Théorie des matrices aléatoires en physique statistique : théorie quantique de la diffusion et systèmes désordonnés

Aurélien Grabsch

université PARIS-SACLAY

NNT : 2018SACLS142

Thèse de doctorat

UNIVERSITÉ PARIS SUD

Comprendre le monde, construire l'avenir

Random Matrices in Statistical Physics: Quantum Scattering and Disordered Systems

Thèse de doctorat de l'Université Paris-Saclay
préparée à l'Université Paris-Sud

École Doctorale n°564 Physique en Île-de-France
Spécialité du doctorat : Physique

Thèse présentée et soutenue à Orsay, le 2 juillet 2018, par

M. Aurélien Grabsch

Composition du Jury :

Mme Cécile Monthus . . . . . Présidente
Directrice de Recherche, CEA Saclay
Institut de Physique Théorique

M. David Dean . . . . . Rapporteur
Professeur, Université de Bordeaux
Laboratoire Ondes et Matière d'Aquitaine

M. Yan Fyodorov . . . . . Rapporteur
Professeur, King's College London
Department of Mathematics

M. Alexander Altland . . . . . Examinateur
Professeur, Université de Cologne
Institute for Theoretical Physics (THP)

M. Jean-Philippe Bouchaud . . . . . Examinateur
Directeur de Recherche, Capital Fund Management

M. Christophe Texier . . . . . Directeur de thèse
Professeur, Université Paris-Sud
Laboratoire de Physique Théorique et Modèles Statistiques

M. Satya Majumdar . . . . . Co-Directeur de thèse
Directeur de Recherche, Université Paris-Sud
Laboratoire de Physique Théorique et Modèles Statistiques

Remerciements

Tout d'abord je tiens à remercier mes directeurs de thèse, Christophe Texier et Satya Majumdar. Ce fut un plaisir de travailler avec eux pendant ces trois années de thèse et j'ai beaucoup appris lors de nos nombreuses discussions.

J'exprime ma reconnaissance à David Dean et à Yan Fyodorov qui ont accepté d'être rapporteurs de ma thèse, et également à Alexander Altland, Jean-Philippe Bouchaud et Cécile Monthus pour avoir participé à mon jury.

Je tiens à faire part de ma gratitude à mes collaborateurs Olivier Giraud, Bertrand Lacroix-A-Chez-Toine, Dmitry Savin, Grégory Schehr et Yves Tourigny, avec qui ce fut toujours un plaisir de travailler.

Je suis également reconnaissant à Alain Comtet dont j'ai eu le plaisir de suivre les cours à l'ENS de Cachan lors de mon année de M1. C'est grâce a lui que j'ai découvert la physique des systèmes désordonnés et c'est sur ses conseils avisés que j'ai par la suite décidé de faire ma thèse au LPTMS.

Je souhaite remercier l'ensemble des membres du LPTMS, en particulier son directeur Emmanuel Trizac pour m'avoir toujours soutenu, Claudine Le Vaou et Karolina Kolodziej pour leur efficacité et leur bienveillance, ainsi que Nicolas Pavloff pour son sens de l'humour. Je remercie aussi mes camarades doctorants et post-doctorants qui ont contribué à la bonne ambiance qui règne au laboratoire, en particulier Thibault dont j'ai partagé le bureau pendant deux ans, et avec qui ce fut toujours un plaisir de discuter et de rigoler.

Je remercie également mes parents qui m'ont soutenu tout au long de mes études, ainsi que mes amis Clément, Jean, Hadrien et Pauline, sans qui ces années à Paris auraient été beaucoup moins agréables.

Contents

Résumé en français

Depuis son introduction par Wishart dans le domaine des statistiques en 1928 [311], le concept de matrice aléatoire a été utilisé dans divers domaines : mathématiques, physique, finance, etc.

En mathématiques, la théorie des matrices aléatoires a été un domaine de recherche très actif. Une de ses applications les plus remarquables est la théorie des nombres. En 1973, Montgomery a conjecturé que la fonction de corrélation a deux points des zéros de la fonction zêta de Riemann est identique à celle des valeurs propres de grandes matrices unitaires aléatoires [237]. Bien que cette conjecture n'ait toujours pas été démontrée, la connexion entre la théorie des nombres et les matrices aléatoires s'est renforcée : la conjecture de Montgomery a été étendue aux fonctions de corrélations à n points, il a été montré que la fonction zêta se comporte comme les polynômes caractéristiques de matrices aléatoires, que des généralisations de la fonction zêta, les fonctions L, sont reliées à d'autres ensembles de matrices aléatoires,... Pour plus de détails, je renvoie aux revues [87, 188, 189], ainsi qu'aux références qu'elles contiennent.

En physique, les matrices aléatoires ont été introduites dans les années 50 par Wigner dans le but d'étudier le noyau atomique [306, 309, 310]. En effet, il est très difficile de décrire analytiquement ce système à N corps en interaction. L'idée de Wigner consiste à simplifier sa description en remplaçant son Hamiltonien par une matrice aléatoire. Cette approche repose sur le principe que les propriétés universelles du système ne doivent pas dépendre de ses détails microscopiques, mais uniquement de propriétés globales, comme les symétries. L'approche de Wigner est similaire à celle de la physique statistique : en physique statistique l'analyse de la dynamique d'un problème à N corps (par exemple un gaz) est remplacée par une information statistique (probabilité d'occupation d'un microétat). De même, au lieu de considérer un modèle microscopique pour le noyau atomique, on se donne une mesure de probabilité sur un ensemble d'Hamiltoniens. Bien que cette approche ne permette pas de décrire les détails du spectre du noyau, elle a permis de décrire correctement des propriétés universelles, comme la distribution de l'espacement entre niveaux d'énergie consécutifs (voir Figure 1).

Les symétries jouent un rôle essentiel dans cette approche, car elles imposent de fortes contraintes sur l'Hamiltonien. Une première classification de matrices aléatoires, qui se base sur deux symétries globales (renversement du temps et rotation du spin),

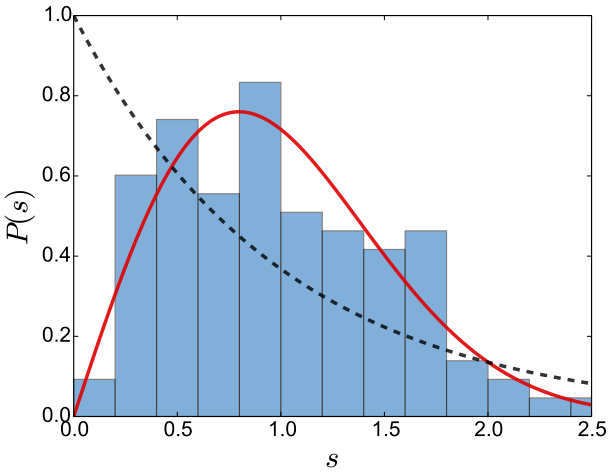

Figure 1: Histogramme représentant l'espacement entre niveaux d'énergie consécutifs (normalisé par l'espacement moyen) des 108 premiers niveaux de ^{166}Er, obtenus par résonance de neutrons lents (les données sont tirées de [205]). Le trait plein représente la prédictions des matrices aléatoires connue sous le nom de *Wigner's surmise* (voir Section 1.2). La ligne en pointillés correspond à la loi de Poisson, qui serait attendue si les niveaux d'énergie étaient des variables aléatoires indépendantes.

a été établie par Dyson dans les années 60 [115, 116]. Cette classification a ensuite été complétée par Altland et Zirnbauer à la fin des années 90 [16, 314] en prenant en compte des symétries discrètes (symétrie chirale et particule-trou).

Bien qu'elle ait d'abord été utilisée en physique nucléaire, la théorie des matrices aléatoires s'est révélée être un puissant outil dans divers domaines de la physique, par exemple pour étudier le transport électronique cohérent [5, 30, 54, 88, 163, 169, 191, 226, 229, 278, 301–303], l'information quantique (entropie d'intrication d'états bipartite) [99, 125, 126, 250, 251, 258], les interfaces fluctuantes en physique statistique [248, 249], les atomes froids [77, 91, 100, 198, 218, 219], la transmission de données dans des canaux entrée multiple sortie multiple (MIMO, *multiple input multiple output*), les verres de spin [2, 22, 52, 142, 144, 149], etc.

De nombreuses applications des matrices aléatoires reposent sur les *ensembles invariants*. Ces ensembles sont entièrement caractérisés par la loi jointe des valeurs propres $\{\lambda_i\}$ de la matrice aléatoire, tandis que les vecteurs propres sont décorrélés des valeurs propres. Les exemples les plus connus sont les trois ensembles Gaussiens (orthogonal, unitaire et symplectique), mais il existe beaucoup d'autres ensembles, comme les ensembles de Laguerre ou de Jacobi qui sont importants pour les applications des matrices aléatoires en transport quantique. Par exemple, le transport des électrons à travers un point quantique (*quantum dot*) à deux terminaux est caractérisé par un jeu de probabilités de transmission $\{T_n\}$. Plusieurs observables physiques peuvent être exprimées à partir de ces transmissions, par exemple la conductance $G = \frac{2e^2}{h}\sum_n T_n$ où e désigne la charge électronique, ou la puissance du bruit de grenaille (*shot noise*) $S = \frac{2e^3|V|}{h}\sum_n T_n(1-T_n)$, où l'on a noté V la différence de potentiel. Si la dynamique des électrons dans le point quantique est de nature chaotique, on peut montrer que les probabilités $\{T_n\}$ sont distribuées comme les valeurs propres de matrices aléatoires dans les ensembles de Jacobi. Les deux quantités physiques susmentionnées sont alors des exemples de *statistiques linéaires* de valeurs propres d'une matrice aléatoire: elles sont de la forme $L = \sum_{i=1}^{N} f(\lambda_i)$, où f est une fonction quelconque (le terme *linéaire* vient du fait que L ne comporte pas de produit de valeurs propres distinctes).

La détermination des propriétés de ces statistiques linéaires a été un domaine de recherche très actif. Les fortes corrélations entre les valeurs propres de matrices aléatoires rendent en effet ce problème très difficile. Plusieurs techniques ont été développées pour étudier les fluctuations typiques de ces observables. Elles ont abouti à la célèbre formule de Dyson-Mehta pour la variance des statistiques linéaires [117], qui a par la suite été étendue par plusieurs personnes, entre autres : Beenakker [28, 29], Basor et Tracy [26], Jancovici et Forrester [181]. La question des fluctuations *atypique* a été considérée plus récemment. Une puissante méthode qui permet d'étudier ces fluctuations atypiques est la technique du *Gaz de Coulomb*, introduite par Dyson et Mehta [115,117]. Dans cette approche, les valeurs propres de matrices aléatoires sont interprétées comme les positions de particules dans un gaz unidimensionnel, avec répulsion logarithmique. La détermination de la distribution d'une statistique linéaire se réduit à l'étude de l'effet d'une contrainte sur la configuration optimale de ce gaz (minimum de l'énergie). Cette contrainte peut potentiellement engendrer des transitions de phases dans le gaz.

Dans cette thèse, je décris comment les puissants outils issus de la théorie des matrices aléatoires, en particulier le gaz de Coulomb, peuvent être utilisés pour étudier des observables variées en physique statistique.

Panorama de cette thèse

Après une introduction générale (page 1) suit un chapitre préliminaire (page 5) dans lequel je donne un aperçu global de la recherche que j'ai menée pendant ma thèse. J'y liste mes principaux résultats, ainsi que mes publications (résumées dans le Tableau 1, page 9). Une partie de ces sujets est abordée plus en détails dans la suite du manuscrit. Pour les autres, je renvoie le lecteur aux articles correspondants.

Première partie : statistiques linéaires et matrices aléatoires

La première partie se concentre sur l'analyse de la distribution (fluctuations typiques et atypiques) de différentes statistiques linéaires de valeurs propres, en utilisant la méthode du gaz de Coulomb.

Le Chapitre 1 est une introduction générale à la théorie des matrices aléatoires. Après avoir discuté les exemples des ensembles Gaussiens et de Laguerre, j'y décris plus particulièrement les propriétés universelles des ensembles invariants.

Le Chapitre 2 introduit la méthode du gaz de Coulomb, qui est l'outil principal de cette première partie. Je donne quelques illustrations de cette méthode dans des cas simples.

Dans le Chapitre 3 j'applique cette méthode pour obtenir la loi jointe de deux statistique linéaire, qui est requise pour étudier le transport AC dans un circuit RC quantique. L'analyse de cette loi jointe nous oblige à imposer deux contraintes sur le gaz de Coulomb, ce qui nous donne un diagramme de phase bidimensionnel pour le gaz de Coulomb (le premier obtenu dans ce contexte).

Au Chapitre 4 j'introduis un nouveau type d'observable, que nous avons baptisé *statistiques linéaires tronquées*. Ce sont des statistiques linéaires dans lesquelles nous avons gardé seulement une fraction des valeurs propres. Nous avons considéré deux cas : soit on ne conserve que les plus grandes (ou les plus petites) valeurs propres, soit n'importe quel sous-ensemble de valeurs propre peut contribuer. Je présente une méthode générale pour analyser ces deux différents cas, et je l'applique à l'étude d'un modèle d'interfaces 1D fluctuantes.

Deuxième partie : fils désordonnés

La deuxième partie de cette thèse se concentre sur l'étude d'un modèle de fil désordonné quasi-1D. Ce projet s'inscrit dans le domaine des systèmes désordonnés, et plus précisément, de la localisation d'Anderson. Il est bien connu que la dimension joue un rôle crucial dans l'étude de la propagation d'une onde dans un milieu aléatoire. À une dimension, il existe de puissants outils analytiques qui permettent de calculer les propriétés de localisation. Cependant, le problème devient beaucoup plus difficile en dimensions supérieures.

Les modèles de fils désordonnés multicanaux représentent une situation intermédiaire entre le probleme purement 1D et les dimensions supérieures. Une des principales méthodes pour étudier ces modèles a été introduite par Dorokhov, Mello, Pereyra et Kumar (DMPK) [106–109, 227] (voir aussi les revues [30, 229]). Cette approche est décrite dans le Chapitre 5.

L'approche DMPK repose en revanche sur une hypothèse d'isotropie qui la restreint a cas quasi-1D. Notre but est de se passer ce cette hypothèse. De plus, notre objectif est également d'étendre au cas multicanal les puissants outils qui existent en 1D. Nous nous intéressons donc à un modèle de fil désordonné : l'équation de Dirac multicanale avec masse aléatoire, qui est introduit au Chapitre 6, dans lequel je le relie à un modèle de matrices aléatoires.

Dans le Chapitre 7, j'utilise la connexion à ce modèle de matrice pour analyser la densité d'états et les propriétés de localisation de ce fil désordonné. Cette approche nous permet d'étendre des résultats connus, en considérant un cas non-isotrope.

Enfin, dans le Chapitre 8 je montre que ce modèle subit une série de transitions de phases de nature topologique, contrôlées par le désordre. Je présente une interprétation simple de ces transitions en terme de condensation de charges dans un gaz de Coulomb.

Introduction

Since its first use by Wishart in the context of Statistics [311], the concept of random matrix has been used in various domains: Mathematics, Physics, Finance, ...

In Mathematics, random matrix theory has been an intense subject of investigation. One of its most remarkable applications is number theory. In 1973, Montgomery conjectured that the pair correlation function of the zeros of the Riemann zeta function (related to the distribution of prime numbers) is the same as for the eigenvalues of random unitary matrices [237]. Although this conjecture still remains to be proved, the connection between random matrices and number theory has been strengthened: Montgomery's conjecture was extended to higher order correlation functions, the Riemann zeta function was shown to behave as the characteristic polynomials of random matrices, a connection between generalisations of the zeta function, known as L-functions, and other ensembles of random matrices was exhibited, ... For more details, see for instance the reviews [87, 188, 189] and references therein.

In Physics, random matrices have first been introduced in the 50s by Wigner to study the atomic nucleus [306, 309, 310]. His idea consists in replacing the exact many body Hamiltonian by a random matrix which captures the essential symmetries of the system. This approach successfully reproduced the correct statistics for the level spacing [224].

Symmetries play a fundamental role in this approach, as they impose strong constraints on the Hamiltonian. A first classification of random Hamiltonian, based on global symmetries, was established by Dyson in the 60s [115, 116]. This classification was completed at the end of the 90s by Altland and Zirnbauer [16, 314].

Although it was first applied in nuclear physics, random matrix theory has proved to be a useful tool in diverse fields of physics, such as electronic quantum transport [5, 30, 54, 88, 163, 169, 191, 226, 229, 278, 301–303], quantum information (entanglement in random bipartite quantum states) [99, 125, 126, 250, 251, 258], the study of fluctuating interfaces in statistical physics [248, 249], cold atoms [77, 91, 100, 198, 218, 219], data transmission in multiple input multiple output (MIMO) channels [187, 241], spin glass [2, 22, 52, 142, 144, 149], ...

Many applications of random matrices involve *invariant ensembles*. These ensembles are fully characterised by the joint distribution of the eigenvalues $\{\lambda_i\}$ of the random matrix, while the eigenvectors are uncorrelated to the eigenvalues. The most famous

examples are the three Gaussian ensembles (orthogonal, unitary and symplectic), but many other ensembles exist, such as the Laguerre or the Jacobi ensembles. These latter have played a central role in the applications of random matrix theory to quantum transport. For example, the electronic transport through a two terminal quantum dot can be characterised by a set of transmission probabilities $\{T_n\}$. Several physical quantities can be related to these transmissions, for example the conductance $G = \frac{2e^2}{h} \sum_n T_n$, where e is the electronic charge or the shot-noise power $S = \frac{2e^3|V|}{h} \sum_n T_n(1-T_n)$, where V is the voltage drop. If the dynamics in the quantum dot is of chaotic nature, the probabilities $\{T_n\}$ were shown to correspond to the eigenvalues of random matrices in the Jacobi ensembles. The two physical observables aforementioned are thus examples of *linear statistics* of eigenvalues of random matrices: they are of the form $L = \sum_{i=1}^{N} f(\lambda_i)$, where f can be any given function.

Determining the statistical properties of these linear statistics has been an intense field of study. The strong correlations between the eigenvalues of random matrices make this problem quite difficult. Several techniques were first developed to study the typical fluctuations. This led to the formula for the variance of linear statistics of Dyson and Mehta [117], which was later extended by several people, among them: Beenakker [28, 29], Basor and Tracy [26], Jancovici and Forrester [181]. More recently, the question of *atypical* fluctuations, was considered. A convenient method to address this problem is to use the *Coulomb gas technique* introduced by Dyson and Mehta [115, 117]. In this approach, the eigenvalues of random matrices are interpreted as the positions of particles in a strongly correlated 1D gas, with logarithmic repulsion. Then, the derivation of the distribution of the linear statistics reduces to minimising the energy of the Coulomb gas under constraints. An interesting feature is the possibility of phase transitions in the underlying Coulomb gas, driven by the constraints.

In this thesis, we apply the powerful tools of random matrix theory, in particular the Coulomb gas method, to study various observables in statistical physics.

Overview of this thesis

First part: linear statistics in random matrix theory

The first part is devoted to the analysis of the full distribution (typical and atypical fluctuations) of different linear statistics, using the Coulomb gas technique.

Chapter 1 gives a general introduction to random matrix theory, and focuses on the universal features of invariant ensembles.

Chapter 2 introduces the Coulomb gas method, which is the main tool used in this first part to analyse the distribution of linear statistics.

In Chapter 3 we apply this method to obtain the joint distribution of two linear statistics, which is required in the study of AC transport in a quantum RC-circuit. The study of this joint distribution leads us to introduce two constraints on the Coulomb gas, resulting in the first two dimensional phase diagram obtained in this context.

We introduce in Chapter 4 a new type of observables, which we called *truncated linear statistics*. These are linear statistics in which only a fraction of the eigenvalues

contribute. We expose a general method to study these truncated linear statistics and apply it to the study of a model of 1D fluctuating interfaces.

Second part: multichannel disordered wires

The second part of this thesis is devoted to the analysis of a model of quasi-1D disordered wire. This project enters into the framework of disordered systems, and more precisely, Anderson localisation. It is well known that dimensionality plays a crucial role in the problem of a wave in a random medium. In one dimension, powerful analytic methods allow to compute the localisation properties. However, the problem is much more challenging in higher dimensions.

Models of multichannel disordered wires represent an intermediate situation between the strictly 1D case and higher dimensions. One of the main methods to study these models was introduced by Dorokhov, Mello, Pereyra and Kumar (DMPK) [106–109,227] (for reviews see [30, 229]). This approach is described in Chapter 5.

The DMPK approach is however based on an isotropy assumption, which restricts it to the quasi-1D geometry. We wished to go beyond this assumption. Furthermore, our aim was to extend the powerful methods that exist for 1D disordered systems to the multichannel models. Therefore, we focus on a model of disordered wire, the mutlichannel Dirac equation with a random mass, which is introduced in Chapter 6, and shown to be linked to a random matrix model.

In Chapter 7 we use this connection to analyse the density of states and the localisation properties of this model.

Finally, in Chapter 8, we show that this model exhibits a series of topological phase transitions, driven by the disorder. We give a simple interpretation of these transitions in terms of the condensation of charges in a Coulomb gas.

Main results

In this preliminary chapter, I give an overview of the research I have conducted during my PhD at LPTMS. I briefly describe my publications related to the questions studied during my PhD, as I have chosen to reproduce only a fraction of them in this manuscript.

Random matrices, Coulomb gas and determinantal processes

A first part of my work is devoted to the study of observables known as *linear statistics* of the eigenvalues of random matrices. These linear statistics play a central role in the applications of random matrices as they can represent many physical quantities: conductance or shot noise of a chaotic quantum dot, kinetic energy of a gas of cold fermions, ... I have studied the distribution of several linear statistics, in various domains of physics, using a technique called *the Coulomb gas method* (described in Chapter 2).

Linear statistics and quantum transport

I have worked on several applications of random matrices to coherent quantum transport. The first one concerns the study of the AC transport properties of a quantum RC-circuit designed from a chaotic quantum dot. These properties can be related to the scattering matrix $\mathcal{S}$ describing the transport of a single electron through the chaotic cavity. More precisely, the AC response is obtained from the energy dependence of the $\mathcal{S}$-matrix, which is encoded in the Wigner-Smith matrix $\mathcal{Q} = -\mathrm{i}\mathcal{S}^\dagger \partial_\varepsilon \mathcal{S}$. Knowing the statistical properties of $\mathcal{Q}$ from Refs. [57, 58] we have studied the distribution of the "mesoscopic capacitance" C_μ and the "charge relaxation resistance" R_q of the circuit. This analysis requires the derivation of the joint distribution of two linear statistics in the Laguerre ensemble of random matrix theory.

1) A. Grabsch and C. Texier, Capacitance and charge relaxation resistance of chaotic cavities —Joint distribution of two linear statistics in the Laguerre ensemble of random matrices, Europhys. Lett. **109**(5), 50004 (2015).

➳ Included as Article 2, page 77.

This letter is the result of the work initiated during my master's internship at LPTMS. It presents only the first results on the Coulomb gas, as the full phase diagram was obtained later during my PhD. For more details, see Chapter 3.

The study of the joint distribution mentioned above was performed using the Coulomb gas technique. In this analysis, I introduced an important simplification of the method, based on a thermodynamic identity (discussed at the end of Section 2.2.5). Besides providing a shortcut through the usual Coulomb gas technique, the use of this thermodynamic identity has allowed to spot a mistake in Ref. [286] and also derive further results.

☞ See the erratum of Ref. [286]

The Coulomb gas method yields only the dominant contribution to the distribution in the limit of large matrix size. We have also studied the subleading corrections to this result, which are essential in the study of the Wigner time delay (related to the density of states) of disordered wires.

2) A. Grabsch and C. Texier, Distribution of spectral linear statistics on random matrices beyond the large deviation function – Wigner time delay in multichannel disordered wires, J. Phys. A **49**, 465002 (2016).

➳ Included as Article 1, page 47.

This work is discussed in Section 2.2.6.

A central concept in the aforementioned project is that of Wigner-Smith time delay matrix $\mathcal{Q}$. The distribution of this matrix was obtained by Brouwer, Frahm and Beenakker [57, 58] for a chaotic quantum dot and by Brouwer and Beenakker [34] for semi infinite disordered wires. These distributions have been derived under the assumption that the mesoscopic system (quantum dot) is connected to a macroscopic system via perfect contacts, or isotropy with respect to the coupling by the disorder (disordered wires). We have extended their result for quantum dots and obtained the distribution of $\mathcal{Q}$ for arbitrary coupling. Our result is briefly discussed in Section 3.1.2.

3) A. Grabsch, D. V. Savin, C. Texier, Wigner-Smith time-delay matrix in chaotic cavities with non-ideal contacts, arXiv:1804.09580 (2018).

The Wigner-Smith matrix $\mathcal{Q}$ is a central object of this thesis: besides Articles 1) and 3) aforementioned, it also appears in 5) (see below) and in 9) (density of states is related to $\operatorname{tr}\mathcal{Q}$) in the context of disordered wires.

Truncated linear statistics

Motivated by applications to coherent transport, we have introduced a new type of observables, which we called *truncated linear statistics*. These are linear statistics in which only a fraction of the eigenvalues contribute. We have developed a general method,

based on the Coulomb gas, to study these truncated linear statistics and applied it to the study of a model of 1D fluctuating interfaces and to analyse the contribution of a finite fraction of channels to the density of states of a chaotic quantum dot.

4) A. Grabsch, S. N. Majumdar, and C. Texier, Truncated Linear Statistics Associated with the Top Eigenvalues of Random Matrices, J. Stat. Phys. **167**(2), 234–259 (2017), updated version arXiv:1609.08296.

➳ Included as Article 3, page 103.

5) A. Grabsch, S. N. Majumdar, and C. Texier, Truncated Linear Statistics Associated with the Eigenvalues of Random Matrices II. Partial Sums over Proper Time Delays for Chaotic Quantum Dots, J. Stat. Phys. **167**(6), 1452–1488 (2017).

➳ Included as Article 4, page 105.

These two articles are the object of Chapter 4.

Cold atoms

The positions of noninteracting fermions in a 1D harmonic trap at zero temperature can be mapped onto the eigenvalues of Gaussian matrices (with unitary symmetry). This mapping allows to study linear statistics of the fermions' positions with the Coulomb gas method. However, this connection is lost at finite temperature. We have introduced a general formalism (based on determinantal processes and statistical mechanics) to study the fluctuations of such observables at finite temperature, in both the canonical and grand canonical ensembles.

6) A. Grabsch, S. N. Majumdar, G. Schehr, and C. Texier, Fluctuations of observables for free fermions in a harmonic trap at finite temperature, SciPost Phys. **4**, 014 (2018).

Our method relies on the statistical properties of the occupation numbers of the energy levels. In the grand canonical ensemble they are independent, but in the canonical one they are strongly correlated. These correlations induce a strong difference in the fluctuations of observables in the different ensembles. To quantify these correlations, we have studied the p-point correlation function of these occupation numbers and applied our results to the study of Bose-Einstein condensation in one dimension.

7) O. Giraud, A. Grabsch, and C. Texier, Correlations of occupation numbers in the canonical ensemble and application to a Bose-Einstein condensate in a one-dimensional harmonic trap, Phys. Rev. A **97**, 053615 (2018).

In two dimensions, several systems of noninteracting fermions can also be described by a random matrix model. For example, the modulus square of the ground state wave function of charged fermions subjected to a magnetic field can be mapped onto the distribution of eigenvalues in the complex Ginibre ensemble. Motivated by the study of extreme value statistics of correlated variables, we have analysed the distribution of the largest (complex) eigenvalue in different matrix ensembles (which corresponds to the position of the farthest fermion). In particular, we have exhibited a universal "intermediate deviation regime" which connects smoothly the typical regime to the left large deviation tail.

8) B. Lacroix-A-Chez-Toine, A. Grabsch, S. N. Majumdar, and G. Schehr, Extremes of 2d Coulomb gas: universal intermediate deviation regime, J. Stat. Mech. **2018**(1), 013203 (2018).

Random matrices and disordered systems

We have considered multichannel disordered wires in the three chiral symmetry classes. We have made a connection with a random matrix model and have given a simple interpretation of the topological phase transitions in terms of the condensation of charges in an underlying Coulomb gas. Furthermore, our approach has allowed us to go beyond the case of isotropic disorder and explore analytically the effect of some anisotropy in the couplings.

9) A. Grabsch and C. Texier, Topological phase transitions in the 1D multichannel Dirac equation with random mass and a random matrix model, Europhys. Lett. **116**, 17004 (2016).

➳ Included as Article 5, page 177.

The work that led to this publication was initiated during a one year internship at the University of Bristol (2014–2015), and later completed during my PhD at LPTMS (in particular the study of the Lyapunov exponents and the numerical simulations, described in Chapter 7, are unpublished). This work is the object of Part II.

This overview of my research is summarised in Table 1.

	Coulomb gas	Linear statistics	Wigner-Smith matrix	Disordered wires	Cold atoms	In this thesis
1)	✓	✓	✓			Chapter 3
2)	✓	✓	✓	✓		Section 2.2.6
3)		✓	✓			Section 3.1.2
4)	✓	✓				Chapter 4
5)	✓	✓	✓			
6)		✓			✓	✗
7)					✓	✗
8)	✓				✓	✗
9)	✓	✓	✓	✓		Part II

Table 1: List of publications with their corresponding topics. The articles related to cold atoms are not described in this thesis.

Part I

Linear statistics in random matrix theory

Chapter 1

Introduction to random matrices

Although it was first used in Statistics by Wishart [311], the idea of random matrices has been introduced in Physics by Wigner to describe the spectra of atomic nuclei [309]. The nucleus is a complex many body system which is very difficult to describe analytically. Wigner's idea is to model it by a simpler Hamiltonian, taken in the form of a $N \times N$ matrix:

$$H = \begin{pmatrix} & \vdots & \\ \cdots & h_{ij} & \cdots \\ & \vdots & \end{pmatrix}, \tag{1.1}$$

where the matrix elements h_{ij} are taken as random. This approach is based on the idea that the universal properties of a system should not depend on its details, but only on global properties, such as symmetries. This observation will lead us to introduce the *invariant ensembles* of random matrices, which are the main objects of this chapter.

Wigner's approach is somewhat similar to the one of statistical physics: in statistical physics the analysis of the dynamics of the many body problem (a fluid for example) is replaced by a statistical information (occupation of microstates). Similarly, instead of considering a microscopic model for the nucleus, one provides some statistical information on the Hamiltonian. Although this approach cannot reproduce the details of the spectrum of the nucleus, it successfully describes some universal properties such as the

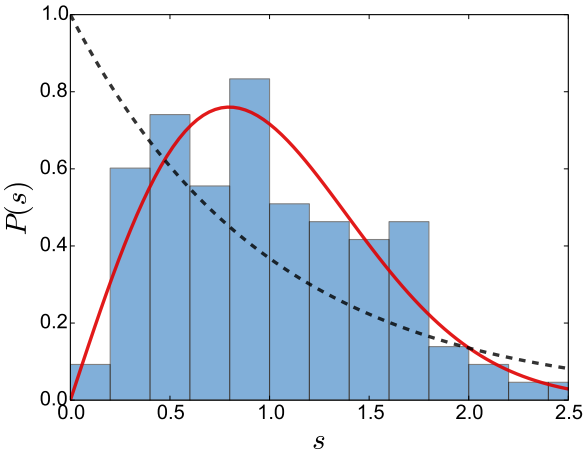

Figure 1.1: Histogram of the levels spacing (normalised by the mean spacing) for the first 108 levels of ^{166}Er obtained by slow neutron resonance (data taken from Ref. [205]). The solid line is the prediction from random matrix theory, known as *Wigner's surmise* (see Section 1.2). The dashed line is the Poisson distribution, which would be expected if the energy levels were independent random variables.

levels statistics (see Fig. 1.1).

In this chapter, we first describe the Wigner-Dyson classification of symmetries in Section 1.1. We then introduce the Gaussian ensembles of random matrices considered by Wigner in Section 1.2. We briefly describe Wishart's earlier work on empirical covariance matrices in Section 1.3. We conclude with Section 1.4 by some general discussion on the invariant ensembles of random matrices.

1.1 The Wigner-Dyson classification

Symmetries have played a central role in Wigner's approach. Following this idea, Dyson introduced a classification of random Hamiltonian based on symmetries [115,116]. Taking into account two symmetries, under time-reversal and spin-rotation, Dyson obtained three different classes which he labelled by an index, called the *Dyson index*, denoted β. As we will see, β can take the values 1, 2 or 4 and is the number of independent real variables per matrix element of H.

In order to represent an Hamiltonian the matrix H must be Hermitian. This matrix can represent either a many body system (such as the atomic nucleus) or a one body system (for example an electron in a chaotic cavity[1]). The presence of other symmetries will impose additional constraints on H.

• If time-reversal symmetry is broken (for example by a magnetic field), there are no further conditions on H. The Hamiltonian can be any Hermitian matrix,

$$H^\dagger = H \,. \tag{1.2}$$

This Hamiltonian can be diagonalised by a unitary matrix, and its spectrum is invariant under unitary transforms

$$H \to U^\dagger H U \,, \quad \text{with} \quad U \in \mathrm{U}(N) \,. \tag{1.3}$$

This class, called the *unitary class*, is associated to the Dyson index $\beta = 2$.

• If the system is invariant under time-reversal, we must impose additional conditions on the Hamiltonian. Time-reversal symmetry is represented by an antiunitary operator T, which can be decomposed as $T = KC$, where K is a unitary matrix and C is the complex conjugation operator. Time-reversal invariance of the Hamiltonian reads

$$H = THT^{-1} = KH^\star K^{-1} = KH^{\mathrm{T}} K^{-1} \,, \tag{1.4}$$

where we used that $H^\dagger = H$ to replace the complex conjugation by a transposition. Acting twice with the operator T, we should recover the original Hamiltonian, thus

$$K^\star K = \kappa \mathbb{1}_N \,, \quad \text{with} \quad \kappa = \pm 1 \,, \tag{1.5}$$

and we used that $K^{-1} = K^\dagger$. We now need to discuss the two possibles cases.

[1] The relation between chaotic dynamics and random matrices has been introduced in the famous work of Bohigas, Giannoni and Schmit [44].

– Let us first consider the case $\kappa = 1$. This situation is realised if the spin is conserved[2], or in many-body systems with integer total angular momentum [308]. We can then choose a basis such that $K = \mathbb{1}_N$, thus the time-reversal symmetry (1.4) reduces to

$$H^{\mathrm{T}} = H \,. \tag{1.6}$$

The corresponding Hamiltonian is therefore a real symmetric matrix. Its spectrum is invariant under orthogonal transforms

$$H \to U^{\mathrm{T}} H U \,, \quad \text{with} \quad U \in \mathrm{O}(N) \,. \tag{1.7}$$

This defines the *orthogonal class*, identified with the Dyson index $\beta = 1$.

– We now consider the case $\kappa = -1$. This situation is realised if spin-rotation symmetry is broken (for example, by spin-orbit coupling in a metallic device). We can choose to represent the matrix K in terms of the second Pauli matrix, as $K = \mathrm{i}\sigma_2$. Time reversal invariance (1.4) implies

$$H = \sigma_2 H^{\mathrm{T}} \sigma_2 \,. \tag{1.8}$$

There are now two ways of seeing the problem. Either we consider that H is a $2N \times 2N$ matrix with complex coefficients, which satisfies (1.8), where σ_2 acts in the spin subspace and should be understood as $\mathbb{1}_N \otimes \sigma_2$. The matrix H can be diagonalised by unitary transforms U that satisfy $U\sigma_2 U^{\mathrm{T}} = \sigma_2$, meaning that U belongs to the compact symplectic group[3] $\mathrm{Sp}(N)$. We can equivalently think of H as a $N \times N$ matrix, with 2×2 matrix coefficients of the form

$$q_0 \mathbb{1}_2 + \mathrm{i} q_1 \sigma_1 + \mathrm{i} q_2 \sigma_2 + \mathrm{i} q_3 \sigma_3 \,, \qquad q_0, q_1, q_2, q_3 \in \mathbb{R}, \tag{1.9}$$

which act on the spin space. These coefficients can be thought of as quaternions, so that H is a $N \times N$ self-adjoint matrix of quaternions, which can be diagonalised by a $N \times N$ "unitary matrix of quaternions"[4]. Since this compact group is isomorphic to the compact symplectic group, we will also denote it $\mathrm{Sp}(N)$. For coherence with the other cases we will follow this second approach, so that H is always a $N \times N$ matrix. Its spectrum being invariant under symplectic transforms

$$H \to U^{-1} H U \,, \quad \text{with} \quad U \in \mathrm{Sp}(N) \,, \tag{1.10}$$

this defines the *symplectic class*, associated to $\beta = 4$ (matrices of quaternions).

Based on time-reversal and spin-rotation symmetries, we have obtained the three Wigner-Dyson classes, indexed by $\beta = 1$, 2 or 4. This classification, known as Dyson's threefold way [116, 224], is summarised in Table 1.1.

[2] If the spin is conserved, we can work in the corresponding subspace, such that we reduce to an effectively spinless Hamiltonian.

[3] The condition $U\sigma_2 U^{\mathrm{T}} = \sigma_2$ means that U belongs to the symplectic group $\mathrm{Sp}(2N)$. The intersection with the unitary group defines the compact symplectic group [171]: $\mathrm{Sp}(N) = \mathrm{Sp}(2N) \cap \mathrm{U}(2N)$.

[4] Since H is a $2N \times 2N$, it has $2N$ eigenvalues. However they all have degeneracy two, so we can effectively treat H as a $N \times N$ matrix of quaternions which can be diagonalised as $H = U^{-1}\mathrm{Diag}(\lambda_1 \mathbb{1}_2, \ldots, \lambda_N \mathbb{1}_2) U$.

Dyson index	TRS	SRS	H	U
$\beta = 1$	yes	yes	real symmetric	orthogonal
$\beta = 2$	no	irrelevant	complex Hermitian	unitary
$\beta = 4$	yes	no	quaternionic self dual	symplectic

Table 1.1: Dyson's threefold way. The different classes are indexed by the Dyson index β which counts the number of independent real parameters per matrix element of H. The presence or not of time-reversal (TRS) and spin-rotation (SRS) symmetries determine the class. The matrix H can be diagonalised by a matrix U, which belongs to a compact group.

1.2 The Gaussian ensembles

Having identified the three Wigner-Dyson classes, we can follow Wigner's idea to study the spectrum of the atomic nucleus. The simplest case consists in considering systems invariant under time-reversal symmetry, and restrict ourselves to the energy levels associated to the same spin states. The transitions between these levels conserve the spin, therefore this corresponds to the orthogonal class $\beta = 1$. The Hamiltonian H is thus a real symmetric matrix, so we only need to fix the matrix elements h_{ij} for $i \leqslant j$. There remains to choose the distribution of these entries. Wigner considered two possibilities:

(i) Either all entries are statistically independent (the so called "Wigner matrices");

(ii) Or from a more physical point of view, the physical properties of a quantum system should not depend on the choice of the basis, therefore the joint distribution of the entries of H must be invariant under a change of basis, i.e., under a rotation (1.7) (the so called "rotationally invariant" ensembles).

It turns out that numerically it is easier to generate the Wigner matrices, but not so easy to generate matrices from a generic rotationally invariant ensemble (because the entries get highly correlated). In contrast, for rotationally invariant ensembles, it is much easier to derive analytically the joint distribution of eigenvalues as we show below.

In particular, there is only one ensemble of random matrices that has independent entries as well as is rotationally invariant: the Gaussian ensemble. This is known as the celebrated Porter-Rosenzweig theorem [263] (see also [224]). We thus consider this specific ensemble, by choosing the matrix entries h_{ij} as independent Gaussian variables:

$$h_{ij} \sim \mathcal{N}(0, \sigma_{ij}) \,, \tag{1.11}$$

where σ_{ij} is the variance of the element h_{ij}. We can thus write the distribution of the matrix H as

$$P(H) = \prod_{i \leqslant j} \left(\frac{1}{\sqrt{2\pi\sigma_{ij}^2}} \, \mathrm{e}^{-h_{ij}^2/2\sigma_{ij}^2} \right) \,, \tag{1.12}$$

with respect to the Lebesgue (uniform) measure

$$\mathrm{d}H = \prod_{i \leqslant j} \mathrm{d}h_{ij} \,. \tag{1.13}$$

If we additionally impose that the distribution is invariant under orthogonal transforms, Eq. (1.7), we obtain very restrictive conditions of the variances σ_{ij}:

$$\sigma_{ij} = \begin{cases} \sigma & \text{if } i = j\,, \\ \dfrac{\sigma}{\sqrt{2}} & \text{if } i < j\,, \end{cases} \qquad (\beta = 1)\,. \tag{1.14}$$

We can understand this easily: the symmetric off diagonal terms being equal, they appear twice in the matrix while the diagonal terms contribute only once. The choice (1.14) compensates this imbalance. Using that

$$\sum_{i \leqslant i} \frac{h_{ij}^2}{2\sigma_{ij}^2} = 2\sum_{i<j} \frac{h_{ij}^2}{2\sigma^2} + \sum_i \frac{h_{ij}^2}{2\sigma^2} = \sum_{i,j} \frac{h_{ij}^2}{2\sigma^2} = \operatorname{tr}(H^{\mathrm{T}} H) = \operatorname{tr}(H^2)\,, \tag{1.15}$$

we can rewrite the distribution (1.12) as

$$P(H) = \frac{1}{2^{N/2}(\pi\sigma^2)^{N(N+1)/4}}\, \mathrm{e}^{-\frac{1}{2\sigma^2}\operatorname{tr}(H^2)}\,, \tag{1.16}$$

which makes explicit the invariance of the distribution under (1.7). For convenience, we will set $\sigma = 1$. We thus define the *Gaussian Orthogonal Ensemble* (GOE) by the distribution

$$P(H) = \frac{1}{G_{N,1}}\, \mathrm{e}^{-\frac{1}{2}\operatorname{tr}(H^2)}\,, \qquad G_{N,1} = 2^{N/2}\, \pi^{N(N+1)/4}\,. \tag{1.17}$$

We can similarly define the *Gaussian Unitary Ensemble* (GUE) and *Gaussian Symplectic Ensemble* (GSE) by filling the matrix H with independent complex or quaternionic Gaussian variables. This defines the three Gaussian ensembles, associated to the distributions

$$\boxed{P(H) = \frac{1}{G_{N,\beta}}\, \mathrm{e}^{-\frac{\beta}{2}\operatorname{tr}(H^2)}\,, \qquad G_{N,\beta} = 2^{N/2} \left(\frac{\pi}{\beta}\right)^{\frac{N}{2}(1+\beta\frac{N-1}{2})}} \tag{1.18}$$

with respect to the associated Lebesgue measures defined in Appendix A.1. The choice $\sigma^2 = 1/\beta$ for the variance of the matrix elements is arbitrary, but will turn out to be convenient in the following as it permits to treat the three cases in a unified way (see for instance Section 2.1.1).

Given the distribution of the matrix H (1.18), we are now interested in its eigenvalues, which represent the energy levels of the nucleus in Wigner's approach. Therefore, we need to make a change of variables to go from the matrix entries h_{ij} to the eigenvalues and eigenvectors of H. Since we are interested only in the eigenvalues, we will then integrate over the eigenvectors to obtain the marginal of the eigenvalues. We thus perform the eigendecomposition

$$X = U^{-1}\Lambda U\,, \quad \Lambda = \operatorname{Diag}(\lambda_1, \dots, \lambda_N)\,, \quad U \in \begin{cases} \mathrm{O}(N) & \text{for } \beta = 1\,, \\ \mathrm{U}(N) & \text{for } \beta = 2\,, \\ \mathrm{Sp}(N) & \text{for } \beta = 4\,. \end{cases} \tag{1.19}$$

The Jacobian of this change of variables in given in Appendix A.1, and reads:

$$\mathrm{d}H = \prod_{i<j} |\lambda_i - \lambda_j|^\beta \prod_{i=1}^N \mathrm{d}\lambda_i \, \mathrm{d}\mu(U) \,, \tag{1.20}$$

where $\mathrm{d}\mu$ is the Haar measure on the corresponding compact group. This Jacobian involves a Vandermonde determinant

$$\det(\lambda_i^{j-1}) = \prod_{i<j} (\lambda_i - \lambda_j) \,, \tag{1.21}$$

which is of central importance as we will soon see. The joint distribution of the eigenvalues and eigenvectors is thus

$$P(\{\lambda_i\}, U) = \frac{1}{G_{N,\beta}} \prod_{i<j} |\lambda_i - \lambda_j|^\beta \prod_{i=1}^N \mathrm{e}^{-\frac{\beta}{2}\lambda_i^2} \,, \tag{1.22}$$

which does not depend on U. This means that the eigenvectors of H are uniformly distributed over the compact group. Therefore, integrating (1.22) over the matrix U, we obtain the joint distribution of the eigenvalues

$$\boxed{\mathcal{P}(\lambda_1, \dots, \lambda_N) = \frac{1}{\tilde{G}_{N,\beta}} \prod_{i<j} |\lambda_i - \lambda_j|^\beta \prod_{i=1}^N \mathrm{e}^{-\frac{\beta}{2}\lambda_i^2}} \tag{1.23}$$

where the normalisation constant $\tilde{G}_{N,\beta}$ is given by

$$\tilde{G}_{N,\beta} = \frac{G_{N,\beta}}{v_{N,\beta}} \,, \quad \text{where} \quad v_{N,\beta} = \int \mathrm{d}\mu(U) = \frac{\pi^{\beta\frac{N(N-1)}{2}} \Gamma\left(\frac{\beta}{2}\right)^N}{\Gamma_{N,\beta}\left(\frac{\beta N}{2}\right)} \,, \tag{1.24}$$

expressed in terms of the multivariate Gamma function $\Gamma_{N,\beta}$, defined in Appendix B (see also Appendix A.1). We thus deduce the normalisation constant as:

$$\tilde{G}_{N,\beta} = 2^{N/2} \left(\frac{\pi}{\beta}\right)^{\frac{N}{2}(1+\beta\frac{N-1}{2})} \frac{\Gamma_{N,\beta}\left(\frac{\beta N}{2}\right)}{\pi^{\beta\frac{N(N-1)}{2}} \Gamma\left(\frac{\beta}{2}\right)^N} = \frac{(2\pi)^{N/2}}{\beta^{\frac{N}{2}(1+\beta\frac{N-1}{2})}} \prod_{j=1}^N \frac{\Gamma\left(\beta\frac{N-j+1}{2}\right)}{\Gamma\left(\frac{\beta}{2}\right)} \,. \tag{1.25}$$

An important feature of the joint distribution of eigenvalues (1.23) is the presence of the Vandermonde determinant, which comes from the Jacobian of the eigendecomposition. This term induces **correlations** between the different eigenvalues. In particular, the joint distribution (1.23) vanishes for $\lambda_i = \lambda_j$ and $i \neq j$. Therefore, the probability of having two eigenvalues close to each other is very small. This induces some effective repulsion between the eigenvalues, as we will see in more details in Chapter 2.

Although we have obtained the joint distribution (1.23) for $\beta = 1$, 2 or 4 from the diagonalisation of Gaussian Wigner matrices, it can be obtained for general $\beta > 0$ by the diagonalisation of a specific type of Wigner matrices: the tridiagonal Dumitriu-Edelman ensembles [113].

Additionally, the joint distribution (1.23) can also be derived by analysing the Dyson Brownian motion [114].

Wigner conjectured that the statistics of the spacing of energy levels of the atomic nuclei should be correctly described by the spacing of eigenvalues in the Gaussian ensembles. He computed the distribution of the levels spacing from the joint distribution of eigenvalues (1.23) for $N = 2$ and $\beta = 1$ (to describe transitions between levels with the same spin), and obtained:

$$P(s) = \frac{\pi s}{2} \mathrm{e}^{-\pi s^2/4} , \qquad s = \frac{|\lambda_1 - \lambda_2|}{\langle |\lambda_1 - \lambda_2| \rangle} , \tag{1.26}$$

where $\langle \cdots \rangle$ denotes the averaging with (1.23). The vanishing of this distribution for $s = 0$ shows the repulsion between the eigenvalue. Wigner conjectured that this form should hold for bigger matrices [307]. Although the shape of the distribution remains similar, its exact form is more complicated for larger values of N [224]. Wigner's conjecture (1.26), known as *Wigner surmise* has first been verified experimentally on the levels of ^{166}Er in Ref. [205] (see Fig. 1.1). A finer agreement was later obtained in Ref. [45] by combining the data from 27 different nuclei (1726 spacings).

Beyond their applications in nuclear physics [45, 205, 309], the Gaussian ensembles have then found applications in many other fields, such as quantum transport (in the Hamiltonian approach, see for instance [148]) and cold atoms [77, 100, 218, 219].

1.3 Wishart matrices – Laguerre ensembles

Before being introduced in physics by Wigner, random matrices have first been studied by Wishart [311] in the context of statistics. His purpose was to analyse the statistical properties of the sample covariance of a series of measurements. Consider a first series of measurements $\{x_i^{(1)}\}_{i=1,\dots,M}$. One can think for example of a set of temperatures in a given city, measured at different times i. The sample (or empirical) mean value of this series is

$$\overline{x^{(1)}} = \frac{1}{M} \sum_{i=1}^{M} x_i^{(1)} . \tag{1.27}$$

We can also define the sample variance[5]

$$\widetilde{\mathrm{var}}(x^{(1)}) = \frac{1}{M-1} \sum_{i=1}^{M} \left(x_i^{(1)} - \overline{x^{(1)}} \right)^2 . \tag{1.28}$$

This latter gives information about the amplitude of fluctuations of the measures $\{x_i^{(1)}\}$ around the empirical mean (1.27). If the $x_i^{(1)}$'s are random variables, these two quantities are also random and one can investigate their probabilistic properties. For instance, if the $x_i^{(1)}$'s are independent and identically distributed, the law of large number states

[5] The factor $\frac{1}{M-1}$, instead of $\frac{1}{M}$ which might be more natural at first sight, in the definition of the sample variance is such that, if the $x_i^{(1)}$'s are independent random variables, the mean of (1.28) is the probabilistic variance $\langle \widetilde{\mathrm{var}}(x^{(1)}) \rangle = \mathrm{Var}(x^{(1)})$.

that both the empirical mean and variance converge towards the probabilistic mean and variance for a large series of samples:

$$\overline{x^{(1)}} \underset{M\to\infty}{\longrightarrow} \left\langle x_i^{(1)} \right\rangle , \qquad \widetilde{\mathrm{var}}(x^{(1)}) \underset{M\to\infty}{\longrightarrow} \mathrm{Var}(x_i^{(1)}) = \left\langle (x_i^{(1)})^2 \right\rangle - \left\langle x_i^{(1)} \right\rangle^2 , \tag{1.29}$$

where $\langle \cdots \rangle$ denotes the averaging with respect to the distribution of the $x_i^{(1)}$'s.

One can also consider different series of measurements $\{x_i^{(j)}\}_{i=1,\dots,M}$ for $j = 1, 2, \dots, N$. In our example, these could represent measurements of temperatures at times i, in different cities labelled by j. We can define the empirical mean and variance for each series as in Eqs. (1.27) and (1.28). We can additionally define the empirical covariance between two different series as

$$\widetilde{\mathrm{cov}}(x^{(a)}, x^{(b)}) = \frac{1}{M-1} \sum_{i=1}^{M} \left(x_i^{(a)} - \overline{x^{(a)}} \right) \left(x_i^{(b)} - \overline{x^{(b)}} \right) . \tag{1.30}$$

This quantity gives information about the correlations between the two different series a and b. We can write this definition in a more compact form by introducing the $M \times N$ matrix of measurements (shifted by their mean)

$$X = \begin{pmatrix} x_1^{(1)} - \overline{x^{(1)}} & \cdots & x_1^{(N)} - \overline{x^{(N)}} \\ x_2^{(1)} - \overline{x^{(1)}} & \cdots & x_2^{(N)} - \overline{x^{(N)}} \\ \vdots & & \vdots \\ x_M^{(1)} - \overline{x^{(1)}} & \cdots & x_M^{(N)} - \overline{x^{(N)}} \end{pmatrix} . \tag{1.31}$$

We can then rewrite (1.30) in terms of the empirical covariance matrix C:

$$\widetilde{\mathrm{cov}}(x^{(a)}, x^{(b)}) = \mathrm{C}_{ab} , \quad \text{with} \quad \mathrm{C} = \frac{1}{M-1} X^{\mathrm{T}} X , \tag{1.32}$$

and $\widetilde{\mathrm{cov}}(x^{(a)}, x^{(a)}) = \widetilde{\mathrm{var}}(x^{(a)})$.

Wishart was interested in the statistical properties of the matrix C. In a typical sample, the entries X_{ij} of (1.31) are correlated. However, even in the uncorrelated case, the spectral properties of the covariance matrix C are nontrivial. Therefore, the knowledge of these properties is essential to distinguish the specific features of a true sample from the universal characteristics of C. Henceforth, Wishart constructed a Null model, by considering random covariance matrices, in which the entries X_{ij} of (1.31) are independent and identically distributed. He choose these entries as Gaussian variables, with zero mean and unit variance. Note that unlike the matrices considered in Section 1.2, this rectangular matrix has no particular symmetry and all its elements are independent. We introduce then the matrix

$$Y = X^{\mathrm{T}} X , \qquad X \text{ of size } M \times N , \qquad X_{ij} \sim \mathcal{N}(0,1) , \tag{1.33}$$

which is, up to a factor, the empirical covariance matrix (1.32). This new matrix is real symmetric, and thus corresponds to the orthogonal symmetry class $\beta = 1$. One can show that its distribution is given by[6] [244, 311]:

$$P(Y) \propto (\det Y)^{\frac{1}{2}(M-N+1)-1} \, \mathrm{e}^{-\frac{1}{2}\operatorname{tr} Y} , \qquad Y > 0 , \tag{1.34}$$

[6] The proof relies on the Jacobian (A.18) given in Appendix A.

for $M \geqslant N$ and $Y > 0$ means that the matrix Y has positive eigenvalues (since it takes the form of a square, see (1.33)). This distribution, called the *Wishart distribution*, is a generalisation of the Gamma distribution to real symmetric matrices. It can be extended to the other symmetry classes by considering matrices X filled with complex or quaternionic coefficients of variance $1/\beta$ (as for the Gaussian ensembles, this choice is arbitrary). The β-Wishart distribution is then

$$\boxed{P(Y) \propto (\det Y)^{\frac{\beta}{2}(M-N+1)-1} \, \mathrm{e}^{-\frac{\beta}{2}\operatorname{tr} Y} \,, \quad Y = X^\dagger X > 0 \,, \quad X_{ij} \sim \mathcal{N}(0, 1/\beta)} \tag{1.35}$$

where we denoted $X^\dagger$ the adjoint[7] of the matrix X.

The Wishart distribution can be extended to the case where the parameter M is not an integer. This generalisation defined the three *Laguerre Ensembles* of random matrix theory (indexed by β), which correspond to the distribution

$$\boxed{P(Y) = \frac{1}{L_{N,\beta}(\alpha)} \, (\det Y)^{\alpha-1-\beta\frac{N-1}{2}} \, \mathrm{e}^{-\frac{\beta}{2}\operatorname{tr} Y} \,, \qquad \alpha > \beta\frac{N-1}{2}} \tag{1.36}$$

where the normalisation constant can be expressed in terms of a multivariate Gamma function, defined in Appendix B.1:

$$L_{N,\beta}(\alpha) = \left(\frac{2}{\beta}\right)^{N\alpha} \Gamma_{N,\beta}(\alpha) = \pi^{\beta N(N-1)/4} \left(\frac{2}{\beta}\right)^{N\alpha} \prod_{j=1}^{N} \Gamma\left(\alpha - \beta\frac{j-1}{2}\right) \,. \tag{1.37}$$

We can recover the Wishart distribution (1.35) by setting $\alpha = \beta M/2$.

As for the Gaussian ensembles, we can look for the distribution of the eigenvalues of the matrix Y. We again perform the eigendecomposition $Y = U^{-1}\Lambda U$, as in Eq. (1.19). The Jacobian is given by Eq. (1.20), and the eigenvalues and eigenvectors again decorrelate. Integration over the eigenvectors gives:

$$\boxed{\mathcal{P}(\lambda_1, \dots, \lambda_N) = \frac{1}{\tilde{L}_{N,\beta}(\alpha)} \prod_{i<j} |\lambda_i - \lambda_j|^\beta \prod_{i=1}^{N} \lambda_i^{\alpha-1-\beta\frac{N-1}{2}} \mathrm{e}^{-\frac{\beta}{2}\lambda_i} \,, \quad \lambda_i > 0} \tag{1.38}$$

where

$$\begin{aligned} \tilde{L}_{N,\beta}(\alpha) &= \pi^{-\beta\frac{N(N-1)}{2}} \left(\frac{2}{\beta}\right)^{N\alpha} \frac{\Gamma_{N,\beta}(\alpha)\Gamma_{N,\beta}\left(\frac{\beta N}{2}\right)}{\Gamma\left(\frac{\beta}{2}\right)^N} \\ &= \left(\frac{2}{\beta}\right)^{N\alpha} \prod_{j=1}^{N} \frac{\Gamma\left(\alpha - \beta\frac{j-1}{2}\right)\Gamma\left(\beta\frac{N-j+1}{2}\right)}{\Gamma\left(\frac{\beta}{2}\right)} \,. \end{aligned} \tag{1.39}$$

As for the Gaussian case discussed in Section 1.2, the Vandermonde determinant in distribution (1.38) induces repulsion between the eigenvalues.

[7] Depending on the symmetry class, it can be a transposition ($\beta = 1$), conjugation and transposition ($\beta = 2$) or the quaternionic conjugation and transposition ($\beta = 4$).

Beyond its original application to the study of empirical covariance [311], the Laguerre ensembles have found many other applications in diverse fields of Mathematics, Physics or Finance [49,50,67,68]. For instance in the context of quantum transport, the (inverse of the) Wigner-Smith matrix which describes quantum scattering in a chaotic quantum dot [57,58,286] (see also Article 2, Article 4 and the reviews [194,284]) or in multichannel disordered wires [34] (also Article 1) belongs to the Laguerre ensembles. These ensembles also appear in the description of quantum entanglement of random bipartite quantum states [250, 251], interface models in statistical physics [249] (see Article 3) and principal component analysis in statistics [214].

In this thesis we will encounter this distribution in Chapter 3 in the context of quantum transport and in Chapter 4 for the statistical description of fluctuating interfaces.

1.4 Invariant ensembles

We have introduced two different sets of random matrices: the Gaussian ensembles (1.18) and the Laguerre ensembles (1.36). These are particular examples of a much broader class of ensembles, known as *invariant ensembles*. These are ensembles which verify the invariance properties (1.3), (1.7) or (1.8). This means that the distribution $P(H)$ of the $N \times N$ matrix H satisfies

$$P(UHU^{-1}) = P(U)\,, \qquad U \in \begin{cases} \mathrm{O}(N) & \text{for } \beta = 1\,, \\ \mathrm{U}(N) & \text{for } \beta = 2\,, \\ \mathrm{Sp}(N) & \text{for } \beta = 4\,. \end{cases} \tag{1.40}$$

In general, we can write such distributions in the form

$$P(H) = \frac{1}{Z_{N,\beta}}\, \mathrm{e}^{-\frac{\beta}{2}\operatorname{tr} V(H)}\,, \tag{1.41}$$

where $Z_{N,\beta}$ is a normalisation constant and V is a function, called *potential*, which verifies $V(UHU^{-1}) = UV(H)U^{-1}$. This is true for any function which can be expressed as a power series. Note that the potential V must be sufficiently confining to ensure the normalisability of (1.41). For example, the Gaussian ensembles (1.18) are obtained by setting $V(x) = x^2$, and the Laguerre ensembles (1.36) correspond to $V(x) = x - [\frac{2}{\beta}(\alpha - 1) - (N-1)] \ln x$. For other examples of invariant ensembles, we can mention the Cauchy ensemble, corresponding to the potential

$$V(x) = \alpha \ln(1 + x^2)\,, \qquad \alpha > N - 1\,. \tag{1.42}$$

The condition on α ensures the normalisability: the probability must decay sufficiently fast at infinity. For example, this ensemble is involved in the proof of the equivalence between the Hamiltonian approach and the stochastic approach to quantum transport, in order to derive the Poisson kernel [54]. Another important ensemble for applications to quantum transport (for the transmission through a quantum dot [24,30,154,301–303]) is the Jacobi ensemble, associated to

$$V(x) = -a \ln x - b \ln(1 - x) \quad \text{for} \quad x \in [0, 1]\,, \qquad a, b > -\frac{2}{\beta}\,. \tag{1.43}$$

Ensembles	Interval	$\mathcal{P}(\lambda_1, \dots, \lambda_N)$
Gaussian	$\lambda_i \in \mathbb{R}$	$\prod_{i<j} \lvert\lambda_i - \lambda_j\rvert^\beta \prod_n \mathrm{e}^{-\frac{\beta}{2}\lambda_n^2}$
Laguerre	$\lambda_i \in \mathbb{R}^+$	$\prod_{i<j} \lvert\lambda_i - \lambda_j\rvert^\beta \prod_n \lambda_n^{\alpha-1-\beta\frac{N-1}{2}} \mathrm{e}^{-\frac{\beta}{2}\lambda_n}$
Cauchy	$\lambda_i \in \mathbb{R}$	$\prod_{i<j} \lvert\lambda_i - \lambda_j\rvert^\beta \prod_n (1+\lambda_n^2)^{-\beta\alpha/2}$
Jacobi	$\lambda_i \in [0,1]$	$\prod_{i<j} \lvert\lambda_i - \lambda_j\rvert^\beta \prod_n \lambda_n^{\frac{\beta a}{2}} (1-\lambda_n)^{\frac{\beta b}{2}}$

Table 1.2: A few ensembles of random matrix theory.

All the ensembles introduced in this chapter are summarised in Table 1.2.

Invariant ensembles play a central role in applications random matrix theory. For these ensembles, the eigenvectors and eigenvalues are statistically independent and one can focus only on the latter. The distribution of the eigenvalues can be easily obtained, as we did for the Gaussian and Laguerre ensembles. Indeed, let us consider the eigendecomposition

$$H = U\Lambda U^{-1}\,, \qquad \Lambda = \mathrm{Diag}(\lambda_1, \dots, \lambda_N)\,, \tag{1.44}$$

where U belongs to the corresponding compact group, fixed by the Dyson index β. The Jacobian of this change of variables is given in Appendix A.1, and reads

$$\mathrm{d}H = \prod_{i<j} |\lambda_i - \lambda_j|^\beta \prod_{i=1}^N \mathrm{d}\lambda_i \, \mathrm{d}\mu(U)\,, \tag{1.45}$$

where $\mathrm{d}\mu(U)$ is the Haar (uniform) measure on the corresponding compact group. The joint distribution of the eigenvalues and eigenvectors is thus

$$P(\{\lambda_i\}, U) = \frac{1}{Z_{N,\beta}} \prod_{i<j} |\lambda_i - \lambda_j|^\beta \prod_{i=1}^N \mathrm{e}^{-\frac{\beta}{2}V(\lambda_i)}\,. \tag{1.46}$$

As in the Gaussian and Laguerre cases, the eigenvalues and eigenvectors are statistically independent. Furthermore, the eigenvectors are uniformly distributed and can easily be integrated over. We obtain

$$\mathcal{P}(\lambda_1, \dots, \lambda_N) = \frac{1}{\tilde{Z}_{N,\beta}} \prod_{i<j} |\lambda_i - \lambda_j|^\beta \prod_{i=1}^N \mathrm{e}^{-\frac{\beta}{2}V(\lambda_i)}\,, \tag{1.47}$$

where the normalisation constant $\tilde{Z}_{N,\beta}$ is related to the one of (1.41) by

$$\tilde{Z}_{N,\beta} = \frac{Z_{N,\beta}}{v_{N,\beta}}\,, \quad \text{where} \quad v_{N,\beta} = \int \mathrm{d}\mu(U) = \frac{\pi^{\beta\frac{N(N-1)}{2}} \Gamma\left(\frac{\beta}{2}\right)^N}{\Gamma_{N,\beta}\left(\frac{\beta N}{2}\right)}\,, \tag{1.48}$$

expressed in terms of the multivariate Gamma function $\Gamma_{N,\beta}$ defined in Appendix B.

We see that the distributions (1.23) and (1.38) obtained for the Gaussian and Laguerre ensembles respectively are specific examples of invariant ensembles. We can stress that the observation made in the Gaussian ensembles is general: the presence of the Vandermonde determinant (which comes from the Jacobian of the eigendecomposition)

induces strong **correlations** between the eigenvalues. Since the distribution (1.47) vanishes for $\lambda_i = \lambda_j$ $(i \neq j)$, the probability of having two eigenvalues close to each other is small. This causes an effective repulsion between the eigenvalues, which we will discuss in more details in Chapter 2.

Chapter 2

The Coulomb gas method and the distribution of linear statistics

In this chapter, we give a general introduction to one of the main tools used in this thesis: the Coulomb gas method. It was first introduced by Dyson and Mehta [115, 117], and has then been applied to many different problems of random matrices, such as the study of the largest eigenvalue [101, 212, 213] (which is required to study the distribution of the number of stationary points in a Gaussian field [22, 52, 142, 144, 149]) or the number of eigenvalues in a given domain [210, 211, 217–219]. It also proved to be very efficient in the study of the electronic transport through a quantum dot [30, 301, 302], data transmission in multiple input multiple output (MIMO) channels [186, 187], principal component analysis [214], bipartite quantum entanglement [99, 125, 250, 251], one dimensional fluctuating interfaces in statistical physics [249] or cold atoms [218, 219]. For references in the mathematical literature, see for instance [36, 37].

The Coulomb gas method is an extremely powerful tool to study invariant ensembles, for which the joint distribution of eigenvalues takes the form[1]

$$\mathcal{P}(\lambda_1, \dots, \lambda_N) \propto \prod_{i<j} |\lambda_i - \lambda_j|^\beta \prod_{i=1}^{N} \mathrm{e}^{-\frac{\beta N}{2} V(\lambda_i)} \,. \tag{2.1}$$

The idea of the Coulomb gas approach is to rewrite this joint distribution of eigenvalues as a Gibbs weight

$$\mathcal{P}(\lambda_1, \dots, \lambda_N) \propto \mathrm{e}^{-\frac{\beta N^2}{2} E(\lambda_1, \dots, \lambda_N)} \,, \tag{2.2}$$

where the Dyson index β plays the role of an inverse temperature and we introduced the "energy"

$$E(\lambda_1, \dots, \lambda_N) = -\frac{1}{N^2} \sum_{i \neq j} \ln |\lambda_i - \lambda_j| + \frac{1}{N} \sum_{i=1}^{N} V(\lambda_i) \,. \tag{2.3}$$

This can be interpreted as the energy of a one-dimensional gas of particles, at positions $\{\lambda_i\}$, trapped in an external potential $V(\lambda)$, which interact with logarithmic repulsion, see Fig. 2.1. This long range repulsion corresponds to the Coulomb interaction of charged

[1] We introduced a factor N in the exponential compared to Eq. (1.47) for convenience, as we will see later.

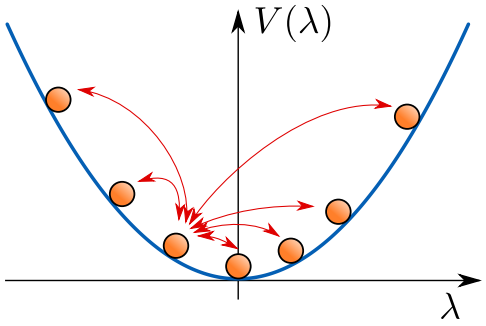

Figure 2.1: In the Coulomb gas approach, the eigenvalues $\{\lambda_i\}$ of a random matrix are mapped onto the positions of particles in a 1D gas with logarithmic interaction, confined by a potential $V(x)$. Here we represented a harmonic potential.

particles in 2D, hence the name of this approach[2]. In the following, we will thus often use the term *charges* to refer to the eigenvalues. This approach is particularly convenient as it permits to forge some physical intuition in random matrix theory by thinking of the eigenvalues as interacting charges.

We expect the typical distribution of charges $\{\lambda_n\}$ to balance the potential and interaction energy. Let us denote λ_{typ} a typical scale for the eigenvalues. The interaction energy scales as

$$\frac{1}{N^2}\sum_{i\neq j}\ln|\lambda_i-\lambda_j| = \mathcal{O}(N^0)\,, \tag{2.4}$$

independently of the scaling of the eigenvalues. While the potential energy has the scaling

$$\frac{1}{N}\sum_{i=1}^{N} V(\lambda_i) = \mathcal{O}(V(\lambda_{\text{typ}}))\,. \tag{2.5}$$

If we assume that the potential is independent of N, these two contributions thus balance each other in (2.3) if the eigenvalues are of order 1 as $N\to\infty$:

$$\lambda_{\text{typ}} = \mathcal{O}(N^0)\,. \tag{2.6}$$

This is why we chose to multiply the potential V by a factor N in (2.1): this ensures that the eigenvalues will not scale with N. Note also that the energy (2.3) is also $\mathcal{O}(N^0)$ as $N\to\infty$.

We can now apply standard tools from statistical mechanics to extract some information from the joint distribution (2.2). Let us first see how we can obtain the typical distribution of eigenvalues for large N (which maximises (2.2)), and then apply this formalism to get the distribution of other observables, known as linear statistics.

2.1 Typical density of eigenvalues

Let us look for the typical distribution of eigenvalues. For large N, the Gibbs weight (2.2) is dominated by the configuration of charges $\{\lambda_n^{(0)}\}$ which minimises the energy (2.3). We can find this configuration by taking the derivative of this energy with respect to each λ_i:

$$\left.\frac{\partial E}{\partial\lambda_i}\right|_{\{\lambda_n^{(0)}\}} = 0 \quad\Rightarrow\quad -\frac{2}{N}\sum_{\substack{j=1\\ j\neq i}}^{N}\frac{1}{\lambda_i^{(0)}-\lambda_j^{(0)}} + V'(\lambda_i^{(0)}) = 0\,, \tag{2.7}$$

[2]Note that it is the 2D Coulomb interaction for a 1D gas. To avoid confusion, the term log-gas is sometimes used in the literature.

where V' denotes the derivative of the potential. This equation can thus be interpreted as a force balance for the charge at position $\lambda_i^{(0)}$: the external force that derives from the potential must balance the sum of the repulsion of all the other charges. To solve this equation in the limit $N \to \infty$, we switch to a continuous description. Introduce the *empirical density* of charges

$$\rho_0(x) = \frac{1}{N} \sum_{i=1}^{N} \delta\left(x - \lambda_i^{(0)}\right) . \tag{2.8}$$

In the large N limit, we can replace the density (2.8) by a continuous one. Equation (2.7) can thus be rewritten as

$$2 \fint \frac{\rho_0(y)}{x-y} \mathrm{d}y = V'(x) , \tag{2.9}$$

where we denoted $\fint$ the Cauchy principal value. This equation holds for all x in the support of the density ρ_0. Our aim is thus to invert this integral equation to obtain the typical (or optimal) density of charges. The inversion process depends on the support of this density. If the density was supported on the whole real line, Eq. (2.9) would correspond to a Hilbert transform, which can be easily inverted [291]. However, this is not the case. The easiest way to prove it is to look at the behaviour for $x \to \infty$ of Eq. (2.9). If ρ_0 was supported on $\mathbb{R}$, we would obtain:

$$\fint \frac{\rho_0(y)}{x-y} \mathrm{d}y \simeq \frac{1}{x} , \quad \text{for} \quad x \to \infty , \tag{2.10}$$

where we used that the density is normalised $\int \rho_0 = 1$. Since the potential V must be confining to ensure the normalisability of the joint distribution (2.1), the force balance (2.9) cannot be satisfied if ρ_0 is supported on $\mathbb{R}$. Therefore, the support of ρ_0 is bounded. Let us suppose that this support is a compact interval $[a, b]$ with $a < b$. In this case, Eq. (2.9) can be inverted using a formula due to Tricomi [296] (see Appendix A.5). We obtain

$$\rho_0(x) = \frac{1}{\pi \sqrt{(x-a)(b-x)}} \left\{ 1 + \fint_a^b \frac{\mathrm{d}t}{\pi} \frac{\sqrt{(t-a)(b-t)}}{t-x} \frac{V'(t)}{2} \right\} . \tag{2.11}$$

This expression can then be evaluated for specific choices of potential V to give an explicit form for the density. This formula holds only if the optimal density has a compact support $[a, b]$. We can expect this to be true if the potential V has a single minimum: in this case, the charges will accumulate at the bottom of the well and spread due to the repulsion. If the potential V has several local minima, we can have more complex densities. This will be discussed in Chapters 3 and 4.

To illustrate this discussion, let us follow explicitly the procedure described above in the case of the Gaussian and Laguerre ensembles.

2.1.1 Wigner semicircle distribution

We consider the three Gaussian ensembles introduced in Section 1.2. We can rewrite the joint distribution of the eigenvalues (1.23) in the form

$$\mathcal{P}(\lambda_1, \dots, \lambda_N) \propto \prod_{i<j} |\lambda_i - \lambda_j|^\beta \prod_{i=1}^{N} \mathrm{e}^{-\frac{\beta N}{2} \lambda_i^2} , \tag{2.12}$$

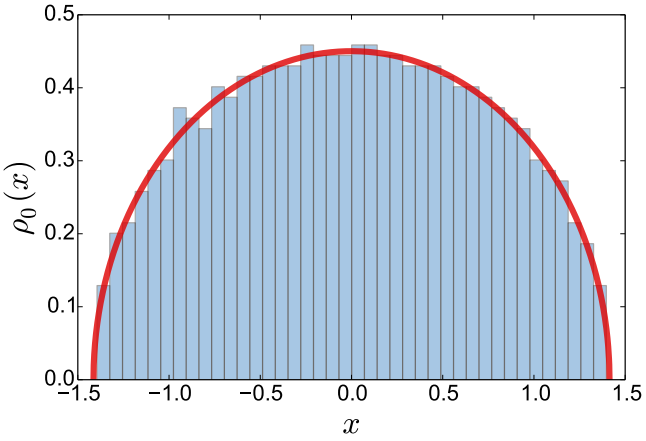

Figure 2.2: Typical density of eigenvalues for Gaussian matrices (GOE, GUE and GSE), i.e. Wigner's semicircle law (2.17) compared to an histogram obtained by diagonalising one GUE matrix of size $N = 1000$.

where we introduced a factor N in the exponential such that this distribution coincides with (2.1), with a harmonic confinement $V(x) = x^2$. This potential having a single minimum, we expect the density ρ_0 to be supported on an interval $[a, b]$ to be determined. Equation (2.11) becomes:

$$\rho_0(x) = \frac{1}{\pi\sqrt{(x-a)(b-x)}} \left\{ 1 + \fint_a^b \frac{\mathrm{d}t}{\pi} \frac{\sqrt{(t-a)(b-t)}}{t-x}\, t \right\} . \tag{2.13}$$

The principal value integral is given in Appendix C, by relation (C.11). We obtain

$$\rho_0(x) = \frac{1}{\pi\sqrt{(x-a)(b-x)}} \left\{ 1 + \frac{(b-a)^2}{8} + \frac{a+b}{2}\, x - x^2 \right\} . \tag{2.14}$$

There only remains to determine the boundaries a and b. Using the symmetry of the problem under the reflection $x \to -x$, we deduce that

$$a = -b\,. \tag{2.15}$$

We thus only need to find the value of b. This can be done using the continuity of ρ_0. Since the density vanishes outside the interval $[a, b]$, we impose that $\rho_0(a) = \rho_0(b) = 0$ in Eq. (2.14). This reduces to imposing that the expression inside the brackets vanishes at these points which yields:

$$b = -a = \sqrt{2}\,. \tag{2.16}$$

Using this result in Eq. (2.14) we obtain the density

$$\boxed{\rho_0(x) = \frac{1}{\pi}\sqrt{2-x^2}} \tag{2.17}$$

This is the celebrated Wigner semicircle law for the distribution of eigenvalues of Gaussian matrices [1, 135, 224]. Wigner first obtained this result by studying the moments of this distribution in the large N limit [306, 310]. Here, we have easily recovered this result by using the Coulomb gas method. Note that the density ρ_0 is the same for all values of β, due to the fact that we have chosen to multiply the potential V by $\beta/2$ in (2.1). It is represented in Fig. 2.2, along with numerical simulations.

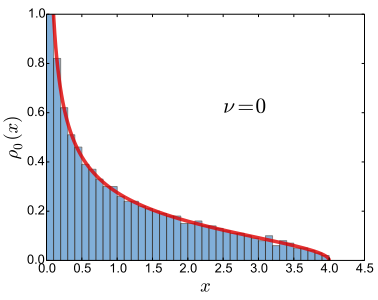

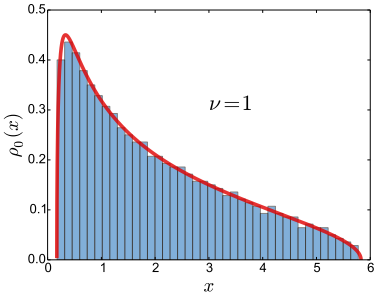

Figure 2.3: Typical density of eigenvalues for Wishard matrices (Laguerre ensembles), i.e. the Marčenko-Pastur distribution. Left: $\nu = 0$, Eq. (2.22). Right: $\nu = 1$, Eq. (2.24). The histograms are obtained by diagonalising matrices of size $N = 1000$.

2.1.2 Marčenko-Pastur distribution

We now consider the Laguerre ensembles described in Section 1.3. We rewrite the joint distribution of eigenvalues (1.38) as

$$\mathcal{P}(\lambda_1, \dots, \lambda_N) \propto \prod_{i<j} |\lambda_i - \lambda_j|^\beta \prod_{i=1}^N \lambda_i^{\frac{\beta N}{2}\nu+\mu-1+\frac{\beta}{2}} \, \mathrm{e}^{-\frac{\beta N}{2}\lambda_i} \,, \quad \lambda_i > 0 \,, \tag{2.18}$$

where we rewrote the parameter α of Eq. (1.38) as

$$\alpha = \frac{\beta N}{2}(\nu + 1) + \mu \,, \quad \nu \geqslant 0 \,, \tag{2.19}$$

in order to isolate its N dependence (the condition $\nu \geqslant 0$ ensures normalisability at leading order in N). In terms of Wishart matrices, this corresponds to the distribution of eigenvalues of matrices $Y = X^\dagger X$, where X is of size $M \times N$ with $M \simeq (\nu+1)N$ for $N \to \infty$, and $X_{ij} \sim \mathcal{N}(0, 1/\beta)$. As in the Gaussian case, we introduced a factor N in the exponential to identify (2.18) with Eq. (2.1), with the potential

$$V(x) = x - \nu \ln x \,, \qquad x > 0 \text{ and } \nu \geqslant 0 \,, \tag{2.20}$$

where we dropped the subleading $\mathcal{O}(N^{-1})$ corrections which are irrelevant at leading order. The domain $x < 0$ is excluded since the eigenvalues are positive. In terms of the Coulomb gas, this condition reduces to confine the gas on the positive axes with a wall at the origin. We can compute the typical density ρ_0 from Eq. (2.11), by using the integrals (C.10) and (C.14). We obtain:

$$\rho_0(x) = \frac{1}{\pi\sqrt{(x-a)(b-x)}} \left\{ 1 + \frac{a+b}{4} - \frac{x}{2} - \frac{\nu}{2}\left(-1 + \frac{\sqrt{ab}}{x} \right) \right\} . \tag{2.21}$$

We now need to distinguish two cases:

- If $\nu = 0$, the potential (2.20) is not repulsive at the origin, thus the charges tend to accumulate there. Therefore, there is no reason to impose $\rho_0(a) = 0$. Instead, we impose $a = 0$. Then, the condition $\rho_0(b) = 0$ yields $b = 4$, such that the density takes the form

$$\boxed{\rho_0(x) = \frac{1}{2\pi}\sqrt{\frac{4-x}{x}}} \tag{2.22}$$

- If $\nu > 0$, the potential (2.20) is repulsive at the origin, so we expect $0 < a < b$. Imposing $\rho_0(a) = \rho_0(b) = 0$, we deduce

$$a = 2 + \nu - 2\sqrt{1+\nu}\,, \quad b = 2 + \nu + 2\sqrt{1+\nu}\,. \tag{2.23}$$

  The typical density then takes the form

$$\boxed{\rho_0(x) = \frac{1}{2\pi x}\sqrt{(x-a)(b-x)}} \tag{2.24}$$

  Note that we can recover (2.22) by taking the limit $\nu \to 0$.

The densities (2.22) and (2.24) have first been derived by Marčenko and Pastur [221]. They are represented in Fig. 2.3 for $\nu = 0$ and $\nu = 1$

2.2 Distribution of linear statistics of eigenvalues

We have seen that the Coulomb gas method is very powerful to obtain the typical density of eigenvalues of a random matrix, in the limit of large matrices $N \to \infty$. We will now apply this method to study other kind of observables, known as *linear statistics*. These are quantities of the form

$$\mathcal{L} = \sum_{n=1}^{N} f(\lambda_n)\,, \tag{2.25}$$

where f can be any given function, not necessarily linear.

Many quantities take the form of linear statistics, such as the number of eigenvalues in a given domain [210, 211, 214, 217–219]. In the context of quantum transport, the conductance and shot noise of a quantum dot can also be expressed as linear statistics [30, 191, 278, 301, 302], as well as the Wigner time delay [164, 284, 286]. Other examples include the mutual information in MIMO channels [186, 187] or the Renyi entropy as a measure of quantum entanglement [99, 125, 250, 251].

2.2.1 From the typical fluctuations to the large deviations

Different methods have been introduced to study observables of the form (2.25). The typical fluctuations can be studied using orthogonal polynomials [224] or Selberg's integral [191, 224, 273, 278]. In particular, a formula[3] for the variance of $\mathcal{L}$ has first been obtained by Dyson and Mehta [117] in the Gaussian ensembles:

$$\mathrm{Var}(\mathcal{L}) \simeq \frac{1}{\beta\pi^2}\int_0^\infty \left|\hat{f}(k)\right|^2 k\,\mathrm{d}k\,, \qquad \hat{f}(k) = \int_{-\infty}^{\infty} \mathrm{e}^{\mathrm{i}kx}\, f(x)\,\mathrm{d}x\,. \tag{2.26}$$

This general formula exhibits a universal scaling in $1/\beta$. Another formula has been derived by Beenakker [28, 29] in the Laguerre ensembles (2.18) (with $\nu = 0$), for applications in coherent quantum transport:

$$\mathrm{Var}(\mathcal{L}) \simeq \frac{1}{\beta\pi^2}\int_0^\infty |F(k)|^2\, k\, \tanh(\pi k)\,\mathrm{d}k\,, \qquad F(k) = \int_{-\infty}^{\infty} \mathrm{e}^{\mathrm{i}kx}\, f(\mathrm{e}^x)\,\mathrm{d}x\,. \tag{2.27}$$

[3] The formula (2.26) was obtained for distributions of the form (2.1), without the factor N in front of the potential V, as in Eq. (1.47). The two are related by a rescaling of the eigenvalues with N, which translates in a rescaling of the linear statistics $\mathcal{L}$.

Several other formulae can be found in the literature, see for instance Refs. [26,33,181].

The question of *atypical fluctuations*, associated to rare events, has been addressed more recently [101,300]. It fits into the framework of large deviations theory, which has been an intense field of study both in Mathematics and Physics. For a review on large deviations, see [293]. In this perspective, the Coulomb gas method has proved to be a very powerful tool to analyse the full distribution (typical and atypical fluctuations) of a linear statistics in the limit $N \to \infty$ [135]. We now show how the Coulomb gas method can be applied for this purpose.

Let us first rescale the linear statistics to manipulate quantities of order $\mathcal{O}(N^0)$. Since the eigenvalues $\{\lambda_n\}$ are $\mathcal{O}(N^0)$, the linear statistics (2.25) is $\mathcal{O}(N)$. Therefore, we introduce the rescaled linear statistics

$$s = \frac{1}{N}\,\mathcal{L} = \frac{1}{N}\sum_{n=1}^{N} f(\lambda_n)\,. \tag{2.28}$$

We can formally write the distribution of s in terms of the joint distribution of the eigenvalues (2.1) as:

$$P_N(s) = \int \mathrm{d}\lambda_1 \cdots \mathrm{d}\lambda_N\, \mathcal{P}(\lambda_1,\ldots,\lambda_N)\, \delta\left(s - \frac{1}{N}\sum_{n=1}^{N} f(\lambda_n)\right)\,, \tag{2.29}$$

which we can rewrite in terms of the energy (2.3):

$$P_N(s) = \frac{\displaystyle\int \mathrm{d}\lambda_1 \cdots \mathrm{d}\lambda_N\, \mathrm{e}^{-\frac{\beta N^2}{2}E(\lambda_1,\ldots,\lambda_N)}\, \delta\left(s - \frac{1}{N}\sum_{n=1}^{N} f(\lambda_n)\right)}{\displaystyle\int \mathrm{d}\lambda_1 \cdots \mathrm{d}\lambda_N\, \mathrm{e}^{-\frac{\beta N^2}{2}E(\lambda_1,\ldots,\lambda_N)}}\,. \tag{2.30}$$

We will now show how to use the Coulomb gas method to analyse this distribution. First, we study the cumulant generating function in Section 2.2.2. Then, we study the distribution $P_N(s)$ in Section 2.2.3. An example is given in Section 2.2.4. Finally, we slightly reformulate the method in Section 2.2.5 to introduce the procedure and the notations we will use in Chapters 3 and 4.

2.2.2 Characteristic function and cumulants

Let us first study the cumulants of the distribution $P_N(s)$ by introducing the moment generating function

$$G_N(\mu) = \left\langle \mathrm{e}^{-\frac{\beta N^2}{2}\mu s} \right\rangle = \int P_N(s)\, \mathrm{e}^{-\frac{\beta N^2}{2}\mu s}\, \mathrm{d}s\,. \tag{2.31}$$

From the distribution (2.30), we obtain

$$G_N(\mu) = \frac{\displaystyle\int \mathrm{d}\lambda_1 \cdots \mathrm{d}\lambda_N\, \exp\left[-\frac{\beta N^2}{2}\left(E(\lambda_1,\ldots,\lambda_N) + \frac{\mu}{N}\sum_{n=1}^{N} f(\lambda_n)\right)\right]}{\displaystyle\int \mathrm{d}\lambda_1 \cdots \mathrm{d}\lambda_N\, \exp\left[-\frac{\beta N^2}{2}E(\lambda_1,\ldots,\lambda_N)\right]}\,. \tag{2.32}$$

Since the energy is of order $\mathcal{O}(N^0)$, we can estimate these integrals for $N \to \infty$ by a saddle point method. The denominator is dominated by the configuration of eigenvalues (or *charges*) that minimises the energy (2.3). This is the optimal configuration $\{\lambda_n^{(0)}\}$, which verifies (2.7). However, the numerator is dominated by the configuration $\{\tilde{\lambda}_n(\mu)\}$, which minimises

$$F(\lambda_1, \dots, \lambda_N; \mu) = E(\lambda_1, \dots, \lambda_N) + \frac{\mu}{N} \sum_{n=1}^{N} f(\lambda_n) \,. \tag{2.33}$$

Taking a derivative with respect to λ_i gives

$$\left.\frac{\partial F}{\partial \lambda_i}\right|_{\{\tilde{\lambda}_n\}} = 0 \quad \Rightarrow \quad -\frac{2}{N} \sum_{\substack{j=1 \\ j \neq i}}^{N} \frac{1}{\tilde{\lambda}_i - \tilde{\lambda}_j} + V'(\tilde{\lambda}_i) + \mu f'(\tilde{\lambda}_i) = 0 \,. \tag{2.34}$$

This equation can, like (2.7), be interpreted as a force balance on the particle located at $\tilde{\lambda}_i$, but with an additional force $\mu f'$. Therefore, we reduced the problem of computing the moment generating function of a linear statistics to studying the effect of an external force on the Coulomb gas. Let us suppose we are able to solve (2.34) for this optimal configuration $\{\tilde{\lambda}_n(\mu)\}$ (we will describe a procedure to do so in a second step). The saddle point estimate of (2.32) gives

$$G_N(\mu) \sim \exp\left[-\frac{\beta N^2}{2}\left(F(\{\tilde{\lambda}_n(\mu)\}; \mu) - E(\{\lambda_n^{(0)}\})\right)\right] \,, \tag{2.35}$$

where the symbol $\sim$ means logarithmic equivalence:

$$\lim_{N\to\infty} -\frac{2}{\beta N^2} \ln G_N(\mu) = F(\{\tilde{\lambda}_n(\mu)\}; \mu) - E(\{\lambda_n^{(0)}\}) \,. \tag{2.36}$$

There remains now to evaluate $F(\{\tilde{\lambda}_n(\mu)\}; \mu)$. Note that we can easily evaluate the second term (energy of the optimal configuration $\{\lambda_n^{(0)}\}$) simply by setting $\mu = 0$:

$$E(\{\lambda_n^{(0)}\}) = F(\{\tilde{\lambda}_n(\mu = 0)\}; \mu = 0) \,. \tag{2.37}$$

We will thus focus on evaluating $F(\{\tilde{\lambda}_n(\mu)\}; \mu)$. This is usually very difficult to do in practice, due to the complex form of the energy (2.3). However, the problem greatly simplifies if we compute the derivative with respect to μ:

$$\frac{\mathrm{d}}{\mathrm{d}\mu} F(\{\tilde{\lambda}_n(\mu)\}; \mu) = \sum_{i=1}^{n} \frac{\mathrm{d}\tilde{\lambda}_i}{\mathrm{d}\mu} \underbrace{\left.\frac{\partial F}{\partial \lambda_i}\right|_{\{\tilde{\lambda}_n(\mu)\}}}_{=0} + \left.\frac{\partial F}{\partial \mu}\right|_{\{\tilde{\lambda}_n(\mu)\}} = \frac{1}{N} \sum_{i=1}^{N} f(\tilde{\lambda}_i(\mu)) \,. \tag{2.38}$$

Therefore, knowing the optimal configuration $\{\tilde{\lambda}_n(\mu)\}$, we can easily compute the value of $F(\{\tilde{\lambda}_n(\mu)\}; \mu)$ by integration of (2.38) with respect to μ (the value for $\mu = 0$ is given by Eq. (2.37)).

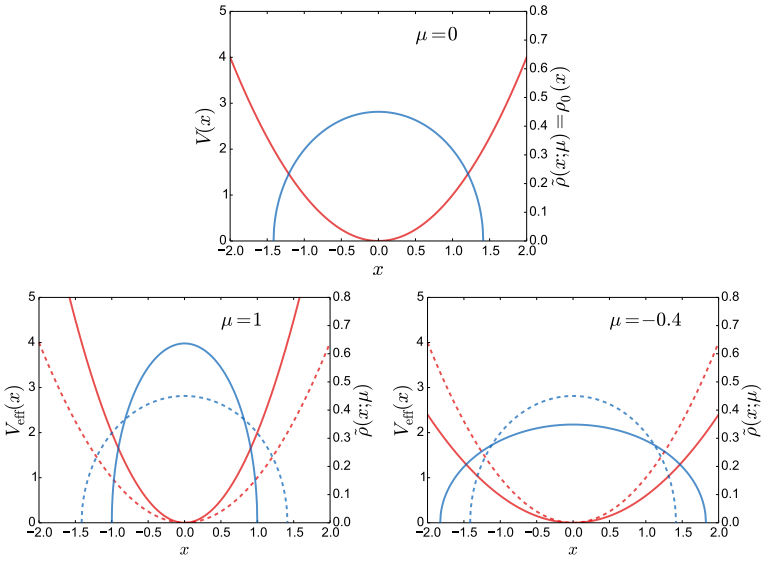

Figure 2.4: Effective potential $V_{\rm eff}(x) = V(x) + \mu f(x)$ (red) to which is subjected the Coulomb gas, along with the corresponding density of charges $\tilde{\rho}(x;\mu)$ (blue). Plots are for the Gaussian ensembles $V(x) = x^2$, with $f(x) = x^2$ (example of Section 2.2.4). Top: the unconstrained case $\mu = 0$. Bottom left: $\mu > 0$, corresponding to a stronger confinement. Bottom right: $\mu < 0$, i.e. weaker confinement (dashed lines are for $\mu = 0$).

Continuous description for the density of eigenvalues

We now come back to finding the solution of the saddle point equation (2.34). For large N, it is convenient to switch to a continuous description. Let us denote

$$\tilde{\rho}(x;\mu) = \frac{1}{N}\sum_{n=1}^{N} \delta\left(x - \tilde{\lambda}_n(\mu)\right) \tag{2.39}$$

the corresponding density of charges for a given value of μ. In the limit $N \to \infty$, Eq. (2.34) becomes

$$\boxed{2\fint \frac{\tilde{\rho}(y;\mu)}{x-y} = V'(x) + \mu f'(x)} \tag{2.40}$$

This equation shows that the density $\tilde{\rho}(x;\mu)$ is the optimal density for the Coulomb gas in the effective external potential

$$V_{\rm eff}(x) = V(x) + \mu f(x)\,. \tag{2.41}$$

Therefore, analysing the distribution of a linear statistics reduces to modifying the potential in which the Coulomb gas is placed. Changing the value of μ thus changes the potential and consequently deforms the density $\tilde{\rho}$ away from the typical one ρ_0, as illustrated in Fig. 2.4).

Equation (2.40) can again be solved explicitly, at least in the simplest cases, by making use of Tricomi's formula (A.42). Solving this equation allows to express the optimal density $\tilde{\rho}$ in terms of the parameter μ. We can now use this solution to rewrite (2.38) as

$$\frac{\mathrm{d}}{\mathrm{d}\mu} F(\{\tilde{\lambda}_n(\mu)\};\mu) \simeq \int \tilde{\rho}(x;\mu)\, f(x)\, \mathrm{d}x\,. \tag{2.42}$$

We can then obtain the expression of $F(\{\tilde{\lambda}_n(\mu)\};\mu)$ by integrating this expression. Therefore, the moment generating function takes the form

$$\boxed{G_N(\mu) \underset{N\to\infty}{\sim} \exp\left[-\frac{\beta N^2}{2}\Psi(\mu)\right] \text{ , with } \frac{\mathrm{d}\Psi}{\mathrm{d}\mu} = \int \tilde{\rho}(x;\mu)\, f(x)\, \mathrm{d}x \,, \quad \Psi(0) = 0} \tag{2.43}$$

This shows that the moment generating function takes a *large deviations* form, where Ψ is called *large deviation function*. We can easily deduce the cumulant generating function, defined as the logarithm of (2.31):

$$\ln G_N(\mu) = -\frac{\beta N^2}{2}\Psi(\mu) = \sum_{k=1}^{\infty} \frac{1}{k!}\left(-\frac{\beta N^2 \mu}{2}\right)^k \left\langle s^k \right\rangle_c \,, \tag{2.44}$$

where we denoted $\left\langle s^k \right\rangle_c$ the k^{th} cumulant of s. Therefore, we obtain directly the cumulants of the linear statistics from the derivatives of the large deviation function Ψ:

$$\left\langle s^k \right\rangle_c \simeq \left(-\frac{2}{\beta N^2}\right)^{k-1} \Psi^{(k)}(0) \,. \tag{2.45}$$

In particular, the variance has the scaling

$$\mathrm{Var}(s) \propto \frac{1}{\beta N^2} \,. \tag{2.46}$$

This specific scaling in $1/N^2$ is a signature of the strong correlations between the eigenvalues of random matrices. In the uncorrelated situation, the relative fluctuations of a sum of independent variables is known to scale as $1/N$ (central limit theorem). The presence of correlations thus strongly reduces the relative fluctuations.

The procedure to compute the cumulants is, in principle, straightforward: one should find the solution $\tilde{\rho}(x;\mu)$ of Eq. (2.40), then compute the large deviation function Ψ from Eq. (2.43) and then expand it as a power series in μ to identify the cumulants. Before carrying out this procedure explicitly on an example in Section 2.2.4, let us first study the full distribution $P_N(s)$.

2.2.3 Distribution of the linear statistics

We have obtained a compact expression for the moment generating function (2.31) in a large deviations form, see Eq. (2.43). This function is the Laplace transform of the distribution $P_N(s)$, see (2.31). We can thus write the distribution as the inverse Laplace transform

$$P_N(s) = \frac{\beta N^2}{2}\frac{1}{2\mathrm{i}\pi}\int_{c-\mathrm{i}\infty}^{c+\mathrm{i}\infty} G_N(\mu)\, \mathrm{e}^{\frac{\beta N^2}{2}s\mu}\mathrm{d}\mu \,, \tag{2.47}$$

where the integral runs over a vertical contour $\mathrm{Re}\,\mu = c$ of the complex plane, located at the right of all (possible) singularities of $G_N(\mu)$. Using the expression (2.43) for the moment generating function, and dropping the prefactors, we obtain

$$P_N(s) \underset{N\to\infty}{\sim} \frac{1}{2\mathrm{i}\pi}\int_{c-\mathrm{i}\infty}^{c+\mathrm{i}\infty} \exp\left[-\frac{\beta N^2}{2}\left(\Psi(\mu) - s\mu\right)\right]\mathrm{d}\mu \,. \tag{2.48}$$

This integral can be evaluated via a saddle point method. The saddle point is given by the value $\mu_\star(s)$, solution of

$$\left.\frac{\mathrm{d}\Psi}{\mathrm{d}\mu}\right|_{\mu_\star(s)} - s = 0 \quad \Rightarrow \quad \int \tilde{\rho}(x;\mu_\star(s))\, f(x)\, \mathrm{d}x = s\,. \tag{2.49}$$

Then, the distribution is given by

$$P_N(s) \underset{N\to\infty}{\sim} \exp\left[-\frac{\beta N^2}{2}\Phi(s)\right]\,, \tag{2.50}$$

where

$$\Phi(s) = \Psi(\mu_\star(s)) - s\mu_\star(s)\,. \tag{2.51}$$

The distribution of the linear statistics also takes a large deviations form, with a large deviation function Φ, which is simply deduced from Ψ by a Legendre transform[4]. The direct consequence is that

$$\frac{\mathrm{d}\Phi}{\mathrm{d}s} = \frac{\mathrm{d}\mu_\star}{\mathrm{d}s}\underbrace{\left.\frac{\mathrm{d}\Psi}{\mathrm{d}\mu}\right|_{\mu_\star(s)}}_{=s} - s\,\frac{\mathrm{d}\mu_\star}{\mathrm{d}s} - \mu_\star(s) = -\mu_\star(s)\,. \tag{2.52}$$

Therefore, we can compute the large deviation function $\Phi(s)$ by direct integration of $\mu_\star(s)$, obtained from Eq. (2.49). Let us denote s_0 such that $\mu_\star(s_0) = 0$. From Eq. (2.51), we have $\Phi(s_0) = 0$ since $\Psi(0) = 0$. Therefore, we can write the distribution as

$$\boxed{P_N(s) \underset{N\to\infty}{\sim} \exp\left[-\frac{\beta N^2}{2}\Phi(s)\right]\,, \quad \Phi(s) = -\int_{s_0}^{s} \mu_\star(s')\,\mathrm{d}s'} \tag{2.53}$$

The value s_0 has then a simple interpretation: since $\Phi(s_0) = \frac{\mathrm{d}\Phi}{\mathrm{d}s}(s_0) = 0$, it is the minimum of the large deviation function, thus the maximum of the distribution $P_N(s)$. s_0 is thus the typical value of the linear statistics (2.25).

The large deviations form (2.53) encodes information about the typical fluctuations around s_0, but also about the tails of the distribution which result from atypical fluctuations. The challenge is to obtain an analytical form for this large deviation function.

2.2.4 A first illustration: a simple solvable example

Having described the general procedure to obtain the distribution of a given linear statistics via the Coulomb gas method, let us illustrate it on an example. We consider the three Gaussian ensembles (GOE, GUE and GSE) introduced in Chapter 1, corresponding to the joint distribution of eigenvalues (2.1), with $V(x) = x^2$. We will consider the linear statistics

$$\mathcal{L} = \sum_{i=1}^{N} \lambda_i^2\,, \tag{2.54}$$

which corresponds to (2.25) for $f(x) = x^2$. We start with this specific example as it is exactly solvable for all N and will thus be a test of the Coulomb gas method. We first derive an exact expression for the distribution of $s = \mathcal{L}/N$, and then apply the Coulomb gas approach.

[4]This property is knwon as the Gärtner-Ellis theorem [120, 170] (see also the review [293]).

Exact distribution

The moment generating function (2.32) takes the form:

$$G_N^{\text{exact}}(\mu) = \frac{\displaystyle\int \mathrm{d}\lambda_1 \cdots \mathrm{d}\lambda_N \, \exp\left[-\frac{\beta N^2}{2}\left(-\frac{1}{N^2}\sum_{i\neq j}\ln|\lambda_i-\lambda_j| + \frac{1}{N}\sum_{i=1}^{N}\lambda_n^2 + \frac{\mu}{N}\sum_{n=1}^{N}\lambda_n^2\right)\right]}{\displaystyle\int \mathrm{d}\lambda_1 \cdots \mathrm{d}\lambda_N \, \exp\left[-\frac{\beta N^2}{2}\left(-\frac{1}{N^2}\sum_{i\neq j}\ln|\lambda_i-\lambda_j| + \frac{1}{N}\sum_{i=1}^{N}\lambda_n^2\right)\right]} . \tag{2.55}$$

Making the change of variables $x_i = \sqrt{1+\mu}\,\lambda_i$ in the numerator, we obtain:

$$G_N^{\text{exact}}(\mu) = \frac{1}{(1+\mu)^{N/2}} \exp\left[-\frac{\beta N^2}{2}\frac{N(N-1)}{N^2}\ln\sqrt{1+\mu}\right] \times \frac{\displaystyle\int \mathrm{d}x_1 \cdots \mathrm{d}x_N \, \exp\left[-\frac{\beta N^2}{2}\left(-\frac{1}{N^2}\sum_{i\neq j}\ln|x_i-x_j| + \frac{1}{N}\sum_{i=1}^{N}x_n^2\right)\right]}{\displaystyle\int \mathrm{d}\lambda_1 \cdots \mathrm{d}\lambda_N \, \exp\left[-\frac{\beta N^2}{2}\left(-\frac{1}{N^2}\sum_{i\neq j}\ln|\lambda_i-\lambda_j| + \frac{1}{N}\sum_{i=1}^{N}\lambda_n^2\right)\right]} . \tag{2.56}$$

The multiple integrals cancel out, and we obtain the exact moment generating function

$$G_N^{\text{exact}}(\mu) = (1+\mu)^{-\frac{N}{2}(1+\beta\frac{N-1}{2})} . \tag{2.57}$$

We can compute the inverse Laplace transform to deduce the exact distribution of $s = \mathcal{L}/N$:

$$P_N^{\text{exact}}(s) = \frac{1}{\Gamma(\frac{N}{2}+\beta N\frac{N-1}{4})}\left(\frac{\beta N^2}{2}\right)^{\frac{N}{2}(1+\beta\frac{N-1}{2})} s^{\frac{\beta N^2}{4}-\frac{N}{2}(\frac{\beta}{2}-1)-1}\,\mathrm{e}^{-\frac{\beta N^2}{2}s} , \tag{2.58}$$

which is a Gamma distribution. This result is valid for all values of N, but in the limit $N\to\infty$ we have

$$-\frac{2}{\beta N^2}\ln P_N^{\text{exact}}(s) = s - \frac{1}{2} - \frac{1}{2}\ln(2s) + \mathcal{O}\left(\frac{1}{N}\right) , \tag{2.59}$$

where we have used Stirling's formula [166]:

$$\ln\Gamma(z) = z\ln z - z + \frac{1}{2}\ln\frac{2\pi}{z} + \mathcal{O}(z^{-1}) . \tag{2.60}$$

The distribution $P_N^{\text{exact}}(s)$ is represented in Fig. 2.5 for different values of N. We will use the exact result (2.58,2.59) to check the validity of the Coulomb gas method.

Approximate distribution from the Coulomb gas

We now apply the procedure of section 2.2 to analyse the large N limit of the distribution of s via the Coulomb gas technique. We first need to solve the integral equation (2.40), for the density $\tilde{\rho}$, which becomes in this case:

$$⨍ \frac{\tilde{\rho}(y;\mu)}{x-y}\mathrm{d}y = (1+\mu)x . \tag{2.61}$$

This equation can be solved using Tricomi's theorem (A.42), assuming that the density $\tilde{\rho}$ has a compact support $[a, b]$. This gives:

$$\tilde{\rho}(y;\mu) = \frac{1}{\pi\sqrt{(x-a)(b-x)}}\left\{1 + (1+\mu)\fint_a^b \frac{\mathrm{d}t}{\pi}\frac{\sqrt{(t-a)(b-t)}}{t-x}\,t\right\} . \tag{2.62}$$

Using relation (C.11) to evaluate the integral, we deduce

$$\tilde{\rho}(y;\mu) = \frac{1}{\pi\sqrt{(x-a)(b-x)}}\left\{1 + (1+\mu)\left[\frac{(b-a)^2}{8} + \frac{a+b}{2}\,x - x^2\right]\right\} . \tag{2.63}$$

The values of a and b are then deduced by imposing that the density vanishes at these points, from which we deduce

$$b = -a = \sqrt{\frac{2}{1+\mu}} \tag{2.64}$$

and

$$\tilde{\rho}(y;\mu) = \frac{1+\mu}{\pi}\sqrt{b^2 - x^2} . \tag{2.65}$$

This optimal density is shown in Fig. 2.4 for different values of μ.

The moment generating function takes the form (2.43), with a large deviation function $\Psi(\mu)$ which can be computed from

$$\frac{\mathrm{d}\Psi}{\mathrm{d}\mu} = \int_a^b \tilde{\rho}(x;\mu)\,x^2\,\mathrm{d}x = \frac{1}{2(1+\mu)} , \quad \text{with } \Psi(0) = 0 . \tag{2.66}$$

Therefore, we obtain

$$\Psi(\mu) = \frac{1}{2}\ln(1+\mu) \quad \Rightarrow \quad G_N(\mu) \sim (1+\mu)^{-\frac{\beta N^2}{4}} , \tag{2.67}$$

which coincides with the large N behaviour of (2.57). From this expression, we can straightforwardly extract the cumulants of the distribution of s by using Eq. (2.45):

$$\left\langle s^k \right\rangle_c \simeq \left(\frac{2}{\beta N^2}\right)^{k-1} (k-1)! . \tag{2.68}$$

We can now obtain the form of the full distribution $P_N(s)$. First, we need to find the value $\mu_\star(s)$ by solving (2.49), which reads:

$$s = \int_a^b \tilde{\rho}(x;\mu_\star(s))\,x^2\,\mathrm{d}x = \frac{1}{2(1+\mu_\star(s))} \quad \Rightarrow \quad \mu_\star(s) = \frac{1}{2s} - 1 . \tag{2.69}$$

The typical value s_0 is the solution of the equation $\mu_\star(s_0) = 0$, which gives $s_0 = 1/2$. We then obtain the large deviation function controlling the large N behaviour of $P_N(s)$ from (2.52):

$$\Phi(s) = -\int_{s_0}^{s} \mu_\star(s')\mathrm{d}s' = s - \frac{1}{2} - \frac{1}{2}\ln(2s) . \tag{2.70}$$

This large deviation function obtained from the Coulomb gas method matches the asymptotic result (2.59) obtained from the exact computation of the distribution (2.58).

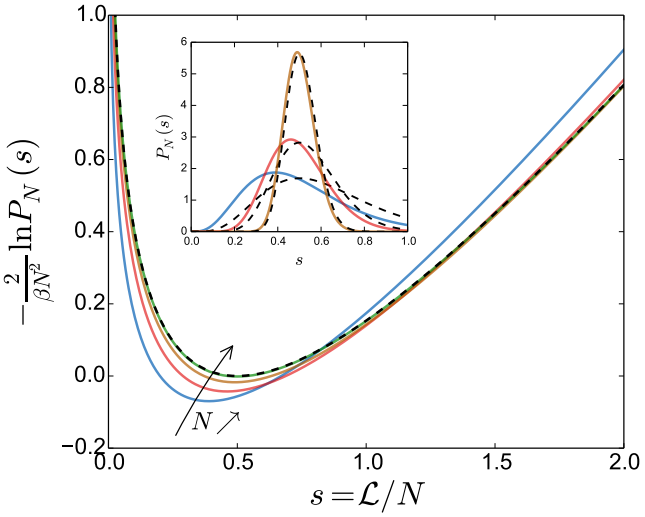

Figure 2.5: Large deviation function $\Phi(s)$ (dashed line), given by Eq. (2.70), compared to the exact result (2.58), for $\beta = 2$, and $N = 3$, 5, 10 and 50. The inset represents the distribution $P_N(s)$ itself. The dashed lines are the asymptotic form (2.53) for $N = 3$, 5 and 10 (normalised).

Comparison between this exact result and the large deviation function (2.70) is shown in Fig. 2.5. The exact form (2.58) rapidly reaches the asymptotic form (2.70): the two are in excellent agreement for $N = 10$ and the curves are indistinguishable in the plot range for $N = 50$. This shows that the behaviour obtained in the limit $N \to \infty$ describes very well the distribution of the linear statistics for values of N relatively small ($N \sim 10 - 50$).

This example validates the use of the Coulomb gas technique to obtain the asymptotic large deviations form of the distribution $P_N(s)$ for $N \to \infty$.

2.2.5 Reformulation in a continuous setting

In Sections 2.2.3 and 2.2.4 we have shown how the Coulomb gas method can be applied to obtain the distribution of a linear statistics in the limit $N \to \infty$. In this section we present a different derivation of Eq. (2.53), as it is often found in the literature (see for instance [88, 101, 102, 300, 301]).

Formulation in terms of functional integrals

Up to now, the continuous approximation was introduced in Section 2.2.2 in order to find the optimal distribution of eigenvalues, i.e. solve Eq. (2.38). We will show that it is possible to start from a fully continuous description by introducing a path integral formalism. Here, we sketch the main ideas of this approach. For a more detailed derivation see Ref. [102].

We again introduce the empirical density of eigenvalues is defined as

$$\rho(x) = \frac{1}{N}\sum_{n=1}^{N} \delta(x - \lambda_n)\,. \tag{2.71}$$

In the limit $N \to \infty$, this density can be replaced by a continuous one, which must satisfy the condition

$$\int \rho(x)\mathrm{d}x = 1\,. \tag{2.72}$$

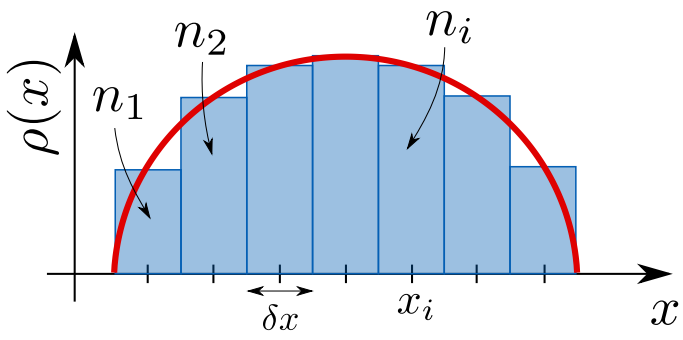

Figure 2.6: An histogram of the eigenvalues $\{\lambda_n\}$, consisting of bins of widths δx at positions x_i containing n_i eigenvalues. In the limit $\delta x \to 0$ it converges to the density $\rho(x)$.

The idea is thus to replace the integration measure over the eigenvalues $\{\lambda_n\}$ by a (functional) measure over the density ρ:

$$\mathcal{P}(\{\lambda_n\})\, \mathrm{d}\lambda_1 \cdots \mathrm{d}\lambda_N \longrightarrow \mathcal{D}\rho\, P[\rho]\, \delta\left(\int \rho(x)\mathrm{d}x - 1\right) , \tag{2.73}$$

where $P[\rho]$ is a functional of the density encoding the weight (2.2) of the configuration $\{\lambda_n\}$ described by ρ. However, this substitution must be done carefully. Indeed, when switching from a discrete description in terms of the eigenvalues $\{\lambda_n\}$ to a continuous one in terms of the density ρ, there is a loss of information which will be accounted for by adding an entropic contribution. This entropy comes from the fact that the permutations of the set $\{\lambda_i\}$ give rise to the same density $\rho(x)$. To estimate this entropy, we construct this density from an histogram of the set $\{\lambda_i\}$. We denote n_i the number of eigenvalues in an interval of size δx around the point x_i, as shown in Fig. 2.6. The number of ways to arrange the eigenvalues $\{\lambda_i\}$ (by permuting them) into the histogram is

$$\frac{N!}{\prod_i n_i!} . \tag{2.74}$$

Taking the logarithm and using Stirling's formula (2.60), we obtain:

$$\ln \frac{N!}{\prod_i n_i!} \simeq N \ln N - N - \sum_i n_i \ln n_i + \sum_i n_i = N \ln N - \sum_i n_i \ln n_i . \tag{2.75}$$

The bins $\{n_i\}$ and the density $\rho(x)$ are related by

$$\frac{n_i}{N} = \rho(x_i)\delta x , \tag{2.76}$$

therefore:

$$\ln \frac{N!}{\prod_i n_i!} \simeq -N \ln \delta x - N \sum_i \rho(x_i)\, \delta x \ln \rho(x_i) . \tag{2.77}$$

In the continuous limit $\delta x \to 0$ we can replace the sum by an integral. We obtain:

$$\frac{N!}{\prod_i n_i!} \simeq (\delta x)^{-N}\, \mathrm{e}^{N\mathscr{S}[\rho]} , \tag{2.78}$$

where we introduced the classical Shannon entropy

$$\boxed{\mathscr{S}[\rho] = -\int \rho(x) \ln \rho(x)\, \mathrm{d}x} \tag{2.79}$$

For simplicity, we can drop the constant factor δx by redefining the normalisation constant of distribution $P[\rho]$ which will multiply the measure. Therefore, when switching to a continuous description, the correct substitution is (at leading order in N):

$$\mathcal{P}(\{\lambda_n\})\,\mathrm{d}\lambda_1\cdots\mathrm{d}\lambda_N \longrightarrow \mathcal{D}\rho\,\mathrm{e}^{N\mathscr{S}[\rho]}\,P[\rho]\,\delta\left(\int\rho(x)\mathrm{d}x-1\right)\,. \tag{2.80}$$

Let us now discuss the probability measure $P[\rho]$, which is the continuous counterpart of Eq. (2.2). It can be obtained by taking the large N limit of the energy (2.3). The potential energy (second term) simply gives

$$\frac{1}{N}\sum_{i=1}^{N}V(\lambda_i)\underset{N\to\infty}{\longrightarrow}\int\rho(x)\,V(x)\,\mathrm{d}x\,. \tag{2.81}$$

However, as already stressed by Dyson [115], we must treat more carefully the self-interaction energy (first term of (2.3)) because of the diagonal terms:

$$-\frac{1}{N^2}\sum_{i\neq j}\ln|\lambda_i-\lambda_j|\simeq-\int\mathrm{d}x\,\rho(x)\left(\int^{x-\frac{\delta\lambda}{2}}+\int_{x+\frac{\delta\lambda}{2}}\right)\mathrm{d}y\,\rho(y)\,\ln|x-y|\,, \tag{2.82}$$

where we excluded from the double integral a region of size $\delta\lambda$, which is the typical gap between two eigenvalues near the point x. This gap can be estimated from the density (2.71) as

$$\delta\lambda\simeq\frac{1}{N\rho(x)}\,. \tag{2.83}$$

With this estimate, Eq. (2.82) becomes

$$-\frac{1}{N^2}\sum_{i\neq j}\ln|\lambda_i-\lambda_j|\simeq-\int\mathrm{d}x\int\mathrm{d}y\,\rho(x)\rho(y)\ln|x-y| -\frac{1}{N}\int\rho(x)\,[\ln(2N\rho(x))-1]\,\mathrm{d}x\,. \tag{2.84}$$

Using that the density is normalised, we get

$$\int\rho(x)\,[\ln(2N\rho(x))-1]\,\mathrm{d}x=\ln(2N)-1-\mathscr{S}[\rho]\,, \tag{2.85}$$

where $\mathscr{S}[\rho]$ is the entropy (2.79). Combining this expression with (2.84) and (2.81), we obtain that the energy (2.3) takes the form:

$$E(\{\lambda_n\})\simeq\mathscr{E}[\rho]+\frac{1}{N}\mathscr{S}[\rho]\,, \tag{2.86}$$

where we have introduced the energy functional

$$\boxed{\mathscr{E}[\rho]=-\int\mathrm{d}x\int\mathrm{d}y\,\rho(x)\rho(y)\ln|x-y|+\int\mathrm{d}x\,\rho(x)V(x)} \tag{2.87}$$

and again dropped the constant terms (included by redefining the normalisation). Combined with (2.80), we have shown that we can substitute the measures as

$$\mathcal{P}(\{\lambda_n\})\,\mathrm{d}\lambda_1\cdots\mathrm{d}\lambda_N \longrightarrow \mathcal{D}\rho\,\mathrm{e}^{-\frac{\beta N^2}{2}\mathscr{E}[\rho]+N\left(1-\frac{\beta}{2}\right)\mathscr{S}[\rho]}\,\delta\left(\int\rho(x)\mathrm{d}x-1\right)\,, \tag{2.88}$$

up to an overall constant for normalisation. For a more rigorous derivation of the relation above, see Ref. [102]. Interestingly, the entropic term vanishes in the unitary case $\beta = 2$.

We can now rewrite the distribution (2.30) of a linear statistics in terms of functional integrals:

$$P_N(s) \simeq \frac{\displaystyle\int \mathcal{D}\rho\, \mathrm{e}^{-\frac{\beta N^2}{2}\mathscr{E}[\rho]+N\left(1-\frac{\beta}{2}\right)\mathscr{S}[\rho]}\, \delta\left(\int \rho(x)\mathrm{d}x - 1\right)\, \delta\left(\int \rho(x) f(x)\mathrm{d}x - s\right)}{\displaystyle\int \mathcal{D}\rho\, \mathrm{e}^{-\frac{\beta N^2}{2}\mathscr{E}[\rho]+N\left(1-\frac{\beta}{2}\right)\mathscr{S}[\rho]}\, \delta\left(\int \rho(x)\mathrm{d}x - 1\right)}\,, \tag{2.89}$$

where the denominator ensures that the distribution is normalised.

Saddle point estimate

In many cases, we are only interested in the leading contributions, as in Sections 2.2.2–2.2.4. We will drop the entropic correction of order N and keep only the $\mathcal{O}(N^2)$ energy term[5]. We thus rewrite the distribution (2.30) as

$$P_N(s) \simeq \frac{\displaystyle\int \mathcal{D}\rho\, \mathrm{e}^{-\frac{\beta N^2}{2}\mathscr{E}[\rho]}\, \delta\left(\int \rho(x)\mathrm{d}x - 1\right)\, \delta\left(\int \rho(x) f(x)\mathrm{d}x - s\right)}{\displaystyle\int \mathcal{D}\rho\, \mathrm{e}^{-\frac{\beta N^2}{2}\mathscr{E}[\rho]}\, \delta\left(\int \rho(x)\mathrm{d}x - 1\right)}\,. \tag{2.90}$$

We can then estimate these functional integral by a saddle point method. Let us consider the numerator first. It is dominated by the density that minimises the energy $\mathscr{E}[\rho]$ under the constraints imposed by the Dirac delta-functions. These constraints can be handled by introducing Lagrange multipliers μ_0 and μ_1. We thus need to minimise

$$\mathscr{F}[\rho;\mu_0,\mu_1;s] = \mathscr{E}[\rho] + \mu_0\left(\int \rho(x)\mathrm{d}x - 1\right) + \mu_1\left(\int \rho(x) f(x)\mathrm{d}x - s\right)\,. \tag{2.91}$$

Taking the functional derivative with respect to ρ yields

$$\frac{\delta\mathscr{F}}{\delta\rho(x)} = 0 \quad \Rightarrow \quad -2\int \rho(y)\ln|x-y|\,\mathrm{d}y + V(x) + \mu_0 + \mu_1 f(x) = 0\,. \tag{2.92}$$

Taking the derivative with respect to x, we recover

$$2\fint \frac{\rho(y)}{x-y}\mathrm{d}y = V'(x) + \mu_1 f'(x)\,, \tag{2.93}$$

i.e. Eq. (2.40), as it should. We now understand the significance of the parameter μ introduced in Section 2.2.2: it coincides with the Lagrange multiplier μ_1 which enforces the constraint $\int \rho f = s$. Solving Eq. (2.93) yields the optimal density as a function of the Lagrange multiplier μ_1. Since it is the same density as in Section 2.2.2, we denote it $\tilde{\rho}(x;\mu_1)$. We can obtain it as a function of the parameter s by enforcing the constraint

$$\int \tilde{\rho}(x;\mu_1) f(x)\mathrm{d}x = s\,. \tag{2.94}$$

[5]Note that here we consider β fixed and let $N \to \infty$ (motivated by Dyson's threefold way, in which $\beta = 1$, 2 or 4). Instead if we let $\beta = \mathcal{O}(N^{-1})$ (using for example Dumitriu-Edelman matrices [113]), we can no longer neglect the entropic term, which then modifies the optimal density [8,9].

Solving this equation for μ_1 yields the Lagrange multiplier as a function of s. We denote $\mu_1^\star(s)$ this solution. We can thus express the density $\rho_\star(x;s)$ which dominates the numerator of (2.90) as

$$\rho_\star(x;s) = \tilde{\rho}(x;\mu_1^\star(s)) \,. \tag{2.95}$$

The optimal density for the denominator can be easily deduced by releasing the constraint, i.e. setting $\mu_1 = 0$. This corresponds to a value s_0, given by $\mu_1^\star(s_0) = 0$. The saddle point for the denominator is thus

$$\rho_0(x) = \rho_\star(x;s_0) = \tilde{\rho}(x;0) \,. \tag{2.96}$$

With these results, we obtain the saddle point estimate of (2.90):

$$P_N(s) \underset{N\to\infty}{\sim} \exp\left[-\frac{\beta N^2}{2}\left(\mathscr{E}[\rho_\star(x;s)] - \mathscr{E}[\rho_0]\right)\right] \,. \tag{2.97}$$

There remains to evaluate the energy of $\rho_\star(x;s)$, given by Eq. (2.87). This can be cumbersome to do in practice, but has been carried out explicitly in a few cases to obtain the distribution $P_N(s)$, see for instance [101, 102, 286, 300, 302]. In Ref. [163] (Article 2) we introduced a great simplification, along the lines of Section 2.2.3. Indeed, the density $\rho_\star$ satisfies all the constraints[6], thus:

$$\mathscr{E}[\rho_\star(x;s)] = \mathscr{F}[\rho_\star(x;s);\mu_0^\star(s),\mu_1^\star(s);s] \,. \tag{2.98}$$

Taking the derivative with respect to s yields:

$$\begin{aligned}\frac{\mathrm{d}}{\mathrm{d}s}\mathscr{E}[\rho_\star(x;s)] &= \int \frac{\partial\rho_\star(x;s)}{\partial s}\underbrace{\left.\frac{\delta\mathscr{F}}{\delta\rho(x)}\right|_{\rho_\star}}_{=0}\mathrm{d}x + \frac{\mathrm{d}\mu_0^\star}{\mathrm{d}s}\underbrace{\left.\frac{\partial\mathscr{F}}{\partial\mu_0}\right|_{\mu_0^\star}}_{=0} + \frac{\mathrm{d}\mu_1^\star}{\mathrm{d}s}\underbrace{\left.\frac{\partial\mathscr{F}}{\partial\mu_1}\right|_{\mu_1^\star}}_{=0} + \left.\frac{\partial\mathscr{F}}{\partial s}\right|_{\mu_1^\star} \\ &= -\mu_1^\star(s) \,.\end{aligned} \tag{2.99}$$

Therefore, we can introduce the large deviation function

$$\boxed{\Phi(s) = \mathscr{E}[\rho_\star(x;s)] - \mathscr{E}[\rho_0] = -\int_{s_0}^{s}\mu_1^\star(s')\mathrm{d}s'} \tag{2.100}$$

and then the distribution of s is given by (2.97). We have made extensive use of Eq. (2.100) in the analysis of different linear statistics [160, 161, 163, 164] (Article 1, Article 2, Article 3 and Article 4), as it greatly simplifies the analysis of the distribution: instead of computing the double integral (2.87), which can be quite cumbersome to do in practice, we only have one (simpler) integration to perform. This relation has also been discussed in Ref. [89].

An interesting feature of this approach is the possibility of phase transitions in the associated Coulomb gas. When changing the value of s, the density $\rho_\star(x;s)$ of the gas can undergo a change – splitting, condensation of one charge, ... – which we can interpret

[6] Imposing the constraint on the normalisation gives the first Lagrange multiplier μ_0 as a function of s. We denote it $\mu_0^\star(s)$.

as a phase transition. These transitions are associated to non-analyticity of the energy $\mathscr{E}$ (or equivalently of the large deviation functions Φ) as a function of s. Phase transitions of various order have been observed in many applications of the Coulomb gas method, for example in quantum transport [88, 163, 286, 301, 302], quantum entanglement [250, 251], models of interface [249], study of the largest eigenvalue [212], etc... For an overview of the different mechanisms, see the Table at the end of Article 3, which we reproduce here in Table 2.1.

Quantity	Ensemble	Order	Type	Reference
Wigner time delay $\sum_i \lambda_i^{-1}$	Laguerre	second	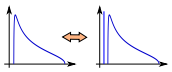	[286]
Renyi entropy $\sum_i \lambda_i^q$	Laguerre	second & third	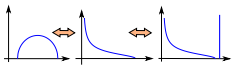	[250, 251]
Conductance $\sum_i \lambda_i$	Jacobi	third	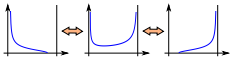	[301, 302]
Shot noise, $\sum_n \lambda_n(1-\lambda_n)$	Jacobi	third	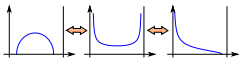	[302]
Moments, $\sum_n \lambda_n^k$	Jacobi	third	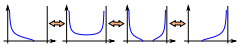	[302]
NS conductance, $\sum_n \lambda_n^2(2-\lambda_n)^{-2}$	Jacobi	third	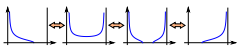	[94]
Largest eigenvalue λ_1	Gaussian, Laguerre	third	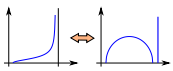	[102] [212, 213]
Index $\sum_n \Theta(\lambda_n)$	Gaussian, Laguerre Cauchy,...	⋆	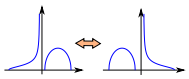	[210, 211] [217, 218]
Index (2D) $\sum_n \Theta(\lvert\lambda_n\rvert - r)$	Complex Ginibre	third		[10]
Mean radius (2D) $\sum_n \lvert\lambda_n\rvert$	Complex Ginibre	fourth		[90]
Center of mass of interf. $\sum_i \sqrt{\lambda_i}$	Laguerre	infinite ⋆⋆	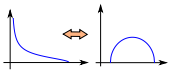	[249]
Truncated $\sum_i^K \sqrt{\lambda_i}$ $\sum_i^K \lambda_i$	Laguerre Jacobi	infinite ∞ & 3rd	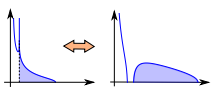	Ref. [161] (Article 3) Chapter 4

Table 2.1: List of different phase transitions observed in the Coulomb gas. The evolution of the density of the gas on each side of the transitions are represented ⋆: the energy has a logarithmic correction at the typical value. ⋆⋆: the density presents a logarithmic correction at the hard edge $\rho(x) \sim -\ln x/\sqrt{x}$ for $x \to 0$. Reproduced from Ref. [161] (Article 3).

2.2.6 A conjecture for subleading corrections

We have introduced the general features of the Coulomb gas method, applied to the study of linear statistics in the limit $N \to \infty$. Usually, the form (2.97) is sufficient to correctly describe the behaviour of the distribution $P_N(s)$. However if the choice of ensemble and of function f is such that the distribution has a power law tail which does not depend on N, it cannot be reproduced by the large deviations form (2.97). In this case, one should look for $1/N$ corrections, beyond the analysis of the large deviation function $\Phi(s)$.

The analysis of these corrections has been an intense field of research, see for instance Refs. [17, 47, 48, 81, 82, 121, 123, 124]. This problem has also been studied from the perspective of field theory, as the study of fields with a high number of components was proposed to model the strong coupling limit [53, 178]. The $1/N$ corrections can be analysed by loop equations [17, 233], which provide recursion between the contributions of different orders to the correlation function. A solution of these loops equation was later found by Eynard [123, 124] in terms of properties of algebraic curves. Usually, these methods provide a rigorous analysis of the $1/N$ corrections to the characteristic function (2.31).

Instead, we have proposed in Ref. [164] to investigate the distribution $P_N(s)$ itself and have formulated a conjecture for the form of this distribution. We briefly sketch here the ideas that led us to this conjecture.

Let us start from the expression (2.89). By expressing the Dirac delta functions as

$$\delta(X) = \frac{\beta N^2}{4\mathrm{i}\pi} \int_{-\mathrm{i}\infty}^{+\mathrm{i}\infty} \mathrm{d}\mu \, \mathrm{e}^{\frac{\beta N^2}{2}\mu X} , \tag{2.101}$$

we can introduce the two Lagrange multipliers μ_0 and μ_1 and rewrite (2.89) as

$$P_N(s) \simeq \frac{\beta N^2}{4\mathrm{i}\pi} \frac{\displaystyle\int_{-\mathrm{i}\infty}^{+\mathrm{i}\infty} \mathrm{d}\mu_0 \int_{-\mathrm{i}\infty}^{+\mathrm{i}\infty} \mathrm{d}\mu_1 \int \mathcal{D}\rho \, \mathrm{e}^{-\frac{\beta N^2}{2}\mathscr{F}[\rho;\mu_0,\mu_1]}}{\displaystyle\int_{-\mathrm{i}\infty}^{+\mathrm{i}\infty} \mathrm{d}\mu_0 \int \mathcal{D}\rho \, \mathrm{e}^{-\frac{\beta N^2}{2}\mathscr{F}[\rho;\mu_0,0]}} , \tag{2.102}$$

where $\mathscr{F}$ is given by

$$\mathscr{F}[\rho;\mu_0,\mu_1] = \mathscr{E}[\rho] + \mu_0 \left(\int \rho(x)\mathrm{d}x - 1 \right) + \mu_1 \left(\int \rho(x) f(x) \mathrm{d}x - s \right) + \frac{1}{N} \left(1 - \frac{2}{\beta} \right) \mathscr{S}[\rho] . \tag{2.103}$$

In the case $\beta = 2$, the entropic term vanishes and the functional $\mathscr{F}$ is quadratic in ρ. Therefore, the functional integrals over ρ in (2.102) are Gaussian. However, the integration is restricted to densities which remain positive $\rho(x) \geqslant 0$, due to the fact that it represents a density of eigenvalues. If we neglect this restriction[7], the functional

[7] This is reasonable if the density $\rho_\star$ of the saddle point never vanishes, as fluctuations around it are not sensitive to the constraint $\rho(x) \geqslant 0$. This is the case for example in the Jacobi ensembles, but not in the Gaussian or Laguerre ensembles.

integrals are Gaussian and the saddle point estimate of Section 2.2.5 is exact[8]. We thus obtain

$$P_N(s) \simeq \frac{N^2}{2\mathrm{i}\pi} \frac{\displaystyle\int_{-\mathrm{i}\infty}^{+\mathrm{i}\infty} \mathrm{d}\mu_0 \int_{-\mathrm{i}\infty}^{+\mathrm{i}\infty} \mathrm{d}\mu_1 \, \mathrm{e}^{-N^2 \mathscr{F}[\tilde{\rho}_\star(x;\mu_0,\mu_1);\mu_0,\mu_1]}}{\displaystyle\int_{-\mathrm{i}\infty}^{+\mathrm{i}\infty} \mathrm{d}\mu_0 \, \mathrm{e}^{-N^2 \mathscr{F}[\tilde{\rho}_\star(x;\mu_0,0);\mu_0,0]}} , \tag{2.104}$$

where we denoted $\tilde{\rho}_\star(x;\mu_0,\mu_1)$ the solution of (2.93) which is not necessarily normalised, as the normalisation condition comes from the integral over μ_0. We have thus reduced the problem from evaluating functional integrals to computing scalar integrals in the complex plane. In principle, a careful saddle point estimate of these integrals should yield the large deviation form (2.97), as well as the prefactor (from the Hessian of $\mathscr{F}[\tilde{\rho}_\star(x;\mu_0,\mu_1);\mu_0,\mu_1]$), which is a $1/N^2$ correction to the large deviation function (2.100). This procedure is however usually difficult to carry out in practice. Nevertheless, explicit computations in simple cases (such as the example of Section 2.2.4) suggest that the distribution (2.104) takes the form

$$P_N(s) \simeq c_{N,2} \sqrt{-\frac{N^2}{2\pi} \frac{\partial \mu_1^\star}{\partial s}} \, \mathrm{e}^{-N^2 \Phi(s)} , \tag{2.105}$$

where $c_{N,2}$ is a constant, Φ is the large deviation function (2.100) and $\mu_1^\star$ the value of the Lagrange multiplier obtained from the saddle point equation (2.94). This is our conjecture for the form of the distribution for $\beta = 2$, which we can extend to general β as

$$P_N(s) \simeq c_{N,\beta} \sqrt{-\frac{\beta N^2}{4\pi} \frac{\partial \mu_1^\star}{\partial s}} \, \exp\left[-\frac{\beta N^2}{2} \Phi(s) + N \left(1 - \frac{\beta}{2}\right) \mathscr{S}[\rho_\star(x;s)] \right] . \tag{2.106}$$

This form allows an easy computation of the distribution from simple properties of the Coulomb gas (the Lagrange multiplier $\mu_1^\star(s)$ and the density $\rho_\star$).

In Article 1 we give more details and we verify the conjecture (2.106) explicitly on several examples (listed in Table 2.2). In all these examples, our conjecture either gives the correct result for the whole distribution (if known), or properly reproduces the exponents controlling the power law tails, up to a constant prefactor.

Coming back to our original motivation, we have analysed in Article 1 the distribution of the Wigner time delay in disordered wires, which is a linear statistics with $f(\lambda) = 1/\lambda$ in the Laguerre ensembles. In this case we have obtained $\mu_1^\star(s) \propto 1/s^3$ for $s \to \infty$, corresponding to $\Phi(s) \to 0$ in this limit. The large deviation function Φ cannot characterise the decay of the probability at infinity. The determination of the prefactor with (2.106) is thus crucial, as it gives $P_N(s) \sim 1/s^2$ for $s \to \infty$.

In all the cases mentioned in Table 2.2, the optimal density $\rho_\star$ which dominates the integrals (2.102) is supported on a single interval $[a,b]$. We have not tested the conjecture (2.106) in a situation where the density is supported on several intervals.

Finally, the most promising way to prove this conjecture seems to make a connection with the loop equations method [47,123,124]. This approach could also clarify the range of applications of Eq. (2.106) to obtain the distribution of linear statistics.

[8] The second derivative $\frac{\delta^2 \mathscr{F}}{\delta\rho(x)\delta\rho(y)} = -2\ln|x-y|$ does not depend on ρ, so the Hessian cancels out between the numerator and the denominator.

Ensemble	$V(x)$	Linear statistics	$f(x)$	References
Laguerre	$x - \nu \ln x$, $\nu \leqslant 0$	trace	x	[164] (Article 1)
Laguerre	$x - \ln x$	Wigner time delay (cavity)	$1/x$	[286]
Laguerre	x	Wigner time delay (wire)	$1/x$	[164] (Article 1)
Jacobi	$0 \leqslant x \leqslant 1$	Conductance	x	[301]

Table 2.2: A few cases on which the conjecture (2.106) has been explicitly tested. These examples are discussed in the conclusion of [164] (Article 1).

Article 1

Distribution of spectral linear statistics on random matrices beyond the large deviation function – Wigner time delay in multichannel disordered wires

A. Grabsch and C. Texier, Distribution of spectral linear statistics on random matrices beyond the large deviation function – Wigner time delay in multichannel disordered wires, J. Phys. A **49**, 465002 (2016).

☞ http://dx.doi.org/10.1088/1751-8113/49/46/465002

Chapter 3

Joint distribution of two linear statistics

In Chapter 2 we have introduced the general method to obtain the distribution of a linear statistics using the Coulomb gas technique. In this Chapter, we describe an application of random matrices to quantum transport which requires the determination of the joint distribution of two linear statistics. Some of the main results have been published in the Letter [163], which is included at the end of this Chapter (Article 2). Here we also present some extensions obtained more recently.

We start in Section 3.1 by giving some generalities about coherent quantum transport and quantum scattering in quantum dots. In Section 3.2 we show that the analysis of the physical properties of a quantum RC-circuit can be reduced to the study the joint distribution of two linear statistics. In Sections 3.3 and 3.4 we analyse this joint distribution using the Coulomb gas method. These results are used in Section 3.5 to study the resistance of the quantum RC-circuit.

3.1 Quantum scattering

3.1.1 Coherent electronic transport

Since the 80s, it has been possible to realise micrometric condensed matter devices in which the electronic phase coherence length becomes larger than the system size at low temperature ($\sim$ 1K). This regime, which is intermediate between the atomic and the macroscopic regimes, and in which quantum coherence plays a crucial role at low temperature, is called the "mesoscopic regime".

A convenient approach to quantum transport is the Landauer-Büttiker formalism, which allows to relate measurable properties (conductance, shot noise, ...) to scattering properties of a single electron. This approach has later been extended to AC transport (admittance, ...) by Büttiker and collaborators. Let us recall a few simple ideas.

The response of mesoscopic devices under stationary (DC) external drive has been extensively studied. In such situations, the mesoscopic system is connected to macroscopic conductors, through which current is injected and collected (Fig. 3.1). At a given energy ε each external lead α allows the propagation of N_α scattering states (like a

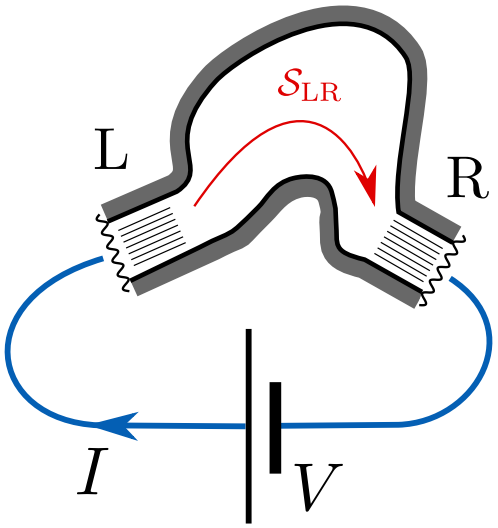

Figure 3.1: A mesoscopic device connected to two perfect leads (L and R), through which is applied a voltage. The subblock of the scattering matrix $\mathcal{S}$ describing transport from contact L to contact R is denoted $\mathcal{S}_{\mathrm{LR}}$.

wave-guide). The contacts between the leads and the cavity are assumed to be perfect. The mesoscopic conductor can thus be described by a scattering matrix $\mathcal{S}(\varepsilon)$ which relates the in-going to out-goint amplitudes of these scattering states. In the case of two contacts (see Fig. 3.1), the DC conductance G_{DC} at zero temperature is given in terms of the scattering matrix $\mathcal{S}$ by the well-known Landauer formula [132]:

$$\langle I \rangle = G_{\mathrm{DC}} V \,, \qquad G_{\mathrm{DC}} = \frac{e^2}{h} \operatorname{tr}(\mathcal{S}_{\mathrm{LR}}^{\dagger} \mathcal{S}_{\mathrm{LR}}) \,, \tag{3.1}$$

where $\mathcal{S}_{\mathrm{LR}}$ is the subblock of the $\mathcal{S}$-matrix which describes scattering from the left to the right lead (at Fermi energy). Taking into account spin degeneracy, this relation becomes $G_{\mathrm{DC}} = (2e^2/h) \operatorname{tr}(\mathcal{S}_{\mathrm{LR}}^{\dagger} \mathcal{S}_{\mathrm{LR}})$. The formula (3.1) can be extended to the multiterminal case, and to finite temperature [71]. In this stationary (DC) setting, the scattering matrix $\mathcal{S}$, which characterises the solution of the Schrödinger equation for one electron in the structure, controls entirely the conductance G_{DC} of the mesoscopic device, i.e. a quantity measurable by simple means.

The DC response of micrometric systems characterises their resistive properties (conductance). It is also natural to probe their capacitive and inductive properties by studying the dynamic response under AC driving (at pulsation ω). These properties are encoded in the complex admittance $G(\omega)$ (or its impedance $Z(\omega) = 1/G(\omega)$). The simplest system we can consider is a quantum RC-circuit, represented in Fig. 3.2. It can be realised experimentally with a chaotic cavity (quantum dot) patterned in a two-dimensional electron gas. This cavity is closed by a quantum point contact which allows the propagation of N scattering modes. The scattering of a wave of energy ε in this cavity can be described by the $N \times N$ scattering matrix $\mathcal{S}(\varepsilon)$. The cavity is capacitively coupled to a metallic gate deposited on top of it or nearby.

A theory for the AC response of coherent conductors has been proposed by Büttiker, Prêtre and Thomas [73–75]. In the absence of interaction between the electrons, the admittance of the RC-circuit takes the form (without spin degeneracy)

$$G_0(\omega) = \frac{e^2}{h} \int \mathrm{d}\varepsilon \, \frac{f(\varepsilon) - f(\varepsilon + \hbar\omega)}{\hbar\omega} \left[N - \operatorname{tr}\left(\mathcal{S}^{\dagger}(\varepsilon) \mathcal{S}(\varepsilon + \hbar\omega) \right) \right] \,, \tag{3.2}$$

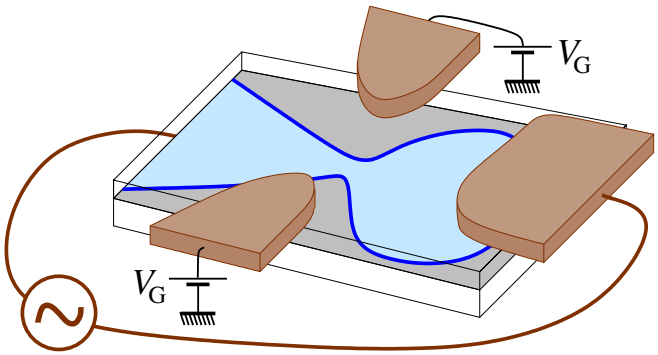

Figure 3.2: A quantum RC-circuit formed with a 2D electron gas and top gates (from Refs. [163, 286]).

where f is the Fermi-Dirac distribution. Here, the matallic gate plays no role. This formula has been generalised to the multiterminal situation in Ref. [72, 265]. At low frequency, expanding this expression in powers of ω, we obtain at zero temperature:

$$G_0(\omega) = \frac{e^2}{h}\left(-\mathrm{i}\omega\ \mathrm{tr}[\mathcal{Q}] + \frac{\omega^2}{2}\,\mathrm{tr}[\mathcal{Q}^2] + \mathcal{O}(\omega^3)\right)\,, \tag{3.3}$$

which is expressed in terms of the Wigner-Smith matrix

$$\boxed{\mathcal{Q} = -\mathrm{i}\hbar\,\mathcal{S}^\dagger \frac{\partial \mathcal{S}}{\partial \varepsilon}\bigg|_{\varepsilon_F}} \tag{3.4}$$

evaluated at the Fermi energy. Unlike the DC case where the transport properties are described by the scattering matrix $\mathcal{S}$ at Fermi energy, the AC response is encoded in the Wigner-Smith matrix $\mathcal{Q}$, another fundamental matrix characterising the energy dependence of the $\mathcal{S}$-matrix. This matrix encodes the temporal aspects of the scattering (see for instance the reviews [97, 284]).

Büttiker, Prêtre and Thomas have stressed the role of electronic interaction in nonlinear AC transport. Within a simple mean field (Hartree) treatment of these interactions, they showed that the admittance of the RC-circuit can be obtained by combining in series the admittance G_0, Eq. (3.2), and the geometric capacitance C_{geo} encoding the Coulomb interaction [74]:

$$\frac{1}{G(\omega)} = \frac{1}{G_0(\omega)} + \frac{1}{-\mathrm{i}\omega C_{\mathrm{geo}}}\,. \tag{3.5}$$

The geometric capacitance C_{geo} characterises the shape of the system, and can be deduced in principle from the Poisson equation. The admittance $G_0(\omega)$ encodes the mesoscopic effects. Combining (3.5) with the expansion (3.3), we obtain at zero temperature, a low frequency expansion of the form

$$Z(\omega) = \frac{1}{G(\omega)} = \frac{1}{-\mathrm{i}\omega C_\mu} + R_q + \mathcal{O}(\omega)\,. \tag{3.6}$$

Thus we have obtained the same form as the one given by the classical electrokinetics theory. However the two coefficients C_μ, the "mesoscopic capacitance", and R_q, the "charge relaxation resistance", now encode information on the quantum dynamics of charges in the device. The mesoscopic capacitance is given (at $T = 0$) by

$$\frac{1}{C_\mu} = \frac{1}{C_{\mathrm{geo}}} + \frac{1}{C_q}\,, \qquad \boxed{C_q = \frac{e^2}{h}\,\mathrm{tr}[\mathcal{Q}]} \tag{3.7}$$

The mesoscopic capacitance is thus obtained by combining two different capacitances in series: the geometric one $C_{\rm geo}$ (coming from the Coulomb energy $Q^2/2C_{\rm geo}$) and the quantum one C_q which comes from the Fermi energy $N\varepsilon_F \sim Q^2/C_q$ (it is an effect of the density of states, and thus is proportional to $\mathrm{tr}[\mathcal{Q}]$).

The second term of the expansion (3.6) is the charge relaxation resistance (at $T = 0$)

$$\boxed{R_q = \frac{h}{2e^2}\frac{\mathrm{tr}[\mathcal{Q}^2]}{\mathrm{tr}[\mathcal{Q}]^2}} \tag{3.8}$$

Equation (3.7) and (3.8) can be extended to finite temperature, by introducing convolutions with the Fermi function: the traces must be replaced by $\int \mathrm{d}\varepsilon(\partial f/\partial\varepsilon)\,\mathrm{tr}[\cdots]$ [74].

We stress that the factor 2 in the denominator of (3.8) does not arise from spin degeneracy. If we include this degeneracy, the charge relaxation resistance becomes

$$R_q = \frac{h}{2_s \times 2e^2}\frac{\mathrm{tr}[\mathcal{Q}^2]}{\mathrm{tr}[\mathcal{Q}]^2}\,. \tag{3.9}$$

In particular the result (3.8) leads to the surprising result that the one-channel contact ($N = 1$) is characterised by the universal value of *half* the quantum resistance $h/(2e^2)$ (named the "Büttiker resistance" [177]), instead of the value $R_{\rm DC} = h/e^2$ which we would obtain for the DC resistance of the contact (Eq. (3.1) for $\mathcal{S}_{\rm LR} \propto \mathbb{1}_N$). This prediction has been verified experimentally [150, 151].

The resistance R_q controls the charge relaxation in the quantum regime through the RC time

$$\tau_{\rm RC} = R_q C_\mu\,. \tag{3.10}$$

This resistance plays an important role in experiments involving charge injection, for example in quantum information ("flying qubit") [127, 128] and quantum optics experiments with electrons [42, 43].

We will now see how to analyse the quantum capacitance C_q and the charge relaxation resistance R_q within a random matrix approach.

3.1.2 The random matrix approach for chaotic quantum dots

In the formalism described above, we have expressed the physical properties of the mesoscopic system (conductance, capacitance, ...) in terms of the scattering matrix $\mathcal{S}(\varepsilon)$ and the Wigner-Smith matrix $\mathcal{Q}$, obtained from $\mathcal{S}$ by (3.4). We now describe how the statistical properties of these matrices can be obtained within a random matrix approach to describe the transport properties through a chaotic quantum dot.

Scattering matrix $\mathcal{S}(\varepsilon)$

If we assume that the dynamics inside the quantum dot is chaotic, the scattering matrix $\mathcal{S}(\varepsilon)$ can be taken as random [6, 30, 55, 64].

➢ Perfect contacts

If the quantum dot is connected to a macroscopic system via perfect contacts (as it was assumed in the previous section), it is natural to assume that the probabilities to

be scattered in any of the N channels are equal. Therefore, the scattering matrix at a given energy ε is uniformly distributed on the unitary group, with only the constraints imposed by symmetries [24, 180]. The different symmetry classes are labelled by the Dyson index β (see Section 1.1):

- Case $\beta = 2$: in the absence of time-reversal symmetry, there is no further restriction on $\mathcal{S}$, which can be any unitary matrix. This ensemble is called *Circular Unitary Ensemble* (CUE).
- Case $\beta = 1$: in the presence of both time-reversal and spin-rotation symmetry, the scattering matrix is symmetric:

$$\mathcal{S}^{\mathrm{T}} = \mathcal{S} \,. \tag{3.11}$$

  The set of unitary matrices satisfying this constraint is called the *Circular Orthogonal Ensemble* (COE).
- Case $\beta = 4$: if spin-rotation symmetry is broken, but time-reversal symmetry is preserved, $\mathcal{S}$ belongs to the *Circular Symplectic Ensemble* (CSE) which corresponds to the set of unitary matrices satisfying

$$\sigma_2 \mathcal{S}^{\mathrm{T}} \sigma_2 = \mathcal{S} \,, \tag{3.12}$$

  where σ_2 is the second Pauli matrix.

Under this assumption, one can study the distributions of quantities which depend on $\mathcal{S}$ at a given energy, such as the DC conductance (3.1), the shot noise [71], ...(see also [30] for a review).

➢ Non ideal contacts

If the quantum dot is connected through non ideal leads, the distribution of the $\mathcal{S}$-matrix can be obtained either from a maximal entropy principle (stochastic approach [30, 229, 230]) or by assuming that the Hamiltonian of the closed system is a random matrix (Hamiltonian approach [209, 298]). In the universal regime the two approaches yield the same result for the distribution of the scattering matrix [54], known as the *Poisson kernel*. It is parametrised only by the mean scattering matrix denoted $\bar{\mathcal{S}}$, as:

$$P(\mathcal{S}) \propto \left|\det(\mathbb{1}_N - \bar{\mathcal{S}}^{\star}\mathcal{S})\right|^{-2-\beta(N-1)} \,. \tag{3.13}$$

The circular ensembles are recovered by setting $\bar{\mathcal{S}} = 0$. This distribution has been successfully applied to the study of coherent transport properties, such as the conductance [30].

Wigner-Smith matrix $\mathcal{Q}(\varepsilon)$

➢ Perfect contacts

The AC response of the quantum dot is encoded in the Wigner-Smith matrix $\mathcal{Q}$, constructed from the derivative of the $\mathcal{S}$-matrix with respect to the energy ε, see Eq. (3.4). Therefore it is not enough to know the distribution of $\mathcal{S}$ at a given energy: we need

information on its energy-dependence, which is a more difficult task. Different theories for this ε-dependence have been proposed, see for instance Refs. [56–58, 146, 148, 159] (see also [140]).

In Refs. [57,58], Brouwer, Frahm and Beenakker have obtained the distribution of the Wigner-Smith matrix $\mathcal{Q}$ in the case of perfect contacts. They showed that $\mathcal{Q}^{-1}$ belongs to the Laguerre ensembles of random matrices[1] (see Section 1.3). More explicitly, denote τ_n the eigenvalues of $\mathcal{Q}$, which are called the *proper time delays*. Introducing the rates $\gamma_n = \tau_H/\tau_n$, where $\tau_H = h/\Delta$ is the Heisenberg time and Δ the mean level spacing, the joint distribution of the γ_i's is given by [57, 58]:

$$\mathcal{P}(\gamma_1, \ldots, \gamma_N) \propto \prod_{i<j} |\gamma_i - \gamma_j|^\beta \prod_{n=1}^{N} \gamma_n^{\beta N/2}\, \mathrm{e}^{-\beta\gamma_n/2}\,, \quad \gamma_n > 0\,, \tag{3.14}$$

where $\beta \in \{1, 2, 4\}$ is the Dyson index associated to the symmetry classes (see Section 1.1). The proper time delays $\{\tau_n = \tau_H/\gamma_n\}$ control the quantum capacitance (3.7),

$$C_q = \frac{e^2}{h} \sum_{i=1}^{N} \tau_i = \frac{e^2}{h} \tau_H \sum_{i=1}^{N} \frac{1}{\gamma_i} \tag{3.15}$$

and the charge relaxation resistance (3.8),

$$R_q = \frac{h}{2e^2} \frac{\sum_{i=1}^{N} \tau_i^2}{\left(\sum_{i=1}^{N} \tau_i\right)^2} = \frac{h}{2e^2} \frac{\sum_{i=1}^{N} 1/\gamma_i^2}{\left(\sum_{i=1}^{N} 1/\gamma_i\right)^2}\,. \tag{3.16}$$

Therefore, knowing the joint distribution (3.14) one should in principle be able to deduce the statistical properties of C_q and R_q. However, this is not an easy task due to the strong correlations between the time delays. For instance, C_q is related to another well-studied quantity: the Wigner time delay

$$\tau_W = \frac{h}{Ne^2} C_q = \frac{1}{N} \operatorname{tr}[\mathcal{Q}] = \frac{\tau_H}{N} \sum_{n=1}^{N} \frac{1}{\gamma_n}\,. \tag{3.17}$$

The distribution of τ_W was first obtained before the result (3.14) of Brouwer, Frahm and Beenakker, for $N = 1$ channel by Gopar, Mello and Büttiker [159]. It was later derived for $N = 2$ channels from (3.14) by Savin, Fyodorov and Sommers [270]. A systematic method was then introduced by Mezzadri and Simm to obtain the cumulants of the distribution, for arbitrary N [232]. The distribution of τ_W was obtained in the large N limit by Texier and Majumdar [286] by using the Coulomb gas method described in Chapter 2. We describe this last result in Section 3.3.

In this chapter, we show how the distribution of the resistance R_q, given by (3.16), can be obtained by the Coulomb gas technique.

➢ Non ideal contacts

In the case of non-ideal contacts, several results have been obtained on the correlations

[1] This result holds in the Wigner-Dyson symmetry classes discussed in Chapter 1. For other symmetry classes (Chiral and Bogoliubov-de Gennes, described in Chapter 5), see for instance Refs. [145, 215, 272].

or the marginal distribution of the time delays, see for instance [146–148, 203, 270, 279]. Most of these results have been obtained using a nonperturbative approach developed in Refs. [148, 203, 279], which can be extended to include effects due to finite absorption [271] or disorder [141, 257].

In Ref. [162], we have obtained the distribution of the Wigner-Smith matrix for the case of non ideal contacts. More precisely, denoting

$$T = 1 - \left|\bar{\mathcal{S}}\right|^2 = \frac{4\kappa}{(1+\kappa)^2} \tag{3.18}$$

the transmission of the contact, the distribution of inverse of the symmetrised Wigner-Smith matrix

$$\Gamma = \mathcal{Q}_s^{-1}\,, \qquad \mathcal{Q}_s = \mathcal{S}^{1/2}\mathcal{Q}\mathcal{S}^{-1/2} = -\mathrm{i}\hbar\mathcal{S}^{-1/2}\frac{\partial\mathcal{S}}{\partial\varepsilon}\mathcal{S}^{-1/2} \tag{3.19}$$

is given by the following matrix integral over Hermitian matrices:

$$P(\Gamma) \propto (\det\Gamma)^{\beta N/2} \int \frac{\mathrm{d}K\ \det(\mathbb{1}_N + K^2)^{\beta N/2}}{\det(\mathbb{1}_N + \kappa^2 K^2)^{1-\beta/2+\beta N}} \exp\left[-\frac{\beta}{2}\kappa\,\mathrm{tr}\left(\frac{\mathbb{1}_N + K^2}{\mathbb{1}_N + \kappa^2 K^2}\Gamma\right)\right]\,. \tag{3.20}$$

In Ref. [162], we have used this representation to study the distribution of the Wigner time delay $\tau_W = \mathrm{tr}[\mathcal{Q}]/N$. However, in this chapter, we will focus on the case of ideal contacts, so that we can use the simpler distribution (3.14).

3.2 The Coulomb gas formulation

In order to make use of the Coulomb gas method introduced in Chapter 2, we rewrite the distribution (3.14) in the form (2.1) by making the change of variables $\gamma_i = Nx_i$. This gives:

$$\mathcal{P}(x_1,\ldots,x_N) \propto \prod_{i<j}|x_i - x_j|^\beta \prod_{n=1}^N \mathrm{e}^{-\frac{\beta N}{2}V(x_n)}\,, \quad V(x) = x - \ln x\,, \quad x_i > 0\,. \tag{3.21}$$

From the discussion of Chapter 2, $x_i = \mathcal{O}(N^0)$, therefore the rates $\gamma_i = \mathcal{O}(N)$. This corresponds to proper times that scale as $1/N$. We can express R_q in terms of the $\{x_i = \gamma_i/N\}$ as:

$$R_q = \frac{h}{2e^2}\frac{\sum_{n=1}^N 1/x_n^2}{\left(\sum_{n=1}^N 1/x_n\right)^2}\,. \tag{3.22}$$

The quantum resistance (3.22) is not of the form (2.25), therefore not a linear statistics. However, it can be expressed in terms of two linear statistics:

$$R_q = \frac{h}{Ne^2}\frac{r}{2s^2}\,, \qquad s = \frac{1}{N}\sum_{n=1}^N \frac{1}{x_n}\,, \quad r = \frac{1}{N}\sum_{n=1}^N \frac{1}{x_n^2}\,, \tag{3.23}$$

where the factor N was introduced such that both s and r are $\mathcal{O}(N^0)$. Our aim is thus to obtain the joint distribution of these two linear statistics,

$$P_N(s,r) = \int \mathrm{d}x_1 \cdots \mathrm{d}x_N \, \mathcal{P}(x_1,\ldots,x_N) \, \delta\left(s - \frac{1}{N}\sum_{n=1}^{N} \frac{1}{x_n}\right) \, \delta\left(r - \frac{1}{N}\sum_{n=1}^{N} \frac{1}{x_n^2}\right) , \quad (3.24)$$

from which we can easily deduce the joint distribution of C_q and R_q. Before entering into the derivation of the distribution, let us first notice that since s and r are expressed in terms of the same variables $\{x_i\}$, some domains in the (s,r) plane are excluded. First, the Cauchy-Schwarz inequality (or Jensen's inequality) imposes that

$$\left(\sum_{i=1}^{N} \frac{1}{x_i}\right)^2 \leqslant N \sum_{i=1}^{N} \frac{1}{x_i^2} \quad \Rightarrow \quad r \geqslant s^2 \, . \quad (3.25)$$

This gives a first forbidden region in the (s,r) plane. Then, from the positiveness of the eigenvalues $x_i \geqslant 0$, we have the second condition

$$r \leqslant N \, s^2 \, . \quad (3.26)$$

The consequence of these restrictions is that the quantum resistance (3.23) is bounded:

$$\boxed{\frac{h}{2Ne^2} \leqslant R_q \leqslant \frac{h}{2e^2}} \quad (3.27)$$

The lower bound corresponds to a situation where all the proper times τ_i are equal. The upper bound is reached when one of the τ_i's becomes much larger than the others. In this case the resistance is dominated by one resonance, and we recover the result of the $N = 1$ channel situation. In the limit $N \to \infty$, we expect the resistance to reach its semiclassical value $R_q \to R_{\mathrm{DC}} = h/(Ne^2)$.

We have reduced the problem to the determination of the joint distribution of two linear statistics in the Laguerre ensembles of random matrices. We will thus apply the Coulomb gas method introduced in Chapter 2 to study this joint distribution in the large N limit. Compared to the case we have analysed in Section 2.2.4, we will see that we need to introduce two constraints on the gas, one for s and one for r. This will yield a richer physics for the Coulomb gas, with a two dimensional phase diagram, in the (s,r) plane. The joint distribution of two linear statistics has been considered by other authors, see for instance Refs. [88, 93].

Instead of working with the eigenvalues $\{\gamma_n = N x_n\}$, we will use the continuous approach, introduced in Section 2.2.5, involving the density

$$\rho(x) = \frac{1}{N}\sum_{n=1}^{N} \delta(x - x_n) \, . \quad (3.28)$$

We replace the measure over the eigenvalues $\{x_n\}$ in (3.24) by a weight for the density:

$$\mathcal{P}(\{x_n\}) \, \mathrm{d}x_1 \cdots \mathrm{d}x_N \longrightarrow \mathrm{e}^{-\frac{\beta N^2}{2}\mathscr{E}[\rho]} \, \delta\left(\int \rho(x)\mathrm{d}x - 1\right) \, \mathcal{D}\rho \, , \quad (3.29)$$

where we introduced the energy

$$\mathscr{E}[\rho] = -\int \mathrm{d}x \int \mathrm{d}y\, \rho(x)\rho(y) \ln|x-y| + \int \rho(x)(x - \ln x)\mathrm{d}x\,. \tag{3.30}$$

This energy is indeed of the form (2.87), with a potential $V(x) = x - \ln x$. The joint distribution (3.24) takes the form:

$$P_N(s,r) \simeq \frac{\displaystyle\int \mathcal{D}\rho\, \mathrm{e}^{-\frac{\beta N^2}{2}\mathscr{E}[\rho]}\, \delta\left(1 - \int \mathrm{d}x\, \rho(x)\right)\, \delta\left(s - \int \frac{\mathrm{d}x}{x}\rho(x)\right)\, \delta\left(r - \int \frac{\mathrm{d}x}{x^2}\rho(x)\right)}{\displaystyle\int \mathcal{D}\rho\, \mathrm{e}^{-\frac{\beta N^2}{2}\mathscr{E}[\rho]}\, \delta\left(1 - \int \mathrm{d}x\, \rho(x)\right)}\,. \tag{3.31}$$

The procedure is the same as for one linear statistics: we look for the density $\rho_\star(x;s,r)$ which dominates the numerator of (3.31) in the limit $N \to \infty$. This can be done by introducing three Lagrange multipliers, one per constraint on ρ, i.e. per delta function. We thus introduce the functional

$$\begin{aligned}\mathscr{F}[\rho;\mu_0,\mu_1,\mu_2;s,r] = \mathscr{E}[\rho] + \mu_0\left(\int \mathrm{d}x\, \rho(x) - 1\right) + \mu_1\left(\int \frac{\mathrm{d}x}{x}\rho(x) - s\right) \\ + \mu_2\left(\int \frac{\mathrm{d}x}{x^2}\rho(x) - r\right)\,.\end{aligned} \tag{3.32}$$

The saddle point is given by $\frac{\delta\mathscr{F}}{\delta\rho(x)} = 0$, which gives

$$2\int \rho(y)\ln|x-y|\,\mathrm{d}y = x - \ln x + \mu_0 + \frac{\mu_1}{x} + \frac{\mu_2}{x^2}\,. \tag{3.33}$$

Taking a derivative with respect to x yields:

$$2\fint \frac{\rho(y)}{x-y}\mathrm{d}y = 1 - \frac{1}{x} - \frac{\mu_1}{x^2} - 2\frac{\mu_2}{x^3}\,. \tag{3.34}$$

Our aim is now to find the solution $\rho_\star(x;s,r)$ of this equation, which satisfies the two constraints

$$\int \rho_\star(x;s,r)\frac{\mathrm{d}x}{x} = s\,, \qquad \int \rho_\star(x;s,r)\frac{\mathrm{d}x}{x^2} = r\,. \tag{3.35}$$

Depending on the values of s and r, we obtain different types of solutions, which we will interpret as different phases for the Coulomb gas. Having found the optimal density $\rho_\star$, the energy of the gas can be computed using an extended version of the thermodynamic identity (2.52)[2]:

$$\frac{\partial\mathscr{E}[\rho_\star(x;s,r)]}{\partial s} = -\mu_1(s,r)\,, \qquad \frac{\partial\mathscr{E}[\rho_\star(x;s,r)]}{\partial r} = -\mu_2(s,r)\,. \tag{3.36}$$

Before studying the joint distribution of s and r, let us first briefly review the results on the marginal distribution of s, obtained in Ref. [286], and present some extensions. We will come back to the determination of $P_N(s,r)$ in a second step (Section 3.4).

[2]Compared to Eq. (2.100), we have dropped the superscript $\star$ for the value Lagrange multipliers after imposing the constraints, in order to lighten the notations.

3.3 Marginal distribution of s: capacitance C_q

We begin by analysing the marginal distribution of s, proportional to the quantum capacitance C_q (or the Wigner time delay τ_W), see Eq. (3.17). Its distribution, denoted $P_N^{(s)}(s)$, thus encodes all the statistical properties of the capacitance. It has been studied by a Coulomb gas technique in Ref. [286] (this article focuses on the Wigner time delay $\tau_W = (h/Ne^2)C_q$). Here we present the main results, which will be useful in the following, and present some extensions.

The marginal of s can be obtained by releasing the constraint on r. This is easily implemented by setting the Lagrange multiplier μ_2 to zero. We are back to determining the distribution of a single linear statistics, in the Laguerre ensembles, as described in Section 2.2.5. In Ref. [286], the authors solve the saddle point equation (3.34) with $\mu_2 = 0$ and obtain two types of solutions, which we now describe.

3.3.1 Phase I: Compact density

The first solution corresponds to an optimal density which has a compact support $[a, b]$:

$$\rho_\star^{(s)}(x; s) = \frac{x + c}{2\pi x^2}\sqrt{(x-a)(b-x)}\,. \tag{3.37}$$

This solution is conveniently parametrised by

$$u = \sqrt{\frac{a}{b}}\,. \tag{3.38}$$

Then, all the parameters are given by

$$v = \sqrt{ab} = 2u\frac{3u^2 - 2u + 3}{(1-u^2)^2}\,, \qquad c = \frac{\mu_1}{v}\,, \tag{3.39}$$

$$\mu_1^{(s)} = -4u^2\frac{(3u^2 - 2u + 3)(u^2 - 6u + 1)}{(1-u^2)^4}\,. \tag{3.40}$$

The parameter u can be related to s via the constraint (3.35), which gives:

$$s = \sigma(u) \overset{\text{(def)}}{=} (1-u)^2\frac{-u^4 + 16u^3 + 2u^2 + 16u - 1}{16u^2(3u^2 - 2u + 3)}\,. \tag{3.41}$$

All these expressions were obtained from Tricomi's theorem, as illustrated in Chapter 2. Additionally, we can compute the corresponding value of r:

$$r = \tau(u) \overset{\text{(def)}}{=} (1-u^2)^4\frac{-u^4 + 12u^3 - 6u^2 + 12u - 1}{64u^4(3u^2 - 2u + 3)^2}\,. \tag{3.42}$$

Note that the typical value of the linear statistics s can be obtained by releasing the constraint:

$$\mu_1^{(s)} = 0 \quad \Rightarrow \quad u_0 = 3 - 2\sqrt{2}\,. \tag{3.43}$$

This corresponds to the density

$$\rho_0(x) = \frac{1}{2\pi x}\sqrt{(x-x_-)(x_+-x)}\,, \quad x_\pm = 3 \pm 2\sqrt{2}\,, \tag{3.44}$$

which is the Marčenko-Pastur distribution discussed in Section 2.1.2. The typical value of s is thus

$$s_0 = \sigma(u_0) = \int \frac{\rho_0(x)}{x}\mathrm{d}x = 1\,. \tag{3.45}$$

Domain of existence

Since the function $s = \sigma(u)$ has a maximum $s_c \simeq 1.17$ reached for $u_c = (1+2^{4/3}-2^{5/3})/3$, this compact phase can exist only for

$$s < s_c = \sigma(u_c) \,. \tag{3.46}$$

Explicit form of the energy

In Ref. [286], the energy associated to the density (3.37) was analysed using the functional (3.30). This integral representation did not permit the authors to obtain an analytic expression for the energy. However, the use of the thermodynamic identity (3.36) yields an explicit form of the energy, by direct integration of (3.40):

$$\mathscr{E}[\rho_\star^{(s)}(x;s)] - \mathscr{E}[\rho_0] = \frac{3}{2}\ln(X(s)-2) + 2\ln(3X(s)-2) + \frac{(X(s)-6)^2}{2(X(s)^2-4)} + 5\ln 2 \,, \tag{3.47}$$

where

$$X(s) = u + \frac{1}{u} = \sigma^{-1}(s) + \frac{1}{\sigma^{-1}(s)} \,. \tag{3.48}$$

From this expression, we recover (and improve) the asymptotics of Ref. [286]:

$$\mathscr{E}[\rho_\star^{(s)}(x;s)] - \mathscr{E}[\rho_0] \simeq \begin{cases} \dfrac{1}{s} + \dfrac{3}{2}\ln s + \dfrac{5}{2}\ln 2 - \dfrac{9}{4} & \text{for } s \to 0 \\ \dfrac{1}{4}(s-1)^2 & \text{for } s \to 1 \,. \end{cases} \tag{3.49}$$

Having described this first phase, which exists only for $s < s_c \simeq 1.17$, we now describe the second solution obtained in Ref. [286].

3.3.2 Phase II: Condensation of one charge

We now investigate the second phase, which permits to reach the large values of

$$s = \frac{1}{N}\sum_{n=1}^{N}\frac{1}{x_n} \,. \tag{3.50}$$

From this expression, it is clear that we can construct a large value of s simply by letting one charge, say x_1, go to zero. This charge thus detaches from the others, so we single it out:

$$s = \frac{1}{Nx_1} + \frac{1}{N}\sum_{n=2}^{N}\frac{1}{x_n} \,. \tag{3.51}$$

For this single charge to give a macroscopic contribution as $N \to \infty$, its position x_1 must scale as $1/N$:

$$x_1 = \frac{1}{N}\frac{1}{s - \dfrac{1}{N}\displaystyle\sum_{n=2}^{N}\frac{1}{x_n}} \,. \tag{3.52}$$

In the large N limit, we will describe the $N-1$ remaining charges by a continuous density ρ_1, such that

$$\rho_\star^{(s)}(x;s) = \frac{1}{N}\,\delta_{x_1}(x) + \rho_1(x)\,. \tag{3.53}$$

Using this ansatz in the equilibrium equation (3.34), we deduce

$$\mu_1^{(s)} = -x_1 + \mathcal{O}(N^{-2})\,. \tag{3.54}$$

Therefore, $\mu_1^{(s)} \to 0$ as $N \to \infty$. The density ρ_1 is thus no longer constrained, so it reaches the optimal one without any constraint, which is the Marčenko-Pastur distribution (3.44):

$$\rho_1(x) \underset{N\to\infty}{\longrightarrow} \rho_0(x)\,. \tag{3.55}$$

The value of x_1 is deduced from Eq. (3.52):

$$s = \frac{1}{N}\frac{1}{s - \displaystyle\int \frac{\rho_0(x)}{x}\mathrm{d}x} = \frac{1}{N(s-1)}\,. \tag{3.56}$$

We can also compute the corresponding value of r, which is given by

$$r = 2 + N(s-1)^2\,. \tag{3.57}$$

A similar scenario was shown to occur in other contexts, for example in the distribution of the largest eigenvalue [47, 101, 102, 212, 300] or for the Renyi entropy [250, 251].

Domain of existence

This phase exists as long as the single charge remains separated from the bulk, that is $x_1 < a$. This gives the condition

$$s > \tilde{s}_c = 1 + 1/(Nx_-)\,. \tag{3.58}$$

Energy of the gas

The corresponding energy can be obtained from (3.54) by using the thermodynamic identity (3.36). This yields

$$\mathscr{E}[\rho_\star^{(s)}(x;s)] - \mathscr{E}[\rho_0] = \frac{1}{N}\ln(s-1) + \mathrm{cte}\,. \tag{3.59}$$

To obtain this constant, it is required to use the integral form of the energy (3.30), which gives

$$\mathscr{E}[\rho_\star^{(s)}(x;s)] - \mathscr{E}[\rho_0] = \frac{1}{N}\ln(s-1) + \frac{\ln N}{N} - \frac{1+2\ln 2}{N} + \mathcal{O}(N^{-2})\,. \tag{3.60}$$

Note that the efficiency of the thermodynamic identity has permitted to spot a mistake in the original version of Ref. [286].

Knowing the explicit from of the density $\rho_\star^{(s)}(x;s)$ for all values of s, we can now study the distribution of s.

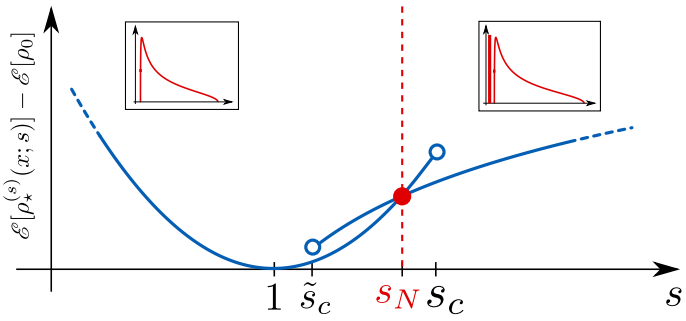

Figure 3.3: Energy of the Coulomb gas associated to the Wigner time delay $\tau_W = \mathrm{tr}[\mathcal{Q}]/N = (h/Ne^2)C_q$. The circles denote the end of existence of each phase. The red point indicates the transition at $s_N \to 1$ as $N \to \infty$. Insets represent the corresponding shape of the density of the Coulomb gas.

3.3.3 Distribution and phase diagram

The Coulomb gas exhibits two possible phases which coexist on a small interval, as shown in Fig. 3.3. To find the position of the phase transition, we need to identify the phase with the lowest energy. The energies (3.47) and (3.60) are represented in Fig. 3.3. They intersect at

$$s_N \simeq 1 + \sqrt{\frac{2\ln N}{N}}\,. \tag{3.61}$$

Therefore, for $s < s_N$, the compact phase is stable, while it is the one with a separate charge for $s > s_N$. In the thermodynamic limit $N \to \infty$, $s_N \to 1$, thus the phase transition occurs at $s = 1$. The energy near this point is given by (3.49) and (3.60), which gives for $N \to \infty$:

$$\mathscr{E}[\rho_\star^{(s)}(x;s)] - \mathscr{E}[\rho_0] \simeq \begin{cases} \dfrac{1}{4}(s-1)^2 & \text{Phase I, i.e. } s < 1 \\ 0 & \text{Phase II, i.e. } s > 1\,. \end{cases} \tag{3.62}$$

In the usual denomination of statistical physics, this corresponds to a second order phase transition.

Having obtained the expression of the energy of the Coulomb gas, Eqs. (3.47) and (3.60), we deduce the distribution of s from (2.97):

$$P_N^{(s)}(s) \sim \exp\left[-\frac{\beta N^2}{2}\left(\mathscr{E}[\rho_\star^{(s)}(x;s)] - \mathscr{E}[\rho_0]\right)\right]\,. \tag{3.63}$$

From the expressions of the energies, the distribution of s is dominated by a Gaussian peak near $s_0 = 1$, with variance

$$\mathrm{Var}(s) \simeq \frac{4}{\beta N^2} \quad \Rightarrow \quad \mathrm{Var}(C_\mu) \simeq \left(\frac{e^2}{h}\right)^2 \frac{4}{\beta N^2}\,. \tag{3.64}$$

We have recovered the result of Refs. [56, 203, 232]. The tails of the distribution are given by:

$$P_N^{(s)}(s) \sim \begin{cases} s^{-3\beta N^2/4}\, \mathrm{e}^{-\beta N^2/(2s)} & \text{for } s \to 0 \\ (s-1)^{-\beta N/2} & \text{for } s \to \infty\,. \end{cases} \tag{3.65}$$

A sketch of this distribution is represented in Fig. 3.4.

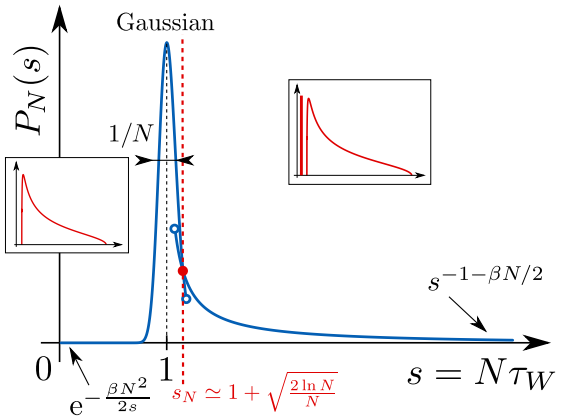

Figure 3.4: Distribution of the Wigner time delay $\tau_W = \mathrm{tr}[\mathcal{Q}]/N = (h/Ne^2)C_q$, derived in Ref. [286] by a Coulomb gas method. Insets represent the shape of the optimal density $\rho_\star(x;s)$ in the two phases $s < s_N$ and $s > s_N$. The circles denote the positions of the end of existence of each phase. Both phases exhibit a metastable region around the transition point s_N. As $N \to \infty$, $s_N \to 1$ and the Coulomb gas undergoes a second order phase transition at $s = 1$.

3.4 Joint distribution

Having studied the marginal distribution of s, we move to the analysis of the joint distribution $P_N(s,r)$. We now have two parameters, therefore we will obtain a two dimensional phase diagram for the Coulomb gas. To the best of our knowledge, this phase diagram reported in Ref. [163] is the first 2D one obtained in the framework of random matrices. Another one has been studied in Ref. [88] soon after.

The case of the marginal of s, corresponding to set the Lagrange multiplier μ_2 to zero, is a line is the (s,r) plane, given by Eqs. (3.41,3.42) and (3.57). Therefore we expect to find again the two phases discussed in Section 3.3, at least on this line. We will see that in addition to these phases, there is an additional one for the Coulomb gas.

3.4.1 Phase I: Compact density

We start by looking for solutions supported on a compact interval $[a,b]$. In this case, Eq. (3.34) can be solved using Tricomi's theorem (see Appendix A.5). We obtain the optimal density in terms of the Lagrange multipliers μ_1 and μ_2 as

$$\tilde{\rho}(x;\mu_1,\mu_2) = \frac{1}{\pi\sqrt{(x-a)(b-x)}}\left[A + \frac{1}{2}\left(\frac{a+b}{2} - x\right) - \frac{1}{2}\left(-1 + \frac{\sqrt{ab}}{x}\right)\right.$$
$$\left. - \frac{\mu_1}{2}\left(\frac{\sqrt{ab}}{x^2} - \frac{a+b}{2x\sqrt{ab}}\right) - \mu_2\left(\frac{\sqrt{ab}}{x^3} - \frac{a+b}{2x^2\sqrt{ab}} - \frac{(a-b)^2}{8x(ab)^{3/2}}\right)\right], \quad (3.66)$$

where A is a constant. The normalization of ρ imposes $A = 1$. The conditions that the density vanishes for $x = a$ and $x = b$ yields

$$12 + 2(b-a) - 4\sqrt{\frac{b}{a}} + 2\mu_1\sqrt{\frac{b}{a}}\left(\frac{1}{b} - \frac{1}{a}\right) - \mu_2\sqrt{\frac{b}{a}}\left(\frac{3}{a^2} - \frac{2}{ab} - \frac{1}{b^2}\right) = 0\,, \quad (3.67)$$

$$12 + 2(a-b) - 4\sqrt{\frac{a}{b}} + 2\mu_1\sqrt{\frac{a}{b}}\left(\frac{1}{a} - \frac{1}{b}\right) - \mu_2\sqrt{\frac{a}{b}}\left(\frac{3}{b^2} - \frac{2}{ab} - \frac{1}{a^2}\right) = 0\,. \quad (3.68)$$

These two equations give a and b, and thus the density, as functions of the Lagrange multipliers μ_1 and μ_2. The density can then be expressed as a function of s and r by

Constraints	Parameters (s, r)	$V_{\text{eff}}(x)$	$\rho_\star$
none	none ($s = s_0$, $r = r_0$)	$x - \ln x$	MP, Eq. (3.44)
$s = \int \frac{\rho(x)}{x} \mathrm{d}x$	s ($r = r(s)$)	$x - \ln x + \frac{\mu_1}{x}$	Eq. (3.37)
$s = \int \frac{\rho(x)}{x} \mathrm{d}x$, $r = \int \frac{\rho(x)}{x^2} \mathrm{d}x$	s, r	$x - \ln x + \frac{\mu_1}{x} + \frac{\mu_2}{x^2}$	Eq. (3.71)

Table 3.1: Optimal density $\rho_\star$ for the Coulomb gas in the presence of constraints. The addition of constraints reduces to place the gas in an effective potential $V_{\text{eff}}(x)$.

imposing the constraints (3.35):

$$-\frac{1}{2} + \frac{6+a+b}{4\sqrt{ab}} - \frac{1}{4}\left(\frac{1}{a}+\frac{1}{b}\right) - \frac{\mu_1}{16}\left(\frac{1}{a}-\frac{1}{b}\right)^2 - \mu_2(a+b)\frac{(a-b)^2}{16(ab)^3} = s\,, \tag{3.69}$$

$$\frac{a^2+6a-2ab+6b+b^2}{8(ab)^{3/2}} - \frac{1}{16}\left(\frac{3}{b^2}+\frac{2}{ab}+\frac{3}{a^2}\right) - \mu_1(a+b)\frac{(a-b)^2}{16(ab)^3} - \frac{\mu_2}{128}(a-b)^2\frac{9a^2+14ab+9b^2}{(ab)^4} = r\,. \tag{3.70}$$

Solving these last two equations give $\mu_1(s,r)$ and $\mu_2(s,r)$. With these results, we can write the optimal density as

$$\rho_\star(x;s,r) = \frac{x^2+px+q}{2\pi x^3}\sqrt{(x-a)(b-x)}\,, \tag{3.71}$$

where the coefficients p and q given by

$$p = \frac{\mu_1}{\sqrt{ab}} + \frac{\mu_2}{(ab)^{3/2}}(a+b)\,, \tag{3.72}$$

$$q = \frac{2\mu_2}{\sqrt{ab}}\,. \tag{3.73}$$

We can recover the optimal density obtained for the marginal distribution of s by setting $\mu_2 = 0$ in these expressions. As shown in Table 3.1, the addition of the constraints changes the form of the density $\rho_\star$. Note that, as for the marginal of s, all these equations can be further simplified by introducing the variables

$$u = \sqrt{\frac{a}{b}}\,, \quad v = \sqrt{ab}\,. \tag{3.74}$$

This change of variable is useful both for numerical and analytical results as all the parameters μ_1, μ_2, s and r can then be expressed as rational fractions of u and v.

Domain of existence

Compared to the case of the marginal of s, the discussion is more involved. The solution (3.71) is valid as long as it remains positive. This imposes the condition

$$Q(x) \overset{\text{(def)}}{=} x^2 + px + q \geqslant 0\,, \quad \forall x \in [a,b]\,. \tag{3.75}$$

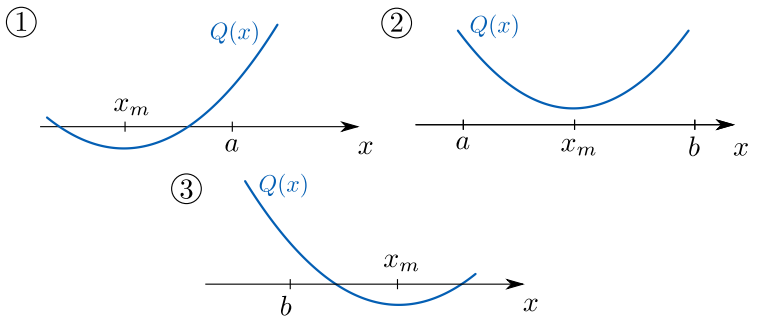

Figure 3.5: The three conditions for the existence of the compact phase, obtained from (3.75).

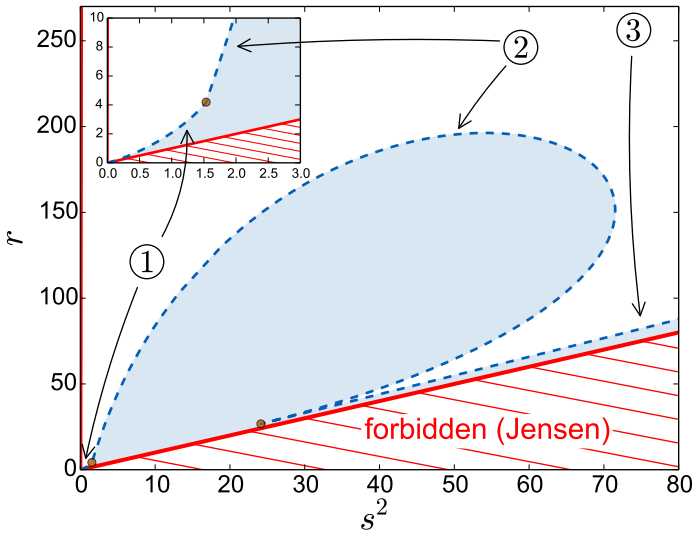

Figure 3.6: Domain of existence of the compact density (shaded region), obtained from (3.75), delimited by the dashed line. Inset is a zoom on the region near the origin. The different conditions shown in Fig. 3.5 are indicated. The transitions between different conditions, denoted by a dot, are associated to a cusp in the boundary of the domain.

This quadratic polynomial has a minimum at

$$x_m = -\frac{p}{2}\,. \tag{3.76}$$

There are now three possibilities, illustrated in Fig. 3.5:

① $x_m < 0$, thus (3.75) can be reduced to $Q(a) \geqslant 0$;

② $x_m \in [a, b]$, therefore (3.75) becomes $Q(x_m) \geqslant 0$;

③ $x_m > b$, and (3.75) gives $Q(b) \geqslant 0$.

These conditions correspond to the blue domain, delimited by the dashed line, shown in Fig. 3.6.

Typical fluctuations

The typical values (s_0, r_0) of the two linear statistics can be easily obtained by releasing the constraints. Setting $\mu_1 = \mu_2 = 0$ in Eqs. (3.67,3.68) yields

$$a = 3 - 2\sqrt{2}\,, \qquad b = 3 + 2\sqrt{2}\,. \tag{3.77}$$

This corresponds to a density of charges given by the Marčenko-Pastur distribution (3.44):

$$\rho_0(x) = \frac{\sqrt{(x-x_-)(x_+-x)}}{2\pi x}\,, \quad x_\pm = 3 \pm 2\sqrt{2}\,. \tag{3.78}$$

We deduce the typical values of s and r as

$$s_0 = \int \frac{\rho_0(x)}{x}\mathrm{d}x = 1\,, \qquad r_0 = \int \frac{\rho_0(x)}{x^2}\mathrm{d}x = 2\,. \tag{3.79}$$

The behaviour of the energy near this point can be obtained by expanding the energy to second order in $s-s_0$ and $r-r_0$. Using the thermodynamic identities (3.36) we obtain

$$\begin{aligned}\mathscr{E}[\rho_\star(x;s,r)] \simeq \mathscr{E}[\rho_0] - \frac{1}{2}(s-s_0)^2\left.\frac{\partial\mu_1}{\partial s}\right|_{(s_0,r_0)} - \frac{1}{2}(r-r_0)^2\left.\frac{\partial\mu_2}{\partial r}\right|_{(s_0,r_0)} \\ - (s-s_0)(r-r_0)\left.\frac{\partial\mu_1}{\partial r}\right|_{(s_0,r_0)}\,.\end{aligned} \tag{3.80}$$

From Eqs. (3.67)–(3.70), we deduce

$$\mathscr{E}[\rho_\star(x;s,r)] \simeq \mathscr{E}[\rho_0] + \frac{5}{2}(s-1)^2 + \frac{1}{16}(r-2)^2 - \frac{3}{4}(s-1)(r-2)\,. \tag{3.81}$$

From Eq. (2.97), we deduce that the joint distribution of s and r is dominated by a Gaussian peak located at (s_0, r_0). We can rewrite (3.81) in terms of a covariance matrix as

$$\mathscr{E}[\rho_\star(x;s,r)] - \mathscr{E}[\rho_0] \simeq \begin{pmatrix}\delta s & \delta r\end{pmatrix}\begin{pmatrix}4 & 24\\ 24 & 160\end{pmatrix}^{-1}\begin{pmatrix}\delta s\\ \delta r\end{pmatrix}\,, \quad \begin{cases}\delta s = s-1\,,\\ \delta r = r-2\,.\end{cases} \tag{3.82}$$

From this expression, we recover the variance of s given by Eq. (3.64), and also deduce

$$\mathrm{Var}(r) \simeq \frac{160}{\beta N^2}\,, \qquad \mathrm{Cov}(s,r) \simeq \frac{24}{\beta N^2}\,. \tag{3.83}$$

The covariance matrix (3.82) has been recently derived by other means [92,93], but our approach will also provide us with information about the full joint distribution of s and r, which is needed to study the resistance R_q.

Asymptotic behaviour near $r = s^2$

We can similarly study the behaviour of the energy near the limit $r = s^2$. Denote $\varepsilon = r - s^2 > 0$. In the limit $\varepsilon \to 0$, Eqs. (3.67)–(3.70) give

$$\mu_1 = -\frac{s}{\varepsilon} + \frac{7}{4}\frac{3-5s}{s^2} + \mathcal{O}(\sqrt{\varepsilon})\,, \tag{3.84}$$

$$\mu_2 = \frac{1}{2\varepsilon} + \frac{23s-17}{8s^2} + \mathcal{O}(\sqrt{\varepsilon})\,. \tag{3.85}$$

The energy can then be deduced from the thermodynamic identities (3.36) by integration of these expressions:

$$\mathscr{E}[\rho_\star(x;s,r)] \simeq -\frac{1}{2}\ln(r-s^2) + \mathcal{O}(1)\,, \quad \text{as } r - s^2 \to 0\,. \tag{3.86}$$

3.4.2 Phase II: Condensation of one charge

As we have seen in Section 3.3, we can reach large values of s and r by letting one charge, for instance the one located at x_1, go to zero as $1/N$. This observation leads us to look for a solution of (3.34) in the form

$$\rho(x) = \rho_1(x) + \frac{1}{N}\,\delta(x - x_1)\,, \tag{3.87}$$

where ρ_1 has a compact support denoted $[a, b]$. For $x \in [a, b]$, Eq. (3.34) becomes

$$\frac{1}{2}\left(1 - \frac{1}{x} - \frac{\mu_1}{x^2} - 2\frac{\mu_2}{x^3}\right) = \fint \frac{\rho_1(x)}{x - y}\mathrm{d}y + \frac{1}{N}\frac{1}{x - x_1}\,. \tag{3.88}$$

Equation (3.34) must also be evaluated for $x = x_1$, which can be interpreted as the force balance on the charge at position x_1:

$$\frac{1}{2}\left(1 - \frac{1}{x_1} - \frac{\mu_1}{x_1^2} - 2\frac{\mu_2}{x_1^3}\right) = \int \frac{\rho_1(x)}{x_1 - x}\mathrm{d}x\,. \tag{3.89}$$

Using Tricomi's theorem, one can compute the expression of the density ρ_1. Imposing the conditions $\rho_1(a) = \rho_1(b) = 0$, the constraints (3.35) and relation (3.89) which fixes the position of the isolated charge, we obtain a set of five equations linking μ_1, μ_2, a, b and x_1 to the parameters s and r. Then the density ρ_1 takes the form

$$\rho_1(x; s, r) = \frac{x^3 + mx^2 + nx + l}{2\pi x^3(x - x_1)}\sqrt{(x - a)(b - x)}\,, \tag{3.90}$$

where we introduced

$$m = \frac{\mu_1}{\sqrt{ab}} + \mu_2\frac{a + b}{(ab)^{3/2}} - x_1\left(\frac{\mu_2}{(ab)^{5/2}}\frac{3a^2 + 2ab + 3b^2}{4} + \frac{1}{\sqrt{ab}} + \mu_1\frac{a + b}{2(ab)^{3/2}}\right)\,, \tag{3.91}$$

$$n = \frac{2\mu_2}{\sqrt{ab}} - x_1\left(\mu_2\frac{a + b}{(ab)^{3/2}} + \frac{\mu_1}{\sqrt{ab}}\right)\,, \tag{3.92}$$

$$l = -2x_1\frac{\mu_2}{\sqrt{ab}}\,. \tag{3.93}$$

Similarly as in the case of the marginal of s, for the charge located at x_1 to give a macroscopic contribution to s and r, it must be of order $\mathcal{O}(N^{-1})$. We thus denote

$$x_1 = \frac{\tilde{x}_1}{N}\,. \tag{3.94}$$

We can expand the equations determining the parameters in the limit $N \to \infty$. As in the compact case, it is not convenient to choose s and r as parameters. Instead, we choose to parametrise the solution by $u = \sqrt{a/b}$ and $\tilde{x}_1$ as this will yield simpler

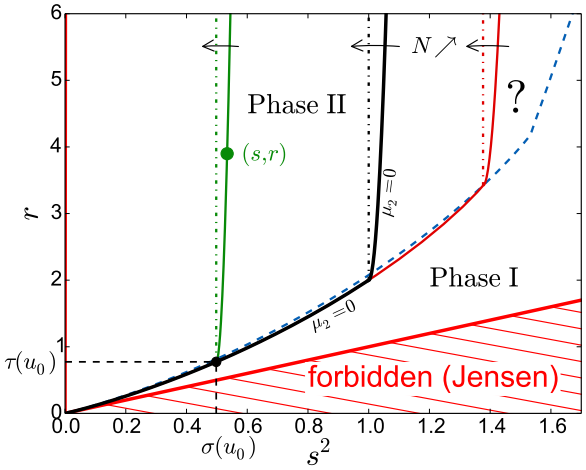

Figure 3.7: Domain of existence of Phase II (shaded), obtained from (3.100,3.101), delimited by the red solid line. The green line is $r = N(s - \sigma(u_0))^2 + \tau(u_0)$. On this line, the energy is given at leading order by its value for $(s = \sigma(u_0), r = \tau(u_0))$. The line $\mu_2 = 0$, corresponding to the case of the marginal of s studied in Section 3.3 is also represented. All the lines are shown for $N = 5000$, while their limit for $N \to \infty$ are represented by dash-dot lines.

expressions than the other possible choices. For fixed u and $\tilde{x}_1$, we obtain:

$$\rho_1(x; s, r) = \rho^{(s)}(x; \sigma(u)) + \mathcal{O}(N^{-1}) , \tag{3.95}$$

$$\mu_1 = \mu_1^{(s)}(u) + \frac{1}{N}\,\mu_1^{(1)}(u, \tilde{x}_1) + \mathcal{O}(N^{-2}) , \tag{3.96}$$

$$\mu_2 = -\frac{1}{2N}\,\tilde{x}_1\,\mu_1^{(s)}(u) - \frac{1}{2N^2}\left(\tilde{x}_1\,\mu_1^{(1)}(u, \tilde{x}_1) + \tilde{x}_1^2\right) + \mathcal{O}(N^{-3}) , \tag{3.97}$$

$$s = \sigma(u) + \frac{1}{\tilde{x}_1} + \frac{1}{N}\,s^{(1)}(u, \tilde{x}_1) + \mathcal{O}(N^{-2}) , \tag{3.98}$$

$$r = \frac{N}{\tilde{x}_1^2} + \tau(u) + \mathcal{O}(N^{-1}) , \tag{3.99}$$

where the functions $\mu_1^{(s)}$, σ and τ are given by Eqs. (3.40), (3.41) and (3.42) respectively. We do not give here the explicit form of the functions $\mu_1^{(1)}(u, \tilde{x}_1)$ and $s^{(1)}(u, \tilde{x}_1)$, which are rational fractions in u and linear in $\tilde{x}_1$.

Domain of existence

We now study the domain in the (s, r) plane in which this phase with a condensed charge exists. The solution must respect two conditions:

1. The density (3.95) must remain positive on its support. At leading order, it is given by the density of the compact phase of Section 3.3, therefore this gives

$$\sigma(u) < s_c . \tag{3.100}$$

2. The separate charge $x_1 = \tilde{x}_1/N$ must remain detached from the bulk, thus

$$\tilde{x}_1 < Na . \tag{3.101}$$

These two conditions correspond to the shaded domain represented in Fig. 3.7.

Energy of the gas

Unlike for Phase I, we can explicitly compute the energy $\mathscr{E}[\rho_\star(x;s,r)]$ in this phase from equations (3.95)–(3.99). The question is again to get the correct parametrisation to find the most compact expressions. The simplest way I found is to first invert the series (3.98) to obtain u in terms of $\tilde{x}_1$ and s, as a power series

$$u = u_0(\tilde{x}_1, s) + \frac{1}{N}\, u_1(\tilde{x}_1, s) + \mathcal{O}(N^{-2})\,. \tag{3.102}$$

The leading coefficient, given by

$$s = \sigma(u_0) + \frac{1}{\tilde{x}_1}\,, \tag{3.103}$$

is of particular interest: instead of parametrising by s and $\tilde{x}_1$, it is more convenient to take s and u_0 as parameters. Indeed, let us denote

$$\mathcal{E}(u_0, s) = \mathscr{E}\left[\rho_\star\left(x; s, r = N(s-\sigma(u_0))^2 + \tau(u_0)\right)\right] \tag{3.104}$$

the energy of the gas, where we used Eq. (3.99) for r. The meaning of this parametrisation is simple: for a given value of u_0, changing s moves us on the parabola $r = N(s-\sigma(u_0))^2 + \tau(u_0)$. The starting point of this curve is $(s = \sigma(u_0), r = \tau(u_0))$, which is on the line $\mu_2 = 0$ corresponding to the case of the marginal discussed in Section 3.3 (see Fig. 3.7).

The derivatives of the energy (3.104) can be computed from the thermodynamic identities (3.36) and the expressions of the Lagrange multipliers (3.96,3.97):

$$\frac{\partial \mathcal{E}}{\partial s} = \frac{1}{N}\frac{1}{s-\sigma(u_0)} + \mathcal{O}(N^{-2})\,, \tag{3.105}$$

$$\frac{\partial \mathcal{E}}{\partial u_0} = \sigma'(u_0)\left[-\mu_1^{(s)}(u_0) + \frac{1}{N}\left(\frac{1}{\sigma(u_0)-s} + 16u_0^2(1+u_0^2)\frac{u_0^2-6u_0+1}{(1-u_0^2)^2}\right) + \mathcal{O}(N^{-2})\right]. \tag{3.106}$$

By integrating these two equations, we obtain the energy of the gas:

$$\mathcal{E}(u_0, s) = \mathscr{E}[\rho_\star^{(s)}(x;s)] + \frac{1}{N}\left[\ln(s-\sigma(u_0)) + \Xi(u_0)\right] + \mathcal{O}(N^{-2})\,, \tag{3.107}$$

where the $\mathcal{O}(N^0)$ term is the energy of the gas for $\mu_2 = 0$, given by Eq. (3.47) and the function Ξ is given by

$$\Xi(u) = \ln\left(32u^2\frac{3u^2-2u+3}{(1+u)^6}\right) + 2(1+u^2)\frac{u^2-6u+1}{(1-u^2)^2} + \ln N - 1 - 2\ln 2\,. \tag{3.108}$$

In this expression, we fixed the constant by identification with (3.60) for $\sigma(u_0) = 1$.

From the exact form of the energy (3.107), we can deduce its asymptotic behaviour near the forbidden region $r = Ns^2$:

$$\mathscr{E}[\rho_\star(x;s,r)] \simeq \frac{2Ns}{Ns^2 - r} \quad \text{for} \quad r \to Ns^2\,. \tag{3.109}$$

3.4.3 Phase III: Split bulk

Up to now, we have described the two phases already obtained for the marginal of s. But these two phases do not describe the full (s, r) plane. We now investigate the nature of the density in the remaining region, see Fig. 3.7.

To get some insight, let us come back to the saddle point equation (3.34). It describes the force balance for a charge at position x, between the repulsion of the other charges, and an external force which derives from the effective potential

$$V_{\text{eff}}(x) = x - \ln x + \frac{\mu_1}{x} + \frac{\mu_2}{x^2} \,. \tag{3.110}$$

If $\mu_1 < 0$ and $\mu_2 > 0$, this effective potential exhibits two local minima. Therefore, the density of charges can split into two bulks, located at each minima. Solving the integral equation (3.34) for a density with two bulks using Tricomi's theorem is more involved, as we will see in Chapter 4. Here, we use another method, based on complex analysis, which is more convenient in this case [216, 218, 219, 248]. For a complex variable z, we introduce the resolvent

$$G(z) = \int \frac{\rho_\star(x; s, r)}{z - x} \mathrm{d}x \,. \tag{3.111}$$

This function is analytic everywhere in the complex plane, except on the support of ρ. Indeed, if $x \in \mathrm{Supp}(\rho)$:

$$G(x + \mathrm{i}\varepsilon) - G(x - \mathrm{i}\varepsilon) = -2\mathrm{i}\varepsilon \int \frac{\rho_\star(y; s, r)}{(x - y)^2 + \varepsilon^2} \mathrm{d}y \underset{\varepsilon \to 0^+}{\longrightarrow} -2\mathrm{i}\pi \rho_\star(x; s, r) \,. \tag{3.112}$$

Therefore, if we can determine the function $G(z)$, we can extract the optimal density $\rho_\star(x; s, r)$ from its cuts. Additionally, since the density is normalised, the resolvent must verify the property

$$G(z) \sim \frac{1}{z} \text{ for } |z| \to \infty \,. \tag{3.113}$$

We can derive an equation on G by multiplying (3.34) by $\frac{\rho_\star(x;s,r)}{z-x}$ and integrating over x. After a few manipulations, we obtain that G is solution of the quadratic equation

$$-G(z)^2 + G(z)\left(1 - \frac{1}{z} - \frac{\mu_1}{z^2} - \frac{2\mu_2}{z^3}\right) - \frac{s + \mu_1 r + \mu_2 t}{z} - \frac{\mu_1 s + 2\mu_2 r}{z^2} - \frac{2\mu_2 s}{z^3} = 0 \,, \tag{3.114}$$

where we used that

$$s = \int \frac{\rho_\star(x; s, r)}{x} \mathrm{d}x = -G(0) \,, \quad r = \int \frac{\rho_\star(x; s, r)}{x^2} \mathrm{d}x = -G'(0) \,, \tag{3.115}$$

and we denoted

$$t = \int \frac{\rho_\star(x; s, r)}{x^3} \mathrm{d}x = -\frac{1}{2} G''(0) \,. \tag{3.116}$$

The normalisation condition (3.113) implies

$$s + \mu_1 r + \mu_2 t = 1 \,, \tag{3.117}$$

so that Eq. (3.114) no longer depends on this unknown parameter t. We can then solve this quadratic equation to get

$$G(z) = \frac{1}{2}\left(1 - \frac{1}{z} - \frac{\mu_1}{z^2} - \frac{2\mu_2}{z^3}\right) \pm \frac{1}{2z^3}\sqrt{P(z)} \,, \tag{3.118}$$

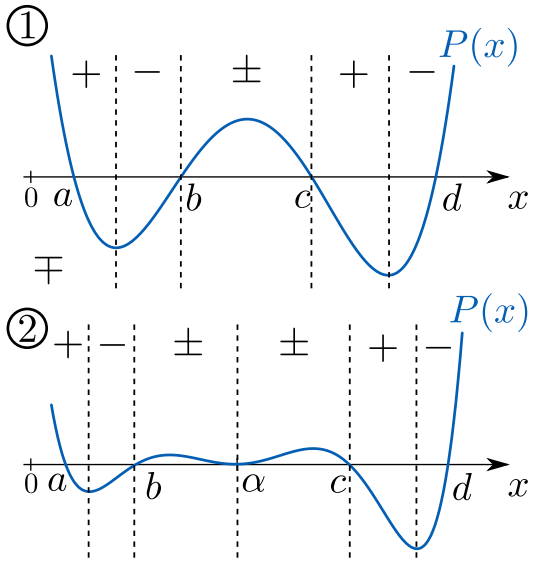

Figure 3.8: Two possibilities for the polynomial P. Either it has 4 positive roots (top), or an additional positive double root, denoted α. Any other possibility would lead to a density $\rho_\star$ with a higher number of supports. The signs are the value of the function $\mathrm{sgG}(x) = \pm 1$. On the support of $\rho_\star$, corresponding to $P(x) < 0$, it is the opposite of the sign of P', see Eq. (3.122). Outside the support, it has to be constant (to be determined), unless $P(x)$ vanishes.

where we introduced the following polynomial of degree six:

$$P(z) = z^6 - 6z^5 + (1 - 2\mu_2(2s+1) - 8\mu_2 r)z^4 + (2\mu_1 - 4\mu_2(2s+1))z^3 + (\mu_1^2 + 4\mu_2)z^2 + 4\mu_1\mu_2 z + 4\mu_2^2 \,. \quad (3.119)$$

The support of the optimal density corresponds to the cuts of (3.118), which are given by $P(x) \leqslant 0$. We can then deduce the density (3.112) using that

$$\mathrm{Im}\, G(z + \mathrm{i}\varepsilon) = \frac{\mathrm{sgG}(x)}{2x^3}\sqrt{P(x) + \mathrm{i}P'(x)\varepsilon} \underset{\varepsilon\to 0^+}{\longrightarrow} \frac{\mathrm{sgG}(x)}{2x^3}\,\mathrm{sign}(P'(x))\sqrt{-P(x)}\,, \quad (3.120)$$

where $\mathrm{sgG}(x) = \pm 1$, depending on the $\pm$ sign in (3.118). We thus obtain

$$\rho_\star(x; s, r) = \frac{1}{2\pi x^3}\sqrt{-P(x)}\,, \quad (3.121)$$

and

$$\mathrm{sgG}(x) = -\,\mathrm{sign}(P'(x)) \quad \text{for} \quad x \in \mathrm{Supp}(\rho_\star)\,. \quad (3.122)$$

If $x \notin \mathrm{Supp}(\rho_\star)$, $G(x)$ is real and continuous from Eq. (3.111). Therefore $\mathrm{sgG}(x)$ is constant outside the support of $\rho_\star$, or can change if the multiplicative factor $P(z)$ vanishes. The possible values of this function are represented in Fig. 3.8.

S We look for an optimal density $\rho_\star$ with a support of the form $[a, b] \cup [c, d]$, with $0 < a < b < c < d$. This implies that a, b, c and d are positive roots of the polynomial P. There are only two possibilities, illustrated in Fig. 3.8:

① a, b, c and d are the only positive roots of P;

② there is another positive root α. This additional root must have multiplicity two, otherwise $\rho_\star$ would have a third support.

To completely solve the problem, we need to determine all the roots of P, which will give the density $\rho_\star$, Eq. (3.121), as well as μ_1 and μ_2. The relations between the roots

and the coefficients of P give six equations, which is not enough to completely determine all the parameters. We thus need another equation. We can make use of Eq. (3.33), which we rewrite in terms of the effective potential (3.110) as

$$\int \rho_\star(y;s,r)\ln|x-y|\,\mathrm{d}y = \mu_0 + V_{\text{eff}}(x)\,, \quad \forall x \in \text{Supp}(\rho_\star)\,. \tag{3.123}$$

This equation depending on the unknown Lagrange multiplier μ_0, which acts as a chemical potential for the Coulomb gas, we will consider the difference between two points, say b and c:

$$V_{\text{eff}}(c) - V_{\text{eff}}(b) = \int \rho_\star(y;s,r)\ln\left|\frac{c-y}{b-y}\right|\mathrm{d}y\,. \tag{3.124}$$

This equation can be interpreted as the chemical equilibrium between the two bulks, supported on $[a,b]$ and $[c,d]$ (this interpretation was proposed in Refs. [216,219]). Using the definition of G, Eq. (3.111), we have

$$\int_b^c G(x)\mathrm{d}x = \int \rho_\star(y;s,r)\ln\left|\frac{c-y}{b-y}\right|\mathrm{d}y\,. \tag{3.125}$$

Therefore, from the expression of G. Eq. (3.118), the condition (3.124) becomes

$$\int_b^c \frac{\text{sgG}(x)}{x^3}\sqrt{P(x)}\mathrm{d}x = 0\,. \tag{3.126}$$

This condition cannot be fulfilled in case (1), where P has only four positive roots, as sgG is constant on $[b,c]$ (see Fig. 3.8). Therefore, we are in the situation (2) and sgG has to change sign when crossing the double root α. The polynomial P thus takes the form

$$P(x) = (x-\alpha)^2(x-a)(x-b)(x-c)(x-d)\,, \tag{3.127}$$

from which we deduce the density (3.121)

$$\rho_\star(x;s,r) = \frac{|x-\alpha|}{2\pi x^3}\sqrt{(x-a)(b-x)(c-x)(d-x)}\,. \tag{3.128}$$

Expanding (3.127) and identifying the coefficients with (3.119), we obtain the set of six equations linking the seven parameters a, b, c, d, α, μ_1 and μ_2 to s and r. The last relation is given by Eq. (3.126), which we can rewrite as

$$\int_b^c \frac{x-\alpha}{2\pi x^3}\sqrt{(x-a)(x-b)(x-c)(x-d)}\,\mathrm{d}x = 0\,. \tag{3.129}$$

since sgG changes sign when crossing the root α. This gives a set of seven equations, which fix all the parameters for a given couple of values (s,r). This set of equations cannot be solved analytically, but it can be implemented numerically to compute these parameters, for each value of s and r.

Domain of existence

The solution (3.128) with two bulks can cease to exist in different situations:

1. the left bulk can vanish if $a = b$;
2. the right bulk can vanish if $c = d$;
3. the two bulks can merge if $b = c$.

In case 1, at the limit the resulting density takes the form

$$\rho_\star(x; s, r) = \frac{(x-\alpha)(x-a)}{2\pi x^3}\sqrt{(x-c)(d-x)}\,, \tag{3.130}$$

which is the optimal density in the compact phase. Similarly for case 2. Therefore, there is an overlap between Phase I and Phase III.

However, in case 3, the resulting density is

$$\rho_\star(x; s, r) = \frac{(x-\alpha)^2}{2\pi x^3}\sqrt{(x-a)(d-x)}\,, \tag{3.131}$$

since $b < \alpha < c$. This density, supported on $[a, d]$, vanishes as a square in the bulk for $x = \alpha$. This coincides with the limit (2) for Phase I. Therefore, the transition from Phases I to Phase III occurs on this line, represented in Fig. 3.6.

Finally, we will see below that this phase extends up to $s = 1$, and overlaps with Phase II. Therefore Phase III completes our description of the whole (s, r) plane.

Asymptotic behaviours

The analysis of the set of equations determining the density $\rho_\star$ in Phase III is rather difficult. We can however analyse some limiting cases. The most interesting one is the limit $b \to 0$, with $a \simeq b$. In this case we obtain

$$\alpha \simeq -2b\ln b\,, \tag{3.132}$$

$$c + d \simeq 6\,, \qquad cd \simeq 1\,, \tag{3.133}$$

$$\mu_1 \simeq 2b\ln b\,, \qquad \mu_2 \simeq -b^2\ln b\,, \tag{3.134}$$

$$s \simeq 1 + \alpha\frac{(b-a)^2}{16b^4}\,, \qquad r \simeq \alpha\frac{(b-a)^2}{16b^5}\,. \tag{3.135}$$

Combining these expressions, we deduce

$$b \simeq \frac{s-1}{r}\,, \tag{3.136}$$

therefore the limit $b \to 0$ is either $r \to \infty$ or $s \to 1^+$ (this shows that Phase III extends to $s = 1$). Combining this expression with Eq. (3.134), we obtain μ_1 and μ_2 in terms of s and r. Using then the thermodynamic identities (3.36), we deduce

$$\mathscr{E}[\rho_\star(x; s, r)] \simeq -\frac{(s-1)^2}{r}\ln\frac{s-1}{r} + \text{cst}\,. \tag{3.137}$$

The constant can be determined by taking the limit $s \to 1$. We then reach the vertical line $\mu_2 = 0$ on which the gas is frozen the ρ_0, thus:

$$\mathscr{E}[\rho_\star(x; s, r)] \simeq -\frac{(s-1)^2}{r}\ln\frac{s-1}{r} + \mathscr{E}[\rho_0]\,. \tag{3.138}$$

3.4.4 Summary and phase diagram

Combining the results of the previous sections, we have obtained the expression of the optimal density of the Coulomb gas for all values of the parameters s and r. The resulting phase diagram is represented in Fig. 3.9.

Knowing the optimal density $\rho_\star(x;s,r)$, the joint distribution of s and r takes the form (2.97)

$$P_N(s,r) \underset{N\to\infty}{\sim} \exp\left[-\frac{\beta N^2}{2}\Phi(s,r)\right], \quad \Phi(s,r) = \mathscr{E}[\rho_\star(x;s,r)] - \mathscr{E}[\rho_0(x)], \tag{3.139}$$

where the Marčenko-Pastur distribution is associated to the typical values of s and r:

$$\rho_0(x) = \rho_\star(x;s_0,r_0), \quad \text{with} \quad \begin{cases} s_0 = 1 \\ r_0 = 2 \end{cases} \tag{3.140}$$

The precise expression of the large deviation function depends on the phase under consideration:

$$\Phi(s,r) = \begin{cases} \Phi_I(s,r) & \text{if } (s,r) \in \text{Phase I}, \\ \Phi_{II}(s,r) & \text{if } (s,r) \in \text{Phase II}, \\ \Phi_{III}(s,r) & \text{if } (s,r) \in \text{Phase III}, \end{cases} \tag{3.141}$$

which can be deduced from the phase diagram given in Fig. 3.9. In particular, we have an analytical expression for the function Φ_{II}, deduced from Eq. (3.107). The other two functions are not known analytically, but can be evaluated numerically. Nevertheless, we have the following behaviours, deduced from Eqs. (3.86,3.138):

$$\Phi_I(s,r) \simeq -\frac{1}{2}\ln(r-s^2), \quad \text{for } r - s^2 \to 0^+, \tag{3.142}$$

$$\Phi_{III}(s,r) \simeq -\frac{(s-1)^2}{r}\ln\frac{s-1}{r}, \quad \text{for } \frac{s-1}{r} \to 0^+. \tag{3.143}$$

The transitions between the phases can be determined, when two phases overlap, by looking for the one with the smallest energy. For Phases I and II, the analysis is similar to the case of the marginal of s, discussed in Section 3.3. The conclusion is also the same: in the limit $N \to \infty$ the transition occurs on the line $\mu_2 = 0$. It is also a **second order** phase transition.

The transition between Phases II and III is more complex, and was not studied into details. As we have seen when studying the energy, the limit $s \to 1$ corresponds to the left bulk (supported on $[a,b]$) going to zero. It is natural to expect that, for finite N, when this bulk contains only 1 charge it becomes the separate charge of Phase II. For $N \to \infty$, we thus expect the transition to occur at the limit $s = 1$, corresponding also to $\mu_2 = 0$. The order of this transition however remains to be determined.

Finally, we have not analysed the transition between Phases I and III, as it is quite difficult to compute analytically the energy in these phases. However, as discussed in Ref. [212], the order of the transition depends only on the scenario for the density (condensation of one charge, splitting of the bulk, ...). The line associated to the condition (2) for Phase I corresponds to the splitting of a compact density into two bulks. Exactly on the transition line, the density vanishes as a square, Eq. (3.131). A similar scenario was shown in Refs. [167,304] to correspond to a **third order** phase transition. Therefore, we expect that this line corresponds to a third order transition, but a direct derivation would still be instructing.

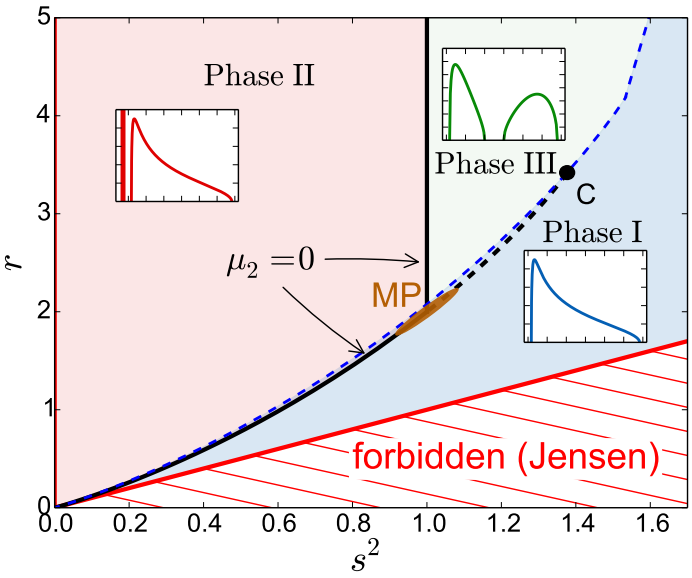

Figure 3.9: Phase diagram for the Coulomb gas, in the presence of two constraints.

3.5 Statistical properties of R_q

Having obtained the full joint distribution of s and r, we can now analyse the distribution of the quantum resistance

$$R_q = \frac{h}{Ne^2}\, r_q \,, \quad r_q = \frac{r}{2s^2} \,. \tag{3.144}$$

3.5.1 Typical fluctuations

As we have seen in Section 3.4.1, the typical values of s and r are given by

$$s_0 = 1 \,, \quad r_0 = 2 \,. \tag{3.145}$$

This corresponds to a typical value of the resistance of

$$\langle r_q \rangle = \frac{r_0}{2s_0^2} = 1 \quad \Rightarrow \quad \langle R_q \rangle \simeq \frac{h}{Ne^2} \,. \tag{3.146}$$

We notice that $\langle R_q \rangle \simeq R_{\rm DC}$, where $R_{\rm DC}$ is the Sharvin resistance of the ballistic quantum point contact given by (3.1), in the large N limit, as expected. We can study the fluctuations around this value from the expression of the large deviation function $\Phi_I(s,r)$ near the point (s_0, r_0), given by Eq. (3.82):

$$\mathrm{Var}(r_q) \simeq \frac{8}{\beta N^2} \quad \Rightarrow \quad \frac{\mathrm{Var}(R_q)}{\langle R_q \rangle^2} \simeq \frac{8}{\beta N^2} \,. \tag{3.147}$$

The variance (3.147) corresponds to a Gaussian peak of the distribution, near the mean:

$$p_N(r_q) \sim \exp\left[-\frac{\beta N^2}{16} (r_q - 1)^2 \right] \,. \tag{3.148}$$

The covariance matrix (3.82) shows that the variables s and r are strongly correlated, and therefore the capacitance C_q and resistance R_q are also correlated:

$$\frac{\mathrm{Cov}(C_q, R_q)}{\sqrt{\mathrm{Var}(C_q)\mathrm{Var}(R_q)}} = \frac{1}{\sqrt{2}} \,. \tag{3.149}$$

3.5.2 Large deviations

The Coulomb gas approach gives access to the full joint distribution of s and r, from which we study the distribution of r_q, away from the typical region. This distribution is given by

$$p_N(r_q) = \int P_N(s,r)\, \delta\Big(r_q - \frac{r}{2s^2}\Big)\, \mathrm{d}s\mathrm{d}r = \int 2s^2\, P_N(s, 2s^2 r_q)\, \mathrm{d}s \,. \tag{3.150}$$

Since the joint distribution $P_N(s,r)$ has the large deviations form (3.139), this integral can be evaluated by a saddle point estimate. One only needs to find the minimum of the large deviation function $\Phi(s,r)$ on a line $r = 2s^2 r_q$.

• Let us consider the case $r_q > 1$. The large deviation function $\Phi(s,r)$ is of order $\mathcal{O}(N^0)$ everywhere, except on the line $\mu_2 = 0$ where it is $\mathcal{O}(N^{-1})$. Therefore, on a given line $r = 2s^2 r_q$, the minimum of $\Phi(s,r)$ is located on the line $\mu_2 = 0$. This latter being given by $r = N(s-1)^2 + 1$, the intersection is solution of

$$\begin{cases} r = 2s^2 r_q \,, \\ r = N(s-1)^2 + 2 \,. \end{cases} \tag{3.151}$$

Solving this set of equations yields that the saddle point of (3.150) is

$$s_* = \frac{N - \sqrt{2N(r_q - 1) + 4r_q}}{N - 2r_q} \,. \tag{3.152}$$

Using that, for $\mu_2 = 0$,

$$\Phi_{II}(s,r) \simeq \frac{1}{N} \ln(s-1) \,, \tag{3.153}$$

we deduce

$$p_N(r_q) \sim \left(\frac{N - 2r_q}{2r_q + \sqrt{2N(r_q - 1) + 4r_q}} \right)^{\beta N/2} \,. \tag{3.154}$$

Near the upper boundary, it reduces to a power law suppression

$$p_N(r_q) \sim \Big(\frac{N}{2} - r_q \Big)^{\beta N/2} \,, \quad r_q \to \frac{N}{2}^- \,. \tag{3.155}$$

• If $r_q < 1$, the analysis is more difficult. We can however study the limit $r_q \to \frac{1}{2}^+$. Denote

$$r_q = \frac{1}{2} + \varepsilon \,. \tag{3.156}$$

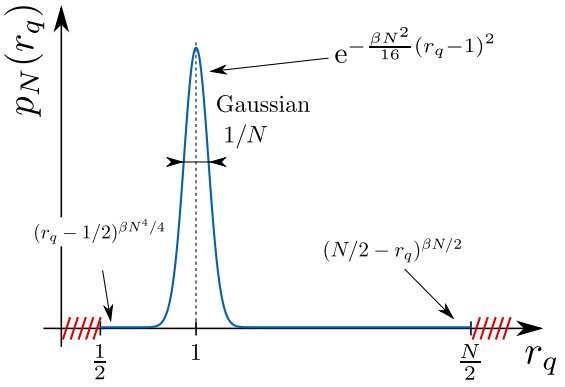

Figure 3.10: Sketch of the distribution of the quantum resistance $R_q = (h/Ne^2)r_q$.

The distribution (3.150) becomes

$$p_N(r_q) \sim \int 2s^2 \, \exp\left[-\frac{\beta N^2}{2}\Phi_I(s, s^2 + 2s^2\varepsilon)\right] \, \mathrm{d}s \,, \tag{3.157}$$

where Φ_I is the large deviation function in Phase I. Its behaviour in the limit $\varepsilon \to 0$ is given by (3.142), from which we deduce the power law suppression

$$p_N(r_q) \sim \left(r_q - \frac{1}{2}\right)^{\beta N^2/4} \,, \quad \text{for } r_q \to \frac{1}{2}^+ \,. \tag{3.158}$$

This concludes our analysis of the distribution of r_q, which is sketched in Fig. 3.10.

Article 2

Capacitance and charge relaxation resistance of chaotic cavities – Joint distribution of two linear statistics in the Laguerre ensemble of random matrices

A. Grabsch and C. Texier, Capacitance and charge relaxation resistance of chaotic cavities —Joint distribution of two linear statistics in the Laguerre ensemble of random matrices, Europhys. Lett. **109**(5), 50004 (2015).

☞ http://dx.doi.org/10.1209/0295-5075/109/50004

Chapter 4

Truncated linear statistics

A lot of effort has been devoted to the analysis of linear statistics. In Chapter 2, we have presented the Coulomb gas technique, which is a very convenient method to study the full distribution of these linear statistics (typical and atypical fluctuations). We have applied this method in Chapter 3 to study the joint distribution of two linear statistics.

In our Refs. [160, 161] (Article 3 and Article 4), we have introduced a new type of observable which we have called *truncated linear statistics*. For a $N \times N$ random matrix with eigenvalues $\{\lambda_i\}$, we define a truncated linear statistics as

$$\tilde{\mathcal{L}} = \frac{1}{N} \sum_{n=1}^{K} f(\lambda_n) \,, \quad \text{with} \quad 1 \leqslant K \leqslant N \,, \tag{4.1}$$

where f can be any given function, not necessarily linear. Compared to the case of the usual linear statistics described in Chapter 2, we have an additional parameter K, which is the number of eigenvalues contributing to $\tilde{\mathcal{L}}$. If $K = N$, we recover the case of the usual linear statistics. For $K < N$, we can consider two possibilities:

(1) We fix the subset of eigenvalues that contribute to (4.1), for example the K largest ones. This case constitutes an intermediate situation between two well-studied problems: the distribution of the full linear statistics ($K = N$) and extreme value statistics when keeping only the largest eigenvalue ($K = 1$), which has been much studied [47, 101, 102, 183, 213, 294, 295, 300] (see also the review [212]).

This situation is relevant for example in the context of data compression or in statistics, for principal component analysis [214, 277] (one keeps a given number of the top eigenvalues, which carry the most relevant information).

This first case is the object of Ref. [161] (Article 3). In this paper, we have applied this question to a model of fluctuating interfaces in statistical physics.

(2) We let any possible subset of K eigenvalues contribute.

We have studied this case in Ref. [160] (Article 4) in the context of quantum scattering. We have studied the contribution to the density of states of a given number of scattering channels in a multiterminal quantum dot.

In order to compare these two cases and make the analysis more concrete we will focus on an example of truncated linear statistics, coming from a model of fluctuating

interfaces discussed in [161] (Article 3). This model was shown to be related to random matrices in Ref. [249]. We describe it in Section 4.1. In Section 4.2, we analyse the case of the truncated linear statistics constrained to select the largest eigenvalues (case (1)). The other situation, in which all the eigenvalues can contribute, is described in Section 4.3 (case (2)).

4.1 A model of fluctuating interfaces

The analysis of the truncated linear statistics will be based on a model of N non intersecting elastic and fluctuating interfaces in $1+1$ dimensions. This model was originally introduced by de Gennes [98], and later studied by Fisher [134] in the context of surface wetting or depositions of atoms on a substrate. Each interface is described by its height $h_n(x)$, with $n = 1, \dots, N$. We will suppose that the interfaces evolve on top of a substrate of size L, located at height zero, so that $h_n(x) > 0$ as shown in Fig. 4.1. For simplicity, we will assume periodic boundary conditions. To each interface can be associated an energy

$$\mathcal{E}[h_n(x)] = \int_0^L \left[\frac{1}{2} \left(\frac{\mathrm{d}h}{\mathrm{d}x} \right)^2 + \mathcal{V}(h_n(x)) \right] \mathrm{d}x \,, \tag{4.2}$$

which is the sum of the elastic energy (first term) and some potential energy. For the choice of the potential, we follow Ref. [249] and choose a sum of harmonic confinement, and a repulsion from the substrate, leading to the form

$$\mathcal{V}(h) = \frac{b^2 h^2}{2} + \frac{\alpha(\alpha-1)}{2h^2} \,, \tag{4.3}$$

with $b > 0$ and $\alpha > 1$. The repulsion in $1/h^2$ can be justified from entropic considerations [134, 249]. The energy of the N interfaces is then simply

$$E_{\text{interf}}[\{h_n(x)\}] = \sum_{n=1}^{N} \mathcal{E}[h_n(x)] \,, \quad \text{with} \quad h_1 > h_2 > \cdots > h_N \,. \tag{4.4}$$

At thermal equilibrium, we can associate to each configuration $\{h_n(x)\}$ a Boltzmann weight

$$P[\{h_n(x)\}] \propto \exp\left\{ -\frac{1}{k_B T} E_{\text{interf}}[\{h_n(x)\}] \right\} \,, \tag{4.5}$$

where k_B is the Boltzmann constant and T the temperature. In the following we set $k_B T = 1$ for convenience. Let us consider the set of heights $\{h_n(x)\}$ at a given point x, see Fig. 4.1. Since we chose periodic boundary conditions the system has translational invariance, thus the joint distribution of the height do not depend on the position x and we will simply denote $\{h_n\}$ the set of heights at a given position x. Their joint distribution was derived in [249] by mapping these heights onto the positions of free fictitious quantum particles. Since the interfaces cannot cross, these particles are fermions. In the limit of large system size $L \to \infty$, their distribution is controlled by the many body ground state wave function $\Psi_0(h_1, \dots, h_N)$. This yields:

$$\mathcal{P}_{\text{interf}}(h_1, \dots, h_N) \propto \prod_{i<j} (h_i^2 - h_j^2)^2 \prod_{n=1}^{N} h_n^{2\alpha} \, \mathrm{e}^{-b h_n^2} \,. \tag{4.6}$$

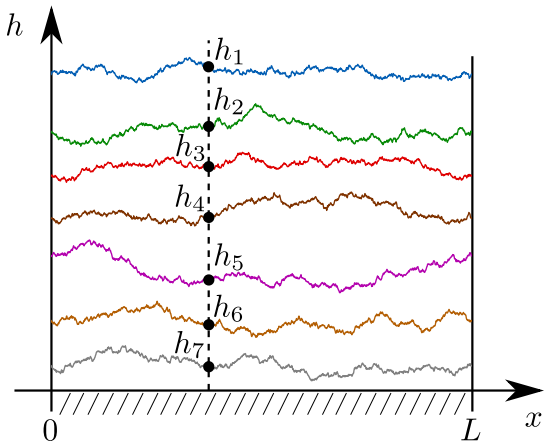

Figure 4.1: Non intersecting Brownian on top of a substrate (at $h = 0$), with periodic boundary conditions. The distribution of a set of heights $\{h_n\}$ at a given position x is independent of x due to translational invariance.

Making the change of variables $\lambda_n = bh_n^2$, this distribution reduces to

$$\mathcal{P}(\lambda_1, \dots, \lambda_N) \propto \prod_{i<j} (\lambda_i - \lambda_j)^2 \prod_{n=1}^{N} \lambda_n^{\alpha - 1/2} \, \mathrm{e}^{-\lambda_n} \,, \quad \lambda_n > 0 \,. \tag{4.7}$$

We recognise the joint distribution of eigenvalues in the Laguerre ensemble (1.38). The Vandermonde determinant simply comes from the condition that the interfaces do not cross. It is raised to the power $\beta = 2$, which is not related to the breaking of time reversal symmetry as usual in applications of random matrices to quantum mechanics, as discussed in Section 1.1. This particular value comes from the fact that the probability density (4.6) is the square of the many body wave function: $\mathcal{P}_{\text{interf}} = |\Psi_0|^2$.

Knowing the joint distribution of heights (4.6,4.7), one can study the statistical properties of observables associated to the set of interfaces $\{h_n\}$. For instance, the centre of mass of all the interfaces is given by

$$G = \frac{1}{N} \sum_{n=1}^{N} h_n = \frac{1}{N\sqrt{b}} \sum_{n=1}^{N} \sqrt{\lambda_n} \,. \tag{4.8}$$

This quantity is a linear statistics, of the form (2.25) with $f(\lambda) = \sqrt{\lambda}$. Its distribution was analysed in Ref. [249] by a Coulomb gas method. Here, we will study the distribution of the centre of mass of the top K interfaces:

$$\tilde{G} = \frac{1}{K} \sum_{n=1}^{K} \sqrt{\lambda_n} \,, \tag{4.9}$$

where we set $b = 1$ for simplicity. We recognise the expression of the truncated linear statistics (4.1), restricted to the top K eigenvalues, with $f(\lambda) = \sqrt{\lambda}$ (case (1)). In Section 4.2 we will analyse the distribution of this quantity in the limit $N \to \infty$ with $\kappa = K/N$ fixed. In a second step, we will release the constraint that only the top K interfaces contribute, and allow any subset of K interfaces contribute (case (2)). This is the object of Section 4.3.

As in the previous chapters, we will study the distribution of (4.9) by a Coulomb gas method. We thus rewrite the joint distribution (4.7) in the form (2.1) by denoting

$\lambda_n = N x_n$. We obtain

$$\mathcal{P}(x_1, \ldots, x_N) \propto \prod_{i<j} (x_i - x_j)^\beta \prod_{n=1}^{N} \mathrm{e}^{-N V(x_n)} \,, \quad x_n > 0 \,, \tag{4.10}$$

where $\beta = 2$ for the interface model, and we introduced the potential

$$V(x) = x - \frac{1}{N}\left(\alpha - \frac{1}{2}\right) \ln x \,, \quad x > 0 \,. \tag{4.11}$$

In the limit $N \to \infty$, for fixed α, this reduces to the linear potential

$$V(x) = x \,, \qquad x > 0 \,. \tag{4.12}$$

From the discussion of Chapter 2, for large N the x_i's remain of order N^0. To consider only quantities which do not scale with N, we introduce

$$s = \frac{\kappa}{\sqrt{N}} \tilde{G} = \frac{1}{N} \sum_{n=1}^{\kappa N} \sqrt{x_n} \,, \qquad \kappa = \frac{K}{N} \,. \tag{4.13}$$

In the following, we will derive the distribution of s, for fixed $\kappa \in]0, 1[$, in the limit $N \to \infty$ in the two situations described above.

4.2 Truncated linear statistics restricted to the largest eigenvalues

In this section, we analyse the distribution of the rescaled centre of mass s of the $K = \kappa N$ highest interfaces. We can rewrite (4.13) as

$$s = \frac{1}{N} \sum_{n=1}^{K} \sqrt{x_n} \,, \quad x_1 > x_2 > \cdots > x_N \,, \tag{4.14}$$

where the x_i's are picked from the joint distribution (4.10), corresponding to the Laguerre ensemble of random matrices. We have adapted the Coulomb gas method described in Chapter 2 to this new type of observable. Here, we will give an overview of the derivation and summarise the main results. The details are published in Ref. [161], which is included at the end of this Chapter (Article 3).

4.2.1 The Coulomb gas formulation

To study the distribution of the truncated linear statistics s, we adapt the Coulomb gas method to this new type of observable. We again interpret the $\{x_i\}$ as the positions of charges in a 1D gas, with density

$$\rho(x) = \frac{1}{N} \sum_{n=1}^{N} \delta(x - x_n) \tag{4.15}$$

and energy

$$\mathscr{E}[\rho] = -\int \mathrm{d}x \int \mathrm{d}y \, \rho(x)\rho(y) \ln|x - y| + \int x \, \rho(x) \, \mathrm{d}x \,, \tag{4.16}$$

where we used (2.87) with the potential (4.12). We can rewrite (4.14) in terms of the density ρ as

$$s = \int_c \sqrt{x}\, \rho(x)\, \mathrm{d}x\,, \tag{4.17}$$

where c is a lower bound which ensures that only the top $K = \kappa N$ eigenvalues contribute to s. This means that c is the position of the K^{th} charge: $c = x_K$. We can re-express this condition as

$$\int_c \rho(x)\, \mathrm{d}x = \kappa\,. \tag{4.18}$$

A dual problem was considered in Ref. [214], in which the authors have studied the distribution of the number of eigenvalues above a fixed threshold in the Laguerre ensembles (see also Refs. [210, 217] for the number of positive eigenvalues in the Gaussian or Cauchy ensembles). In their case, c is the fixed threshold, and the fraction κ of eigenvalues above it is a random quantity. Here we fix this fraction κ while the boundary c can fluctuate.

Following the procedure of Section 2.2.5, we should find the minimum of the energy (4.16), under the constraints (4.17) and (4.18), with the condition that ρ is normalised to unity. We thus introduce the functional

$$\mathscr{F}[\rho;\kappa,s;\mu_0^{(1)},\mu_0^{(2)},\mu_1] = \mathscr{E}[\rho] + \mu_0^{(1)}\left(\int^c \rho(x)\mathrm{d}x - (1-\kappa)\right) + \mu_0^{(2)}\left(\int_c \rho(x)\mathrm{d}x - \kappa\right) + \mu_1\left(\int_c \sqrt{x}\,\rho(x)\,\mathrm{d}x - s\right)\,, \tag{4.19}$$

where $\mu_0^{(1)}$, $\mu_0^{(2)}$ and μ_1 are Lagrange multipliers enforcing the constraints. The minimum is given by $\frac{\delta\mathscr{F}}{\delta\rho(x)} = 0$. Taking a derivative with respect to x gives

$$2\fint \frac{\rho_\star(y;\kappa,s)}{x-y}\mathrm{d}y = 1 + \begin{cases} 0 & \text{for } x < c\,, \\ \dfrac{\mu_1}{2\sqrt{x}} & \text{for } x > c\,. \end{cases} \tag{4.20}$$

As in Section 2.2.5, we can again interpret this equation as a force balance on the charge located at position x. But this time, the additional force coming from the constraint on s acts only on the fraction κ of the rightmost charges. Depending on the sign of μ_1, this force pushes these charges either towards or away from the origin, as illustrated in Fig. 4.2. We will thus distinguish these two cases in the following.

In order to solve Eq. (4.20), it is convenient to split the density into two parts: one which contains to rightmost $K = \kappa N$ charges, which we denote ρ_2, and the second which contains the other charges, denoted ρ_1:

$$\rho_\star(x;\kappa,s) = \begin{cases} \rho_1(x) & \text{for } x < c\,, \\ \rho_2(x) & \text{for } x > c\,. \end{cases} \tag{4.21}$$

We will denote $[a,b]$ the support of ρ_1, and $[c,d]$ the support of ρ_2. The force balance equation (4.20) rewrites

$$2\int_a^b \frac{\rho_1(y)}{x-y}\mathrm{d}y + 2\fint_c^d \frac{\rho_2(y)}{x-y}\mathrm{d}y = 1 + \frac{\mu_1}{2\sqrt{x}} \qquad \text{for } x > c\,, \tag{4.22}$$

$$2\fint_a^b \frac{\rho_1(y)}{x-y}\mathrm{d}y + 2\int_c^d \frac{\rho_2(y)}{x-y}\mathrm{d}y = 1 \qquad \text{for } x < c\,. \tag{4.23}$$

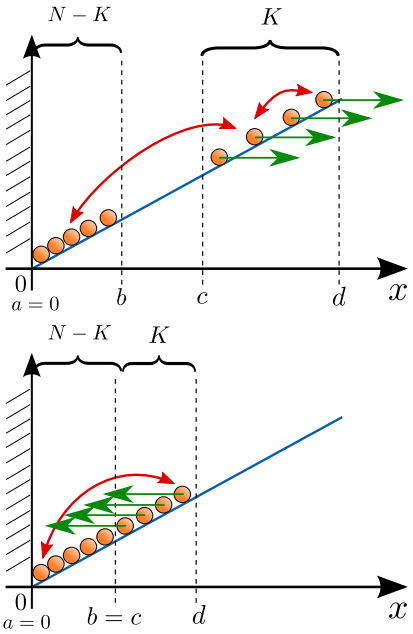

Figure 4.2: Coulomb gas in the external potential (4.12), with a wall at $x = 0$ coming from the positivity of the eigenvalues. The constraint on s translates in an additional external force applied only on the $K = \kappa N$ rightmost charges. If $\mu_1 < 0$, this force pulls these charges away from the origin (top). If $\mu_1 > 0$, it pushed them, and consequently the whole gas, towards the bottom of the well (bottom).

The procedure to solve this type of coupled equations was introduced in Refs. [210, 211], in the study the distribution of the number of positive eigenvalues of Gaussian matrices (which is a linear statistics). The method relies on Tricomi's theorem (see Appendix A.5). We first solve Eq. (4.23) to express ρ_1 in terms of ρ_2. We then plug the result in Eq. (4.22), which gives an equation on ρ_1 only. Solving this equation then yields ρ_1 and thus $\rho_\star$. We will not perform explicitly this derivation here, as it is quite cumbersome. We refer to the appendix of Article 3. We only list the results here.

Optimal density

The optimal density without constraint is obtained by setting $\mu_1 = 0$. Then, solving Eq. (4.20) we recover the Marčenko-Pastur distribution introduced in Section 2.1.2:

$$\rho_0(x) = \frac{1}{2\pi}\sqrt{\frac{4-x}{x}}\,. \tag{4.24}$$

The divergence at the origin corresponds to an accumulation of charges at the bottom of the well. As usual, relaxing the constraint corresponds to the typical density, associated to the typical value s_0, given by (4.17):

$$s_0(\kappa) = \int_{c_0}^{4} \sqrt{x}\,\rho_0(x)\,\mathrm{d}x = \frac{(4-c_0)^{3/2}}{3\pi}\,, \tag{4.25}$$

where c_0 is determined by (4.18):

$$\kappa = \int_{c_0}^{4} \rho_0(x)\,\mathrm{d}x = \frac{2}{\pi}\arccos\frac{\sqrt{c_0}}{2} - \frac{\sqrt{c_0(4-c_0)}}{2\pi}\,. \tag{4.26}$$

These two equations give a parametric representation of the line $s_0(\kappa)$ in the (κ, s) plane. It is the solid line represented in Fig. 4.4. For a given value of κ, it gives the most probable value $s_0(\kappa)$ of the truncated linear statistics.

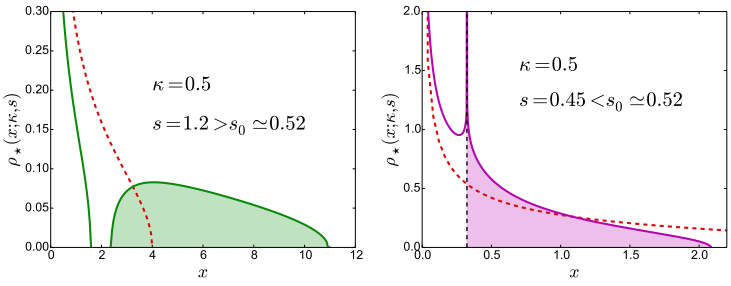

Figure 4.3: Optimal density $\rho_\star(x; s, r)$ (solid line), compared to the Marčenko-Pastur density ρ_0 (dashed) obtained when releasing the constraint. Left: Phase I, Right: Phase II. The shaded areas correspond to the κN rightmost charges.

Phase I: $\mu_1 < 0$

The case $\mu_1 < 0$ corresponds to an additional force that pulls the rightmost charges to the right, away from the origin. Since the other charges are not subjected to this force, we do not expect them to move much. Therefore, the density $\rho_\star$ should split into two disjoint bulks, corresponding to $b < c$. This is illustrated in Fig. 4.2 (top). Since the rightmost charges are pulled towards the large x, this corresponds to a value of s, given by (4.17), larger than the typical value $s_0(\kappa)$.

We can check that this heuristic argument is correct by solving Eqs. (4.22,4.23). Remarkably, this can be done analytically, and yields a compact expression:

$$\rho_\star(x;\kappa,s) = \frac{\mu_1}{2\pi^2}\frac{\mathrm{sign}(x-c)}{\sqrt{d-b}}\sqrt{\frac{(c-x)(b-x)}{x(d-x)}}\,\Pi\left(\frac{d-c}{d-x},\sqrt{\frac{d-c}{d-b}}\right), \tag{4.27}$$

where Π is the complete elliptic integral of the third kind defined by Eq. (C.3). This density is represented in Fig. 4.3 (left).

We can easily estimate the leading behaviour of the energy in the limit $s \to \infty$ by a heuristic argument. For large s, the κN rightmost charges are pushed towards infinity. The typical position x_{typ} of these charges is obtained from (4.17), which gives

$$s \simeq \kappa\sqrt{x_{\mathrm{typ}}} \quad \Rightarrow \quad x_{\mathrm{typ}} \simeq s^2/\kappa^2\,. \tag{4.28}$$

The energy of these charges is dominated by their potential energy, thus

$$\mathscr{E}[\rho_\star(x;\kappa,s)] \simeq \int_c \rho_\star(x;\kappa,s)V(x)\mathrm{d}x \simeq \kappa\, V(x_{\mathrm{typ}}) \simeq s^2/\kappa\,, \tag{4.29}$$

where we introduced an additional factor κ since only the κN rightmost charges contribute. This heuristic derivation is validated by a precise analytic computation, which also yields the next term:

$$\mathscr{E}[\rho_\star(x;\kappa,s)] = \frac{s^2}{\kappa} + \kappa(3\kappa-4)\ln s + \mathcal{O}(1) \quad \text{for} \quad s \to \infty\,. \tag{4.30}$$

Phase II: $\mu_1 > 0$

We now consider the second case, $\mu_1 > 0$. It corresponds to an additional force that pushes the rightmost charges towards the origin. It thus corresponds to $s < s_0(\kappa)$. In

this case, the solution of Eqs. (4.22,4.23) give a simpler result:

$$\rho_\star(x;\kappa,s) = \frac{1}{2\pi}\sqrt{\frac{d-x}{x}} + \frac{\mu_1}{4\pi^2\sqrt{x}} \ln \frac{\sqrt{d-c}+\sqrt{d-x}}{\left|\sqrt{d-c}-\sqrt{d-x}\right|} \,. \tag{4.31}$$

This density is supported on the interval $[0,d]$ (here $b=c$). Remarkably, this density exhibits a logarithmic divergence *in the bulk*, at $x=c$, where the two densities ρ_1 and ρ_2 meet:

$$\rho_\star(x;\kappa,s) \simeq -\frac{\mu_1}{4\pi^2\sqrt{c}} \ln|x-c| \;, \quad \text{for} \quad x \to c \,. \tag{4.32}$$

This singularity is clearly visible in Fig. 4.3 (right). We stress that this is very unusual in the framework of the Coulomb gas to obtain such a behaviour for a density of eigenvalues. A logarithmic divergence has already been exhibited at the edge of a density in Ref. [249], with a behaviour $-\ln x/\sqrt{x}$. However, this behaviour comes from the specific linear statistics discussed in this paper. Here, the logarithmic singularity in the bulk comes from the new type of constraint on the gas induced from the consideration of truncated linear statistics. We have shown that the logarithmic divergence (4.32) is **universal** with respect to the matrix ensemble and the function f of the truncated linear statistics (as long as it is monotonous). See Ref. [161], included at the end of this Chapter.

As in the previous phase, we can analyse heuristically the behaviour of the energy for $s \to 0$. This corresponds to pushing the rightmost charges towards the origin. Therefore, all the charges are confined in a small domain of typical size

$$x_{\text{typ}} \simeq s^2/\kappa^2 \,, \tag{4.33}$$

which corresponds to a typical spacing $\delta x \simeq x_{\text{typ}}/N$. The energy is then dominated by the repulsion between the charges, thus

$$\mathscr{E}[\rho_\star(x;\kappa,s)] \simeq -\int \mathrm{d}x \int \mathrm{d}y \; \rho_\star(x;\kappa,s)\rho_\star(y;\kappa,s) \ln|x-y| \simeq -\ln \delta x \simeq -2\ln s \,. \tag{4.34}$$

This behaviour can similarly be checked from a careful analytical computation.

Phase diagram and transition

For a fixed value of κ (corresponding to a vertical line in the phase diagram in Fig. 4.4), the parameter s drives a phase transition in the Coulomb gas. This transition occurs for $s = s_0(\kappa)$, corresponding to $\mu_1 = 0$. At the transition point, the density is given by the Marčenko-Pastur distribution (4.24). For $s > s_0(\kappa)$, the density of the gas has a gap, while for $s < s_0(\kappa)$ it exhibits a logarithmic singularity.

The order of the transition is obtained by studying the behaviour of the energy $\mathscr{E}[\rho_\star(x;\kappa,s)]$ at the transition. One can show that all the derivatives of the energy are continuous on each side of the transition point $s_0(\kappa)$. However, the energy is not analytic at this point:

$$\mathscr{E}[\rho_\star(x;\kappa,s_0(\kappa)+\varepsilon)] - \mathscr{E}[\rho_\star(x;\kappa,s_0(\kappa)-\varepsilon)] = \mathcal{O}(\varepsilon\, \mathrm{e}^{-\gamma/\varepsilon}) \quad \text{as } \varepsilon \to 0^+ \,, \tag{4.35}$$

where

$$\gamma = \frac{\sqrt{4-c_0}}{\pi}(4 - c_0 + c_0 \ln c_0/4) \tag{4.36}$$

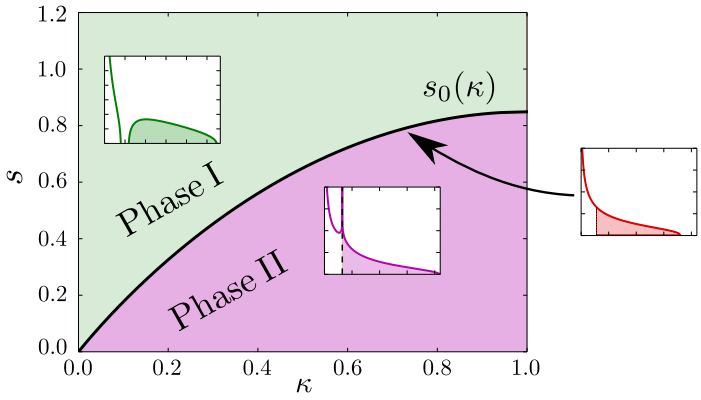

Figure 4.4: Phase diagram for the Coulomb gas.

and c_0 is obtained from Eq. (4.26). Therefore, following the usual terminology of statistical physics, this corresponds to an *infinite order* phase transition. The details are given in Article 3.

4.2.2 Distribution of the truncated linear statistics

Having obtained the optimal density $\rho_\star(x;\kappa,s)$ for all values of κ and s, we can now analyse the distribution of the truncated linear statistics (4.14). From the analysis of Section 2.2.5, it is given by

$$P^{(\mathrm{top})}_{N,\kappa}(s) \sim \exp\left[-\frac{\beta N^2}{2}\Phi_\kappa(s)\right] , \quad \Phi_\kappa(s) = \mathscr{E}[\rho_\star(x;\kappa,s)] - \mathscr{E}[\rho_0(x)] , \tag{4.37}$$

where only $\beta = 2$ is relevant for the interface model. The large deviation function Φ_κ can be conveniently studied by making use of the thermodynamic identity (2.100):

$$\frac{\mathrm{d}\Phi_\kappa}{\mathrm{d}s} = -\mu_1 . \tag{4.38}$$

This large deviation function Φ_κ is represented in Fig. 4.5.

Typical fluctuations

The typical value of s, given by $\mu_1 = 0$, is $s_0(\kappa)$ obtained from Eqs. (4.25,4.26). We deduce the mean value of the centre of mass (4.9):

$$\left\langle \tilde{G} \right\rangle = \frac{\sqrt{N}}{\kappa} s_0(\kappa) . \tag{4.39}$$

The fluctuations near this point can be obtained from the behaviour of μ_1 near 0. We obtain

$$\Phi_\kappa(s) = \frac{\pi^2}{4 - c_0 + c_0 \ln c_0/4}[s - s_0(\kappa)]^2 + \mathcal{O}([s - s_0(\kappa)]^3) , \tag{4.40}$$

where c_0 is given by (4.26). This corresponds to a Gaussian peak of the distribution near $s = s_0(\kappa)$. We straightforwardly deduce

$$\mathrm{Var}(s) = \frac{2}{\pi^2 \beta N^2}\left(4 - c_0 + c_0 \ln \frac{c_0}{4}\right) . \tag{4.41}$$

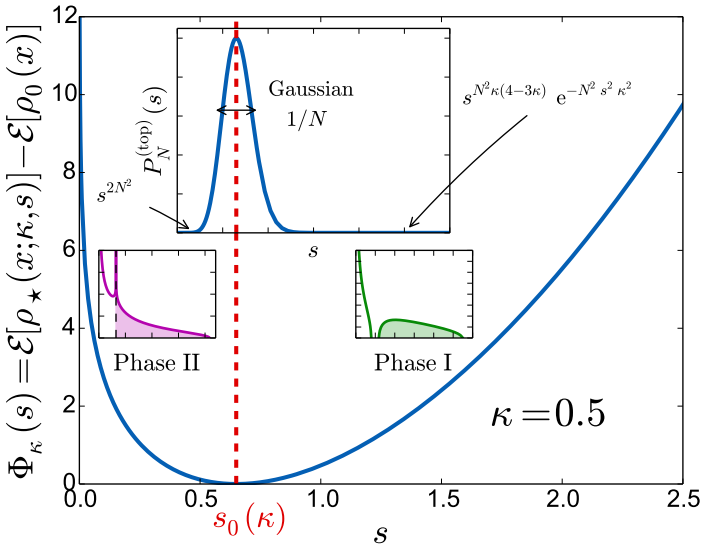

Figure 4.5: Large deviation function $\Phi_\kappa(s)$, associated to the distribution of the centre of mass of the κN highest interfaces (inset, for $\beta = 2$). The optimal density $\rho_\star$ for the Coulomb gas is also shown for the two phases. The phase transition occurs at $s = s_0(\kappa)$, represented by the vertical dashed line.

We recognise the usual scaling of the variance in $1/\beta N^2$, characteristic of the fluctuations of a linear statistics.

Large deviations for $s \to \infty$

This asymptotic form (4.30) yields the behaviour

$$P_{N,\kappa}^{(\mathrm{top})}(s) \sim s^{\beta N^2 \kappa(4-3\kappa)/2}\, \mathrm{e}^{-\beta N^2 s^2/2\kappa} \quad \text{for} \quad s \to \infty\,. \tag{4.42}$$

Large deviations for $s \to 0$

We deduce from (4.34):

$$P_{N,\kappa}^{(\mathrm{top})}(s) \sim s^{\beta N^2} \quad \text{for} \quad s \to 0\,, \tag{4.43}$$

which does not depend on κ. This fact can be understood easily: unlike the case $s \to \infty$, the energy is dominated by the interaction part and involves all the charges, as they are all confined by the wall at $x = 0$. Therefore, the energy of the gas is independent of κ.

A sketch of the distribution $P_{N,\kappa}^{(\mathrm{top})}(s)$, along with the behaviours (4.40), (4.42) and (4.43), is represented in Fig. 4.5.

4.2.3 A universal mechanism

We have analysed in details the distribution of the truncated linear statistics (4.14) in the Laguerre ensemble (4.10). For fixed $\kappa = K/N$, we have shown that in the limit $N \to \infty$ the underlying Coulomb gas undergoes a phase transition of infinite order, located at the most probable value of s, given by $s_0(\kappa)$.

Furthermore, we can show that for any choice of function f for the linear statistics, provided it is monotonous, and any matrix ensemble, the Coulomb gas will always exhibit an infinite order phase transition, at the typical value $s_0(\kappa)$ determined by

$$s_0(\kappa) = \int_{c_0} f(x)\, \rho_0(x)\, \mathrm{d}x\,, \tag{4.44}$$

where ρ_0 is the typical density of eigenvalues in the matrix ensemble under consideration, and c_0 is fixed by

$$\kappa = \int_{c_0} \rho_0(x)\, \mathrm{d}x \,. \tag{4.45}$$

This transition delimits two phases: one with a gap in the density and one with a logarithmic divergence in the bulk. Depending on the choice of f the Coulomb gas may have other phase transitions, but the neighbourhood of the typical value $s_0(\kappa)$ is always characterised by the universal mechanism described above. This is proved in the Appendix of Article 3.

4.2.4 Singular nature of the limits $\kappa \to 0$ and $\kappa \to 1$

Note that in the case $\kappa = 1$ studied in Ref. [249], with the same function $f(x) = \sqrt{x}$, the Coulomb gas undergoes infinite order phase transition at the typical value $s_0(1)$. We can straightforwardly take the limit $\kappa \to 1$ in the results above to obtain the distribution of the full linear statistics. We stress that this is not the case in general (for arbitrary f). For most linear statistics ($\kappa = 1$) the Coulomb gas does not undergo an infinite order phase transition at the typical value $s_0(1)$, as it does for $\kappa < 1$. Therefore the limit $\kappa \to 1$ is singular and we cannot recover the phase diagram at $\kappa = 1$ from the one obtained for $\kappa < 1$. An example is given in the conclusion of Ref. [161] (Article 3).

The limit $\kappa \to 0$ is also singular. Indeed, the extreme case corresponds to take only $K = 1$ eigenvalue, which is thus the largest. This corresponds to $\kappa = 1/N$, which cannot be studied by our Coulomb gas method, as it would require to obtain the subdominant contribution in $1/N$ whereas the Coulomb gas provides only the dominant one.

The singularity of these limits comes from the non-commutativity of the limits $\kappa \to 0$ (or $\kappa \to 1$) and $N \to \infty$. It would be interesting to study more closely these limits to see how the universal mechanism described here transitions to the ones known for the largest eigenvalue ($\kappa = 1/N$) [47, 101, 102, 212, 213, 300] and for the full linear statistics ($\kappa = 1$) [77, 94, 210, 211, 214, 217, 218, 249–251, 286, 301, 302].

4.3 Unconstrained truncated linear statistics

In the previous Section we have studied the distribution of the truncated linear statistics (4.13), with the condition that only the largest eigenvalues contribute. We now relax this constraint and consider the situation where the $x_i's$ involved in

$$s = \frac{1}{N} \sum_{n=1}^{K} \sqrt{x_n} \,, \tag{4.46}$$

are not necessarily ordered, such that any subset of $K = \kappa N$ eigenvalues can contribute to s. This problem has been studied in Ref. [160] (Article 4), for a different linear statistics from motivations from quantum scattering in a chaotic quantum dot. Here, in order to compare with the case where only the largest eigenvalues contribute, we will analyse the distribution of (4.46).

4.3.1 A new matrix ensemble

Our approach is based on the Coulomb gas method, which treats the eigenvalues as indistinguishable variables. Therefore, to keep track of the eigenvalues of interest, we must introduce an additional set of N random variables, denoted $\{n_i\}$, defined as

$$n_i = \begin{cases} 1 & \text{if } x_i \text{ contributes to } s\,, \\ 0 & \text{otherwise.} \end{cases} \tag{4.47}$$

The condition that we select a fixed number $K = \kappa N$ of eigenvalues becomes

$$\sum_{i=1}^{N} n_i = K = \kappa N\,. \tag{4.48}$$

We can then rewrite the truncated linear statistics (4.46) as a sum over all the eigenvalues:

$$s = \frac{1}{N}\sum_{n=1}^{N} n_i \sqrt{x_i}\,. \tag{4.49}$$

In this form, since we have restored the symmetry under the permutation of the x_i's, we can now suppose that the eigenvalues are ordered, $x_1 > x_2 > \cdots > x_N$. Note that the case of the largest eigenvalues discussed in Section 4.2 is obtained by imposing $n_1 = n_2 = \cdots = n_K = 1$ and $n_{K+1} = \cdots = n_N = 0$. Here, we consider the case where the n_i's are no longer fixed. This corresponds to introduce the joint distribution of the two sets of random variables:

$$\boxed{\mathscr{P}_{N,\kappa}(\{x_i\},\{n_i\}) \propto \mathcal{P}(\{x_i\})\, \mathbb{1}_{x_1>x_2>\cdots>x_N}\, \delta_{\sum n_i,\kappa N}} \tag{4.50}$$

where $\mathcal{P}(\{x_i\})$ is the joint distribution of the eigenvalues (4.10) and

$$\mathbb{1}_{x_1>x_2>\cdots>x_N} = \prod_{i=1}^{N} \Theta(x_i - x_{i+1}) \tag{4.51}$$

ensures that the eigenvalues are ordered (Θ is the Heaviside step function).

Within this new ensemble (4.50), our aim is to determine the distribution of the truncated linear statistics (4.49), which is given by

$$P_{N,\kappa}(s) = \sum_{\{n_i\}} \int \mathrm{d}x_1 \cdots \mathrm{d}x_N\, \mathscr{P}_{N,\kappa}(\{x_i\},\{n_i\})\, \delta\left(s - \frac{1}{N}\sum_{i=1}^{N} n_i\sqrt{x_i}\right)\,, \tag{4.52}$$

in the limit $N \to \infty$. We will again use the Coulomb gas method and write

$$\mathscr{P}_{N,\kappa}(\{x_i\},\{n_i\}) \propto \mathrm{e}^{-\frac{\beta N^2}{2} E[\{x_n\}]}\, \mathbb{1}_{x_1>x_2>\cdots>x_N}\, \delta_{\sum n_i,\kappa N}\,, \tag{4.53}$$

where the energy of the gas is

$$E[\{x_n\}] = -\frac{1}{N^2}\sum_{i\neq j} \ln|x_i - x_j| + \frac{1}{N}\sum_{i=1}^{N} x_i\,, \tag{4.54}$$

which is $\mathcal{O}(N^0)$. In the limit $N \to \infty$, we will again perform a saddle point estimate to find the optimal configurations of $\{x_i\}$ and $\{n_i\}$ that dominate (4.52).

Remark: Relation with the thinned ensembles

The ensemble (4.50) is related to the *thinned ensembles* introduced by Bohigas and Pato [46] to describe the transition from the spectral statistics of random matrices (strongly correlated) to Poisson statistics (independent variables). These ensembles have been well-studied in the literature, see for instance Refs. [38, 80, 199]. The thinned ensembles are obtained by removing each eigenvalue x_i with a given probability κ. They correspond to the distribution

$$\mathscr{P}^{(\text{thinned})}_{N,\kappa}(\{x_i\},\{n_i\}) \propto \mathcal{P}(\{x_i\})\, \mathbb{1}_{x_1>x_2>\cdots>x_N}\, \kappa^{\sum n_i}(1-\kappa)^{\sum n_i}\,. \tag{4.55}$$

This is somehow a "grand canonical" version of the problem we consider here, as the final number of eigenvalues obtained can fluctuate while we impose it to be fixed to κN in (4.50). Because of the strong correlations between the variables, it is far from obvious that the two ensembles are equivalent.

4.3.2 Typical density of eigenvalues

In the absence of constraint, the typical configuration of charges $\{x_i^{(0)}\}$ is given by the minimum of the energy (4.54):

$$\left.\frac{\partial E}{\partial x_i}\right|_{\{x_i^{(0)}\}} = 0\,. \tag{4.56}$$

As we have seen in Section 4.2, in the limit $N \to \infty$, this optimal configuration is associated to the Marčenko-Pastur distribution $\rho_0(x)$, given by Eq. (4.24).

In Section 4.2 we restricted to the contribution of the largest eigenvalues. From the typical density ρ_0 we deduced the typical value $s_0(\kappa)$ (maximum of $P^{(\text{top})}_{N,\kappa}$) simply by selecting the $K = \kappa N$ largest eigenvalues, see Eqs. (4.25,4.26). Here, we have the freedom to choose any subset of K eigenvalues to contribute to s. We can thus construct $\binom{N}{K}$ different values of s, without moving the eigenvalues, therefore without any energy cost for the Coulomb gas. The maximal accessible value is given by $s_0(\kappa)$ (selecting the largest eigenvalues, cf. Fig. 4.6, left). Conversely, the minimal accessible value $s_1(\kappa)$ is obtained by selecting the smallest eigenvalues (see Fig. 4.6, right). Thus,

$$s_1(\kappa) = \int_0^{b_0} \sqrt{x}\, \rho_0(x)\, \mathrm{d}x\,, \tag{4.57}$$

where b_0 is given by

$$\kappa = \int_0^{b_0} \rho_0(x)\, \mathrm{d}x\,. \tag{4.58}$$

In the entire interval $[s_1(\kappa), s_0(\kappa)]$, the Coulomb gas is frozen to its optimal density ρ_0 (minimum of the energy), and only the n_i's fluctuate. Outside this interval we have to deform the density ρ, as we have done in Section 4.2. The phase diagram of the Coulomb gas thus involves (at least) two critical lines, $s_0(\kappa)$ and $s_1(\kappa)$.

We will come back to the analysis of the typical fluctuations in Section 4.3.4, but first we will analyse the large deviations, outside the interval $[s_1(\kappa), s_0(\kappa)]$.

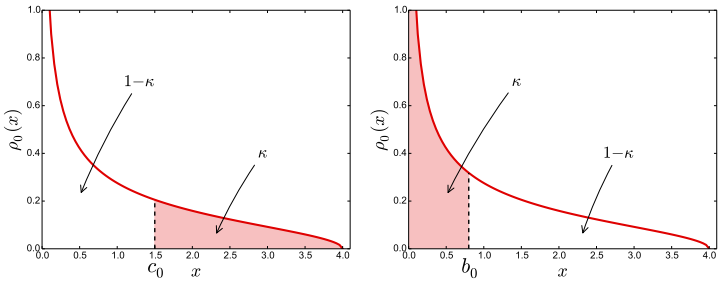

Figure 4.6: The two extreme cases obtained from the Marčenko-Pastur distribution (4.24): either we select only the top eigenvalues (left), or the smallest (right).

4.3.3 Large deviations

To analyse the distribution (4.52), let us first study the atypical fluctuations, corresponding to small or large values of s.

Phase I

Consider the limit $s \to \infty$. From the expression of s, Eq. (4.46), it corresponds to $x_i \to \infty$ for all i such that $n_i = 1$:

$$x_i \to \infty \quad \text{if} \quad n_i = 1 \quad \Rightarrow \quad s \to \infty \,. \tag{4.59}$$

The other $N-K$ eigenvalues, which do not contribute to s, are not constrained, therefore they remain of order 1. The limit $s \to \infty$ thus selects only the largest eigenvalues:

$$n_1 = n_2 = \cdots = n_K = 1 \,, \quad n_{K+1} = \cdots = n_N = 0 \,. \tag{4.60}$$

The problem thus reduces to the case studied in Section 4.2, and we can directly transpose our results here. Therefore the distribution (4.52) is dominated by the density of eigenvalues $\rho_\star(x;\kappa,s)$ given by (4.27). In particular, its asymptotic behaviours are related to the behaviours of the energy (4.30,4.40):

$$\mathscr{E}[\rho_\star(x;\kappa,s)] - \mathscr{E}[\rho_0] \simeq \begin{cases} \dfrac{s^2}{\kappa} + \kappa(3\kappa-4)\ln s & \text{for } s \to \infty \,, \\ \alpha_0 (s - s_0(\kappa))^2 & \text{for } s \to s_0(\kappa)^+ \,, \end{cases} \tag{4.61}$$

where

$$\alpha_0 = \frac{\pi^2}{4 - c_0 + c_0 \ln c_0/4} \tag{4.62}$$

is obtained from (4.40), and c_0 is given by (4.26).

This derivation is valid as long as only the largest eigenvalues contribute to s. This is true if the gap between the two supports of $\rho_\star(x;\kappa,s)$ is larger than the typical spacing of the eigenvalues, which is of order N^{-1}. In the limit $N \to \infty$, this reduces to the condition

$$s > s_0(\kappa) \,, \tag{4.63}$$

where $s_0(\kappa)$ is given by Eqs. (4.25,4.26).

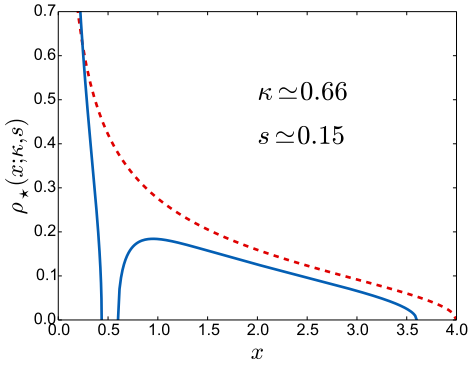

Figure 4.7: Optimal density for the Coulomb gas, given by Eq. (4.65). Only the fraction κ of charges contained in the left bulk contribute to s. The dashed lined is the Marčenko-Pastur distribution (4.24).

Phase III

The other limit can be studied similarly. If $s \to 0$, all the eigenvalues contributing to (4.49) must go to zero, which means they are the smallest:

$$n_1 = \cdots = n_{N-K-1} = 0\,, \quad n_{N-K} = \cdots = n_N = 1\,. \tag{4.64}$$

We can then adapt the derivation presented in the Appendix of Article 3 to consider the smallest eigenvalues. We obtain again an optimal density of charges with two disjoint supports $[0,b]$ and $[c,d]$, of the form:

$$\rho_\star(x;\kappa,s) = \frac{\mu_1}{2\pi}\sqrt{\frac{(b-x)(d-x)(c-x)}{x}}\fint_0^b \frac{\mathrm{d}t}{2\pi}\frac{1}{t-x}\frac{1}{\sqrt{(b-t)(c-t)(d-t)}}\,, \tag{4.65}$$

where the principal value is needed only if $x \in [0,b]$. The values of b, c, d and μ_1 are obtained from the conditions that this density vanishes at b, c and d (which have already been implemented to obtain the form (4.65)), along with the constraints

$$s = \int_0^b \sqrt{x}\,\rho_\star(x;\kappa,s)\,\mathrm{d}x\,, \qquad \kappa = \int_0^b \rho_\star(x;\kappa,s)\,\mathrm{d}x\,. \tag{4.66}$$

Note that this seems to give too many conditions, but one of them is redundant as it was used in the derivation of (4.65). This density is represented in Fig. 4.7.

As before, this phase exists as long as the two bulks remain separated by a gap. The limit of existence is thus $b = c$, which corresponds to

$$s < s_1(\kappa)\,, \tag{4.67}$$

where $s_1(\kappa)$ is given by Eqs. (4.57,4.58).

The behaviour of the energy of the gas can be studied similarly as in Section 4.2. We obtain

$$\mathscr{E}[\rho_\star(x;\kappa,s)] - \mathscr{E}[\rho_0] \simeq \begin{cases} -2\kappa^2 \ln s & \text{for } s \to 0\,, \\ \alpha_1 (s - s_1(\kappa))^2 & \text{for } s \to s_1(\kappa)^-\,, \end{cases} \tag{4.68}$$

where

$$\alpha_1 = \frac{\pi^2}{\sqrt{4-b_0} + \frac{b_0-8}{4} - \frac{b_0}{4}\ln\left(\sqrt{4-b_0} + \frac{8-b_0}{4}\right)} \tag{4.69}$$

and b_0 is given by Eq. (4.58).

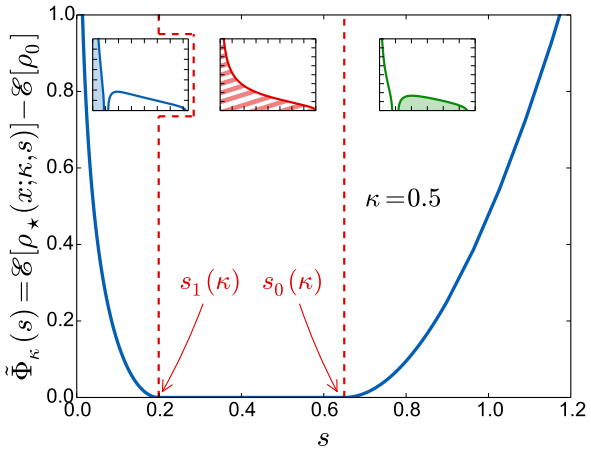

Figure 4.8: Large deviation function (energy of the Coulomb gas) as a function of s, for $\kappa = 0.5$. In the interval $[s_1(\kappa), s_0(\kappa)]$ it is exactly zero as the Coulomb gas is frozen to the Marčenko-Pastur distribution (4.24). The optimal densities $\rho_\star$ in each regions are represented in the insets.

Large deviation function – Second order phase transition

We have obtained the configuration of the charges $\{x_i\}$, associated to the density $\rho_\star(x;\kappa,s)$, that dominates the distribution (4.52). The density takes three different forms, depending on the value of s. We will see that in the interval $[s_1(\kappa), s_0(\kappa)]$, the density is frozen to the Marčenko-Pastur distribution ρ_0 (Phase II), such that the energy of the gas is stuck to its minimal value $\mathscr{E}[\rho_0]$. For $s > s_0(\kappa)$, the fraction κ of the rightmost charges detach from the others and the density splits into two bulks (Phase I). As s increases, these charges move further away from the origin. We thus recover the situation of Section 4.2. Conversely, for $s < s_1(\kappa)$, the leftmost charges detach, and move towards the origin (Phase III). All these phases are represented on the phase diagram in Fig. 4.9. We can regroup the behaviours of the energy in Phases I and III near $s_0(\kappa)$ and $s_1(\kappa)$ respectively, Eqs. (4.61) and (4.68), as

$$\mathscr{E}[\rho_\star(x;\kappa,s)] - \mathscr{E}[\rho_0] \simeq \begin{cases} \alpha_0[s - s_0(\kappa)]^2 & \text{for } s \to s_0(\kappa)^+ , \quad \text{(Phase I)}, \\ 0 & \text{for } s \in [s_1(\kappa), s_0(\kappa)] , \quad \text{(Phase II)}, \\ \alpha_1[s - s_1(\kappa)]^2 & \text{for } s \to s_1(\kappa)^- , \quad \text{(Phase III)}. \end{cases} \tag{4.70}$$

We thus deduce that the two phase transitions are of *second order*.

Having obtained the density $\rho_\star(x;\kappa,s)$, we deduce the form of the distribution from (2.97):

$$P_{N,\kappa}(s) \sim \mathrm{e}^{-\frac{\beta N^2}{2}\tilde{\Phi}_\kappa(s)} , \quad \tilde{\Phi}_\kappa(s) = \mathscr{E}[\rho_\star(x;\kappa,s)] - \mathscr{E}[\rho_0(x)] . \tag{4.71}$$

The large deviation function $\tilde{\Phi}_\kappa$ is represented in Fig. 4.8. This analysis gives no information on the distribution in the interval $[s_1(\kappa), s_0(\kappa)]$ since the Coulomb gas is frozen. In this interval, the distribution is thus controlled by the fluctuations of the n_i's, which we now investigate.

4.3.4 Typical fluctuations: mapping to a free fermions model

We have obtained the distribution $P_{N,\kappa}(s)$ outside the interval $[s_1(\kappa), s_0(\kappa)]$ using the Coulomb gas technique. In this case the eigenvalues contributing to s are either the smallest or the largest, which corresponds to a frozen configuration $\{n_i\}$, while the eigenvalues $\{x_i\}$ fluctuate.

In the interval $[s_1(\kappa), s_0(\kappa)]$, all the values of s can be obtained from the optimal density ρ_0, as discussed in Section 4.3.2. Therefore, there are two possibilities:

- Either we move the eigenvalues away from their optimal configuration $\{x_i^{(0)}\}$. This corresponds to deform the density $\rho_\star$, which results in an energy cost of order N^2.
- Or we let the eigenvalues rest to their optimal configuration $\{x_i^{(0)}\}$ while letting the $\{n_i\}$ fluctuate. In this case, there is no energy cost from the Coulomb gas, but only an entropic cost from the fluctuations of the set $\{n_i\}$ (different configurations $\{n_i\}$ can give the same value of s). This entropy cost is of order N.

In the limit $N \to \infty$, we thus expect that the density of charges $\rho_\star$ will remain frozen to its optimal configuration ρ_0, and only the $\{n_i\}$ will fluctuate. Indeed, the distribution of s is given by

$$P_{N,\kappa}(s) \propto \sum_{\{n_i\}} \int \mathrm{d}x_1 \cdots \mathrm{d}x_N \, \mathrm{e}^{-\frac{\beta N^2}{2} E[\{x_n\}]} \, \delta_{\sum n_i, \kappa N} \, \delta\left(s - \frac{1}{N} \sum_{i=1}^{N} n_i f(x_i) \right) . \tag{4.72}$$

A saddle point evaluation of the integral over the x_i's thus yields

$$P_{N,\kappa}(s) \propto \sum_{\{n_i\}} \delta_{\sum_i n_i, \kappa N} \, \delta\left(s - \frac{1}{N} \sum_{i=1}^{N} n_i f(x_i^{(0)}) \right) , \quad f(x) = \sqrt{x} , \tag{4.73}$$

where $\{x_i^{(0)}\}$ is the optimal configuration that minimises the energy (4.54). We now introduce a convenient representation of this distribution in terms of the microcanonical partition function for $K = \kappa N$ particles, on N energy levels

$$\varepsilon_i = N f(x_i^{(0)}) \tag{4.74}$$

and total energy

$$E = \sum_i n_i \varepsilon_i = N s . \tag{4.75}$$

The n_i's play the role of occupation number for these K fictitious particles. Since $n_i = 0$ or 1 because an eigenvalue either contributes or not to s, these particles are fermions. We have thus reduced the problem of determining the distribution of s to computing

$$\Omega(K, E) = \sum_{\{n_i\}} \delta_{\sum_i n_i, K} \, \delta\left(E - \sum_{i=1}^{N} n_i \varepsilon_i \right) \tag{4.76}$$

for K free fermions with total energy E on the N energy levels (4.74). This is a textbook computation in statistical physics [105,260,261,288], which we reproduce here. The idea is to consider generating functions, such as

$$Z(K, \tilde{\beta}) = \int \Omega(K, E) \, \mathrm{e}^{-\tilde{\beta} E} \, \mathrm{d}E = \sum_{\{n_i\}} \delta_{\sum_i n_i, K} \, \mathrm{e}^{-\tilde{\beta} \sum_i n_i \varepsilon_i} , \tag{4.77}$$

which is the canonical partition function for K fermions at inverse temperature $\tilde{\beta}$, which we denoted with a tilde to distinguish it from the Dyson index β. Here, the number

of level N, which is the dimension of the one body Hilbert space, plays the role of a volume. We also introduce the grand canonical partition function

$$Z_{\mathrm{GC}}(z,\tilde{\beta}) = \sum_{K=0}^{N} z^K \, Z(K,\tilde{\beta}) = \sum_{\{n_i\}} z^{\sum_i n_i} \, \mathrm{e}^{-\tilde{\beta}\sum_i n_i \varepsilon_i} \, , \tag{4.78}$$

where $z = \mathrm{e}^{\tilde{\beta}\mu}$ is the fugacity and μ the chemical potential. This last sum can be easily evaluated and has the standard form of the grand canonical partition function for non interacting fermions:

$$Z_{\mathrm{GC}}(\tilde{\beta},z) = \prod_{i=1}^{N} \left(1 + z \, \mathrm{e}^{-\tilde{\beta}\varepsilon_i}\right) \, . \tag{4.79}$$

In the thermodynamic limit, we deduce the expression of the grand potential (defined here without the usual factor $1/\tilde{\beta}$)

$$\mathcal{J}(\tilde{\beta},z) = \lim_{N\to\infty} -\frac{1}{N} \ln Z_{\mathrm{GC}}(\tilde{\beta},z) = -\int \rho_0(x) \, \ln\left(1 + z \, \mathrm{e}^{-\tilde{\beta}f(x)}\right) \mathrm{d}x \, , \tag{4.80}$$

where ρ_0 is the optimal density (4.24). The procedure is now straightforward: knowing the grand canonical partition function, we will successively deduce the canonical and microcanonical ones by using the equivalence of ensembles in the thermodynamic limit $N \to \infty$ through a Legendre transform.

Canonical ensemble: cumulant generating function

We can obtain the canonical partition function in terms of its grand canonical counterpart by inverting (4.78):

$$Z(K,\tilde{\beta}) = \frac{1}{2\mathrm{i}\pi} \oint \frac{Z_{\mathrm{GC}}(\tilde{\beta},z)}{z^{K+1}} \mathrm{d}z \, , \tag{4.81}$$

where the integral runs over a contour enclosing once the origin in the counter-clockwise direction. Using Eq. (4.80), we can evaluate this integral in the limit $N \to \infty$ via a saddle point estimate. The saddle point determines the fugacity to the value $z_{\mathrm{can}}(\kappa,\tilde{\beta})$ such that the mean (grand canonical) number of fermions is K:

$$z \left.\frac{\partial \ln Z_{\mathrm{GC}}}{\partial z}\right|_{z_{\mathrm{can}}} = K \quad \Rightarrow \quad \int \frac{\rho_0(x)}{\mathrm{e}^{\tilde{\beta}f(x)}/z_{\mathrm{can}} + 1} = \kappa \, . \tag{4.82}$$

We then deduce the free energy (defined without the usual factor $1/\tilde{\beta}$)

$$\mathcal{F}(\kappa,\tilde{\beta}) = \lim_{N\to\infty} -\frac{1}{N} \ln Z(\kappa N,\tilde{\beta}) = \kappa \ln z_{\mathrm{can}}(\kappa,\tilde{\beta}) + \mathcal{J}(\tilde{\beta}, z_{\mathrm{can}}(\kappa,\tilde{\beta})) \, . \tag{4.83}$$

This whole procedure simply shows that the free energy $\mathcal{F}$ can be deduced from the grand potential $\mathcal{J}$ by a Legendre transform, as it is well-known.

Since the truncated linear statistics under consideration is given by $Ns = \sum_i n_i \varepsilon_i$, the canonical partition function (4.77) is proportional to the moment generating function of s:

$$Z(\kappa N,\tilde{\beta}) \propto \left\langle \mathrm{e}^{-N\tilde{\beta}s} \right\rangle \, . \tag{4.84}$$

The normalisation is simply obtained by setting $\tilde{\beta} = 0$, thus:

$$\left\langle \mathrm{e}^{-N\tilde{\beta}s} \right\rangle = \frac{Z_(\kappa N, \tilde{\beta})}{Z(\kappa N, 0)} \,. \tag{4.85}$$

By taking the logarithm, we directly obtain that the cumulant generating function is controlled by the free energy:

$$\frac{1}{N} \ln \left\langle \mathrm{e}^{-N\tilde{\beta}s} \right\rangle \underset{N\to\infty}{\longrightarrow} \mathcal{F}(\kappa, 0) - \mathcal{F}(\kappa, \tilde{\beta}) \,. \tag{4.86}$$

We then get the cumulants of s by expanding the generating function

$$\ln \left\langle \mathrm{e}^{-N\tilde{\beta}s} \right\rangle = \sum_{k=0}^{\infty} \frac{(-N\tilde{\beta})^k}{k!} \left\langle s^k \right\rangle_{\mathrm{c}} \underset{N\to\infty}{\simeq} N \left(\mathcal{F}(\kappa, 0) - \mathcal{F}(\kappa, \tilde{\beta}) \right) \,. \tag{4.87}$$

Expanding $\mathcal{F}$ near $\tilde{\beta} = 0$, we obtain the scaling

$$\left\langle s^k \right\rangle_c \propto N^{-k+1} \,, \qquad 0 < K < N \,. \tag{4.88}$$

This can be compared to the scaling of the full linear statistics ($K = N$), Eq. (2.45):

$$\left\langle s^k \right\rangle_c \propto \beta^{-k+1} N^{-2k+2} \,, \qquad K = N \,. \tag{4.89}$$

We notice that, for the truncated linear statistics, the cumulants do not depend on the Dyson index β. This is due to the fact that β controls the distribution of the x_i's, which are frozen here. Furthermore, the cumulants are much larger in the case of truncated linear statistics. Indeed, for the full linear statistics, they are controlled by the fluctuations of ρ, which induces an energy cost of order N^2. However here the scaling comes from the fluctuations of the n_i's, which are associated to an entropy cost of order N^1, as we will see.

Expanding (4.83) near $\tilde{\beta} = 0$, we obtain the first two cumulant as:

$$\langle s \rangle = \kappa \int \rho_0(x) f(x) \, \mathrm{d}x \,, \tag{4.90}$$

$$\boxed{\mathrm{Var}(s) = \frac{\kappa(1-\kappa)}{N} \left[\int \rho_0(x) f(x)^2 \, \mathrm{d}x - \left(\int \rho_0(x) f(x) \, \mathrm{d}x \right)^2 \right]} \tag{4.91}$$

These expressions are quite general and should hold for any regular function f. Similar expressions have been obtained recently for linear statistics in the thinned ensembles, see for instance [38]. In our case we have $f(x) = \sqrt{x}$, thus:

$$\langle s \rangle = \frac{8\kappa}{3\pi} \,, \tag{4.92}$$

$$\mathrm{Var}(s) = \frac{\kappa(1-\kappa)}{N} \left(1 - \frac{64}{9\pi^2} \right) \,. \tag{4.93}$$

We notice that the variance vanishes for $\kappa = 0$ and $\kappa = 1$. This is due to the fact that Eq. (4.93) is only the leading term of a $1/N$-expansion of the variance. When taking $\kappa = 1$ (full linear statistics), the leading term vanishes and one should recover the usual scaling of $1/\beta N^2$ of the linear statistics. The fact that $\mathrm{Var}(s)$ also vanishes for $\kappa \to 0$ is straightforward from the symmetry $\kappa \leftrightarrow 1 - \kappa$ which follows from the fermionic nature of the fictitious particles (particle-hole symmetry).

Microcanonical ensemble: distribution of the truncated linear statistics

Knowing the moments generating function (4.85), the distribution can be obtained by Laplace inversion. Again, in the limit $N \to \infty$, we can perform a saddle point estimate, which reduces to computing the Legendre transform of the free energy (4.83). The temperature is fixed to its microcanonical value $\tilde{\beta}_{\rm mic}(\kappa, s)$ by imposing that the mean (canonical) energy is $E = Ns$:

$$\left.\frac{\partial \mathcal{F}}{\partial \tilde{\beta}}\right|_{\tilde{\beta}_{\rm mic}} = s \quad \Rightarrow \quad \int \frac{\rho_0(x)}{\mathrm{e}^{\tilde{\beta}_{\rm mic} f(x)}/z_{\rm mic} + 1} f(x)\, \mathrm{d}x = s \,, \tag{4.94}$$

where

$$z_{\rm mic}(\kappa, s) = z_{\rm can}(\kappa, \tilde{\beta}(\kappa, s)) \,. \tag{4.95}$$

We deduce that

$$\lim_{N\to\infty} \frac{1}{N} \ln \Omega(K = \kappa N, E = Ns) = \mathcal{S}(\kappa, s) \,, \tag{4.96}$$

where the entropy $\mathcal{S}$ is given by

$$\mathcal{S}(\kappa; s) = \tilde{\beta}_{\rm mic}(\kappa, s) s - \mathcal{F}(\kappa, \tilde{\beta}_{\rm mic}(\kappa, s)) \,. \tag{4.97}$$

We can easily show that it verifies the thermodynamic identity

$$\boxed{\frac{\mathrm{d}\mathcal{S}(\kappa, s)}{\mathrm{d}s} = \tilde{\beta}_{\rm mic}(\kappa, s)} \tag{4.98}$$

This relation is analogous to (2.100) which we have extensively used in the context of the Coulomb gas.

Therefore the distribution $P_{N,\kappa}(s)$, which is the inverse Laplace transform of (4.85) is[1]:

$$P_{N,\kappa}(s) \underset{N\to\infty}{\sim} \exp\left[-N \Xi_\kappa(s)\right] \,, \tag{4.99}$$

where the large deviation function is obtained by combining (4.85,4.96,4.97):

$$\Xi_\kappa(s) = -\mathcal{S}(\kappa, s) - \mathcal{F}(\kappa, 0) \,. \tag{4.100}$$

Denoting $s_\star$ the value of s which verifies

$$\tilde{\beta}_{\rm mic}(\kappa, s_\star) = 0 \,, \tag{4.101}$$

we clearly have from (4.97) that

$$\mathcal{S}(\kappa, s_\star) = -\mathcal{F}(\kappa, 0) \,. \tag{4.102}$$

The large deviation function is then a difference of entropy:

$$\boxed{\Xi_\kappa(s) = \mathcal{S}(\kappa, s_\star) - \mathcal{S}(\kappa, s)} \tag{4.103}$$

The meaning is quite clear: the number of configurations $\{n_i\}$ which correspond to the same value s is exactly $\mathrm{e}^{N\mathcal{S}(\kappa,s)}$. It is thus expected that the distribution is controlled

[1] Here, the notation $\underset{N\to\infty}{\sim}$ means $-\frac{1}{N} \ln P_{N,\kappa}(s) \to \Xi_\kappa(s)$ for $N \to \infty$.

by an entropy effect. Note that this entropy comes from the fluctuations of the $\{n_i\}$, therefore is not related to the entropy $\mathscr{S}[\rho]$, described in Section 2.2.5, which associated to the Coulomb gas.

Note also that the values $\tilde{\beta}_{\rm mic}$ and $z_{\rm mic}$ of the inverse temperature and the fugacity are obtained by summing over all the eigenvalues (or levels), with a weight given by the Fermi-Dirac distribution

$$\overline{n_i} = \frac{1}{\exp(\tilde{\beta} f(x_i))/z + 1} \,, \tag{4.104}$$

see Eqs. (4.82) and (4.94). The parameter $\tilde{\beta}$, which is the inverse temperature for the fictitious fermions, can be either positive or negative. This unusual situation arises from the fact that the spectrum $\varepsilon_i = f(x_i)$ is bounded both below and above. The Fermi-Dirac distribution (4.104) interpolates between two step functions: it either selects the smallest eigenvalues for $\tilde{\beta} \to +\infty$, or the largest ones for $\tilde{\beta} \to -\infty$, as shown in Fig. 4.9.

Let us now analyse the behaviour of the large deviation function (4.103). From the identity (4.98), the point $s_\star$ is the maximum of the entropy, thus the maximum of the probability $P_{N,\kappa}(s)$, i.e. the typical value of the truncated linear statistics. In terms of the fermions, the behaviour near this point can be obtained from an infinite temperature expansion $\tilde{\beta} \to \pm\infty$. We obtain

$$\Xi_\kappa(s) \simeq \frac{(s-s_\star)^2}{2\sigma_\kappa^2} \,, \qquad \sigma_\kappa^2 = \frac{\kappa(1-\kappa)}{N}\left(1 - \frac{64}{9\pi^2}\right) . \tag{4.105}$$

The behaviour near the edges $s_0(\kappa)$ and $s_1(\kappa)$ are obtained from zero temperature expansions $\tilde{\beta} \to 0^\pm$, which follow from a Sommerfeld expansion [260]:

$$\Xi_\kappa(s) \simeq C_\kappa - \begin{cases} \pi b_0 \sqrt{\dfrac{2\rho_0(b_0)}{3}(s - s_1(\kappa))} & \text{for } s \to s_1(\kappa)^+ \,, \\ \pi c_0 \sqrt{\dfrac{2\rho_0(c_0)}{3}(s_0(\kappa) - s)} & \text{for } s \to s_0(\kappa)^- \,, \end{cases} \tag{4.106}$$

where c_0 and b_0 are given by Eqs. (4.26,4.58) and

$$C_\kappa = -\kappa \ln \kappa - (1-\kappa)\ln(1-\kappa) \,. \tag{4.107}$$

This value, which is the maximum of Ξ_κ, has a simple interpretation. The probability $P_{N,\kappa}(s)$ is the (normalised) number of configurations $\{n_i\}$ among the $\binom{N}{K}$ which gives the value s. For $s = s_0(\kappa)$ or $s = s_1(\kappa)$, there is only one configuration (largest or smallest eigenvalues), thus:

$$-\frac{1}{N}\ln P_{N,\kappa}(s_0(\kappa)) \simeq \frac{1}{N}\ln\binom{N}{K} \underset{N\to\infty}{\longrightarrow} C_\kappa \,, \tag{4.108}$$

and similarly for $s_1(\kappa)$.

4.3.5 Numerical simulations

To check our results, I have performed a numerical analysis of the distribution of the truncated linear statistics by two different means:

1. Direct simulations of s by diagonalisation of Wishart matrices (constructed as described in Section 1.3). This gives access to the typical fluctuations controlled by the large deviation function (4.103).

2. Computation of the optimal density of the Coulomb gas $\rho_\star(x;\kappa,s)$ which minimises the energy under constraints, by Monte Carlo simulations.

For more details, see Article 4. The results of these simulations are in perfect agreement with our analytical computations.

4.3.6 Summary and phase diagram

We have obtained the distribution of the truncated linear statistics s (4.46) for all values of s, in the large deviations form:

$$P_{N,\kappa}(s) \underset{N\to\infty}{\sim} \begin{cases} \exp\left[-\dfrac{\beta N^2}{2}\tilde{\Phi}_\kappa(s)\right] & \text{for } s<s_1(\kappa) \text{ or } s>s_0(\kappa)\,, \\ \exp\left[-N\,\Xi_\kappa(s)\right] & \text{for } s\in[s_1(\kappa),s_0(\kappa)]\,, \end{cases} \tag{4.109}$$

where the large deviation function

$$\tilde{\Phi}_\kappa(s) = \mathscr{E}[\rho_\star(x;\kappa,s)] - \mathscr{E}[\rho_0(x)] \tag{4.110}$$

is controlled by the energy of the Coulomb gas, while

$$\Xi_\kappa(s) = \mathcal{S}(\kappa,s_\star) - \mathcal{S}(\kappa,s) \tag{4.111}$$

comes from the entropy of the occupation numbers $\{n_i\}$. The particular behaviour of the distribution, with two different scalings with N and N^2 has a simple meaning:

- For $s>s_0(\kappa)$ (Phase I) and $s<s_1(\kappa)$ (Phase III), the occupation numbers $\{n_i\}$ are frozen and select only the largest or the smallest eigenvalues. The distribution $P_{N,\kappa}(s)$ is thus controlled by the fluctuations of the eigenvalues $\{x_i\}$, which induce an energy cost for the Coulomb gas. This yields the usual scaling $\beta N^2/2$ of the large deviations form.

- For $s\in[s_1(\kappa),s_0(\kappa)]$ (Phase II), the Coulomb gas is frozen to its optimal configuration, given by the Marčenko-Pastur distribution (4.24). The distribution $P_{N,\kappa}(s)$ is then controlled by the entropy of the occupation numbers $\{n_i\}$. This gives the linear scaling in N.

This is summarised in the phase diagram shown in Fig. 4.9.

This analysis is universal: it does not depend on the matrix ensembles or the linear statistics under consideration. In particular, the whole discussion of Section 4.3.4 is valid for any typical density of eigenvalues ρ_0 and monotonous function f for the linear

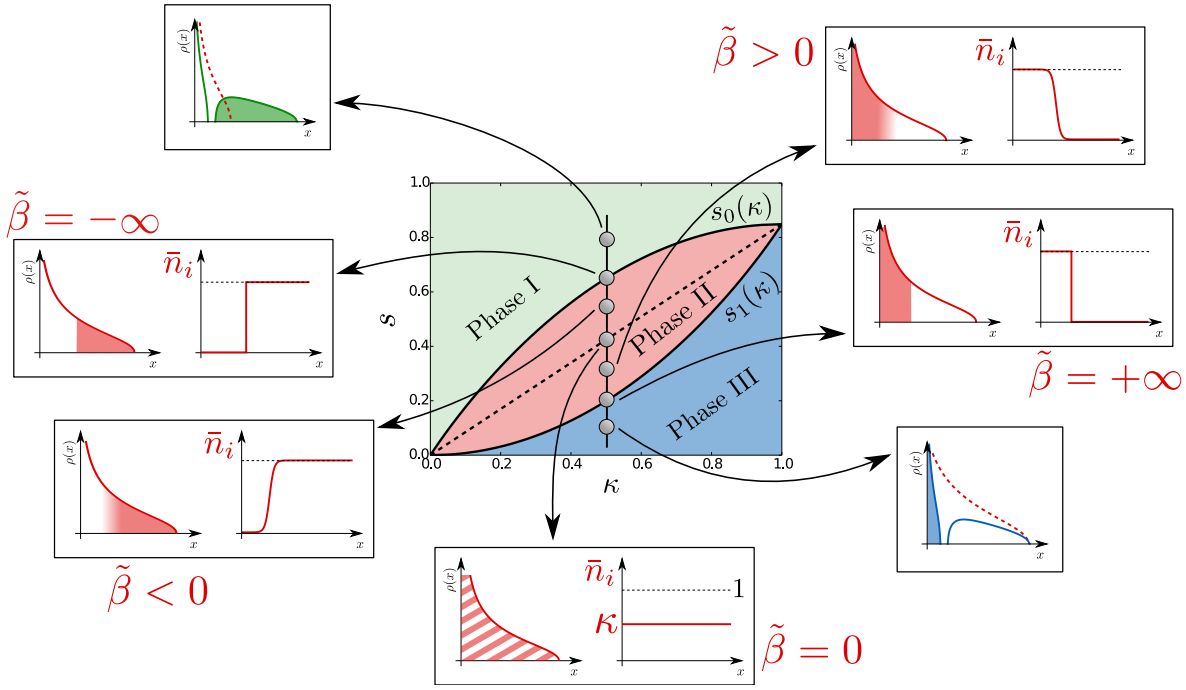

Figure 4.9: Phase diagram for the Coulomb gas. For a given value of κ, the evolution of the density $\rho_\star$ of the Coulomb gas and of the mean occupation numbers $\overline{n_i}$ are represented.

statistics. Similar features should also occur for non-monotonous functions, but a more detailed analysis is still required.

There also remains to understand more precisely the connection with the thinned ensembles briefly mentioned in Section 4.3.1. These ensembles correspond to removing eigenvalues with a given probability, which is a "grand canonical" version of the problem studied here. As we have studied the distribution of the truncated linear statistics in the thermodynamic limit $N \to \infty$ by computing thermodynamic quantities, we expect that the two problems should be similar. However the equivalence of ensemble is not so trivial for these strongly correlated systems and should be investigated more precisely.

Article 3

Truncated linear statistics associated with the top eigenvalues of random matrices

A. Grabsch, S. N. Majumdar, and C. Texier, Truncated Linear Statistics Associated with the Top Eigenvalues of Random Matrices, J. Stat. Phys. **167**(2), 234–259 (2017).

☞ http://dx.doi.org/10.1007/s10955-017-1755-5

Article 4

Truncated linear statistics associated with the eigenvalues of random matrices II. Partial sums over proper time delays for chaotic quantum dots

A. Grabsch, S. N. Majumdar, and C. Texier, Truncated Linear Statistics Associated with the Eigenvalues of Random Matrices II. Partial Sums over Proper Time Delays for Chaotic Quantum Dots, J. Stat. Phys. **167**(6), 1452–1488 (2017).

☞ http://dx.doi.org/10.1007/s10955-017-1780-4

Part II

Multichannel disordered wires

Chapter 5

Introduction to disordered wires

Electronic transport in disordered systems has been extensively studied since the pioneering work of Anderson in the 50s [18]. In a perfect cristal the eigenstates are extented waves. The introduction of disorder might induce localisation of the states, i.e. exponential decay of the wave function in space. Dimensionality plays a crucial role in the theory of Anderson localisation [122, 195]. In the strictly one dimensional case, powerful analytical methods allow to obtain exact results [206]. However, these 1D models cannot reproduce all the phenomenology which exists in higher dimensions, such as the Anderson transition from localised to extended states. In one dimension, all the states are localised, for all disorder strength. In higher dimensions, there are no analytical method to study such systems at all disorder strength. Therefore, one relies either on weak disorder perturbative expansions or numerical methods.

In this framework, models of disordered wires have been introduced to study the transport properties in metallic wires, which have a width W much smaller than their length L. These models describe a quasi-1D situation, between the purely 1D case and higher dimensions. They have attracted a lot of attention in the theory of disordered systems [30, 122], both for analytical and numerical purposes.

Numerical studies of localisation, in any dimension $d \geqslant 2$, rely on the scaling approach [195]. This method is based on exact numerical computations of the localisation length $\xi(W)$ for a quasi-1D system, with a finite cross-section W. The results obtained for different finite size W allow to determine a scaling function, from which the localisation length $\xi(\infty)$ of the infinite system is extracted.

The quasi-1D models of disordered wires allow to study an intermediate situation, between the strictly 1D case and higher dimensions. Under the assumption of ergodicity in the transverse direction (isotropy), these models have been studied analytically. In particular, they properly describe a *diffusive* regime which does not exist in strictly 1D systems.

The analytical study of quasi-1D disordered systems relies on three complementary approaches. The first one is the diagramatic approach [3, 4], which is a perturbative method valid for weak disorder. This approach cannot reach the strongly localised regime, but allows to study the crossover between different symmetry classes, the decoherence and dephasing, ... The second approach, based on non linear σ-models, has permitted to study different types of observables [11–14, 234, 235, 313] (for reviews,

see [118,119,143]), such as density-density correlations, localisation length, conductance, etc.... We will not discuss this approach in more details, as we will follow the third one introduced in the 80s by Dorokhov, Mello, Pereyra and Kumar (DMPK) [106–109, 227] (for reviews see [30,229]). Their approach is based on the analysis of the transport properties of the wire, characterised by a transfer matrix or equivalently a scattering matrix. Their central result is the celebrated DMPK equation, which describes the evolution of the transmission eigenvalues along the wire. This approach relies on a global analysis of the problem, based on symmetries. The DMPK equation describes disordered wires in the presence or absence of time-reversal and spin-rotation symmetry, corresponding to the Wigner-Dyson classes discussed in Chapter 1. This equation has allowed to successfully describe several physical properties of disordered wires, such as the conductance. For a review, see Ref. [30]. Section 5.1 will give a description of the DMPK approach, which will allow us to stress the difference with the approach developed in this thesis.

At the end of the 90s, the original Wigner-Dyson classification was extended by Altland and Zirnbauer [15,16,314] to account for two other discrete symmetries encountered in particle or condensed matter physics: the chiral and particle-hole symmetries. The DMPK approach has thus been applied to study disordered wires belonging to these new symmetry classes. We describe these new symmetry classes and the corresponding extensions of the DMPK equation in Section 5.2.

In the 2000s, a renewed interest for these multichannel disordered wires arose from the perspective of topological insulators and superconductors. These models have turned out to provide a convenient framework to analytically study the effect of disorder on topological phases. For more details, see Section 5.3.

5.1 The DMPK equation

Here we recall the DMPK method, which is one of the standard approach to study quasi-1D systems [30]. Let us consider a disordered wire of length L with a finite width W. This wire is connected to two perfect leads, as shown in Fig. 5.1. The scattering states at Fermi energy define N propagating modes, called *channels*. We describe these states by a N-components wave function Ψ. It satisfies the Schrödinger equation

$$H\Psi = E\Psi\,, \qquad H = -\mathbb{1}_N \frac{\mathrm{d}^2}{\mathrm{d}x^2} + V(x)\,, \qquad \Psi = \begin{pmatrix} \psi_1 \\ \vdots \\ \psi_N \end{pmatrix}\,, \tag{5.1}$$

where the potential $V(x)$ is a $N \times N$ matrix. As discussed in Chapter 1, the symmetries of the system impose some constraint on the Hamiltonian, and thus on the matrix V. If the system breaks time-reversal symmetry, V can be any complex Hermitian matrix (Dyson index $\beta = 2$). If time reversal symmetry is conserved this matrix can be either real symmetric ($\beta = 1$) if spin is conserved or quaternionic self-dual ($\beta = 4$). See Chapter 1 for a more detailed discussion of these symmetries.

The approach of Dorokhov, Mello, Pereyra and Kumar [106–109, 227] is based on a transfer matrix formalism. To introduce this formalism, it is natural to consider a scattering situation. We connect a disordered wire of length L to two perfect leads, as shown in Fig. 5.1. In our model, this corresponds to set $V(x) = 0$ for $x < 0$ and

Figure 5.1: A scattering situation of a disordered wire of size L connected to two perfect leads. On each side, the wave function is the superposition of ingoing and outgoing plane waves.

$x > L$. In these two regions, the wave function of energy $E = k^2$ can be expressed as a superposition of incoming and outgoing waves:

$$\Psi_E(x) = \frac{1}{\sqrt{4\pi k}} \begin{cases} A_L^{\text{in}}\, \mathrm{e}^{\mathrm{i}kx} + A_L^{\text{out}}\, \mathrm{e}^{-\mathrm{i}kx} & \text{for } x < 0\,, \\ A_R^{\text{out}}\, \mathrm{e}^{\mathrm{i}kx} + A_R^{\text{in}}\, \mathrm{e}^{-\mathrm{i}kx} & \text{for } x > L\,, \end{cases} \tag{5.2}$$

where the amplitudes $A_{L,R}^{\text{in,out}}$ are N-components vectors and the prefactor is chosen so that $\int \Psi_E^\dagger(x)\Psi_{E'}(x)\mathrm{d}x = \delta(E - E')$.

We now introduce the $2N \times 2N$ scattering matrix $\mathcal{S}$ which relates the outgoing amplitudes to the incoming ones:

$$\begin{pmatrix} A_L^{\text{out}} \\ A_R^{\text{out}} \end{pmatrix} = \mathcal{S} \begin{pmatrix} A_L^{\text{in}} \\ A_R^{\text{in}} \end{pmatrix} . \tag{5.3}$$

This matrix has to conserve the probability current $\mathcal{J}^{\text{in}} = \mathcal{J}^{\text{out}}$, where the incoming and outgoing currents are given by

$$\mathcal{J}^{\text{in}} = \frac{1}{4\pi}\left[(A_L^{\text{in}})^\dagger A_L^{\text{in}} + (A_R^{\text{in}})^\dagger A_R^{\text{in}}\right] = \frac{1}{4\pi}(X^{\text{in}})^\dagger X^{\text{in}}\,, \quad \text{where } X^{\text{in}} = \begin{pmatrix} A_L^{\text{in}} \\ A_R^{\text{in}} \end{pmatrix} , \tag{5.4}$$

$$\mathcal{J}^{\text{out}} = \frac{1}{4\pi}(X^{\text{out}})^\dagger X^{\text{out}} = \frac{1}{4\pi}(X^{\text{in}})^\dagger\, \mathcal{S}^\dagger\mathcal{S}\, X^{\text{in}}\,, \text{where } X^{\text{out}} = \begin{pmatrix} A_L^{\text{out}} \\ A_R^{\text{out}} \end{pmatrix} . \tag{5.5}$$

This implies that the scattering matrix is unitary:

$$\mathcal{S} \in \mathrm{U}(2N)\,. \tag{5.6}$$

This matrix can be decomposed in blocks of size $N \times N$:

$$\mathcal{S} = \begin{pmatrix} r & t' \\ t & r' \end{pmatrix} . \tag{5.7}$$

where r and t represent respectively the reflection and transmission of a wave coming from the left. Similarly, r' and t' are the reflection and transmission matrices for a wave coming from the right side.

The idea of DMPK is to study the evolution of the eigenvalues $\{T_n\}$ of the transfer matrix $tt^\dagger$ when the length L of the wire is increased by δL. To obtain the evolution of these eigenvalues through a small slice δL we use perturbation theory. We describe the first part of the wire by the scattering matrix (5.7), and the small part of length δL by the scattering matrix

$$\tilde{\mathcal{S}} = \begin{pmatrix} \tilde{r} & \tilde{t}' \\ \tilde{t} & \tilde{r}' \end{pmatrix} , \tag{5.8}$$

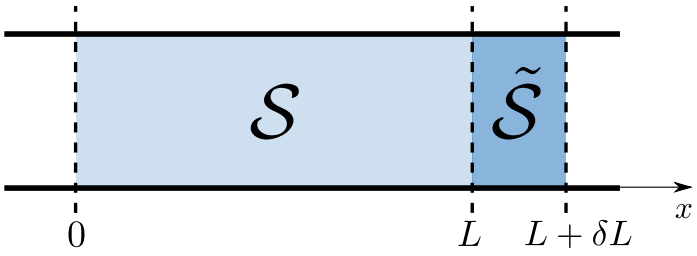

Figure 5.2: The wire of length $L+\delta L$ is artificially separated in two parts. The first section of length L is described by a scattering matrix $\mathcal{S}$, while the additional slice of length δL is described by a scattering matrix $\tilde{\mathcal{S}}$.

as shown in Fig. 5.2. To account for the disorder, the matrix $\tilde{\mathcal{S}}$ is taken to be random. We will assume that the disorder couples all the channels equivalently, such that a wave injected in one channel will come out from any channel with equal probability. This isotropy assumption restricts this approach to the quasi-1D geometry.

We want to study the transmission matrix $t+\delta t$ of the wire of length $L+\delta L$. Let us thus consider a wave coming from the left of the wire. This wave can be directly transmitted through both systems, which corresponds to a transmission matrix $\tilde{t}t$. It can also be transmitted once trough the first section, and then undergo a series of internal reflections before coming out to the right of the wire. Summing all these possibilities yields:

$$t+\delta t = \tilde{t}t + \tilde{t}r'\tilde{r}\tilde{t} + \tilde{t}(r'\tilde{r})^2 t + \cdots = \tilde{t}(1-r'\tilde{r})^{-1}t\,, \tag{5.9}$$

thus

$$\delta t = \left[\tilde{t}(1-r'\tilde{r})^{-1} - 1\right] t\,. \tag{5.10}$$

We now need to specify the distribution of the matrices $\tilde{t}$ and $\tilde{r}$ which describe the transmission and reflection by the small slice δL. Heuristically, if δL is small compared to the mean free path ℓ, we expect that the small slice δL will transmit incoming waves with probability close to 1. We expect that the reflection probability is proportional to δL (this can be proved with a microscopic model [3,4,287]), and thus we write:

$$\left\langle \mathrm{tr}(\tilde{t}\tilde{t}^\dagger) \right\rangle = N\left(1 - \frac{\delta L}{\ell}\right)\,, \tag{5.11}$$

where $\langle\cdots\rangle$ denotes the averaging with respect to the matrix $\tilde{t}$. The length ℓ characterises the strength of the disorder: it is the "elastic mean free path"[1]. If we set for convenience $\ell = 1$, this means that the eigenvalues $\{\tilde{T}_n\}$ of $\tilde{t}\tilde{t}^\dagger$ are close to unity:

$$\tilde{T}_n = 1 - \mathcal{O}(\delta L)\,. \tag{5.12}$$

We can actually express the scattering matrix $\tilde{\mathcal{S}}$ in terms of these eigenvalues as [220,227]

$$\tilde{\mathcal{S}} = \begin{pmatrix} U & 0 \\ 0 & V \end{pmatrix} \begin{pmatrix} -\sqrt{1-\mathcal{T}} & \sqrt{\mathcal{T}} \\ \sqrt{\mathcal{T}} & \sqrt{1-\mathcal{T}} \end{pmatrix} \begin{pmatrix} U' & 0 \\ 0 & V' \end{pmatrix}\,, \quad \mathcal{T} = \mathrm{Diag}(\tilde{T}_1,\ldots,\tilde{T}_N)\,, \tag{5.13}$$

where U, U', V and V' are $N\times N$ unitary matrices. In the absence of time reversal symmetry ($\beta = 2$), the only condition is that $\tilde{S}$ is unitary and thus all the matrices U, U', V and V' are distinct. In the presence of both time-reversal and spin-rotation

[1] We use here the definition of the mean free path used in the random matrix approach, which differs from the one used in the microscopic (diagrammatic) approach [283].

symmetry ($\beta = 1$), the scattering matrix is also symmetric, which implies that $U' = U^T$ and $V' = V^T$. Therefore, only two unitary matrices are required to parametrise $\tilde{\mathcal{S}}$. The case $\beta = 4$ corresponding to the presence of time-reversal symmetry but breaking of spin-rotation symmetry can be discussed in a similar way [30,227]. This parametrisation yields

$$\tilde{r} = -U\,\sqrt{1-\mathcal{T}}\,U'\,, \quad \tilde{t} = V\,\sqrt{\mathcal{T}}\,U'\,. \tag{5.14}$$

Knowing that the transmission eigenvalues $\{\tilde{T}_n\}$ are close to unity, Eq. (5.12), we deduce that the eigenvalues of the increment δt, given by Eq. (5.10), are of order $\mathcal{O}(\sqrt{\delta L})$. We can thus apply perturbation theory to compute the variations of the eigenvalues of $tt^\dagger$ when the wire length is increased by δL. Let us denote $\{T_n\}$ the eigenvalues of $tt^\dagger$, and $\{|w_n\rangle\}$ the eigenvectors. To second order in perturbation theory, we have:

$$\delta T_n = \langle w_n|\delta(tt^\dagger)|w_n\rangle + \sum_{m(\neq n)} \frac{\left|\langle w_m|\delta(tt^\dagger)|w_n\rangle\right|^2}{T_n - T_m} + \mathcal{O}((\delta L)^{3/2})\,, \tag{5.15}$$

where the variation of the matrix $tt^\dagger$ is given by

$$\delta(tt^\dagger) = (\delta t)t^\dagger + t(\delta t)^\dagger = \left[\tilde{t}(1-r'\tilde{r})^{-1} - 1\right] tt^\dagger + \text{h.c.} \tag{5.16}$$

and h.c. denotes the Hermitian conjugate. The idea is now to compute $\langle \delta T_n\rangle$ and $\langle \delta T_n\, \delta T_m\rangle$ with respect to the unitary matrices U, V, U' and V', at leading order in δL. We thus need the distribution of these matrices over the unitary group. Following the DMPK approach, we assume that these matrices have uniform distribution over $\mathrm{U}(N)$. This implies that the slice δL couples all the channels of the wire in the same way. Under this rather strong isotropy assumption, one can evaluate the averages over the unitary group using the formulae given in Appendix A.4. At leading order, this gives [30]:

$$\langle \delta T_n\rangle = \left[-T_n + \frac{2T_n}{\beta N + 2 - \beta}\left(1 - T_n + \frac{\beta}{2}\sum_{m(\neq n)} \frac{T_n + T_m - 2T_nT_m}{T_n - T_m}\right)\right]\delta L\,, \tag{5.17}$$

$$\langle \delta T_n\, \delta T_m\rangle = \frac{4T_n^2(1-T_n)}{\beta N + 2 - \beta}\,\delta_{nm}\,\delta L\,, \tag{5.18}$$

and all higher moments vanish at order δL. These equations allow us to write Langevin equations describing the evolution of the transmission eigenvalues $\{T_n\}$ through the slice, as $\delta L \to 0$:

$$\frac{\mathrm{d}T_n}{\mathrm{d}L} = \langle \delta T_n\rangle + \sum_{m=1}^{N} \langle \delta T_n\, \delta T_m\rangle\, \xi_m\,, \tag{5.19}$$

where $\{\xi_m\}$ are Gaussian white noises of unit variance. Since (5.17,5.18) relate the variations of the transmissions to their value before entering the additional disordered slice, the Langevin equations must be understood in the Itô sense. We can thus write the associated Fokker-Planck equation for the distribution $P(\{T_n\}; L)$ of the eigenvalues for a wire of length L:

$$\frac{\partial}{\partial L}P(\{T_n\}; L) = \sum_{n=1}^{N}\frac{\partial}{\partial T_n}\left(-\langle T_n\rangle\, P + \frac{1}{2}\sum_{m=1}^{N}\frac{\partial}{\partial T_m}\langle \delta T_n\, \delta T_m\rangle\, P\right)\,. \tag{5.20}$$

We can make the change of variable $\lambda_n = (1-T_n)/T_n$ to write this equation in the form originally given in Refs. [108, 227]:

$$\frac{\partial}{\partial L}P(\{\lambda_n\};L) = \frac{2}{\beta N + 2 - \beta}\sum_{n=1}^{N}\frac{\partial}{\partial\lambda_n}\left[\lambda_n(1+\lambda_n)J_0(\{\lambda_n\})\frac{\partial}{\partial\lambda_n}\left(\frac{P(\{\lambda_n\};L)}{J_0(\{\lambda_n\})}\right)\right], \tag{5.21}$$

where we introduced

$$J_0(\{\lambda_n\}) = \prod_{i<j}|\lambda_i - \lambda_j|^\beta . \tag{5.22}$$

This Fokker-Planck equation is the celebrated DMPK equation describing the evolution of the transmission eigenvalues upon increasing the length L of the wire. This equation has been solved in an other form, by introducing the variables $\{x_n\}$ defined by

$$\lambda_n = \sinh^2 x_n , \qquad T_n = \frac{1}{\cosh^2 x_n} , \qquad x_n \geqslant 0 . \tag{5.23}$$

In terms of these variables, the DMPK equation reads:

$$\frac{\partial}{\partial L}P(\{x_i\};L) = \frac{1}{2(\beta N + 2 - \beta)}\sum_{n=1}^{N}\frac{\partial}{\partial x_n}\left[J(\{x_i\})\frac{\partial}{\partial x_n}\left(\frac{P(\{x_i\};L)}{J(\{x_i\})}\right)\right], \tag{5.24}$$

with

$$J(\{x_i\}) = \prod_{i<j}\left|\sinh^2 x_i - \sinh^2 x_j\right|^\beta \prod_i \sinh(2x_i) . \tag{5.25}$$

In this form, the DMPK equation has been solved exactly in the case $\beta = 2$ by mapping (5.24) onto a Schrödinger equation for noninteracting particles [31, 32]. A much more complex solution has then been found in the other symmetry classes $\beta = 1$ and $\beta = 4$ [78]. However, the knowledge of these exact solutions is not required to study some physical observables, such as the conductance. These observables can be obtained in the limiting cases (conducting or localised regimes) from an asymptotic analysis of Eq. (5.24).

The conductance G can be expressed in terms of the transmission eigenvalues via the Landauer forumla [132, 200]:

$$G = \frac{2e^2}{h}\sum_{n=1}^{N} T_n = \frac{2e^2}{h}\sum_{n=1}^{N}\frac{1}{\cosh^2 x_n} , \tag{5.26}$$

where the factor 2 comes from spin degeneracy. Knowing the statistical properties of the x_n's, encoded in the DMPK equation (5.24), allows the study of the distribution of the conductance.

In the limit $L \to \infty$, for fixed number N of channels, the variables $\{x_n\}$ decouple as $x_1 \gg x_2 \gg \cdots \gg x_N \gg 1$. In this limit, they all become independent Brownian motions, such that the solution of the DMPK equation (5.24) factorises into a product of Gaussian distributions [30], with

$$\langle x_n\rangle = \gamma_n L , \quad \mathrm{Var}(x_n) \propto L , \quad \gamma_n = \frac{\beta(N-n)+1}{\beta(N-1)+2} . \tag{5.27}$$

The scales $\{\gamma_n\}$ are called Lyapunov exponents. The system is thus characterised by two length scales: $1/\gamma_1 = \mathcal{O}(N^0)$ and $1/\gamma_N = \mathcal{O}(N)$. The transport properties of the wire depend on the ratios of the length L with these two scales.

Metallic regime

For $1 \ll L \ll N$, one can show from the DMPK equation (5.24) that the conductance decays linearly with the wire's length [228]:

$$\langle G \rangle \sim G_0 \frac{N\ell}{L} , \tag{5.28}$$

which coincides with Ohm's law. The main success of the DMPK approach is to correctly describe this metallic regime which does not exist in the strictly one dimensional case $N = 1$.

If $L \ll 1$, the transmission eigenvalues are close to unity. The wire is thus perfectly conducting:

$$G \simeq N G_0 . \tag{5.29}$$

Localised regime

If $L \gg N$, the statistics of $\{x_n\}$ are given by (5.27). Therefore, the conductance (5.26) is dominated by the smallest term, associated to x_N:

$$G \simeq G_0 \frac{1}{\cosh^2 x_N} \simeq 4\, G_0\, \mathrm{e}^{-2x_N} , \quad G_0 = \frac{2e^2}{h} , \tag{5.30}$$

from which we deduce, using Eq. (5.27):

$$\langle \ln G/G_0 \rangle \simeq -2 \langle x_N \rangle \simeq -\frac{2L}{\beta(N-1)+2} \quad \text{for } L \gg N . \tag{5.31}$$

We recover the well-known exponential decay of the conductance with the system size L, characteristic of a *localised regime* [30].

All these results rely on the DMPK equation (5.21), originally derived for the three Wigner-Dyson classes. We describe in Section 5.2 the extension of the DMPK equation to the other symmetry classes.

Remark: extension of the DMPK approach

As we have seen above, the DMPK equation is based on the isotropy assumption: the disorder couples all the channels in the same way. The consequence is that the DMPK equation (5.39) is restricted to the quasi-1D geometry, as all the information about the spatial structure is lost.

In order to describe higher dimensional systems, several approaches have been proposed to extend the DMPK formalism. For instance, an extension based on a specific model for the transfer matrix have been studied in Ref. [231]. Another approach consists in introducing phenomenological parameters for the averages over the unitary matrices

U, V, U' and V', see Eq. (5.14), instead of considering them uniformly distributed. See for instance Refs. [110–112, 245–247]. For example, in the Wigner-Dyson orthogonal class ($\beta = 1$), the generalised DMPK equation takes the form [112, 245]

$$\frac{\partial P}{\partial L} = \frac{1}{2\gamma} \sum_{n=1}^{N} K_{nn} \frac{\partial}{\partial x_n} J(\{x_i\}) \frac{\partial}{\partial x_n} J^{-1}(\{x_i\}) P \,, \tag{5.32}$$

where

$$J(\{x_i\}) = \prod_{i<j} \left| \sinh^2 x_i - \sinh^2 x_j \right|^{\gamma_{ij}} \prod_{i=1}^{N} |\sinh(2x_i)| \;, \quad \gamma_{ij} = \frac{2K_{ij}}{K_{ii}} \,. \tag{5.33}$$

This equation is controlled by a matrix K_{ij} of phenomenological parameters which describe the anisotropy of the unitary matrices U, V, U' and V' (see Eq. (5.14)). Relating this matrix K to the microscopic parameters of a specific model of disorder is however rather difficult.

5.2 New symmetry classes

The original Wigner-Dyson classification takes into account two symmetries: time-reversal and spin-rotation symmetries, which hold for the entire spectrum. At the end of the 90's, Altland and Zirnbauer [15, 16, 314] extended this original classification by taking into account two additional discrete symmetries, which arise only at a specific value of the energy (usually taken as zero) in the one-body problem: the chiral symmetry and the particle-hole symmetry. The DMPK equation was thus extended to describe disordered wires belonging to these new symmetry classes. In this section, we first describe the additional symmetries and in a second step we present the extension of the DMPK formalism to these new classes.

5.2.1 The chiral classes

The chiral symmetry plays a role both in particle physics, in particular in quantum chromodynamics [275, 297, 299], and in condensed matter [41, 152, 153, 207, 292], as it is carried by the Dirac equation. It is associated with Hamiltonians of the form

$$H = \begin{pmatrix} 0 & h \\ h^\dagger & 0 \end{pmatrix} \,, \tag{5.34}$$

where h is an operator acting on a given subspace. Such Hamiltonians exhibit the symmetry

$$\sigma_z H \sigma_z = -H \,, \tag{5.35}$$

where σ_z is the third Pauli matrix, acting in a given "isospin" space. The chiral symmetry maps an eigenstate ψ_ε of H with energy ε to another eigenstate with opposite energy $-\varepsilon$.

As in the Wigner-Dyson case, the presence or absence of time-reversal and spin-rotation symmetry gives rise to a set of three chiral classes, see Table 5.1.

5.2.2 The Bogoliubov-de Gennes classes

The remaining symmetry classes arise in the study of superconductors, which are usually described using the Bardeen–Cooper–Schrieffer (BCS) theory [25]. The central element of this theory is that the interactions of the electrons with the cristal can lead to the pairing of electrons into Cooper pairs. Let us consider a lattice model, and introduce the electronic creation and annihilation operators $c_i^\dagger$ and c_i, defined for each lattice site i. The dynamics of the electrons is described within a mean field (BCS) approach. This leads to the Bogoliubov-de Gennes (BdG) Hamiltonian[2]

$$\hat{H} = \sum_{i,j} h_{ij} c_i^\dagger c_j + \frac{1}{2} \sum_{i,j} \left(\Delta_{ij} c_i^\dagger c_j^\dagger - \Delta_{ij}^\star c_i c_j \right) , \tag{5.36}$$

with $h^\dagger = h$ and $\Delta^T = -\Delta$ to ensure Hermiticity. In this expression, h is the Hamiltonian controlling the evolution of free electrons on the lattice, and Δ represents the superconducting gap, which is the order parameter. The excitations of this Hamiltonian are called quasi-particles.

We can rewrite the Hamiltonian (5.36) in a matrix form by introducing the spinor $\psi^\dagger = (\{c_i^\dagger\}, \{c_i\})$:

$$\hat{H} = \frac{1}{2} \psi^\dagger H \psi , \qquad H = \begin{pmatrix} h & \Delta \\ -\Delta^\star & -h^T \end{pmatrix} , \tag{5.37}$$

where the minus signs appear due to the anticommutation relations $\{c_i, c_j^\dagger\} = \delta_{ij}$. This Hamiltonian exhibits the particle-hole symmetry

$$\tau_x H^T \tau_x = -H , \tag{5.38}$$

where τ_x is the first Pauli matrix in the particle-hole space (Nambu space).

This additional symmetry, combined with time-reversal and spin-rotation symmetry gives rise to the Bogoliubov-de Gennes classes. Note that unlike in the Wigner-Dyson or chiral cases, spin-rotation symmetry plays a role even if time-reversal symmetry is broken because it combines with the particle-hole symmetry in a nontrivial way. Therefore, this yields a set of four Bogoliubov-de Gennes classes, summarised in Table 5.1.

5.2.3 DMPK equation for the new classes

The original derivation of the DMPK equation presented in Section 5.1 has been extended to the additional chiral and BdG classes, in order to study the transport properties of chiral or superconducting disordered wires [59–63, 65, 66, 79, 242, 243, 292]. These studies have shown that, for all the symmetry classes, the DMPK equation can be written in the form

$$\frac{\partial P}{\partial L} = \frac{1}{2\gamma} \sum_{n=1}^{N} \frac{\partial}{\partial x_n} J(\{x_i\}) \frac{\partial}{\partial x_n} J^{-1}(\{x_i\}) P , \tag{5.39}$$

[2] In the BCS approach, Δ is a scalar. Here we present the Bogoliubov-de Gennes formalism which describes an inhomogeneous superconductor, in which Δ can be inhomogeneous in space.

	Name	TRS	p-h S	ch. S	SRS	m_0	m_l	m_s
Wigner-Dyson	AI (orthogonal)	$+1$	no	no	yes	1	1	0
	A (unitary)	no	no	no	indiff.	2	1	0
	AII (symplectic)	-1	no	no	no	4	1	$\star\star$
Chiral	BDI (chiral orth.)	$+1$	$+1$	yes	yes	1	0	0
	AIII (chiral unit.)	no	no	yes	indiff.	2	0	0
	CII (chiral sympl.)	-1	-1	yes	no	4	0	0
BdG	D	no	$+1$	no	no	1	0	0
	DIII	-1	$+1$	yes	no	2	0	$\star$
	C	no	-1	no	yes	4	3	0
	CI	$+1$	-1	yes	yes	2	2	0

Table 5.1: Classification of disordered sytems based on four symmetries: time-reversal (TRS), particle-hole (p-h S), chiral (ch. S) and spin-rotation (SRS). The names of the different classes come from the Cartan classification of the symmetry group. m_0, m_l and m_s are the multiplicity of the ordinary, long and short roots for the corresponding symmetric space. If N is even, $\star = \star\star = 0$, while for odd N, $\star = 2$ and $\star\star = 4$.

where J is given by:

$$J(\{x_i\}) = \begin{cases} \displaystyle\prod_{i<j}\prod_{\pm} |\sinh(x_i \pm x_j)|^{m_0} \prod_{k=1}^{N} \sinh(2x_k)^{m_l} \sinh(x_k)^{m_s} \,, & x_i > 0 \,, \quad \text{W-D and BdG,} \\ \displaystyle\prod_{i<j} |\sinh(x_i - x_j)|^{m_0} \,, & x_i \in \mathbb{R} \,, \quad \text{chiral.} \end{cases} \tag{5.40}$$

and the constant γ is

$$\gamma = \begin{cases} m_0(N-1) + m_l + 1 \,, & \text{W-D and BdG classes,} \\ \dfrac{1}{2}[m_0(N-1) + 2] \,, & \text{chiral classes.} \end{cases} \tag{5.41}$$

The parameters m_0, m_l and m_s, known as the multiplicity of the ordinary, long and short roots for the corresponding symmetric space, are given in Table 5.1. For the Wigner-Dyson classes, the parameter m_0 is simply the Dyson index β.

The DMPK equation (5.39) in these new classes has permitted to analyse the transport and localisation properties of disordered wires [59–63, 65, 208, 242, 243], as well as the density of states [61, 66, 292].

5.3 Topological phase transitions

More recently, models of multichannel disordered wires have attracted a lot of interest, from the perspective of their topological properties. These are materials characterised by a quantum number of topological nature.

The most famous example of a non trivial topological state in condensed matter physics is the integer quantum Hall effect in two dimensional electronic systems. The

						topological index		
		TRS	p-h S	ch. S	SRS	0D	1D	2D ⋯
Wigner-Dyson	AI (orthogonal)	+1	no	no	yes	$\mathbb{Z}$		
	A (unitary)	no	no	no	indiff.	$\mathbb{Z}$		$\mathbb{Z}$
	AII (symplectic)	−1	no	no	no	$\mathbb{Z}$		$\mathbb{Z}_2$
Chiral	BDI (chiral orth.)	+1	+1	yes	yes	$\mathbb{Z}_2$	$\mathbb{Z}$	
	AIII (chiral unit.)	no	no	yes	indiff.		$\mathbb{Z}$	
	CII (chiral sympl.)	−1	−1	yes	no		$\mathbb{Z}$	
BdG	D	no	+1	no	no	$\mathbb{Z}_2$	$\mathbb{Z}_2$	$\mathbb{Z}$
	DIII	−1	+1	yes	no		$\mathbb{Z}_2$	$\mathbb{Z}_2$
	C	no	−1	no	yes			$\mathbb{Z}$
	CI	+1	−1	yes	yes			

Table 5.2: Periodic table of topological insulators. In any dimension, 3 classes can exhibit topological phases indexed by an integer ($\mathbb{Z}$), while 2 can host topological phases indexed by a parity index ($\mathbb{Z}_2$). The other classes are topologically trivial. This table has periodicity 8 with the dimension.

Hall conductance σ_{xy} of a conductor placed in a strong magnetic field, at low temperature, is quantised and only takes values which are multiple of the quantum conductance [76, 182]

$$\sigma_{xy} = n\frac{e^2}{h}\,, \quad n \in \mathbb{N}^*\,. \tag{5.42}$$

The integer n was shown to be of topological nature [172, 290]: it is a winding number which characterises the bulk properties of the system. A value $n \neq 0$ indicates a non trivial insulator.

Another possible explanation for the quantisation of the Hall resistance has been proposed by Büttiker [70] and emphasises the role of edge states [172] . The existence of edge states (chiral channels propagating along the boundary) corresponds to the interface between two different insulating phases: the Hall state in the sample and the trivial insulating phase outside. In the quantum Hall effect, the number of edge states is given by the filling factor n which appears in (5.42). This was shown to be a general feature of topological insulators and topological superconductors, and has been named the *bulk-edge correspondence* [269].

The topological properties of a system are constrained by symmetries. In any dimension, among the ten symmetry classes discussed in Section 5.2, only five of them can support non trivial topological phases. This property is encoded in the *periodic table of topological insulators* [193, 269], summarised in Table 5.2. $\mathbb{Z}$ corresponds to topological phases classified by with a winding number while $\mathbb{Z}_2$ insulators are characterised by a parity index. For example, the quantum Hall effect corresponds to the $\mathbb{Z}$ index for 2D systems in the unitary Wigner-Dyson class (class A).

The main interest for topological phases rely in their robustness. Indeed, it requires a great perturbation to change a topological property. Therefore, the introduction of small disorder is expected leave the topological index unchanged. This property has lead to the proposal of using topological states for quantum computing [7, 192], which are

topologically protected from decoherence. However, strong enough disorder can drive topological phase transitions [240, 264, 268].

Multichannel disordered wires have provided a convenient framework to study the effect of disorder on topological phases, and in particular how the disorder can drive topological phase transitions. In the quasi-1D geometry, Table 5.2 indicates that models belonging to the three chiral classes and two BdG classes can exhibit non trivial topological phases. They were indeed shown to exhibit topologically protected Majorana zero modes [192, 255]. The number of these modes plays the role of a topological index.

Chapter 6

Model and tools

In this chapter, we introduce a model of disordered wires which we will analyse in details in the next chapters: the multichannel Dirac equation with a random mass. In the stricly one dimensional case, this model is associated with the following Hamiltonian:

$$\mathcal{H} = \mathrm{i}\sigma_2\partial_x + m(x)\sigma_1 \,. \tag{6.1}$$

It arises in different contexts in condensed matter physics, such as disordered metals at half filling [156, 157], organic conductors [281], random spin chains [23, 129–131, 133, 223, 274, 280], superconductors with random gap [35, 204]. It has also been studied in statistical physics, due to its relation with the Sinai model [21, 158, 190, 276]: the square of the Hamiltonian (6.1) can be mapped onto the Fokker-Planck operator describing the diffusion of a classical particle subjected to a random force, the famous "Sinai problem" [51, 131, 201, 238].

The DMPK approach introduced in Chapter 5 relies on global considerations, based on symmetries. This method is restricted to the analysis of the universal properties of the system. However, it can also be important to understand the crossover between different universal regimes. Such an example is the transition between the GOE and GUE: the two ensembles describe universal properties for zero and strong magnetic field respectively. However, the full crossover[1] would be needed to compare to experimental data (for example, a conductance curve).

In the case of the Dirac equation (6.1), the two universal points are located at zero energy $\varepsilon = 0$ (chiral classes) and infinity (Wigner-Dyson classes, see Table 5.1). Exact results from the DMPK approach are only available in these two universal limiting cases. Here, we present a detailed analysis the multichannel version of the model (6.1), from which we derive the universal and non-universal properties.

6.1 The model

We consider the multichannel Dirac equation

$$\mathcal{H}\Psi(x) = \varepsilon\Psi(x) \,, \tag{6.2}$$

[1] Several models have been introduced to study this crossover from a random matrix point of view, see for instance Refs. [225, 259]

where Ψ is a $2N$-components spinor, and the Dirac Hamiltonian $\mathcal{H}$ is of the form

$$\mathcal{H} = \mathrm{i}\,\sigma_2 \otimes \mathbb{1}_N\,\partial_x + \sigma_1 \otimes M(x) = \begin{pmatrix} 0 & \partial_x + M(x) \\ -\partial_x + M(x) & 0 \end{pmatrix}, \tag{6.3}$$

with σ_i a Pauli matrix and the mass $M(x)$ is a $N \times N$ matrix. It can be either real symmetric ($\beta = 1$), complex Hermitian ($\beta = 2$) or quaternionic self-dual ($\beta = 4$). The Hamiltonian (6.3) exhibits the chiral symmetry:

$$\boxed{\sigma_3 \mathcal{H} \sigma_3 = -\mathcal{H}} \tag{6.4}$$

Therefore, the system lies in one of the three chiral classes, see Table 5.1 page 118, specified by the Dyson index β.

We now describe our model of disorder. The minimal model consists in taking the random mass $M(x)$ in the form of a Gaussian white noise, $\langle M_{ab}(x) M_{cd}(x') \rangle \propto \delta(x - x')$. However, there remains to specify the choice of correlations between the channels.

Isotropic noise

A first possibility is to pick the mass from the distribution

$$P[M(x)] \propto \exp\left\{ -\frac{1}{2} \int \mathrm{d}x\, \mathrm{tr}\left[(M(x) - \mu g \mathbb{1}_N)^2 \right] \right\}, \quad \text{with } M(x)^\dagger = M(x)\,. \tag{6.5}$$

It is invariant under the transformation

$$M(x) \to U^\dagger M(x) U\,, \tag{6.6}$$

where U belongs to the corresponding symmetry group:

$$U \in \begin{cases} \mathrm{O}(N)\,, & \text{for } \beta = 1\,, \\ \mathrm{U}(N)\,, & \text{for } \beta = 2\,, \\ \mathrm{Sp}(N)\,, & \text{for } \beta = 4\,. \end{cases} \tag{6.7}$$

Therefore, this distribution corresponds to an isotropic situation with respect to channel exchange (as in the DMPK approach), since the noise couples all the channels in the same manner.

Partially anisotropic noise

We wish to go beyond the isotropy assumption which is central in the DMPK approach. We will consider a more general distribution of the noise:

$$P[M(x)] \propto \exp\left\{ -\frac{1}{2} \int \mathrm{d}x\, \mathrm{tr}\left[(M(x) - \mu G) G^{-1} (M(x) - \mu G) \right] \right\}, \quad M(x)^\dagger = M(x)\,, \tag{6.8}$$

where $\mu \in \mathbb{R}$ and G is a positive self-adjoint matrix which controls the correlations of the matrix elements of M. In this model, the correlations and the mean value $\langle M(x) \rangle = \mu G$ are controlled by the **same** matrix G. Without loss of generality, we can assume that it is diagonal

$$G = \mathrm{Diag}(g_1, \ldots, g_N)\,. \tag{6.9}$$

We can tune the N parameters $\{g_i\}$ which control the strength of the noise, and the parameter μ controlling the mean. We thus have $N+1$ parameters, unlike the only 2 available in the isotropic model (6.5) (μ and $g = g_1 = \cdots = g_N$). The parameter $\mu = \langle M \rangle G^{-1}$ is the mass-over-disorder ratio, and will play a prominent role in the following.

In particular, this model permits to change the number of channels by letting one of the elements of G, say g_N, to zero. Indeed, in this limit, the noise becomes

$$M(x) \to \begin{pmatrix} \tilde{M}(x) & 0 \\ 0 & 0 \end{pmatrix}, \quad \text{for } g_N \to 0\,, \tag{6.10}$$

where $\tilde{M}$ is a $(N-1)\times(N-1)$ matrix, distributed according to (6.8), with the matrix $G = \mathrm{Diag}(g_1, \ldots, g_{N-1})$. In this limit, we thus obtain $N-1$ channels coupled by the disorder, and one independent free channel.

Fully anisotropic noise

The most general kind of disorder takes the form

$$P[M(x)] \propto \exp\left\{-\frac{1}{2}\int \mathrm{d}x\, \mathrm{tr}\left[A^{-1}(M(x)-\mu G)B^{-1}(M(x)-\mu G)\right]\right\}, \tag{6.11}$$

where $\mu \in \mathbb{R}$ and A, B and G are positive self-adjoint matrices. In this model, one can tune independently the mean and variance of each matrix element of M.

Although the most general form of the noise (6.11) permits to reach the two dimensional limit (by coupling only the nearest neighbour channels), it is too complex to get analytical results. Instead, we will consider the intermediate model (6.8), from which we will be able to obtain analytical results.

6.2 The scattering problem

Let us now introduce the scattering formulation, which will be shown to provide a convenient way to study both the spectral and topological properties. We consider the Dirac equation (6.2) on the half line $x > 0$. We suppose that the disorder is restricted to a finite region $[0, L]$, on which the mass is picked from the distribution (6.8). For $x > L$, we set $M(x) = 0$. At $x = 0$, we impose the boundary condition by setting $M(x) = \pm\infty$ on the domain $x < 0$. This ensures total reflection of any wave coming from the right, see Fig. 6.1.

The $N = 1$ channel case

Let us first consider the simpler case of $N = 1$, corresponding to a purely one dimensional system. In the region $x > L$, Eq. (6.2) reduces to the free Dirac equation. Therefore the solutions take the form of plane waves:

$$\begin{pmatrix} -1 \\ \mathrm{i} \end{pmatrix} \mathrm{e}^{\mathrm{i}\varepsilon(x-L)}, \quad \text{and} \quad \begin{pmatrix} 1 \\ \mathrm{i} \end{pmatrix} \mathrm{e}^{-\mathrm{i}\varepsilon(x-L)}. \tag{6.12}$$

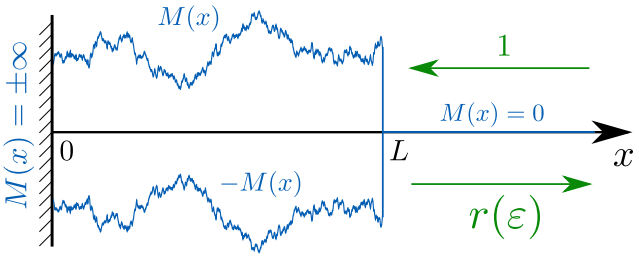

Figure 6.1: A scattering situation. A wave incoming from the right on the disordered region $[0, L]$ is completely reflected. The amplitude of the reflected wave is controlled by the reflection matrix $r(\varepsilon)$. We represented the mass and its opposite to remember that non-zero mass implies a gapped spectrum.

If we consider a wave coming from the right with amplitude 1, the amplitude of the reflected wave is controlled by the reflection coefficient $r(\varepsilon)$ (see Eq. 5.7). The solution is the superposition of the incoming and outgoing plane waves:

$$\psi_\varepsilon(x) = \begin{pmatrix} 1 \\ \mathrm{i} \end{pmatrix} \mathrm{e}^{-\mathrm{i}\varepsilon(x-L)} + r(\varepsilon) \begin{pmatrix} -1 \\ \mathrm{i} \end{pmatrix} \mathrm{e}^{\mathrm{i}\varepsilon(x-L)} \,. \tag{6.13}$$

Since the wave is totally reflected, the reflection coefficient is of modulus one:

$$|r(\varepsilon)| = 1 \,. \tag{6.14}$$

Additionally, the chiral symmetry (6.4) links the solutions for positive and negative energies:

$$\psi_{-\varepsilon}(x) \propto \sigma_3 \psi_\varepsilon(x) = \begin{pmatrix} 1 \\ -\mathrm{i} \end{pmatrix} \mathrm{e}^{\mathrm{i}(-\varepsilon)(x-L)} + r(\varepsilon) \begin{pmatrix} -1 \\ -\mathrm{i} \end{pmatrix} \mathrm{e}^{-\mathrm{i}(-\varepsilon)(x-L)} \,, \tag{6.15}$$

which corresponds to the superposition of an outgoing wave of amplitude 1 and an incoming wave of amplitude $r(\varepsilon)$. The reflection coefficient $r(-\varepsilon)$ at energy $-\varepsilon$ is defined from an incoming wave of unit amplitude. We thus multiply $\sigma_3\psi_\varepsilon$ by $-1/r(\varepsilon) = -r(\varepsilon)^\star$ to obtain the true scattering state for energy $-\varepsilon$:

$$\psi_{-\varepsilon}(x) = r(\varepsilon)^\star \begin{pmatrix} -1 \\ \mathrm{i} \end{pmatrix} \mathrm{e}^{\mathrm{i}(-\varepsilon)(x-L)} + \begin{pmatrix} 1 \\ \mathrm{i} \end{pmatrix} \mathrm{e}^{-\mathrm{i}(-\varepsilon)(x-L)} \,. \tag{6.16}$$

Comparing with (6.13), we deduce that the reflection coefficient for energy $-\varepsilon$ is

$$r(-\varepsilon) = r(\varepsilon)^\star \,. \tag{6.17}$$

This symmetry of the reflection coefficient is the direct consequence of the chiral symmetry (6.4).

Inside the disordered region, the spinor

$$\psi_\varepsilon = \begin{pmatrix} \varphi \\ \xi \end{pmatrix} \tag{6.18}$$

is solution of the Dirac equation (6.2). At the origin, we can choose two possible boundary conditions, depending on the convention for the mass (see Ref. [285] and references therein), either

$$\xi(0) = 0 \quad \text{if} \quad M(x) = +\infty \quad \text{for} \quad x < 0 \,, \tag{6.19}$$

or

$$\varphi(0) = 0 \quad \text{if} \quad M(x) = -\infty \quad \text{for} \quad x < 0\,. \tag{6.20}$$

We will often choose the second one, but for the moment we will keep these two possibilities.

The integrated density of states $\mathcal{N}_L(\varepsilon)$ of the system of size L can be easily obtained from the reflection coefficient r' via the Krein-Friedel relation [95, 137, 138, 196]:

$$\mathcal{N}_L(\varepsilon) = \frac{1}{2\pi}\,\delta(\varepsilon) = \frac{1}{2\mathrm{i}\pi}\ln r(\varepsilon)\,. \tag{6.21}$$

This relation connects a property of the scattering states (the scattering phase δ) to the spectrum of the isolated system of length L. This relation can be understood easily: let us consider the spectral problem on $[0, L]$. The n^{th} eigenmode ψ_n, of energy ε_n, satisfies boundary conditions both at $x = 0$ and $x = L$. If we take for example $M(x) = -\infty$ for $x < 0$ and $M(x) = +\infty$ for $x > L$, then $\varphi_n(0) = 0$ and $\varphi_n(L) = 0$. The scattering states (6.13) can be related to these normalised eigenmodes by imposing that they satisfy the boundary conditions. The condition at $x = 0$ is satisfied by construction, and the one at $x = L$ gives

$$1 - r(\varepsilon_n) = 0 \quad \Rightarrow \quad r(\varepsilon_n) = \mathrm{e}^{2\mathrm{i}\pi n}\,, \tag{6.22}$$

in the case $M(x) = +\infty$ for $x > L$. Therefore, the phase of the reflection coefficient changes by 2π when going from one eigenmode to the next.

The $N > 1$ case

Let us now consider the multichannel situation. The Dirac equation (6.2) has N independent solutions. For convenience, we regroup them into a $2N \times N$ "spinor":

$$\Psi(x) = \begin{pmatrix} \Phi(x) \\ \Xi(x) \end{pmatrix}\,, \tag{6.23}$$

where Φ and Ξ are $N \times N$ matrices which represent the "components" of the spinor Ψ. As in the 1D case, in the domain $x > L$, the solutions take the form the superposition of plane waves:

$$\Psi(x) = \begin{pmatrix} \mathbb{1}_N \\ \mathrm{i}\,\mathbb{1}_N \end{pmatrix} \mathrm{e}^{-\mathrm{i}\varepsilon(x-L)} + \mathbb{1}_2 \otimes r(\varepsilon) \begin{pmatrix} -\mathbb{1}_N \\ \mathrm{i}\,\mathbb{1}_N \end{pmatrix} \mathrm{e}^{\mathrm{i}\varepsilon(x-L)}\,, \quad x > L\,, \tag{6.24}$$

where the reflection matrix r is of size $N \times N$. The discussions on the 1D case straightforwardly generalise to the multichannel case: the total reflection of the incoming wave implies that the reflection matrix is unitary:

$$r(\varepsilon) \in \mathrm{U}(N)\,, \tag{6.25}$$

and the chiral symmetry implies

$$\boxed{r(-\varepsilon) = r(\varepsilon)^\dagger} \tag{6.26}$$

This matrix encodes all the information about the disordered region. For example, the integrated density of states is encoded in the phase $\delta(\varepsilon)$ of the determinant of r:

$$\mathcal{N}_L(\varepsilon) = \frac{1}{2\pi}\,\delta(\varepsilon) = \frac{1}{2\pi\mathrm{i}}\ln\det r(\varepsilon)\,, \quad \det r(\varepsilon) = \mathrm{e}^{\mathrm{i}\delta(\varepsilon)}\,. \tag{6.27}$$

The reflection matrix is a convenient object to characterise the disordered system. However, we will now introduce another matrix, related to r, which is more practical for analytic computations.

6.3 The Riccati matrix

It has been shown that the analysis of one dimensional solvable models can be conveniently handled by introducing a Riccati variable [84–86, 139, 165, 173, 206]. To extend this idea to the multichannel case, we introduce the Riccati matrix

$$Z_\varepsilon(x) = -\varepsilon\,\Xi(x)\Phi(x)^{-1}\,, \tag{6.28}$$

where Φ and Ξ are the two components of the matrix spinor (6.23). Using that they satisfy the Dirac equation (6.2), we can show that the Riccati matrix obeys the equation

$$\partial_x Z_\varepsilon(x) = -\varepsilon^2 - Z_\varepsilon(x)^2 - M(x)Z_\varepsilon(x) - Z_\varepsilon(x)M(x)\,. \tag{6.29}$$

The initial condition at $x = 0$ follows from the one on the spinor Ψ, Eqs. (6.19,6.20):

$$\begin{cases} M(x) = +\infty \text{ for } x < 0 \;\;\Rightarrow\;\; \Xi(0) = 0 \;\;\Rightarrow\;\; Z_\varepsilon(0) = 0\,\mathbb{1}_N\,, \\ M(x) = -\infty \text{ for } x < 0 \;\;\Rightarrow\;\; \Phi(0) = 0 \;\;\Rightarrow\;\; Z_\varepsilon(0) = \infty\mathbb{1}_N\,. \end{cases} \tag{6.30}$$

To stress the importance of this matrix, let us first show how its relation with the reflection matrix $r(\varepsilon)$. From Eq. (6.24), we have:

$$\Phi(L) = \mathbb{1}_N - r(\varepsilon)\,, \quad \Xi(L) = \mathrm{i}[\mathbb{1}_N + r(\varepsilon)]\,. \tag{6.31}$$

From the definition of Z_ε (6.28), we deduce:

$$Z_\varepsilon(L) = -\mathrm{i}\varepsilon[\mathbb{1}_N + r(\varepsilon)][\mathbb{1}_N - r(\varepsilon)]^{-1}\,. \tag{6.32}$$

This relation can be inverted to express the reflection matrix as

$$\boxed{r(\varepsilon) = [\varepsilon - \mathrm{i}Z_\varepsilon(L)][\varepsilon + \mathrm{i}Z_\varepsilon(L)]^{-1}} \tag{6.33}$$

Therefore, we have reduced the problem of determining the reflection matrix to integrating the differential equation (6.29) on $[0, L]$.

When the mass $M(x)$ is a Gaussian white noise, (6.29) is a stochastic differential equation *on the matrix* Z_ε. This equation involving a multiplicative noise, we should specify in which sense we interpret it. The Gaussian white noise can be thought of as a spatially correlated noise in the limit of zero correlation length. If we assume that these correlations are symmetric in space, the limit of zero correlations yields a stochastic equation in the Stratonovich sense [155].

If L is large enough, we expect the process $Z_\varepsilon(x)$ to become stationary. Our aim will be to find this stationary distribution.

But first, let us discuss the symmetries of the stochastic equation (6.29). Since the Riccati matrix and its adjoint[2] satisfy the same initial condition $Z_\varepsilon(0)^\dagger = Z_\varepsilon(0)$ and also the same differential equation since $M^\dagger = M$, we deduce that this matrix is self-adjoint:

$$Z_\varepsilon(x)^\dagger = Z_\varepsilon(x)\,. \tag{6.34}$$

Additionally, using that $\partial_x(Z_\varepsilon^{-1}) = -Z_\varepsilon^{-1}(\partial_x Z_\varepsilon)Z_\varepsilon^{-1}$, we can easily show that $Y_\varepsilon(x) = -\varepsilon^2\, Z_\varepsilon^{-1}$ also satisfies (6.29), but with the mass replaced by its opposite: $M(x) \to -M(x)$. The initial condition having no influence on the stationary properties of the stochastic process, we have:

$$Z_\varepsilon(x;M) \overset{\text{(law)}}{=} -\varepsilon^2\, Z_\varepsilon(x;-M)^{-1}\,, \tag{6.35}$$

where $Z_\varepsilon(x;M)$ denotes the solution of (6.29) for the mass $M(x)$, and we denoted equality in law to indicate that the two stochastic processes have the same stationary distribution. This property is a consequence of the supersymmetry of the Dirac equation (see Ref. [86] for a discussion of the $N = 1$ channel case).

6.3.1 Fokker-Planck equation

We stress an important difference between the DMPK method and the approach we follow here. The DMPK approach is based on a Fokker-Planck equation for the *eigenvalues* of the transmission matrix. Here, instead of considering the eigenvalues of the Riccati matrix, we study the *full matrix* Z_ε. We will thus write a Fokker-Planck equation for the matrix process $Z_\varepsilon(x)$. This central difference is crucial to go beyond the isotropic case and study the effect of introducing some anisotropy between the channels.

Let us denote $f(Z;x)$ the distribution of the matrix Z_ε, at position x. The Fokker-Planck equation associated to the SDE (6.29) takes the form

$$\frac{\partial}{\partial x} f(Z;x) = \mathscr{G}^\dagger f(Z;x)\,, \tag{6.36}$$

where $\mathscr{G}^\dagger$ is a second order differential operator with respect to the elements of Z. The notation comes from the fact that this operator is the adjoint of another operator, called the generator of the diffusion, which plays a central role for stochastic processes [254]. We will first derive the expression of the operator $\mathscr{G}^\dagger$, and in a second step look for the stationary distribution $f(Z)$, solution of

$$\mathscr{G}^\dagger f(Z) = 0\,. \tag{6.37}$$

To write this operator, we need to express the matrix Z_ε in terms of independent real components. Since this matrix is self-adjoint, it has

$$N\left(\beta\frac{N-1}{2}+1\right) \tag{6.38}$$

independent real parameters. We now need to distinguish the different values of β. For simplicity, we will drop the index ε and simply denote Z the Riccati matrix.

[2] We denote $\dagger$ the adjoint in the generic case: for $\beta = 1$ it is a transpose, for $\beta = 2$ a conjugate transpose and for $\beta = 4$ a quaternionic conjugate transpose.

Orthogonal case $\beta = 1$

In this case, the matrices Z and M being real symmetric, we only need to consider their upper-triangular parts. Let us first focus on the noise $M(x)$. We can rewrite the distribution (6.8) in terms of the matrix elements:

$$P[M(x)] \propto \prod_{n=1}^{N} \exp\left\{-\int \frac{\mathrm{d}x}{\sigma_{nn}}(M_{nn}(x) - \mu g_n)^2\right\} \prod_{m<n} \exp\left\{-\int \frac{\mathrm{d}x}{\sigma_{mn}} M_{mn}(x)^2\right\} , \quad (6.39)$$

where we denoted:

$$\sigma_{mn} = \begin{cases} g_n & \text{for } m = n , \\ \dfrac{g_n g_m}{g_n + g_m} & \text{for } m \neq n . \end{cases} \quad (6.40)$$

In this form, it is clear that each matrix element is an independent Gaussian white noise, with mean $\mu g_n \delta_{mn}$ and variance σ_{mn}. Therefore, we will denote

$$M_{mn} = \mu g_n \, \delta_{mn} + \sqrt{\sigma_{mn}} \, \xi_{mn} , \quad (6.41)$$

where ξ_{mn} is a Gaussian white noise of unit variance and zero mean.

Let us now write the equation satisfied by each independent component of the Riccati matrix Z. From the Eq. (6.29), we can straightforwardly write the equation satisfied by each matrix element:

$$\partial_x Z_{mn}(x) = [-Z^2 - \varepsilon^2 - \mu G Z - \mu Z G]_{mn} + \sum_{k \leqslant l} B_{mn,kl}(Z) \, \xi_{kl} , \quad (6.42)$$

where we restricted the summation to $k \leqslant l$ to consider only *independent* noises, and we introduced

$$B_{mn,kl}(Z) = -\sqrt{\sigma_{kl}} \, \frac{2 - \delta_{kl}}{2} (Z_{mk}\delta_{nl} + Z_{ml}\delta_{nk} + Z_{ln}\delta_{km} + Z_{kn}\delta_{lm}) . \quad (6.43)$$

From this set of coupled stochastic equations, we can write the Fokker-Planck equation satisfied by the upper triangular matrix elements of Z in the form (6.36), with the generator

$$\mathscr{G}^\dagger = \sum_{m \leqslant n} \frac{\partial}{\partial Z_{mn}} \Big[Z^2 + E + \mu G Z + \mu Z G\Big]_{mn} + \frac{1}{2} \sum_{m \leqslant n} \sum_{k \leqslant l} \sum_{a \leqslant b} \frac{\partial}{\partial Z_{mn}} B_{mn,kl}(Z) \frac{\partial}{\partial Z_{ab}} B_{ab,kl}(Z) . \quad (6.44)$$

It is possible to write this equation in a compact way, using the matrix structure of the equation. In order to do so, we introduce a matrix differential operator $\frac{\partial}{\partial Z}$ which takes into account the symmetries of Z (see Appendix A.2). It is defined as

$$\left(\frac{\partial}{\partial Z}\right)_{mn} = \frac{1 + \delta_{mn}}{2} \frac{\partial}{\partial Z_{mn}} . \quad (6.45)$$

This specific form of the operator has been chosen to take into account that the diagonal terms appear only once, while the off-diagonal terms appear twice (since $Z_{ij} = Z_{ji}$). Using this operator, the generator (6.44) can be rewritten in the compact form

$$\mathscr{G}^\dagger = \mathrm{tr}\left\{\frac{\partial}{\partial Z}\left(Z^2 + E\ + \mu GZ + \mu ZG)\right\}\right. \\ \left. + 2\ \mathrm{tr}\left\{\frac{\partial}{\partial Z} Z\left[\tilde{\sigma} \circ \left[\frac{\partial}{\partial Z} Z + \left(\frac{\partial}{\partial Z} Z\right)^T\right]\right]\right\}, \tag{6.46}$$

where $[A \circ B]_{mn} = A_{mn} B_{mn}$ is the Hadamard product and we introduced the modified matrix of variances:

$$\tilde{\sigma}_{ab} = \frac{2 - \delta_{ab}}{2} \sigma_{ab} \,. \tag{6.47}$$

Unitary case $\beta = 2$

In this case, the matrices M and Z are complex Hermitian. We can decompose the matrix elements of the noise into real and imaginary parts:

$$M_{mn} = \mu g_n \, \delta_{mn} + \sqrt{\sigma_{mn}}(\xi_{mn} + \mathrm{i}\zeta_{mn}) \,, \tag{6.48}$$

where ξ_{mn} and ζ_{mn} are two independent Gaussian white noises of unit variance and zero mean, and σ_{mn} is given by Eq. (6.40). The Hermiticity of the matrix M imposes the conditions

$$\xi_{mn} = \xi_{nm} \,, \quad \zeta_{mn} = -\zeta_{nm} \,. \tag{6.49}$$

As in the previous case, we can write a stochastic equation for each matrix element of the Riccati matrix:

$$\partial_x Z_{mn}(x) = [-Z^2 - \varepsilon^2 - \mu GZ - \mu ZG]_{mn} + \sum_{k \leqslant l} B_{mn,kl}(Z)\, \xi_{kl} + \sum_{k<l} C_{mn,kl}(Z)\, \zeta_{kl} \,, \tag{6.50}$$

where $B_{mn,kl}(Z)$ is given by Eq. (6.43) and

$$C_{mn,kl}(Z) = -\sqrt{\sigma_{kl}}\,(Z_{mk}\delta_{nl} - Z_{ml}\delta_{nk} + Z_{ln}\delta_{km} - Z_{kn}\delta_{lm}) \,. \tag{6.51}$$

Having expressed the SDE in terms of independent Gaussian white noises, we can now write the generator of the diffusion. We could decompose the matrix Z into independent real elements, as we did for the noise $M(x)$. However, it is simpler to consider the two complex-conjugate off diagonal elements Z_{mn} and Z_{nm} as independent variables. In doing so, we can write the corresponding generator as:

$$\mathscr{G}^\dagger = \sum_{m,n} \frac{\partial}{\partial Z_{mn}} \left[Z^2 + E + \mu GZ + \mu ZG\right]_{mn} \\ + \frac{1}{2} \sum_{m,n} \sum_{k \leqslant l} \sum_{a,b} \frac{\partial}{\partial Z_{mn}} B_{mn,kl}(Z) \frac{\partial}{\partial Z_{ab}} B_{ab,kl}(Z) \\ + \frac{1}{2} \sum_{m,n} \sum_{k<l} \sum_{a,b} \frac{\partial}{\partial Z_{mn}} C_{mn,kl}(Z) \frac{\partial}{\partial Z_{ab}} C_{ab,kl}(Z) \,. \tag{6.52}$$

As before, we can rewrite this complex expression in terms of the matrix differential operator $\frac{\partial}{\partial Z}$, which now takes the simple form:

$$\left(\frac{\partial}{\partial Z}\right)_{mn} = \frac{\partial}{\partial Z_{mn}}\,, \tag{6.53}$$

since all matrix elements are now independent. The generator (6.52) can then be rewritten as

$$\begin{aligned}\mathscr{G}^\dagger = &\operatorname{tr}\left\{\left(\frac{\partial}{\partial Z}\right)^T \left[Z^2 + E + \mu GZ + \mu ZG\right]\right\} \\ &+ \operatorname{tr}\left\{\left[\frac{\partial}{\partial Z}Z^T + \left(\left(\frac{\partial}{\partial Z}\right)^T Z\right)^T\right]^T \tilde{\sigma}\circ\left[\left(\frac{\partial}{\partial Z}\right)^T Z + \left(\frac{\partial}{\partial Z}Z^T\right)^T\right]\right\}.\end{aligned} \tag{6.54}$$

Symplectic case $\beta = 4$

I did not write explicitly the generator $\mathscr{G}^\dagger$ of the Fokker-Planck equation in the quaternionic case, as the procedure becomes quite cumbersome. But we expect the results obtained for $\beta = 1$ and $\beta = 2$ to generalise to $\beta = 4$.

6.3.2 Stationary distribution

The Fokker-Planck equation (6.36) cannot be solved analytically to give $f(x; Z)$ for all x. Therefore, we will focus on the stationary distribution $f(Z)$, which is solution of Eq. (6.37). The (adjoint) generator $\mathscr{G}^\dagger$ is given by Eq. (6.46) for $\beta = 1$ and Eq. (6.54) for $\beta = 2$. This gives a partial differential equation of second order, with complex structure. To get some insight, let us first look at the well-studied $N = 1$ case [51, 86].

In the strictly 1D case, Eq. (6.37) reduces to the ordinary differential equation

$$2g\frac{\mathrm{d}}{\mathrm{d}z}z\frac{\mathrm{d}}{\mathrm{d}z}(zf(z)) + \frac{\mathrm{d}}{\mathrm{d}z}[(z^2 + \varepsilon^2 + 2\mu g z)f(z)] = 0\,. \tag{6.55}$$

For purely imaginary energy $\varepsilon = \mathrm{i}k$, this Fokker-Planck equation admits the following stationary solution [51, 86]:

$$f(z) = \mathcal{C}^{-1}\, z^{-\mu-1}\, \mathrm{e}^{-\frac{1}{2g}(z+k^2/z)}\,, \tag{6.56}$$

where the normalisation constant $\mathcal{C}$ depends on the energy k and the mass over disorder ratio μ. Knowing this result for $N = 1$, we can try to guess to form of the solution for the multichannel case. We take the ansatz:

$$f(Z) = \mathcal{C}_{N,\beta}^{-1}\,(\det Z)^{-\mu-\alpha}\,\exp\left\{-\frac{1}{2}\operatorname{tr}\left[G^{-1}(Z + k^2 Z^{-1})\right]\right\}\,, \tag{6.57}$$

where α is a constant to be determined. For small values of N, this ansatz can be verified using a symbolic computation program, such as MATHEMATICA, by plugging this form into the Fokker-Planck equation (6.37). By doing so, we find the following values of α:

	$\beta = 1$	$\beta = 2$
$N = 1$	$\alpha = 1$	$\alpha = 1$
$N = 2$	$\alpha = 3/2$	$\alpha = 2$
$N = 2$	$\alpha = 2$	$\alpha = 3$

These results seem to indicate that α takes the value

$$1 + \beta \frac{N-1}{2} \, . \tag{6.58}$$

This can be proved analytically by plugging the ansatz (6.57) into the stationary Fokker-Planck equation (6.37). The matrix derivatives can be evaluated using the properties given in Appendix A.2. Then, after rather lengthy but elementary calculations, one can prove that the left hand side of Eq. (6.37) reduces to zero, proving that (6.57) is the stationary distribution of the Riccati process.

To summarise, we have proved that the stationary distribution associated to the stochastic process (6.29), for purely imaginary energy $\varepsilon = \mathrm{i}k$ is:

$$\boxed{f(Z) = \mathcal{C}_{N,\beta}^{-1} \, (\det Z)^{-\mu-1-\beta\frac{N-1}{2}} \, \exp\left\{ -\frac{1}{2} \operatorname{tr}\left[G^{-1}(Z + k^2 Z^{-1}) \right] \right\}} \tag{6.59}$$

where the normalisation constant $\mathcal{C}_{N,\beta}$ depends on k, μ and the matrix G. Using that the Lebesgue measure $\mathrm{d}Z$ verifies (see Appendix A.1)

$$\mathrm{d}(Z^{-1}) = (\det Z)^{-2-\beta(N-1)} \mathrm{d}Z \, , \tag{6.60}$$

we can easily check that the distribution (6.59) is invariant under the change $Z \to k^2 Z^{-1}$, provided that we replace μ by $-\mu$:

$$f_\mu(Z)\mathrm{d}Z = f_{-\mu}(k^2 Z^{-1})\mathrm{d}(k^2 Z^{-1}) \, . \tag{6.61}$$

This relation is exactly the supersymmetry (6.35) for $\varepsilon = \mathrm{i}k$.

We stress that the stationary distribution (6.59) permits to go beyond the DMPK formalism, as we have introduced some anisotropy between the channels, controlled by the matrix G. We can recover the isotropic situation by setting $G = g\mathbb{1}_N$. By doing so, the distribution (6.59) becomes invariant under transforms $Z \to U^\dagger Z U$, with U belonging to the associated symmetry group, see Eq. (6.7). The consequence is that the eigenvalues and eigenvectors of Z decouple, and we can focus only on the eigenvalues $\{z_n\}$ (the distribution of the eigenvectors is uniform). The joint distribution of the eigenvalues can be obtained by integration over the matrix U:

$$f(\{z_i\}) = \mathcal{C}_{N,\beta}^{-1} \prod_{i<j} |z_i - z_j|^\beta \prod_{i=1}^N z_i^{-\mu-1-\beta\frac{N-1}{2}} \, \mathrm{e}^{-\frac{1}{2g}(z_i + k^2/z_i)} \, , \tag{6.62}$$

where we have re-defined the normalisation constant, to absorb the volume of the symmetry group $\int \mathrm{d}\mu(U)$ which plays no role.

The stationary distribution (6.59) is the central object of our approach. In the next chapters, we will extract most of the information about the system, such as the density of states, from this distribution.

Chapter 7

Density of states and localisation properties

In the previous Chapter, we have introduced the Riccati matrix Z_ε and obtained its stationary distribution $f(Z)$ for purely imaginary energy $\varepsilon = \mathrm{i}k$. We will now relate this distribution to physical properties of the system, such as the density of states and the localisation length. We discuss in Section 7.3 a method to compute these quantities numerically.

7.1 Density of states

As we have seen in Chapter 6, the Riccati matrix Z_ε is simply related to the reflection matrix r by relation (6.33). Since the scattering matrix encodes all the spectral information of the system, so does the Riccati matrix. In this section, we will first introduce a convenient way to derive the density of states from the stationary distribution (6.59). Then using this method, we will obtain exact expressions for the density of states under the form of determinants, which will allow us to study its behaviour for $\varepsilon \to 0$.

The simplest way to relate the density of states to the Riccati matrix is to consider a *closed* system of size L. We thus consider the Dirac equation (6.2,6.3) on the interval $[0, L]$, and impose the boundary conditions $M(x) = -\infty$ for $x < 0$ and $x > L$ (the discussion is the same for the other possible boundary condition $M(x) = +\infty$). Denote $\psi_n = (\varphi_n \ \chi_n)^T$ the spinor associated to the energy ε_n. The first component verifies $\varphi_n(0) = \varphi_n(L) = 0$.

7.1.1 Analytic continuation and characteristic function

In order to relate this spectral problem to the reflection matrix introduced in the previous chapter, we need to change our perspective. Instead of diagonalising the Dirac Hamiltonian, let us set for any energy ε the initial value problem:

$$\mathcal{H}\Psi(\varepsilon; x) = \varepsilon\Psi(\varepsilon; x)\,, \quad \Psi(\varepsilon; x) = \begin{pmatrix} \Phi(\varepsilon; x) \\ \Xi(\varepsilon; x) \end{pmatrix}\,, \ \Phi(\varepsilon; 0) = 0 \text{ and } \Xi(\varepsilon; 0) = \mathbb{1}_N\,. \tag{7.1}$$

where we constructed a "matrix spinor" Ψ containing all N independent solutions. This differential equation can then be integrated on the interval $[0, L]$ to give $\Psi(\varepsilon; x)$. If ε is set to one of the eigenvalues of $\mathcal{H}$, say ε_n, the corresponding spinor ψ_n, which is also a solution of the Dirac equation, can be expressed as a linear combination of the independent solutions contained in $\Psi(\varepsilon_n; x)$. The second boundary condition $\varphi_n(L) = 0$ implies that this linear combination of the columns of $\Phi(\varepsilon_n; x)$ vanishes at $x = L$. Equivalently, $\det \Phi(\varepsilon_n; L) = 0$. This properties allows to easily determine the *integrated density of states* (IDoS), denoted $\mathcal{N}_L(\varepsilon)$, which is the number of eigenstates of energy smaller than ε. The idea is to count the number of times $\det \Phi$ vanishes (or equivalently changes sign) between 0 and ε. A convenient way to perform this counting relies on analytical properties of Ψ, and thus of $\det \Phi(\varepsilon; L)$, in the energy ε. Indeed, since $\det \Phi(\varepsilon; L)$ changes sign when crossing one eigenvalue ε_n, its logarithm picks up a shift:

$$\ln \det \Phi(\varepsilon_n^+ + \mathrm{i}0^+; L) = \ln \det \Phi(\varepsilon_n^- + \mathrm{i}0^+; L) - \mathrm{i}\pi \,. \tag{7.2}$$

Therefore, the IDoS is given by:

$$\mathcal{N}_L(\varepsilon) = -\frac{1}{\pi} \operatorname{Im}[\ln \det \Phi(\varepsilon + \mathrm{i}0^+; L)] \,. \tag{7.3}$$

There only remains to relate $\det \Phi$ to the Riccati matrix Z_ε. Since the matrix spinor Ψ verifies the Dirac equation (6.2), we have

$$-\partial_x \Phi + M\Phi = \varepsilon \Xi \,. \tag{7.4}$$

Combining this equation with the definition of the Riccati matrix (6.28) yields a first order differential equation on Φ involving Z_ε:

$$\partial_x \Phi(\varepsilon; x) = (Z_\varepsilon(x) + M(x))\Phi(\varepsilon; x) \,. \tag{7.5}$$

This differential equation cannot be integrated easily due to the fact that the matrices $Z_\varepsilon + M$ do not necessarily commute at different points. However, this equation on the matrix Φ allows us to derive a differential equation on its determinant using Jacobi's formula [262]:

$$\partial_x \det \Phi = \det \Phi \ \operatorname{tr}\left[(\partial_x \Phi)\Phi^{-1}\right] \,, \tag{7.6}$$

which yields:

$$\partial_x \det \Phi(\varepsilon; x) = \det \Phi(\varepsilon; x) \ \operatorname{tr}\left[Z_\varepsilon(x) + M(x)\right] \,. \tag{7.7}$$

This is now a first order scalar differential equation, which can be integrated easily on $[0, L]$:

$$\ln \det \Phi(\varepsilon; L) = \int_0^L \operatorname{tr}\left[Z_\varepsilon(x) + M(x)\right] \mathrm{d}x \,. \tag{7.8}$$

Therefore, the IDoS (7.3) of the system on $[0, L]$ reduces to

$$\mathcal{N}_L(\varepsilon) = -\frac{1}{\pi} \operatorname{Im}\left\{\int_0^L \operatorname{tr}\left[Z_{\varepsilon+\mathrm{i}0^+}(x) + M(x)\right] \mathrm{d}x\right\} \,. \tag{7.9}$$

Since Z_ε and M are random processes, this integrated density of states is also random. Instead, we will consider the IDoS per unit length, in the limit of large system size:

$$\mathcal{N}(\varepsilon) = \lim_{L\to\infty} \frac{1}{L} \mathcal{N}_L(\varepsilon) = -\frac{1}{\pi} \operatorname{Im}\left\{\lim_{L\to\infty} \frac{1}{L} \int_0^L \operatorname{tr}\left[Z_{\varepsilon+\mathrm{i}0^+}(x) + M(x)\right] \mathrm{d}x\right\} \,. \tag{7.10}$$

As we have discussed in Section 6.3, the Riccati process Z_ε is stationary. Therefore for large L, we obtain

$$\lim_{L\to\infty} \frac{1}{L}\int_0^L \mathrm{tr}\,[Z_\varepsilon(x)+M(x)]\,\mathrm{d}x = \langle \mathrm{tr}(Z_\varepsilon+M)\rangle \ , \tag{7.11}$$

where the averaging of Z_ε is performed using its stationary distribution.

Let us define the *characteristic function*

$$\boxed{\Omega(\varepsilon) = \langle \mathrm{tr}(Z_\varepsilon+M)\rangle} \tag{7.12}$$

for all ε complex, which is an important concept for one dimensional systems(see the monograph [206] for a review and Refs. [84–86, 165] for recent articles). Combining Eqs. (7.10,7.11), we deduce that the integrated density of states per unit length of the semi-infinite system is simply given by[1]

$$\boxed{\mathcal{N}(\varepsilon) = -\frac{1}{\pi}\,\mathrm{Im}\,\Omega(\varepsilon+\mathrm{i}0^+)\ , \quad \varepsilon>0} \tag{7.13}$$

We thus need to compute the average of the Riccati matrix with respect of its stationary distribution. We managed to obtain this distribution (6.59) only for purely imaginary energy $\varepsilon = \mathrm{i}k$. Hence, we will compute the characteristic function $\Omega(\mathrm{i}k)$ on the imaginary axis, and deduce its value for real energy by analytic continuation [173, 206]. Using the form of the stationary distribution $f(Z)$ given by Eq. (6.59), we can formally write

$$\langle Z_{\varepsilon=\mathrm{i}k}\rangle = {\mathcal{C}_{\beta,\mu}}^{-1}\int \mathrm{d}Z\ Z\,(\det Z)^{-\mu-1-\beta\frac{N-1}{2}}\exp\left\{-\frac{1}{2}\,\mathrm{tr}\left[G^{-1}(Z+k^2Z^{-1})\right]\right\}\ , \tag{7.14}$$

where the normalisation constant is given by

$$\mathcal{C}_{\beta,\mu} = \int \mathrm{d}Z\,(\det Z)^{-\mu-1-\beta\frac{N-1}{2}}\exp\left\{-\frac{1}{2}\,\mathrm{tr}\left[G^{-1}(Z+k^2Z^{-1})\right]\right\}\ . \tag{7.15}$$

To obtain the density of states, one should in principle compute these two integrals. However, we will show that it is only required to compute the normalisation constant $\mathcal{C}_{\beta,\mu}$. Let us first make the change of variable $Y = G^{1/2}ZG^{1/2}$ in the integral (7.15). From Appendix A.1, the Jacobian of this change of variable is $\mathrm{d}Z = (\det G)^{-1-\beta\frac{N-1}{2}}\mathrm{d}Y$, thus:

$$\mathcal{C}_{\beta,\mu} = (\det G)^{\mu}\int \mathrm{d}Y\,(\det Y)^{-\mu-1-\beta\frac{N-1}{2}}\ \exp\left\{-\frac{1}{2}\,\mathrm{tr}\left[G^{-2}Y+k^2Y^{-1}\right]\right\}\ . \tag{7.16}$$

Recalling that $G = \mathrm{Diag}(g_1,\dots,g_N)$, we have

$$\det G = \prod_{i=1}^N g_i\ , \quad \text{and} \quad \mathrm{tr}\left[G^{-2}Y+k^2Y^{-1}\right] = \sum_{i=1}^N\left(\frac{Y_{ii}}{g_i^2}+k^2(Y^{-1})_{ii}\right)\ . \tag{7.17}$$

[1] Equations (7.12) and (7.13), together with the discussion of Section 6.2, show the connection between the spectral and scattering properties: counting the divergences of Z_ε corresponds to count the number of resonances. This is equivalent to extracting the density of states from the Wigner-Smith matrix $\mathcal{Q}$ discussed in Section 3.1 as $\rho(\varepsilon) \simeq \mathrm{tr}[\mathcal{Q}(\varepsilon)]/h$.

Therefore, taking the derivative of $\mathcal{C}_{\beta,\mu}$ with respect to a diagonal element g_p gives

$$\frac{\partial \mathcal{C}_{\beta,\mu}}{\partial g_p} = \frac{\mu}{g_p}\mathcal{C}_{\beta,\mu} + \frac{1}{g_p^3}\langle Y_{pp}\rangle\, \mathcal{C}_{\beta,\mu}\,. \tag{7.18}$$

Using that $Y_{pp} = g_p Z_{pp}$, this last relation reduces to

$$\frac{g_p^2}{\mathcal{C}_{\beta,\mu}}\frac{\partial \mathcal{C}_{\beta,\mu}}{\partial g_p} = \mu g_p + \langle Z_{\varepsilon=\mathrm{i}k}\rangle_{pp} = \langle \mu G + Z_{\varepsilon=\mathrm{i}k}\rangle_{pp}\,. \tag{7.19}$$

Thus, the p^{th} diagonal elements of $\langle Z_{\varepsilon=\mathrm{i}k} + \mu G\rangle$ can be easily expressed as derivatives of $\mathcal{C}_{\beta,\mu}$ with respect to the diagonal elements of the matrix G. This allows us to express the characteristic function (7.12) as:

$$\boxed{\Omega(\mathrm{i}k) = \sum_{i=1}^{N} g_i^2 \frac{\partial}{\partial g_i} \ln \mathcal{C}_{\beta,\mu}} \tag{7.20}$$

Our aim is now to compute $\mathcal{C}_{\beta,\mu}$, given by Eq. (7.15), in order to deduce the density of states of the system.

7.1.2 High energy limit

Let us first notice that the normalisation constant $\mathcal{C}_{\beta,\mu}$ given by Eq. (7.15) can be expressed in terms of a Bessel function of matrix argument $\mathbb{K}_{N,\beta}$, defined in Appendix B, as

$$\mathcal{C}_{\beta,\mu} = 2^{N(1+\beta\frac{N-1}{2})}\, k^{-N\mu}\, \mathbb{K}_{N,\beta}(-\mu|kG^{-1}, kG^{-1})\,. \tag{7.21}$$

Although this formula gives an explicit expression of $\mathcal{C}_{\beta,\mu}$ in terms of a special function, it is not very useful to study in details the density of states. However, it permits an easy study of the limit $k \to \infty$ by using the asymptotic form of $\mathbb{K}_{N,\beta}$ given by (B.34). Indeed, we obtain:

$$\mathbb{K}_{N,\beta}(\lambda|kG^{-1}, kG^{-1}) \underset{k\to\infty}{\simeq} \left(\frac{\pi}{2k}\right)^{\frac{N}{2}(1+\beta\frac{N-1}{2})} \frac{\prod_i \sqrt{g_i}}{\prod_{i<j}(g_i^{-1}+g_j^{-1})^{\beta/2}}\, \mathrm{e}^{-k\,\mathrm{tr}[G^{-1}]}(1+\mathcal{O}(k^{-1}))\,. \tag{7.22}$$

Using now Eq. (7.20), we deduce

$$\Omega(\mathrm{i}k) = Nk + \frac{1}{2}\,\mathrm{tr}[G] + \frac{\beta}{2}\sum_{j\neq i}\frac{g_i g_j}{g_i+g_j} + \mathcal{O}(k^{-1})\,. \tag{7.23}$$

Analytical continuation to $k = -\mathrm{i}\varepsilon$ straightforwardly gives

$$\Omega(\varepsilon) = -\mathrm{i}N\varepsilon + \frac{1}{2}\,\mathrm{tr}[G] + \frac{\beta}{2}\sum_{j\neq i}\frac{g_i g_j}{g_i+g_j} + \mathcal{O}(\varepsilon^{-1})\,. \tag{7.24}$$

Therefore, we deduce the density of states from (7.13):

$$\mathcal{N}(\varepsilon) \underset{\varepsilon\to\infty}{\simeq} \frac{N\varepsilon}{\pi}\,, \quad \Rightarrow \quad \rho(\varepsilon) \underset{\varepsilon\to\infty}{\simeq} \frac{N}{\pi}\,. \tag{7.25}$$

As expected, at high energy the density of states reaches the asymptotic value N/π, which is the value for the free Dirac equation

7.1.3 Isotropic case

We first study the isotropic case $G = g\mathbb{1}_N$ which is more simple. The effect of anisotropy will be studied in the next Section. We want to evaluate

$$\mathcal{C}_{N,\beta} = \int \mathrm{d}Z \, (\det Z)^{-\mu-1-\beta\frac{N-1}{2}} \, \exp\left\{-\frac{1}{2g}\,\mathrm{tr}\left[Z + k^2 Z^{-1}\right]\right\} . \tag{7.26}$$

As we have shown in Section 6.3.2, in this isotropic case the eigenvalues and eigenvectors of Z decouple. The integral over the eigenvectors is trivial and is just a constant (the volume of the symmetry group). There only remains to evaluate the integral over the eigenvalues, denoted $\{z_n\}$:

$$\mathcal{C}_{N,\beta} = \int \mathrm{d}z_1 \cdots \mathrm{d}z_N \prod_{i<j} |z_i - z_j|^\beta \prod_{i=1}^N z_i^{-\mu-1-\beta\frac{N-1}{2}} \, \mathrm{e}^{-\frac{1}{2g}(z_i + k^2/z_i)} , \tag{7.27}$$

where we conveniently redefined the normalisation constant to absorb the volume of the symmetry group. We can now apply diverse tools from random matrix theory to evaluate this integral. The procedure depends on the symmetry class, and thus on the value of β.

Unitary case $\beta = 2$

We begin with the simplest case of $\beta = 2$. The integral (7.27) can be evaluated using Andréief's relation, see Appendix A.3. The result takes the form of a determinant:

$$\mathcal{C}_{N,2} = N! \det\left[\int \mathrm{d}z \, z^{i+j-2-\mu-N} \, \mathrm{e}^{-\frac{1}{2g}(z+k^2/z)}\right]_{1\leqslant i,j\leqslant N} . \tag{7.28}$$

We recognise the integral representation of the modified Bessel function K_ν, also known as the MacDonald function [166],

$$K_\nu(x) = \frac{x^\nu}{2} \int_0^\infty \mathrm{d}z \, z^{-\nu-1} \, \mathrm{e}^{-\frac{1}{2}(z+x^2/z)} . \tag{7.29}$$

This allows us to express the normalisation in the compact form:

$$\boxed{\mathcal{C}_{N,2} = N! \, 2^N \, k^{-N\mu} \det\left[K_{i+j-1-\mu-N}(k/g)\right]_{1\leqslant i,j\leqslant N}} \tag{7.30}$$

Orthogonal case $\beta = 1$

In the orthogonal case $\beta = 1$, the normalisation constant (7.27) reads

$$\mathcal{C}_{N,1} = \int_0^\infty \mathrm{d}z_1 \cdots \mathrm{d}z_N \prod_{i<j} |z_i - z_j| \prod_{i=1}^N \phi(z_i) , \quad \phi(z) = z^{-\mu-1-\frac{N-1}{2}} \, \mathrm{e}^{-\frac{1}{2g}(z+k^2/z)} . \tag{7.31}$$

This multiple integral can be computed using De Bruijn's formula [96], given in Appendix A.3. The result can be expressed as a Pfaffian:

$$\boxed{\mathcal{C}_{N,1} = N! \, \mathrm{pf}[A(\mu, g)]} \tag{7.32}$$

where $A(\mu, g)$ is a skew-symmetric matrix, whose expression depend on the parity of N. For even N, it is of size $N \times N$, with elements given by

$$A_{ij}(\mu, g) = \int_0^\infty \mathrm{d}z_1 \mathrm{d}z_2 \ \mathrm{sign}(z_1 - z_2)\, z_1^{i-1} z_2^{j-1}\, \phi(z_1)\, \phi(z_2)\,, \quad 1 \leqslant i, j \leqslant N\,. \tag{7.33}$$

For odd N, $A(\mu, g)$ is a matrix of size $(N+1) \times (N+1)$. Its elements are given by (7.33) for $1 \leqslant i, j \leqslant N$. The last row and columns read

$$A_{i,N+1}(\mu, g) = -A_{N+1,i}(\mu, g) = \int_0^\infty \mathrm{d}z\, z^{i-1}\, \phi(z) = 2\, k^{\mu+i-\frac{N-1}{2}} K_{\frac{N+1}{2}-\mu-1}(k/g)\,. \tag{7.34}$$

The expression (7.32) for the normalisation constant is more complex that it $\beta = 2$ counterpart (7.30), but this expression still permits a numerical evaluation of the normalisation constant.

Symplectic case $\beta = 4$

Although the expression of the stationary distribution (6.59) has only been proved for $\beta = 1$ or 2, we assume it still holds for $\beta = 4$. In this case, the normalisation constant (7.27) can also be expressed as a Pfaffian, of a skew-symmetric matrix of size $2N \times 2N$ (see Appendix A.3). Explicitly, this gives:

$$\boxed{\mathcal{C}_{N,4} = N!\, 2^N\, k^{-N\mu}\, \mathrm{pf}\left[(j-i) K_{i+j-\mu-1-2N}(k/g)\right]_{1 \leqslant i,j \leqslant 2N}} \tag{7.35}$$

Summary and comments

In all cases, we have obtained compact expressions (7.30,7.32,7.35) for the normalisation constant $\mathcal{C}_{N,\beta}$. Combining these expressions with (7.13,7.20) allows to compute the density of states

$$\rho(\varepsilon) = \partial_\varepsilon \mathcal{N}(\varepsilon) \tag{7.36}$$

after analytic continuation $k \to -\mathrm{i}\varepsilon$. This density of states is plotted in Fig. 7.1 for different values of μ and number of channels.

The low energy behaviour of the density of states displays non trivial dependence in the number of channels N and the mass over disorder ratio μ. For example, in the case $\mu = 0$, its behaviour depends on the parity of N. This observation has already been made in Ref. [292] in the isotropic case, by using the DMPK equation (see Section 5.2). Here, we have also obtained the μ-dependence of the density of states, which will be a crucial step in order to deduce the topological properties of the system (see Chapter 8).

But before discussing in more details the low energy behaviour, we first consider the non-isotropic situation.

7.1.4 Non-isotropic case

In the general case, the integral in Eq. (7.15) is not invariant under transforms $Z \to U^\dagger Z U$. Nevertheless, it is still useful to introduce the eigenvalues and eigenvectors of Z:

$$Z = U^\dagger \mathcal{Z} U\,, \quad \mathcal{Z} = \mathrm{Diag}(z_1, \ldots, z_N)\,, \tag{7.37}$$

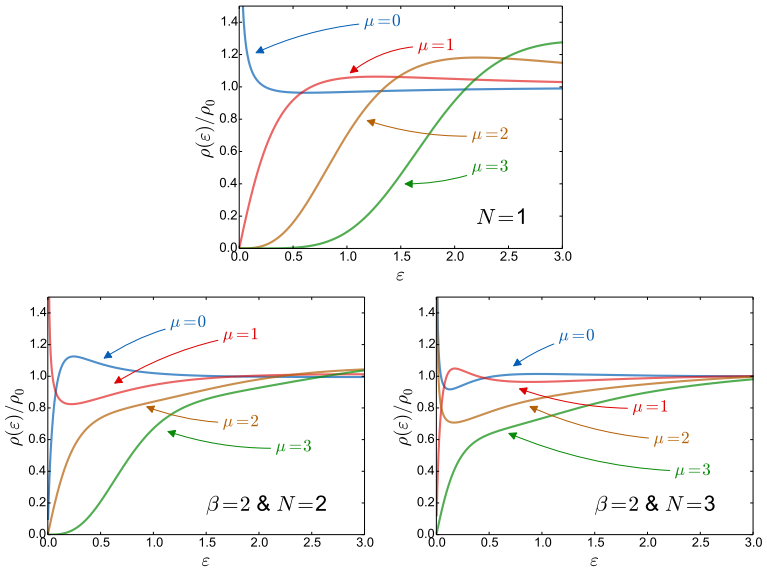

Figure 7.1: Density of states $\rho(\varepsilon)$ in the isotropic case $G = \mathbb{1}_N$ for different numbers N of channels and different values of μ, in the case $\beta = 2$. The DoS is normalised by the free density of states $\rho_0 = N/\pi$. The case $N = 1$ is independent of the Dyson index β.

and U belong to the corresponding group, Eq. (6.7). However, this time the integrals over the eigenvalues and the eigenvectors do not decouple:

$$\mathcal{C}_{N,\beta} = \int \mathrm{d}\mu(U) \int \mathrm{d}z_1 \cdots \mathrm{d}z_N \prod_{i<j} |z_i - z_j|^\beta \, (\det \mathcal{Z})^{-\mu-1-\beta\frac{N-1}{2}} \times \exp\left\{-\frac{1}{2}\operatorname{tr}\left[UG^{-1}U^\dagger(\mathcal{Z} + k^2\mathcal{Z}^{-1})\right]\right\} . \tag{7.38}$$

The dependence in the eigenvectors contained in the matrix U is encoded in the trace

$$\operatorname{tr}\left[UG^{-1}U^\dagger(\mathcal{Z} + k^2\mathcal{Z}^{-1})\right] = \sum_{p=1}^{N} [UG^{-1}U^\dagger]_{pp}\left(z_p + \frac{k^2}{z_p}\right) . \tag{7.39}$$

To make the computations more tractable, we introduce

$$w_n(z, U; G) = z^{-\mu-1-\beta\frac{N-1}{2}} \exp\left[-\frac{1}{2}(UG^{-1}U^\dagger)_{nn}\left(z + \frac{k^2}{z}\right)\right] , \tag{7.40}$$

so that the normalisation constant takes the form

$$\mathcal{C}_{N,\beta} = \int \mathrm{d}\mu(U) \int \mathrm{d}z_1 \cdots \mathrm{d}z_N \prod_{i<j} |z_i - z_j|^\beta \prod_{n=1}^{N} w_n(z_n, U; G) . \tag{7.41}$$

The integral over the matrix U cannot be performed analytically in general. It can be done only in the unitary case via the Harish-Chandra-Itzykson-Zuber integral (see Appendix A.4). But even in this case, the remaining integral over the eigenvalues is still quite complicated and does not provide a useful representation to analyse the density of states. Furthermore, because we also aim to discuss the other symmetry classes, we will follow a different approach. We will not evaluate the integral over U, but only the integral over the eigenvalues $\{z_n\}$, similarly as in Section 7.1.3. This will give a more compact expression for $\mathcal{C}_{N,\beta}$, which we will be able to analyse.

Unitary case $\beta = 2$

To perform the integral over the eigenvalues, we cannot simply apply Andréief's identity (A.27) because the weights w_m given by (7.40) are not the same for all eigenvalues. Nevertheless, we can adapt the proof of this identity given in Ref. [19] to our situation. Let us expand one Vandermonde determinant as a sum over all permutations σ of length N:

$$\prod_{i<j}(z_i - z_j) = \det[z_i^{j-1}]_{1\leqslant i,j\leqslant N} = \sum_{\sigma\in S_N} \epsilon(\sigma) \prod_{p=1}^{N} z_p^{\sigma(p)-1} , \tag{7.42}$$

where $\epsilon(\sigma) = \pm 1$ is the signature of the permutation σ and S_N the group of permutations. Using this expression in Eq. (7.41) gives:

$$\mathcal{C}_{N,2} = \sum_{\sigma\in S_N} \epsilon(\sigma) \int \mathrm{d}\mu(U) \int \mathrm{d}z_1 \cdots \mathrm{d}z_N \prod_{i<j}(z_i - z_j) \prod_{p=1}^{N} z_p^{\sigma(p)-1} \prod_{n=1}^{N} w_n(z_n, U; G) . \tag{7.43}$$

The idea to simplify this expression is to get rid of the sum over the permutations. To do so, let us permute the eigenvalues in the integral with the same permutation σ: $z_i \to z_{\sigma(i)}$, or equivalently

$$\mathcal{Z} \to P_\sigma^\dagger \mathcal{Z} P_\sigma , \quad \text{where } [P_\sigma]_{ij} = \delta_{i,\sigma(j)} . \tag{7.44}$$

This corresponds to also permute the eigenvectors as $U \to P_\sigma^\dagger U$. The permutation matrix P_σ is unitary, so the Haar measure $\mathrm{d}U$ is invariant under this permutation. The normalisation constant becomes:

$$\mathcal{C}_{N,2} = \sum_{\sigma\in S_N} \epsilon(\sigma) \int \mathrm{d}\mu(U) \int \mathrm{d}z_1 \cdots \mathrm{d}z_N \prod_{i<j}(z_{\sigma(i)} - z_{\sigma(j)}) \prod_{p=1}^{N} z_{\sigma(p)}^{\sigma(p)-1} \prod_{n=1}^{N} w_n(z_{\sigma(n)}, P_\sigma^\dagger U; G) . \tag{7.45}$$

From the fact that the Vandermonde is a determinant, we have

$$\prod_{i<j}(z_{\sigma(i)} - z_{\sigma(j)}) = \epsilon(\sigma) \prod_{i<j}(z_i - z_j) . \tag{7.46}$$

Additionally, one can simply check that

$$w_n(z, P_\sigma^\dagger U; G) = w_{\sigma(n)}(z, U; G) . \tag{7.47}$$

Using these properties and relabelling the indices, we obtain:

$$\begin{aligned} \mathcal{C}_{N,2} &= \sum_{\sigma\in S_N} \int \mathrm{d}\mu(U) \int \mathrm{d}z_1 \cdots \mathrm{d}z_N \prod_{i<j}(z_i - z_j) \prod_{p=1}^{N} z_p^{p-1} \, w_p(z_p, U; G) , \\ &= N! \int \mathrm{d}\mu(U) \int \mathrm{d}z_1 \cdots \mathrm{d}z_N \prod_{i<j}(z_i - z_j) \prod_{p=1}^{N} z_p^{p-1} \, w_p(z_p, U; G) . \end{aligned} \tag{7.48}$$

Similarly, expanding the second Vandermonde as (7.42) gives

$$\begin{aligned} \mathcal{C}_{N,2} &= N! \sum_{\sigma\in S_N} \epsilon(\sigma) \int \mathrm{d}\mu(U) \int \mathrm{d}z_1 \cdots \mathrm{d}z_N \prod_{p=1}^{N} z_p^{\sigma(p)-1} z_p^{p-1} \, w_p(z_p, U; G) , \\ &= N! \int \mathrm{d}\mu(U) \sum_{\sigma\in S_N} \epsilon(\sigma) \prod_{p=1}^{N} \int \mathrm{d}z_p \, z_p^{p-1+\sigma(p)-1} \, w_p(z_p, U; G) , \\ &= N! \int \mathrm{d}\mu(U) \, \det\left[\int \mathrm{d}z \, z^{i+j-2} \, w_i(z, U; G) \right]_{1\leqslant i,j\leqslant N} , \end{aligned} \tag{7.49}$$

where in the last line we re-expressed the sum over permutations as a determinant. The last integral over z can be computed and expressed as a modified Bessel function (7.29). This finally gives the expression of the normalisation in terms of an integral over the unitary group:

$$\boxed{\mathcal{C}_{N,2} = N!\, 2^N\, k^{N\mu} \int_{\mathrm{U}(N)} \mathrm{d}\mu(U)\ \det\left[K_{i+j-1-\mu-N}(k[UG^{-1}U^\dagger]_{ii})\right]_{1\leqslant i,j\leqslant N}} \tag{7.50}$$

This expression is more complicated than the one obtained previously in the isotropic case (7.27), because of the integral over the unitary group. But for small number of channels, this integral can be evaluated numerically by parametrising the matrix U and expressing the integral in terms of these parameters.

Orthogonal case $\beta = 1$

In the orthogonal case, we can adapt De Bruijn's proof [96] to our situation. By performing a very similar derivation as in the $\beta = 2$ case, we obtain the normalisation constant as an integral over the orthogonal group:

$$\boxed{\mathcal{C}_{N,1} = N! \int_{\mathrm{O}(N)} \mathrm{d}\mu(U)\ \mathrm{pf}\,[A(\mu, U, G)]} \tag{7.51}$$

where the skew-symmetric matrix A is given by:

$$A_{ij}(\mu, U, G) = \int_0^\infty \mathrm{d}z_1 \mathrm{d}z_2\ \mathrm{sign}(z_1 - z_2)\, z_1^{i-1} z_2^{j-1}\, w_i(z_1, U; G)\, w_j(z_2, U; G)\,, \tag{7.52}$$

where w_n is given by (7.40). If N is odd, we should add one column and one row given by

$$\begin{aligned} A_{m,N+1}(\mu, U, G) = -A_{N+1,m}(\mu, U, G) &= \int_0^\infty \mathrm{d}x\, x^{m-1} w_m(x, U; G) \\ &= 2k^{m-\mu-\frac{N+1}{2}} K_{m-\mu-\frac{N+1}{2}}\left(k[UG^{-1}U^\dagger]_{mm}\right)\,. \end{aligned} \tag{7.53}$$

Symplectic case $\beta = 4$

We did not study explicitly the case $\beta = 4$, but we expect that relation (7.35) can be extended to the anisotropic situation by introducing an additional integral over the symplectic group $\mathrm{Sp}(N)$, as in relations (7.50,7.51) obtained for $\beta = 1$ and $\beta = 2$.

Summary and comments

In the non-isotropic situation, we have obtained several exact expressions for the normalisation $\mathcal{C}_{N,\beta}$, Eqs. (7.50,7.51), in terms of integrals over a compact group. This additional integral makes the numerical evaluation of these expressions more difficult, but for small number of channels it can be done by introducing parametrisations of the matrices. Then, the density of states can be evaluated by using (7.13,7.20), after analytic continuation $k \to -\mathrm{i}\varepsilon$. The result is shown in Fig. 7.2.

We notice some difference with the isotropic case in the crossover regime $\varepsilon \sim ||G||$, but the low energy behaviour seems to be similar in the two cases. We will now study this behaviour in more details.

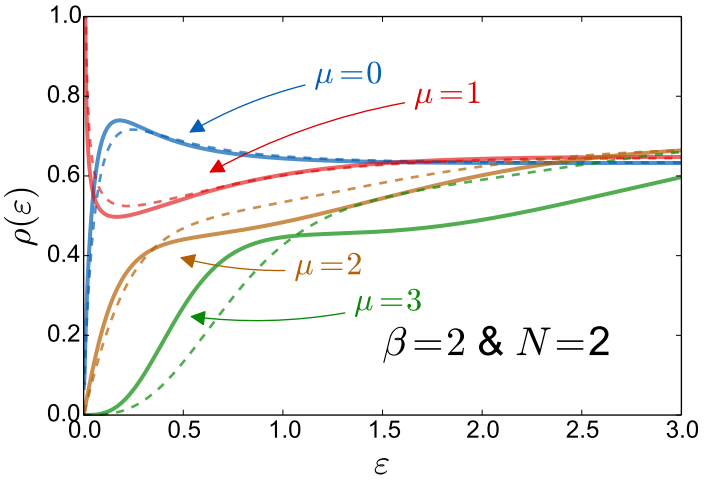

Figure 7.2: Density of states in the anisotropic case $G = \mathrm{Diag}(\frac{1}{2}, \frac{3}{2})$ (solid lines) compared to the isotropic case $G = \mathbb{1}_2$ (dashed lines), for $N = 2$ and $\beta = 2$ and different values of μ.

7.1.5 Low energy behaviour

We have shown that the density of states can be obtained from the normalisation constant $\mathcal{C}_{N,\beta}$ via relations (7.13,7.20). Having obtained compact expressions for this normalisation constant (7.50,7.51), we can now analyse the low energy behaviour of $\mathcal{C}_{N,\beta}$ to deduce the low energy properties of the DoS. Since the integrated density of states $\mathcal{N}(\varepsilon)$ is obtained from a derivative of the logarithm of $\mathcal{C}_{N,\beta}$, the leading low energy term of the expansion is not sufficient, and we need to obtain the next to leading order term. In the following we will show that the low energy expansion for $\varepsilon = \mathrm{i}k$ reads

$$\mathcal{C}_{N,\beta} \simeq A(\mu, G)k^{\theta}[1 + B(\mu, G)k^{\alpha} + o(k^{\alpha})] \,. \tag{7.54}$$

This implies that the expansion of the characteristic function obtained from Eq. (7.20) takes the form

$$\Omega(\varepsilon = \mathrm{i}k) = \tilde{A} + \tilde{B}\, k^{\alpha} + o(k^{\alpha}) \,. \tag{7.55}$$

After analytic continuation $k \to -\mathrm{i}\varepsilon$, taking the imaginary part gives that the integrated density of states behaves as

$$\mathcal{N}(\varepsilon) \sim \varepsilon^{\alpha} \,. \tag{7.56}$$

Our aim is now to compute this exponent α, which will be a central quantity. In the next Chapter, we will show that this exponent characterises the topological properties of the disordered wire.

Unitary case $\beta = 2$

As before, we start with the case $\beta = 2$. We will first discuss the isotropic case $G = g\mathbb{1}_N$, which is simpler. In this case for $\varepsilon = \mathrm{i}k$, $\mathcal{C}_{N,2}$ is given by a determinant involving modified Bessel functions (7.30). The $k \to 0$ properties of the normalisation constant come from the expansion of the Bessel functions [166]:

$$K_{\nu}(z) \sim \begin{cases} z^{-|\nu|}\,(1 + A_{\nu} z^2 + o(z^2)) & \text{for } |\nu| \geqslant 1 \,, \\ z^{-|\nu|}\,(1 + B_{\nu} z^{2|\nu|} + o(z^{2|\nu|})) & \text{for } |\nu| < 1 \,. \end{cases} \tag{7.57}$$

We now need to plug this expression into the determinant (7.30) and expand it to get the two leading orders in k. Many terms will give contributions to the same order, but

since we are only interested in the powers of k and not the prefactors, we only need to exhibit one of these terms. For example, the product of all diagonal elements give a leading order contribution. We can check explicitly for small N that this contribution is not cancelled out by other combination of the matrix elements. To get the exponent α of the next to leading order term, introduce

$$\nu = \mu - N + n \in]0, 1[\,, \tag{7.58}$$

with $n \in \{1, \dots, N\}$. We will now distinguish two cases, depending on the parity of n.

• Odd n: Let us study again the product of all diagonal elements. In this product, the Bessel function with the smallest index is K_ν, which gives a contribution $k^{-\nu}(1+B_\nu k^{2\nu})$ from Eq. (7.57). Thus, the product of diagonal elements has the expansion of the form $k^\eta(1+B_\nu k^{2\nu})$. There are many other contributions to the determinant of the same order in k, but we can check for $N = 2$ or $N = 3$ that these do not cancel out. Therefore, the normalisation constant behaves as $\mathcal{C}_{\beta,2} \sim k^\eta(1 + Bk^{2\nu})$, from which we deduce the exponent

$$\alpha = 2\nu = 2(\mu - N + n)\,, \quad \mu - N + n \in]0, 1[\,. \tag{7.59}$$

• Even n: We can proceed as in the previous case, but this time the smallest index is $\nu - 1$. The same argument gives $\mathcal{C}_{N,2} \sim k^\eta(1 + Bk^{2(1-\nu)})$, thus

$$\alpha = 2(1 - \nu) = 2(1 - (\mu - N + n))\,, \quad \mu - N + n \in]0, 1[\,. \tag{7.60}$$

• For $|\mu| > N - 1$, we can similarly prove that α becomes linear:

$$\alpha = 2\,|\mu - (N - 1)|\ . \tag{7.61}$$

These three results (7.59,7.60,7.61) show that the exponent α exhibits a saw behaviour, as shown in Fig. 7.3. There remains to study the case where μ is an integer (this corresponds to $\nu = 0$ or 1):

$$\mu = N - m\,, \qquad m \in \{1, \dots, 2N - 1\}\,. \tag{7.62}$$

In this case, there is at least one modified Bessel function with index $\nu = 0$ in the determinant. For $k \to 0$, it has the behaviour

$$K_0(z) \sim -\ln z + \mathcal{O}(1)\,. \tag{7.63}$$

We can perform the same analysis as before, with this additional contribution, by distinguishing on the parity of m.
• Odd m: with our previous results, this would correspond to $\alpha = 0$. We have an expansion of the form

$$\mathcal{C}_{N,2} \simeq A(\mu, g)k^\eta \ln k \left(1 + \frac{B(\mu, g)}{\ln k}\right)\,, \tag{7.64}$$

from which we can deduce the characteristic function from Eq. (7.20). After analytic continuation $k \to -\mathrm{i}\varepsilon$, we obtain the IDoS:

$$\mathcal{N}(\varepsilon) \sim \frac{1}{(\ln \varepsilon)^2} \quad \text{for} \quad \alpha = 0\,. \tag{7.65}$$

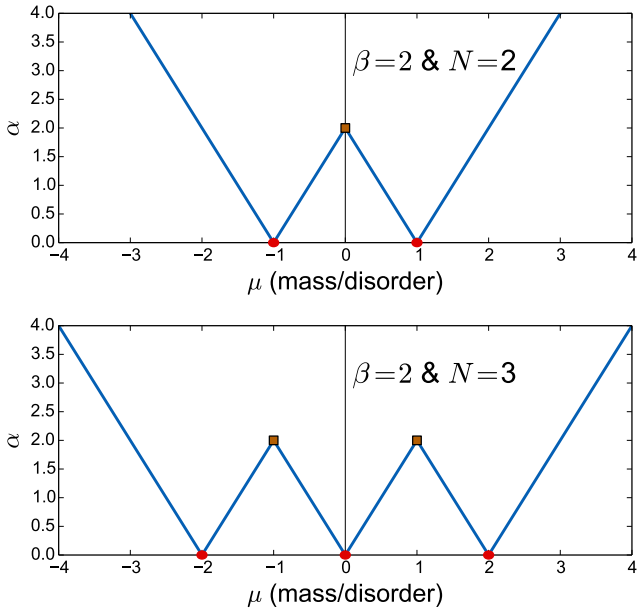

Figure 7.3: Exponent α controlling the low energy behaviour of the density of states $\mathcal{N}(\varepsilon) \sim \varepsilon^{\alpha}$, for $\beta = 2$ and different numbers of channels. This exponent exhibits a saw behaviour, given by Eqs. (7.59,7.60,7.61). When α reaches a local maximum, denoted by ■, the behaviour is $\mathcal{N}(\varepsilon) \sim \varepsilon^{\beta} |\ln \varepsilon|$. When α vanishes, denoted by ●, the integrated density of states has the superuniversal behaviour $\mathcal{N}(\varepsilon) \sim 1/(\ln \varepsilon)^2$, independent of β.

We recover the result obtained in Refs. [14, 61, 292] for odd N and $\mu = 0$.
• Even m: this corresponds to a local maximum $\alpha = 2$. A similar computation yields

$$\mathcal{C}_{N,2} \simeq A(\mu, g) k^{\eta} \left(1 + B(\mu, g)\, (k \ln k)^2\right) , \tag{7.66}$$

from which we deduce

$$\mathcal{N}(\varepsilon) \sim \varepsilon^2 \, |\ln \varepsilon| \quad \text{for} \quad \alpha = 2 \, . \tag{7.67}$$

We again recover the behaviour obtained in [14, 61, 292] for even N and $\mu = 0$.

These last two behaviours complete our low energy analysis of the density of states.

All our discussion in the isotropic case can be straightforwardly extended to the non isotropic situation. In this latter case, there is an additional integral over the unitary matrix U, Eq. (7.50). For a given U, we have an expansion of the form:

$$N!\, 2^N \, k^{N\mu} \det \left[K_{i+j-1-\mu-N}(k[UG^{-1}U^{\dagger}]_{ii})\right]_{1 \leqslant i,j \leqslant N} \simeq A(\mu, UG^{-1}U^{\dagger}) k^{\eta} \left[1 + B(\mu, UG^{-1}U^{\dagger})\, k^{\alpha} + o(k^{\alpha})\right] . \tag{7.68}$$

Integrating this expression over the unitary matrix U gives $\mathcal{C}_{N,2}$. Assuming that the prefactors do not vanish after integration (which we can check for $N = 2$), we obtain the same $k \to 0$ expansion as in the isotropic case. This shows that, for any matrix G, $\mathcal{N}(\varepsilon) \sim \varepsilon^{\alpha}$, where α is given by (7.59,7.60,7.61). This exponent has the saw behaviour shown in Fig. 7.3.

Orthogonal case $\beta = 1$

A similar analysis can be performed in the orthogonal case, but even in isotropic case the normalisation constant takes a more complicated form, see Eq. (7.32). We first need to obtain the low energy behaviour of the matrix elements A_{ij} given by (7.33). The leading order can be obtained directly from the double integral representation. The

next order is trickier to extract. A convenient way to do so is to make the change of variables $z_1 = kx$ and $z_2 = ky$ in Eq. (7.33). This gives:

$$A_{i,j} = k^{i+j+2\mu-N-1} B_{i+\mu-\frac{N+1}{2}, j+\mu-\frac{N+1}{2}}(k/g), \tag{7.69}$$

where we have introduced:

$$B_{\alpha,\beta}(k/g) = \int_0^\infty \mathrm{d}x \int_0^\infty \mathrm{d}y \ \mathrm{sign}(x-y)\, x^{\alpha-1} y^{\beta-1}\, e^{-\frac{k}{2g}(x+y+1/x+1/y)} \,. \tag{7.70}$$

From this expression, we can show that $B_{\alpha,\beta}$ satisfy the following relations

$$(\alpha+\beta)B_{\alpha,\beta}(t) + t\partial_t B_{\alpha,\beta}(t) = -tB_{\alpha-1,\beta}(t) - tB_{\alpha,\beta-1}(t) \,, \tag{7.71}$$

$$(\alpha-\beta)B_{\alpha,\beta}(t) + t\partial_t B_{\alpha,\beta}(t) = -tB_{\alpha-1,\beta}(t) - tB_{\alpha,\beta-1}(t) - 4K_{\alpha+\beta}(2t) \,. \tag{7.72}$$

We can make use of these relations to obtain the behaviour of $B_{\alpha,\beta}(k)$ as $k \to 0$:

$$B_{\alpha,\beta}(k) \sim k^{-\xi(\alpha,\beta)}(1 + \mathcal{O}(k^{\eta(\alpha,\beta)})) \,, \tag{7.73}$$

where

$$\xi(\alpha,\beta) = \max(|\alpha+\beta|, |\alpha-\beta|) \,, \quad \text{and} \quad \eta(\alpha,\beta) = 2\min(1, |\alpha|, |\beta|) \,. \tag{7.74}$$

We also have the specific behaviours:

$$B_{\mu,0} \sim -k^{-|\mu|} \ln k \,, \tag{7.75}$$

$$B_{\mu,\pm1} \sim k^{-|\mu|-1}(1 + \mathcal{O}(k^2 \ln k)) \,, \quad \text{for } \mu > 1 \,, \tag{7.76}$$

$$B_{\mu,\pm1} \sim k^{-|\mu|-1}(1 + \mathcal{O}(k^{2\mu})) \,, \quad \text{for } 0 < \mu < 1 \,, \tag{7.77}$$

$$B_{\pm\frac{1}{2},\mp\frac{1}{2}} \sim k^{-1}(1 + \mathcal{O}(k(\ln k)^2)) \,. \tag{7.78}$$

If N is odd, in addition to these matrix elements, we should add one line and one column to the matrix A, which are given by (7.34). The $k \to 0$ behaviour of these additional elements can straightforwardly be obtained from (7.57).

We will now use these expansions to study $\mathrm{pf}(A) = \sqrt{\det A}$ as $k \to 0$. Let us denote

$$\nu = \mu - (N - 2n - 1)/2 \in]0, 1[\,, \quad \text{with } n \in \{1, \dots, N\} \,. \tag{7.79}$$

It is easier to compute $\det(A)$ by decomposing the skew-symmetric matrix A in blocks (both for odd and even N) as:

$$A = \begin{pmatrix} \tilde{A} & \tilde{B} \\ -\tilde{B}^T & \tilde{C} \end{pmatrix} \,, \tag{7.80}$$

where we introduced $\tilde{A}$ of size $n \times n$, which verifies

$$A_{pm} = \tilde{A}_{pm} = -\tilde{A}_{mp} \sim k^{4\nu+2(m+p-2n-2)}(1 + \mathcal{O}(k^2)) \,, \tag{7.81}$$

$\tilde{B}$ of size $n \times (N-n)$, with

$$A_{pm} = \tilde{B}_{p,m-n} \sim k^{2\nu+2(n-p-1)} \begin{cases} 1 + \mathcal{O}(k^{2\min(\nu,1-\nu)}) & \text{for } p = n \,,\ m = n+1 \,, \\ 1 + \mathcal{O}(k^2) & \text{otherwise} \,, \end{cases} \tag{7.82}$$

and $\tilde{C}$ of size $(N-n)\times(N-n)$, where

$$A_{pm} = \tilde{C}_{p-n,m-n} = -\tilde{C}_{m-p,n-p} = 1 + \begin{cases} \mathcal{O}(k^{2\nu}) & \text{for } m = n+1\,,\ p = n+1\,, \\ \mathcal{O}(k^2) & \text{otherwise.} \end{cases} \tag{7.83}$$

The determinant of A is then computed using the formula for the determinant of a block matrix:

$$\det(A) \sim \det(\tilde{C}_{N,n})\det(\tilde{A}_n + \tilde{B}_{N,n}\tilde{C}_{N,n}^{-1}\tilde{B}_{N,n}^T)\,. \tag{7.84}$$

Finally the behaviour of $\mathcal{C}_{N,1}$ for $k\to 0$ follows from $\mathrm{pf}(A) = \sqrt{\det(A)} \sim k^\sigma(1+O(k^\alpha))$, where

$$\alpha = 2\min(\nu, 1-\nu)\,. \tag{7.85}$$

As in the $\beta = 2$ case, we obtain a power low behaviour, whose exponent has again a saw dependence on μ. We can similarly study the cases where α reaches a local extremum, and obtain similar result to the case $\beta = 2$.

These results can be extended to the case of non isotropic disorder, controlled by the matrix G. As for the unitary case, one should add a matrix integral over the orthogonal group, which does not change the low energy behaviour of the DoS.

Symplectic case $\beta = 4$

In the symplectic case we have not explicitly computed the low energy behaviour from the pfaffian (7.35). We expect that the simple dependence in β observed for $\beta = 1$ and 2 can be extended to the symplectic case. We have verified this assumption on the $N = 2$ channels case, but the general analysis remains to be done.

Low energy density of states: summary

We have shown, for any matrix G, that the low energy behaviour of the integrated density of states has the form of a power law

$$\boxed{\mathcal{N}(\varepsilon) \sim \varepsilon^\alpha} \tag{7.86}$$

where the exponent α has a saw behaviour with μ, as shown in Fig. 7.3. This exponent has the following scaling with the Dyson index β:

$$\alpha_\beta(\mu) = \frac{\beta}{2}\,\alpha_{\beta=2}\left(\frac{2}{\beta}\,\mu\right)\,. \tag{7.87}$$

When this exponent reaches a local maximum, the behaviour of the IDoS receives an additional logarithmic contribution:

$$\boxed{\mathcal{N}(\varepsilon) \sim \varepsilon^\beta\,|\ln\varepsilon| \quad \text{for} \quad \alpha = \beta} \tag{7.88}$$

While for $\alpha = 0$, the behaviour is

$$\boxed{\mathcal{N}(\varepsilon) \sim \frac{1}{(\ln\varepsilon)^2} \quad \text{for} \quad \alpha = 0} \tag{7.89}$$

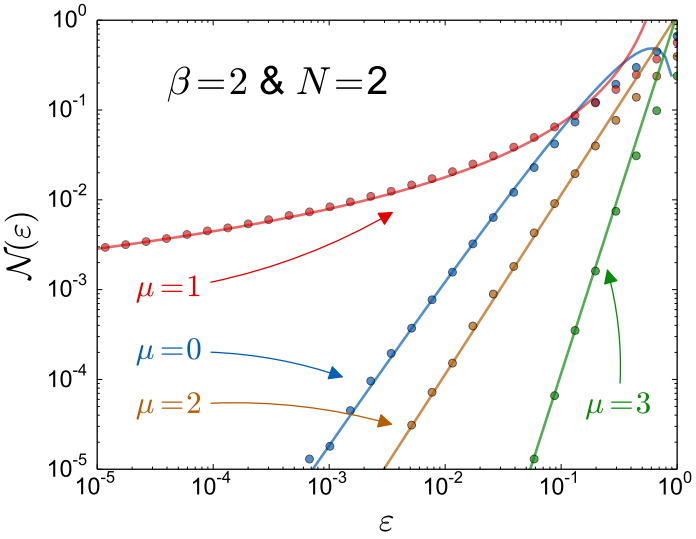

Figure 7.4: Low energy behaviour of the integrated density of states $\mathcal{N}(\varepsilon)$ for $N = 2$ channels and $\beta = 2$, in the non-isotropic case $G = \mathrm{Diag}(\frac{1}{2}, \frac{3}{2})$. The points are obtained from numerical simulations, the lines are the analytic results for low energy (7.86,7.88,7.89).

which does not depend on the Dyson index β. This phenomenon of universality across different symmetry classes is called *superuniversality* [168]. In Chapter 8, we will show that the vanishing of this exponent α is associated to a phase transition of topological nature.

We have checked the low energy behaviour of the density of states numerically, see Fig. 7.4. The numerical results are in excellent agreement with the power low behaviour (7.86), as well as the two behaviours (7.88,7.89), over several decades.

7.2 Lyapunov spectrum

For one dimensional and quasi-one dimensional systems, it is well known that the eigenstates are localised in the presence of disorder. A good indicator of the localisation properties is given by the Lyapunov exponents which measure the exponential growth of the envelope of the wave function. They can be defined in two different ways, depending on the choice of point of view. We can either study the growth of the $2N$-components spinor ψ, which will give us a set of $2N$ Lyapunov exponents (one per component). This is the point of view we will adopt in Section 7.3 to compute the Lyapunov exponents numerically. However here, we will define them from the first component ϕ of the spinor (which is itself a N-components vector). In this case, we will get N Lyapunov exponents which we will denote $\gamma_1, \ldots, \gamma_N$. They can be obtained from the matrix-components of the spinor Ψ, defined in Eq. (7.1), using Oseledec's ergodic multiplicative theorem [256] (see also Ref. [185]). This theorem states that the eigenvalues of the matrix

$$\frac{1}{2x} \ln[\Phi^\dagger(x)\Phi(x)] \tag{7.90}$$

are self-averaging, and converge to the Lyapunov exponents $\{\gamma_n\}$ when $x \to \infty$. Our aim is to introduce a method to compute these exponents and analyse their properties.

As we will see explicitly at zero energy, these two perspective give the same Lyapunov spectrum. Indeed, the $2N$ Lyapunov exponents controlling the evolution of the spinor ψ are simply $\{\gamma_n\}$ and $\{-\gamma_n\}$.

7.2.1 Lyapunov spectrum at zero energy

At zero energy $\varepsilon = 0$, the Dirac equation (6.2,6.3) reduces to

$$\begin{cases} \partial_x \varphi(x) = M(x)\varphi(x) \,, \\ \partial_x \xi(x) = -M(x)\xi(x) \,, \end{cases} \tag{7.91}$$

or equivalently for the matrix-components Φ and Ξ:

$$\begin{cases} \partial_x \Phi(x) = M(x)\Phi(x) \,, \\ \partial_x \Xi(x) = -M(x)\Xi(x) \,, \end{cases} \tag{7.92}$$

We will only focus on the equation for Φ, and introduce a method to compute its Lyapunov exponents $\{\gamma_n\}$. The Lyapunov exponents of the second one are simply their opposite $\{-\gamma_n\}$. This shows explicitly that considering the full spinor ψ gives the Lyapunov spectrum $\{\gamma_n, -\gamma_n\}$.

We study the first order differential equation

$$\partial_x \Phi(x) = M(x)\Phi(x) \,, \tag{7.93}$$

and aim to compute the associated Lyapunov exponents. The solution of this equation takes the form of a ordered exponential

$$\Phi(x) = \mathtt{T}\, \mathrm{e}^{\int_0^x M(t)\mathrm{d}t} \,, \tag{7.94}$$

which must be understood formally as the power series of the exponential, in which the matrices M always appear ordered with respect to their argument. This is ensured by the presence of the ordering operator $\mathtt{T}$, defined as:

$$\mathtt{T}[M(t)M(t')] = \begin{cases} M(t)M(t') & \text{if } t > t' \,, \\ M(t')M(t) & \text{if } t < t' \,. \end{cases} \tag{7.95}$$

However the formal solution (7.94) is not very helpful to study the solution $\Phi(x)$ and compute the Lyapunov exponents.

To circumvent the difficulty of solving Eq. (7.93), we introduce another formalism. The idea of this approach is the following: take any initial vector $\varphi_1(0)$ and evolve it with (7.93), that is $\partial_x \varphi_1(x) = M(x)\varphi_1(x)$. This vector grows exponentially, with the largest Lyapunov exponent, say γ_1:

$$||\varphi_1(x)|| \sim \mathrm{e}^{\gamma_1 x} \,. \tag{7.96}$$

To obtain the second largest Lyapunov exponent, say γ_2, we need to follow two independent vectors φ_1 and φ_2. Considered independently, both will grow with rate γ_1. However, the volume (here surface) of the parallelogram delimited by these two vectors (see Fig. 7.5) will also grow exponentially, with rate $\gamma_1 + \gamma_2$. The square of this volume can be conveniently computed from the determinant:

$$\begin{vmatrix} \varphi_1(x)^\dagger \varphi_1(x) & \varphi_1(x)^\dagger \varphi_2(x) \\ \varphi_2(x)^\dagger \varphi_1(x) & \varphi_2(x)^\dagger \varphi_2(x) \end{vmatrix} \,. \tag{7.97}$$

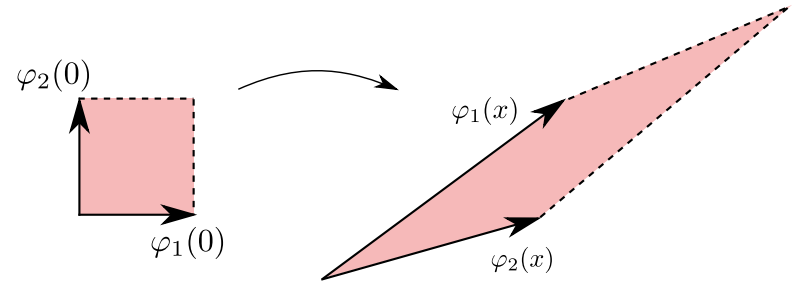

Figure 7.5: Evolution of independent vectors φ_1 and φ_2 with Eq. (7.93). Each vector taken independently will grow with rate γ_1, but the surface enclosed by the two vectors will grow with rate $\gamma_1 + \gamma_2$.

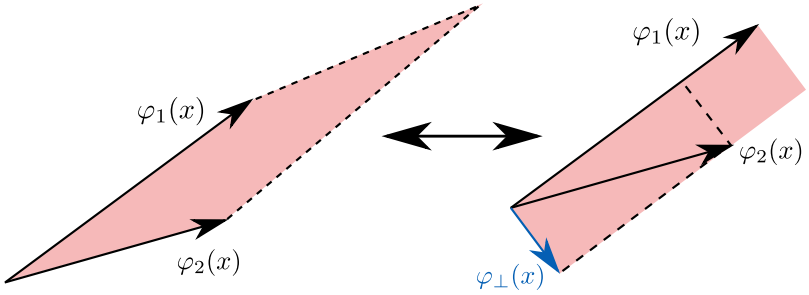

Figure 7.6: The surface enclosed by the two vectors $\varphi_1(x)$ and $\varphi_2(x)$ is also the surface delimited by $\varphi_1(x)$ and $\varphi_\perp(x)$, the component of $\varphi_2(x)$ orthogonal to $\varphi_1(x)$.

This is valid for any independent solutions of Eq. (7.93). All the solutions being encoded in the matrix $\Phi(x)$, we can rewrite this determinant in terms of Φ. Indeed, the determinant of the top left subblock of $\Phi(x)^\dagger\Phi(x)$ is exactly (7.97). Mathematically, this is called the second principal minor of $\Phi(x)^\dagger\Phi(x)$, and denoted $|\Phi(x)^\dagger\Phi(x)|_2$. This discussion can be extended to a set of n vectors $\varphi_1, \dots, \varphi_n$ to obtain the top n Lyapunov exponents from the n^{th} principal minor of $\Phi^\dagger\Phi$ [185, 256]:

$$\boxed{\lim_{x\to\infty} \frac{1}{2x} \ln |\Phi(x)^\dagger\Phi(x)|_n = \sum_{i=1}^{n} \gamma_i \,, \qquad \gamma_1 > \gamma_2 > \cdots > \gamma_N} \tag{7.98}$$

where $|\Phi^\dagger\Phi|_n$ is the determinant of the top-left subblock of $\Phi^\dagger\Phi$ of size $n \times n$. The discussion above is not a rigorous proof of this relation, but it gives some insight to understand it.

To make use of relation (7.98), we will slightly rephrase the problem. Eq. (7.98) relies on this idea of studying the volume enclosed by independent vectors. These vectors can be conveniently chosen as the columns of the matrix $\Phi(x)$. For simplicity, let us look at the first two columns, which we denote $\varphi_1(x)$ and $\varphi_2(x)$. The first vector φ_1 will grow exponentially with rate γ_1, and so will the second vector φ_2. Let us however decompose the second vector as

$$\varphi_2(x) = \varphi_{||}(x) + \varphi_\perp(x) \,, \tag{7.99}$$

where $\varphi_{||}$ is proportional to φ_1, while $\varphi_\perp$ is orthogonal to φ_1. The volume enclosed by φ_1 and φ_2 is the same as the one delimited by φ_1 and $\varphi_\perp$, as shown in Fig. 7.6. This volume, which grows with rate $\gamma_1 + \gamma_2$, is easily computed as $||\varphi_1|| \times ||\varphi_\perp||$. Since $||\varphi_1||$ grows with rate γ_1, we obtain

$$||\varphi_\perp(x)|| \sim \exp(\gamma_2 x) \,. \tag{7.100}$$

Therefore, the growth of the component of φ_2 orthogonal to φ_1 is controlled by the second Lyapunov exponent γ_2. This means that, to obtain the Lyapunov exponents, we should follow a set of orthogonal vectors. In general, this can be done by applying a Gram–Schmidt algorithm to the columns of Φ to orthogonalise them. At the matrix level, this procedure reduces to compute the QR-decomposition of Φ:

$$\Phi(x) = Q(x)R(x)\,, \tag{7.101}$$

where Q is orthogonal ($\beta = 1$), unitary ($\beta = 2$) or symplectic ($\beta = 4$) and R is upper triangular with positive diagonal elements. The last condition implies the uniqueness of the matrices Q and R. Using this decomposition in Eq. (7.93) gives

$$Q'(x)R(x) + Q(x)R'(x) = M(x)Q(x)R(x)\,, \tag{7.102}$$

where Q' and R' denote the derivatives of Q and R. Let us multiply this equation by $Q^{-1} = Q^\dagger$ on the left, and R^{-1} on the right:

$$Q^\dagger(x)Q'(x) + R'(x)R^{-1}(x) = Q^\dagger(x)M(x)Q(x)\,. \tag{7.103}$$

Since R is upper triangular, so are R^{-1} and $R'R^{-1}$. Therefore, looking at the matrix elements of this equation on the lower triangular part yields:

$$[Q^\dagger(x)Q'(x)]_{mn} = [Q^\dagger(x)M(x)Q(x)]_{mn}\,, \quad m > n\,. \tag{7.104}$$

This gives a set of equations governing the evolution of the matrix Q. Looking now at the diagonal elements of (7.103), we obtain

$$[Q^\dagger(x)Q'(x)]_{nn} + \frac{R'_{nn}(x)}{R_{nn}(x)} = [Q^\dagger(x)M(x)Q(x)]_{nn}\,, \tag{7.105}$$

where we used that $(R^{-1})_{nn} = (R_{nn})^{-1}$ which follows from the fact that R is upper triangular. Since $Q^\dagger MQ$ is self-adjoint, its diagonal elements are real. And so is R_{nn} by definition. Therefore $[Q^\dagger Q']_{nn}$ is also real. Additionally, taking the derivative of $Q^\dagger Q = \mathbb{1}_N$ gives

$$Q^\dagger Q' + (Q')^\dagger Q = Q^\dagger Q' + (Q^\dagger Q')^\dagger = 0\,, \tag{7.106}$$

from which we deduce that $\mathrm{Re}[(Q^\dagger Q')_{nn}] = 0$. Thus,

$$[Q^\dagger(x)Q'(x)]_{nn} = 0\,, \tag{7.107}$$

which implies that

$$\frac{R'_{nn}(x)}{R_{nn}(x)} = \partial_x \ln R_{nn} = [Q^\dagger(x)M(x)Q(x)]_{nn}\,. \tag{7.108}$$

We have thus obtained a set of coupled equations (7.104,7.106,7.108) which controls the evolution of the QR-decomposition of Φ. We can summarise these equations as

$$\boxed{\begin{cases} Q^\dagger Q' = \mathbb{A} \circ (Q^\dagger M Q)\,, \\ \partial_x \ln R_{nn} = (Q^\dagger M Q)_{nn}\,, \end{cases}} \qquad \text{(Stratonovich)} \tag{7.109}$$

where $[A \circ B]_{mn} = A_{mn} B_{mn}$ is the Hadamard product, and

$$\mathbb{A} = \begin{pmatrix} 0 & -1 & \cdots & -1 \\ 1 & \ddots & \ddots & \vdots \\ \vdots & \ddots & \ddots & -1 \\ 1 & \cdots & 1 & 0 \end{pmatrix} . \tag{7.110}$$

Having obtained Eq. (7.109) which describes the evolution of the matrix Q and the diagonal elements of R, we will now relate these to the Lyapunov exponents obtained from Eq. (7.98). From the QR-decomposition, we have $\Phi(x)^\dagger \Phi(x) = R(x)^\dagger R(x)$. Therefore, all the information of the localisation is contained in the matrix R. Denote R_n the upper-left subblock of R of size $n \times n$:

$$R(x) = \begin{pmatrix} R_n(x) & \star \\ 0 & \star \end{pmatrix} , \tag{7.111}$$

where we have denoted $\star$ any other non-zero subblock. We thus have:

$$\Phi(x)^\dagger \Phi(x) = R(x)^\dagger R(x) = \begin{pmatrix} R_n(x)^\dagger R_n(x) & \star \\ 0 & \star \end{pmatrix} . \tag{7.112}$$

The determinant of the top-left subblock is given by:

$$|\Phi(x)^\dagger \Phi(x)|_n = \det[R_n(x)^\dagger R_n(x)] = \prod_{i=1}^{n} R_{ii}(x)^2 . \tag{7.113}$$

Consequently, Eq. (7.98) reduces to

$$\frac{1}{2x} \ln |\Phi(x)^\dagger \Phi(x)|_n = \sum_{i=1}^{n} \frac{1}{x} \ln R_{nn}(x) \underset{x\to\infty}{\longrightarrow} \sum_{i=1}^{n} \gamma_n . \tag{7.114}$$

Taking the difference between the equations for n and $n-1$ gives the expression of the n^{th} Lyapunov exponent:

$$\boxed{\gamma_n = \lim_{x\to\infty} \frac{1}{x} \ln R_{nn}(x)} \tag{7.115}$$

This relation shows that the Lyapunov exponents can be obtained from the diagonal elements of the matrix R.

The first consequence is that the sum of all Lyapunov exponents can be obtained easily. From Eq. (7.115), we have

$$\sum_{n=1}^{N} \gamma_n = \lim_{x\to\infty} \frac{1}{x} \sum_{n=1}^{N} \ln R_{nn}(x) . \tag{7.116}$$

Using Eq. (7.109), we can write

$$\partial_x \sum_{n=1}^{N} \ln R_{nn}(x) = \mathrm{tr}[Q^\dagger M Q] = \mathrm{tr}\, M(x) , \tag{7.117}$$

therefore,

$$\frac{1}{x}\sum_{n=1}^{N}\ln R_{nn}(x)=\frac{1}{x}\int_0^x \operatorname{tr} M(x')\mathrm{d}x' \underset{x\to\infty}{\longrightarrow} \operatorname{tr}\langle M\rangle=\mu\operatorname{tr} G\,. \tag{7.118}$$

This proves that the sum of all Lyapunov exponents is simply

$$\boxed{\sum_{n=1}^{N}\gamma_n=\mu\ \operatorname{tr} G\,,\quad \text{for}\quad \varepsilon=0} \tag{7.119}$$

In the one dimensional case $N=1$, we recover the value of the Lyapunov exponent at zero energy [165].

We would like now to obtain each Lyapunov exponent independently. We can go one step further than (7.115) by solving the equation on R_{nn} (7.109), which gives

$$\frac{1}{x}\ln R_{nn}(x)=\frac{1}{x}\int_0^x (Q^\dagger M Q)_{nn}\,. \tag{7.120}$$

For large x, the r.h.s. converges to $\left\langle Q^\dagger M Q\right\rangle$ by ergodicity. However, this mean value is difficult to compute because the noise M and the matrix Q are correlated. This is due to the fact that Eq. (7.109) is to be interpreted in the Stratonovich way, which introduces nontrivial correlations between the matrices Q and M. This problem can be solved by converting the set of equations (7.109) to their Itô form. This procedure is quite cumbersome, but can be carried out explicitly. This gives the Itô form of the equations satisfied by the diagonal elements of R:

$$\partial_x \ln R_{nn}=\mathcal{D}_{n,\beta}(G,Q)+(Q^\dagger M Q)_{nn}\qquad (\text{Itô}), \tag{7.121}$$

where the drift correction is

$$\begin{aligned}\mathcal{D}_{n,\beta}(G,Q)=\beta\sum_{k,l}\frac{g_k g_l}{g_k+g_l}\sum_a \mathbb{A}_{an}Q^\dagger_{ak}Q_{ka}Q^\dagger_{nl}Q_{ln}\\ +(2-\beta)\sum_{k,l}\frac{g_k g_l}{g_k+g_l}\sum_a \mathbb{A}_{an}Q^\dagger_{nk}Q_{ka}Q^\dagger_{nl}Q_{la}\,.\end{aligned} \tag{7.122}$$

We recall that $G=\mathrm{Diag}(g_1,\dots,g_N)$ and the matrix $\mathbb{A}$ is given by (7.110). Integrating equation (7.121) gives the expression of the Lyapunov exponents (7.115):

$$\gamma_n=\langle\mathcal{D}_{n,\beta}(G,Q)\rangle+\left\langle (Q^\dagger M Q)_{nn}\right\rangle\,, \tag{7.123}$$

where the averaging must be done over the stationary distribution of the matrix Q, and over the noise M. Since this relation is obtained from the Itô form of the stochastic equations, Q and M are uncorrelated, thus we can average them independently. Using that $\langle M\rangle=\mu G$, this yields:

$$\gamma_n=\langle\mathcal{D}_{n,\beta}(G,Q)\rangle+\mu\left\langle (Q^\dagger G Q)_{nn}\right\rangle\,, \tag{7.124}$$

where the brackets denote averaging over the stationary distribution of Q.

To compute the Lyapunov spectrum $\{\gamma_n\}$, we should first find the stationary distribution of Q from its stochastic equation (7.109), and then use it to compute the averages in Eq. (7.124). We will now apply this procedure to compute the Lyapunov exponents in a few simple cases in which this procedure can be carried out explicitly.

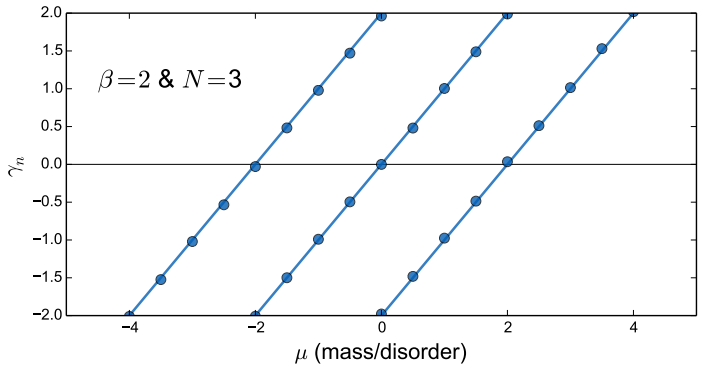

Figure 7.7: Lyapunov exponents for $N = 3$ and $\beta = 2$ as a function of the mass over disorder ration μ, in the isotropic case $G = \mathrm{Diag}(1, 1, 1)$. The lines are obtained from Eq. (7.126), the points from numerical simulations.

Isotropic case

The simplest case is $G = g\mathbb{1}_N$. The drift (7.122) reduces to

$$\mathcal{D}_{n,\beta}(G, Q) = \frac{\beta g}{2}(N + 1 - 2n) \,, \tag{7.125}$$

which does not depend on Q. Therefore the averaging (7.124) is trivial for this term. Additionally, since $Q^\dagger Q = \mathbb{1}_N$, we have $\left\langle Q^\dagger G Q \right\rangle = g \left\langle \mathbb{1}_N \right\rangle = g\mathbb{1}_N$. Therefore, the Lyapunov exponents (7.124) reduce to

$$\boxed{\gamma_n = \mu g + \frac{\beta g}{2}(N + 1 - 2n)} \tag{7.126}$$

This expression for the Lyapunov exponents at zero energy is known in the literature [62, 208]. It was first derived for $\beta = 1$ by Le Jan and Newman independently [202, 252]. These Lyapunov exponents are equally spaced, and depend linearly on the mass over disorder ratio μ. They are represented as function of μ in Fig. 7.7.

Non-isotropic case for $N = 2$ channels

In the general case, it is extremely difficult to find the stationary distribution of the matrix Q associated to the stochastic equation (7.109). Nevertheless this can be done for small number of channels, when the matrix Q can be parametrised by a few real variables. For example, for $N = 2$ channels in the case $\beta = 1$ the matrix Q is orthogonal and can be written as

$$Q = \begin{pmatrix} \cos\theta & -\sin\theta \\ \sin\theta & \cos\theta \end{pmatrix} \,, \tag{7.127}$$

and the Haar measure is simply $\mathrm{d}Q = \mathrm{d}\theta$. While for $\beta = 2$, the unitary matrix Q can be parametrised as

$$Q = \mathrm{e}^{\mathrm{i}\phi} \begin{pmatrix} \mathrm{e}^{\mathrm{i}\psi} & 0 \\ 0 & \mathrm{e}^{-\mathrm{i}\psi} \end{pmatrix} \begin{pmatrix} \cos\theta & -\sin\theta \\ \sin\theta & \cos\theta \end{pmatrix} \begin{pmatrix} \mathrm{e}^{\mathrm{i}\delta} & 0 \\ 0 & \mathrm{e}^{-\mathrm{i}\delta} \end{pmatrix} \,, \tag{7.128}$$

with Haar measure $\mathrm{d}Q = 2\,|\sin(2\theta)|\,\mathrm{d}\phi\mathrm{d}\psi\mathrm{d}\delta\mathrm{d}\theta$. In both cases, rewriting the stochastic equation (7.109) in terms of the parameters of Q allows to find the stationary solution, which takes the form

$$f(Q) \propto [(Q^\dagger G Q)_{11}]^{\mu-\beta/2} [(Q^\dagger G Q)_{22}]^{-\mu-\beta/2} \,. \tag{7.129}$$

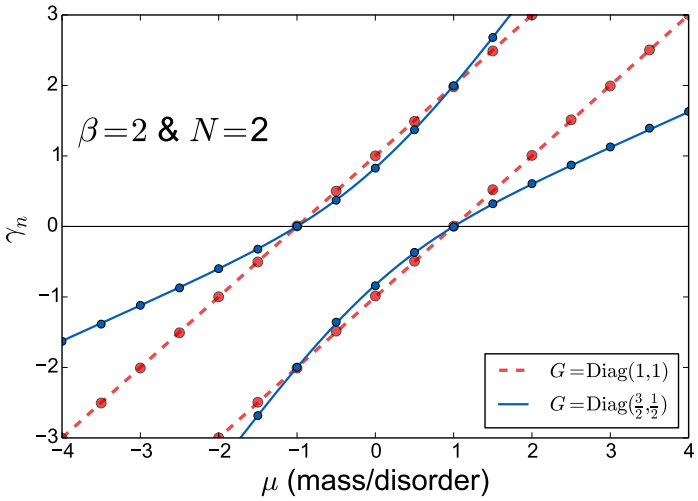

Figure 7.8: Lyapunov exponents for $N = 2$ and $\beta = 2$ as a function of the mass over disorder ration μ, in the non-isotropic case $G = \mathrm{Diag}(g_1, g_2)$. The lines are obtained from Eq. (7.130), the points from numerical simulations.

This explicit solution yields integral representations for the Lyapunov exponents (7.124). For $\beta = 2$, these integrals can be computed analytically and gives the rather complex expression

$$\gamma_1 = \mu^2 (g_1 g_2)^\mu \frac{g_1 + g_2}{g_1^{2\mu} - g_2^{2\mu}} \left[\mathrm{B}\left(\frac{g_1}{g_1 + g_2}; 1 + \mu, -\mu \right) - \mathrm{B}\left(\frac{g_2}{g_1 + g_2}; 1 + \mu, -\mu \right) \right] + \mu \frac{(g_1 - g_2)^3}{g_1^{2\mu} - g_2^{2\mu}} \frac{g_1^{2\mu}}{6 g_1 g_2} \mathrm{F}_1\left(2, -\mu + 1, \mu + 1, 4; 1 - \frac{g_2}{g_1}, 1 - \frac{g_1}{g_2} \right) + 2 \frac{g_1 g_2}{g_1 + g_2} , \quad (7.130)$$

where $\mathrm{B}(z; a, b)$ is the incomplete Beta-function, and F_1 is the Appell hypergeometric function with two arguments [20, 27]:

$$\mathrm{F}_1(a, b, b', c; x, y) = \sum_{m \geqslant 0} \sum_{n \geqslant 0} \frac{(a)_{m+n} (b)_m (b')_n}{(c)_{m+n} m! n!} x^m y^n , \quad (a)_n = \frac{\Gamma(a + n)}{\Gamma(a)} . \quad (7.131)$$

The second Lyapunov exponent can be deduced from the relation (7.119). This result allows to plot the Lyapunov exponents as a function of μ, as shown in Fig. 7.8. In particular, we notice that they vanish for the same values $\mu = \pm 1$ as in the isotropic case, independently of the anisotropy.

Effect of anisotropy on the Lyapunov spectrum at $\varepsilon = 0$

The complexity of the expression (7.130) for the $N = 2$ channels case leaves almost no hope to find closed expressions for the Lyapunov exponents in the general case for N channels. We thus rely on numerical computations for higher number of channels (the method is described in Section 7.3.1). To see the effect of anisotropy, we show in Fig. 7.9 the Lyapunov exponents $\{\gamma_n\}$ for $N = 5$ channels, with disorder $G = \mathrm{Diag}(1, 1, 1, 1, g_N)$, as a function of g_N. For $g_N = 1$, we recover the isotropic situation (7.126). For $g_N = 0$, there is no disorder in the N^{th} channel, which decouples from the others. This corresponds to a delocalised channel, along with 4 isotropically coupled channels. For $0 < g_N < 1$, the Lyapunov spectrum interpolated between these situations. In particular, we notice that the well-known linear Lyapunov spectrum [62, 208] is recovered only

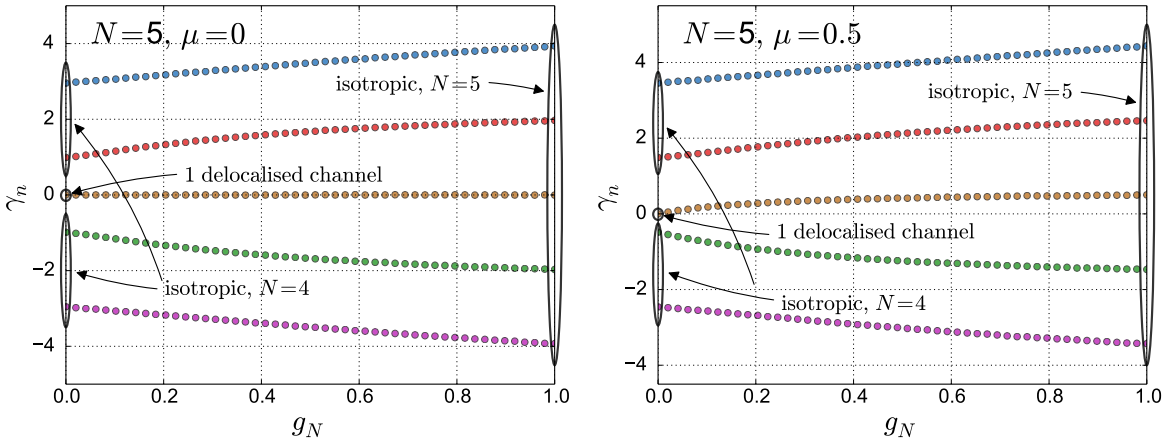

Figure 7.9: Lyapunov exponents for $N = 5$, $\beta = 2$ and $G = \mathrm{Diag}(1, 1, 1, 1, g_N)$ as a function of g_N, obtained by numerical simulations. Left: $\mu = 0$, Right: $\mu = 0.5$.

in the isotropic situations. If isotropy is broken, the Lyapunov exponents are no longer equally spaced.

For $\mu = 0$, we notice that one Lyapunov exponent remains exactly zero, independently of the anisotropy. This observation is consistent with the the one made on the $N = 2$ channels case (see Fig. 7.8). Therefore, it seems that, independently of the isotropy, the n^{th} Lyapunov exponent will vanish for

$$\mu = \frac{\beta}{2}(2n - N - 1) \,. \tag{7.132}$$

As we have seen in Section 7.1 the exponent α which controls the low energy behaviour of the density of states also vanishes for these particular values of μ. In the next Chapter, we will show that these values of μ are associated to phase transitions of topological nature.

7.2.2 Energy dependence of the Lyapunov exponents

Having extensively studied the zero energy case $\varepsilon = 0$, let us now briefly discuss the Lyapunov spectrum away from the Dirac point. Our starting point is the Dirac equation (6.2,6.3), which yields

$$\begin{cases} \partial_x \varphi(x) = M(x)\varphi(x) - \varepsilon\, \xi(x) \,, \\ \partial_x \xi(x) = -M(x)\xi(x) + \varepsilon\, \varphi(x) \,. \end{cases} \tag{7.133}$$

We can use the Riccati matrix (6.28) to reduce the equation on φ to a first order differential equation:

$$\partial_x \varphi(x) = [Z_\varepsilon(x) + M(x)]\varphi(x) \,. \tag{7.134}$$

We can then reproduce the derivation of Section 7.2.1 with this new equation. Regrouping again the independent solutions into the matrix $\Phi = QR$, Eq. (7.109) becomes in this case

$$\boxed{\begin{cases} Q^\dagger Q' = \mathbb{A} \circ [Q^\dagger (Z_\varepsilon + M) Q] \,, \\ \partial_x \ln R_{nn} = [Q^\dagger (Z_\varepsilon + M) Q]_{nn} \,, \end{cases}} \tag{7.135}$$

where the matrix $\mathbb{A}$ is given by (7.110). The Lyapunov exponents are then obtained from the diagonal elements R_{nn}, Eq. (7.115). The main difference from the zero energy case discussed above is the presence of the Riccati matrix Z_ε, which is coupled to the matrix Q. This makes the problem much more challenging.

We stress an important difference with the case of zero energy discussed in Section 7.2.1:

(i) At $\varepsilon = 0$ the two components φ and ξ of the spinor ψ decouple. We thus focused on φ only and we extracted N Lyapunov exponents $\{\gamma_n\}$, which can be either positive or negative. The second component ξ is associated to a second set of Lyapunov exponents, which are simply $\{-\gamma_n\}$ (see Eq. (7.91)).

(ii) Here at $\varepsilon \neq 0$, the two components of ψ remain coupled, and their evolution is described by Eq. (7.133). It is thus associated to $2N$ Lyapunov exponents which come in pairs $\{\gamma_n, -\gamma_n\}$. However, we have reduced the problem to Eq. (7.134) which involves only the component φ by introducing the Riccati matrix. In doing so, we select only the N largest Lyapunov exponents of the set $\{\gamma_n, -\gamma_n\}$, which we denote $\{\hat\gamma_n = |\gamma_n|\}$.

Therefore, the Lyapunov exponents $\{\hat\gamma_n\}$ extracted from Eq. (7.135) are always positive.

Sum of the Lyapunov exponents

Proceeding as in Section 7.2.1, we can easily obtain the the sum of all the Lyapunov exponents $\{\hat\gamma_n\}$ associated to (7.134) as

$$\boxed{\sum_{n=1}^{N} \hat\gamma_n(\varepsilon) = \langle Z_\varepsilon + M \rangle = \operatorname{Re} \Omega(\varepsilon + \mathrm{i}0^+)} \tag{7.136}$$

where Ω is the characteristic function (7.12) introduced in Section 7.1. We stress that this relation differs from Eq. (7.119) which we obtained at zero energy:

- at $\varepsilon = 0$, Eq. (7.119) involves the Lyapunovs $\{\gamma_n\}$ which can be either positive or negative, and gives $\sum_n \gamma_n = \mu \operatorname{tr} G$;
- At finite energy, Eq. (7.136) involves the positive Lyapunovs $\{\hat\gamma_n\}$. Therefore, taking the limit $\varepsilon \to 0$ in this last relation yields $\sum_n \hat\gamma_n(0) = \sum_n |\gamma_n(0)|$, which in general differs from (7.119).

Relation (7.136) is a generalisation of the formula used for one dimensional systems [84–86, 165, 206]. Combining (7.136) with Eq. (7.13), we have shown that the characteristic function Ω takes the form

$$\boxed{\Omega(\varepsilon + \mathrm{i}0^+) = \sum_{n=1}^{N} \hat\gamma_n(\varepsilon) - \mathrm{i}\pi\, \mathcal{N}(\varepsilon)} \tag{7.137}$$

This relation shows that the sum of all the Lyapunov exponents and the density of states are the real and imaginary parts of the same analytic function. This is a consequence of the Thouless relation [197, 236]:

$$\frac{\hat\gamma_1(\varepsilon) + \cdots + \hat\gamma_N(\varepsilon)}{N} = \int \mathrm{d}\varepsilon'\, \rho(\varepsilon') \ln|\varepsilon - \varepsilon'| + \text{const.}\,, \tag{7.138}$$

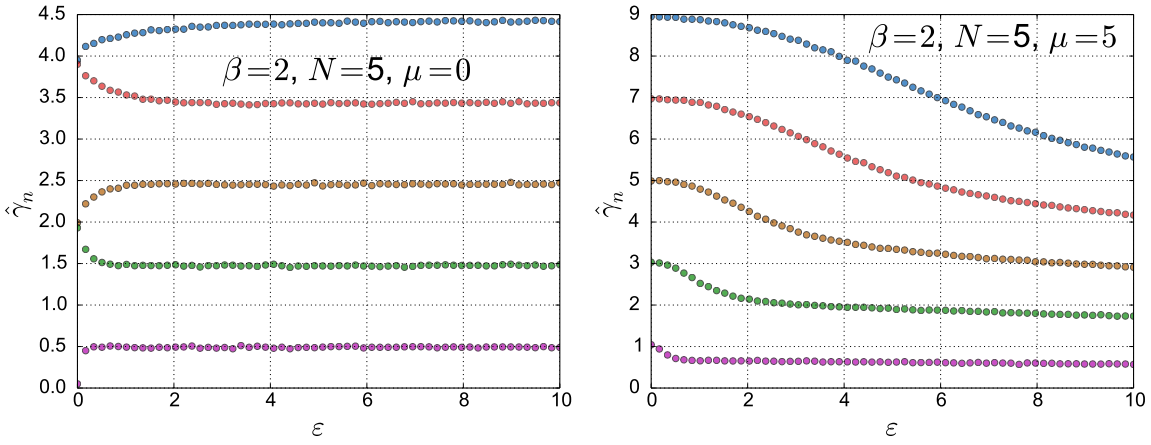

Figure 7.10: Lyapunov exponents for $N = 5$, $\beta = 2$ and $G = \mathbb{1}_5$ as a function of the energy ε, obtained by numerical simulations. Left: $\mu = 0$, Right: $\mu = 5$.

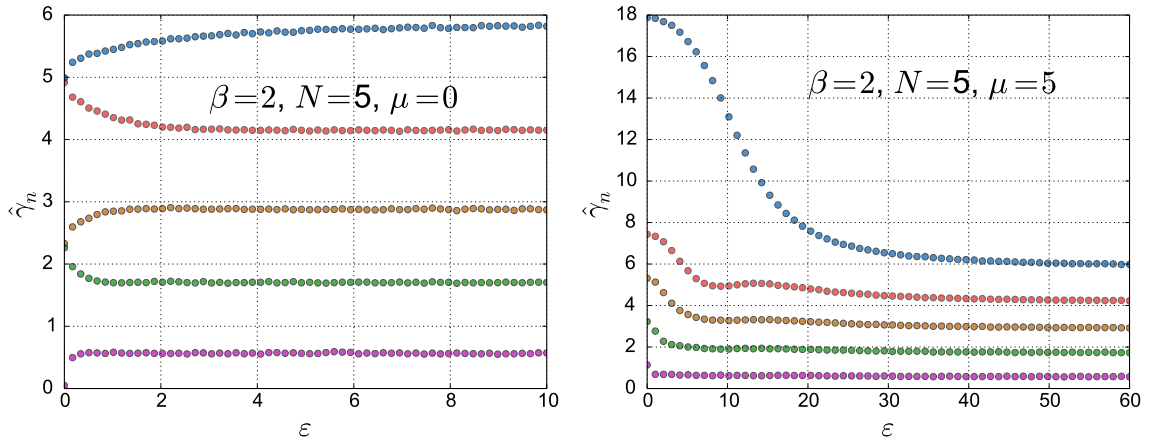

Figure 7.11: Lyapunov exponents for $N = 5$ and $\beta = 2$ in the anisotropic case $G = \mathrm{Diag}(1, 1, 1, 1, 3)$ as a function of the energy ε, obtained by numerical simulations. Left: $\mu = 0$, Right: $\mu = 5$.

which relates the sum of the Lyapunov exponents to the density of states. This relation was first derived in the strictly one dimensional case by Herbert, Jones and Thouless [175, 289].

Individual Lyapunov exponents

Although the sum of the Lyapunov exponents can be easily obtained from Eq. (7.136), studying each exponent $\hat{\gamma}_n$ independently is much more difficult. We thus rely on numerical simulations (the algorithm is described below, in Section 7.3.1).

The Lyapunov exponents, in the isotropic case $G = \mathbb{1}_N$ are represented in Fig. 7.10, for $N = 5$ channels in the unitary case $\beta = 2$. We clearly see, as noted before, that they are all positive. Let us make a few comments.

- In the limit $\varepsilon \to 0$, we can check that the Lyapunov exponents coincide with the

absolute value of (7.126) obtained previously,

$$\hat{\gamma}_n = |\gamma_n| = \left| \mu g + \frac{\beta g}{2}(N+1-2n) \right| , \quad n \in \{1, \dots, N\} . \tag{7.139}$$

The absolute value can cause a degeneracy of the Lyapunov spectrum $\{\hat{\gamma}_n\}$ at $\varepsilon = 0$, for instance for $\mu = 0$, as can be seen in Fig 7.10 (left);

- For $\varepsilon \to \infty$, the Lyapunov exponents become equally spaced, and do not depend on μ. They coincide with the spectrum obtained in the Wigner-Dyson symmetry classes (compare for instance with Eq. (5.27)): they present the scaling

$$\hat{\gamma}_n = (1 + \beta(N-n))\hat{\gamma}_N , \quad n \in \{1, \dots, N\} , \tag{7.140}$$

where $\hat{\gamma}_N$ is the smallest Lyapunov exponent;

- The crossover between the two universal values, for $\varepsilon = 0$ (chiral classes) and for $\varepsilon \to \infty$ (Wigner-Dyson classes), occurs at different values of the energy for different Lyapunov exponents: the smallest exponents reach rapidly their limit, while the largest converge more slowly.

The Lyapunov spectrum in the **anisotropic** case $G = \mathrm{Diag}(1, 1, 1, 1, 3)$ is represented in Fig. 7.11. The phenomenology is qualitatively similar to the isotropic case, except that the Lyapunov exponents are no longer equally spaced, neither at $\varepsilon = 0$ (as we already noticed in Section 7.2.1) nor for $\varepsilon \to \infty$. The linearity of the Lyapunov spectrum with the index n seems to be a specific feature of the isotropic case.

7.3 Numerical simulations

We have obtained analytical results for the density of states and the sum of the Lyapunov exponents for the multichannel Dirac equation with a random mass. Our aim is now to perform numerical simulations to check these results. Furthermore, since we were only able to study the sum analytically, we can use these simulations to study the energy dependence of the spectrum of Lyapunov exponents γ_n.

To perform numerical simulations, it is convenient to consider a different version of the problem. We still consider the Dirac equation (6.2,6.3), with a random mass taking the form of impurities placed at positions $\{x_n\}$:

$$M(x) = \sum_n W_n \, \delta(x - x_n) , \quad x_n = n \, \delta x , \tag{7.141}$$

where the $N \times N$ matrices W_n are picked from the distribution

$$P[W_n] \propto \exp\left\{ -\frac{1}{2\,\delta x} \mathrm{tr}\left[(W_n - \mu G \, \delta x) G^{-1} (W_n - \mu G \, \delta x) \right] \right\} . \tag{7.142}$$

In the limit $\delta x \to 0$, this reduces to the multichannel Dirac equation (6.8) [40, 266, 282].

Between two impurities, the evolution of a spinor $\psi(x)$ satisfies the free Dirac equation

$$\begin{pmatrix} 0 & \partial_x \mathbb{1}_N \\ -\partial_x \mathbb{1}_N & 0 \end{pmatrix} \begin{pmatrix} \varphi \\ \xi \end{pmatrix} = \varepsilon \begin{pmatrix} \varphi \\ \xi \end{pmatrix} , \quad \psi = \begin{pmatrix} \varphi \\ \xi \end{pmatrix} , \tag{7.143}$$

which we can rewrite as

$$\partial_x \begin{pmatrix} \varphi \\ \xi \end{pmatrix} = \begin{pmatrix} 0 & -\varepsilon\, \mathbb{1}_N \\ \varepsilon\, \mathbb{1}_N & 0 \end{pmatrix} \begin{pmatrix} \varphi \\ \xi \end{pmatrix} . \tag{7.144}$$

Therefore, the evolution between two impurities is straightforward:

$$\begin{pmatrix} \varphi(x_{n+1}^-) \\ \xi(x_{n+1}^-) \end{pmatrix} = \begin{pmatrix} \cos(\varepsilon\, \delta x)\mathbb{1}_N & -\sin(\varepsilon\, \delta x)\mathbb{1}_N \\ \sin(\varepsilon\, \delta x)\mathbb{1}_N & \cos(\varepsilon\, \delta x)\mathbb{1}_N \end{pmatrix} \begin{pmatrix} \varphi(x_n^+) \\ \xi(x_n^+) \end{pmatrix} . \tag{7.145}$$

There remains only to study the effect of an impurity at x_n. To do so, we can rewrite the Dirac equation (6.2,6.3) near the impurity at x_n in the form

$$\begin{cases} \partial_x \left[\exp\left(W_n\, \Theta(x - x_n)\right) \xi\right] & = \varepsilon\, \exp\left(W_n\, \Theta(x - x_n)\right) \varphi\, , \\ -\partial_x \left[\exp\left(-W_n\, \Theta(x - x_n)\right) \varphi\right] & = \varepsilon\, \exp\left(-W_n\, \Theta(x - x_n)\right) \xi\, , \end{cases} \tag{7.146}$$

where Θ is the Heaviside step function. Integrating on a small interval $[x_n - t, x_n + t]$ and letting $t \to 0$ yields

$$\begin{cases} \varphi(x_n^+) = \mathrm{e}^{W_n}\, \varphi(x_n^-)\, , \\ \xi(x_n^+) = \mathrm{e}^{-W_n}\, \xi(x_n^-)\, . \end{cases} \tag{7.147}$$

Therefore the evolution of the spinor ψ can be described by the product of matrices

$$\psi(x_n^+) = A_n\, \psi(x_{n-1}^+)\, , \tag{7.148}$$

where

$$A_n = \begin{pmatrix} \mathrm{e}^{W_n} & 0 \\ 0 & \mathrm{e}^{-W_n} \end{pmatrix} \begin{pmatrix} \cos(\varepsilon\, \delta x)\mathbb{1}_N & -\sin(\varepsilon\, \delta x)\mathbb{1}_N \\ \sin(\varepsilon\, \delta x)\mathbb{1}_N & \cos(\varepsilon\, \delta x)\mathbb{1}_N \end{pmatrix} . \tag{7.149}$$

The value of the spinor at position x_n can be deduced from the value at the origin using the product

$$\psi(x_n^+) = \Pi_n \psi(0^+)\, , \quad \text{where } \Pi_n = A_n A_{n-1} \cdots A_1\, . \tag{7.150}$$

We set for convenience $\Pi_0 = \mathbb{1}_{2N}$. This product of random matrices has already been considered in the literature, for example in Ref. [85] in the strictly one dimensional case $N = 1$.

Having rephrased our problem in terms of a product of random matrices, we will now see how this new formulation is useful to obtain numerically the Lyapunov exponents and the density of states.

7.3.1 Lyapunov exponents

As we have seen in Section 7.2.1, the QR-decomposition is a powerful way to extract the Lyapunov exponents. We now present the discrete version of this method, which is convenient to study the product of random matrices (7.150). We thus introduce the QR-decomposition[2] of Π_n:

$$\Pi_n = Q_n R_n\, , \tag{7.151}$$

[2]Note that in the continuous version of Section 7.2.1 we introduced the QR-decomposition of the $N \times N$ matrix Φ while here we decompose the $2N \times 2N$ matrix Π_n.

where Q_n is orthogonal ($\beta = 1$), unitary ($\beta = 2$) or symplectic ($\beta = 4$) and R_n is an upper triangular matrix, with positive real diagonal elements. This condition on the diagonal elements of R_n ensures the uniqueness of the decomposition, which is important for numerical purposes. The idea is to follow the evolution of the matrices Q_n and R_n with n. Initially, since $\Pi_0 = \mathbb{1}_{2N}$, we have:

$$Q_0 = \mathbb{1}_{2N} \quad \text{and} \quad R_0 = \mathbb{1}_{2N} \,. \tag{7.152}$$

From the definition of Π_n (7.150) we have

$$\Pi_{n+1} = A_{n+1}\Pi_n = A_{n+1}Q_nR_n \,. \tag{7.153}$$

Let us now introduce the QR-decomposition of $A_{n+1}Q_n$:

$$A_{n+1}Q_n = \tilde{Q}_n\tilde{R}_n \,, \tag{7.154}$$

with the same conditions as for (7.151). From the unicity of the QR-decomposition, we can straightforwardly deduce

$$\Pi_{n+1} = Q_{n+1}R_{n+1} \,, \quad \text{where} \quad \begin{cases} Q_{n+1} = \tilde{Q}_n \,, \\ R_{n+1} = \tilde{R}_nR_n \,. \end{cases} \tag{7.155}$$

From the discussion of Section 7.2.1, the Lyapunov exponents can be extracted from the diagonal elements of R_n [103, 104]:

$$\gamma_i = \lim_{n\to\infty} \frac{1}{n} \ln[(R_n)_{ii}] \,. \tag{7.156}$$

The evolution of these diagonal elements, given by Eq. (7.155), can be rewritten as

$$\ln[(R_{n+1})_{ii}] = \ln[(\tilde{R}_n)_{ii}] + \ln[(\tilde{R}_n)_{ii}] \,, \tag{7.157}$$

thus

$$\ln[(\tilde{R}_n)_{ii}] = \sum_{k=1}^{n} \ln[(\tilde{R}_k)_{ii}] \,. \tag{7.158}$$

This gives the final expression of the Lyapunov exponents:

$$\gamma_i = \lim_{n\to\infty} \frac{1}{n} \sum_{k=1}^{n} \ln[(\tilde{R}_k)_{ii}] \,. \tag{7.159}$$

Therefore, the Lyapunov exponents can be computed using the following procedure:

1. Initialise $Q_1 = \mathbb{1}_{2N}$ and $\{\xi_i = 0\}$;
2. Compute the QR-decomposition of $A_nQ_n = \tilde{Q}_n\tilde{R}_n$;
3. Set $Q_{n+1} = \tilde{Q}_n$ and increment $\xi_i \leftarrow \xi_i + \ln[(\tilde{R}_n)_{ii}]$
4. Repeat from 2;
5. Return $\{\gamma_i = \xi_i/n\}$.

Note that since most QR-decomposition algorithms do not respect the condition that the diagonal elements of the matrix R be positive, it is required to make the correction

$$Q \to QD\,, \quad R \to D^\dagger R\,, \qquad \text{where } D_{ij} = \frac{R_{ii}}{|R_{ii}|}\delta_{ij}\,, \tag{7.160}$$

to ensure uniqueness of the QR-decomposition.

I used this procedure to obtain numerically the Lyapunov spectrum in different situations. See Figs. 7.7 and 7.8 for the Lyapunov spectrum at zero energy, both in the isotropic and anisotropic cases. See also Figs. 7.10 and 7.11 for the evolution of the Lyapunov spectrum with the energy.

7.3.2 Density of states

The numerical evaluation of the density of states is based on a node counting theorem, also known as Sturm Liouville oscillation theory in the mathematical literature [305]. We proceed as in Section 7.1 and introduce the eigenstates ψ_n of the Dirac Hamiltonian (6.3) restricted to the finite interval $[0, L]$:

$$\mathcal{H}\psi_n = \varepsilon_n \psi_n\,, \quad \psi_n = \begin{pmatrix} \varphi_n \\ \xi_n \end{pmatrix}\,, \quad n \in \mathbb{N}\,, \tag{7.161}$$

with $\xi_n(0) = \xi_n(L) = 0$ (we could similarly choose the other boundary condition $\varphi_n(0) = \varphi_n(L) = 0$). We also consider the initial value problem

$$\mathcal{H}\Psi(\varepsilon; x) = \varepsilon\Psi(\varepsilon; x)\,, \quad \Psi(\varepsilon; x) = \begin{pmatrix} \Phi(\varepsilon; x) \\ \Xi(\varepsilon; x) \end{pmatrix}\,, \quad \text{with } \Psi(\varepsilon; 0) = \begin{pmatrix} \mathbb{1}_N \\ 0 \end{pmatrix}\,, \tag{7.162}$$

where we again introduced the "matrix spinor" Ψ containing the N independent solutions.

The node-counting theorem [305] states that the number of eigenstates of energy $\varepsilon_n < \varepsilon$ is exactly the number of zeros of $\det \Xi(\varepsilon; x)$ in the open interval $]0, L[$. This number is exactly the integrated density of states $\mathcal{N}_L(\varepsilon)$:

$$\mathcal{N}_L(\varepsilon) = \text{number of zeros of } \det \Xi(\varepsilon; x) \text{ in }]0, L[\,. \tag{7.163}$$

It is a random number, but in the limit of large system size $L \to \infty$, it can be used to obtain the mean IDoS per unit length

$$\mathcal{N}(\varepsilon) = \lim_{L\to\infty} \frac{1}{L}\mathcal{N}_L(\varepsilon)\,, \tag{7.164}$$

which is deterministic from the ergodic property.

However, the matrices Φ and Ξ are not convenient objects for numerical purposes, since they grow exponentially. We will thus re-express the IDoS in terms of the matrix Q obtained from the QR-decomposition discussed in Section 7.3.1. Let us again consider the initial value problem $\mathcal{H}\Psi = \varepsilon\Psi$, with a full $2N \times 2N$ matrix Ψ. We thus denote

$$\Psi(\varepsilon, x) = \begin{pmatrix} \Phi(\varepsilon; x) & \tilde{\Phi}(\varepsilon; x) \\ \Xi(\varepsilon; x) & \tilde{\Xi}(\varepsilon; x) \end{pmatrix}\,, \quad \text{with} \quad \Psi(\varepsilon; 0) = \mathbb{1}_{2N} = \begin{pmatrix} \mathbb{1}_N & 0 \\ 0 & \mathbb{1}_N \end{pmatrix}\,. \tag{7.165}$$

The first column is the "matrix spinor" obtained from the initial value problem (7.162) with $\Xi(\varepsilon;0) = 0$. The second column corresponds to the other possible boundary condition $\tilde{\Phi}(\varepsilon;0) = 0$. Let us consider the QR-decomposition of this square matrix:

$$\Psi(\varepsilon, x) = Q(x)R(x)\,, \tag{7.166}$$

where Q is orthogonal ($\beta = 1$), unitary ($\beta = 2$) or symplectic ($\beta = 4$), and R is upper triangular with positive real diagonal elements. Let us decompose these matrices in blocks of size $N \times N$:

$$Q(x) = \begin{pmatrix} Q_{11}(x) & Q_{12}(x) \\ Q_{21}(x) & Q_{22}(x) \end{pmatrix}\,, \quad R(x) = \begin{pmatrix} R_{11}(x) & R_{12}(x) \\ 0 & R_{22}(x) \end{pmatrix}\,. \tag{7.167}$$

The matrices Φ and Ξ are thus given by

$$\Phi(x) = Q_{11}(x)R_{11}(x)\,, \quad \Xi(x) = Q_{21}(x)R_{11}(x)\,. \tag{7.168}$$

Therefore, $\det \Xi = \det Q_{21} \times \det R$. Since the matrix R encodes the envelope of the spinor, its determinant is positive, and only $\det Q_{21}$ can vanish. This gives us the final expression of the IDoS from (7.163):

$$\boxed{\mathcal{N}_L(\varepsilon) = \text{number of zeros of } \det Q_{21}(x) \text{ in }]0, L[\,.} \tag{7.169}$$

Since the matrix Q belongs to a compact group its elements are bounded, and so are those of Q_{21}. This makes this expression well-suited for numerical computations. This discussion can be straightforwardly extended to the discretised model (7.141). The integrated density of states $\mathcal{N}(\varepsilon)$ can thus be obtained from the product of matrices (7.150) as follows:

1. Initialise $Q_1 = \mathbb{1}_{2N}$ and $N_0 = 0$;
2. Compute the QR-decomposition of $A_n Q_n = \tilde{Q}_n \tilde{R}_n$;
3. Set $Q_{n+1} = \tilde{Q}_n$, extract the lower left subblock Q_{21} of size N of Q_{n+1};
4. If $\det Q_{21}$ changed sign when going from step n to $n+1$, increment N_0 by one;
5. Repeat from 2;
6. Return N_0/L (since $\mathcal{N}(\varepsilon) = \lim_{L\to\infty} N_0/L$).

This procedure can be implemented in the same algorithm as the one described in Section 7.3.1 to compute the Lyapunov spectrum and the IDoS simultaneously, in a very efficient way.

I implemented this algorithm to compute the density of states. The numerical results are in excellent agreement with the numerical computations, see Fig. 7.12. I also checked the low energy behaviours obtained in Section 7.1 numerically. Since the analytical results do not provide the prefactor, I obtained it via a fit of the numerical data. The results are again in perfect agreement, see Fig. 7.4. The power law behaviour of the density of states is correctly reproduced over several orders of magnitude.

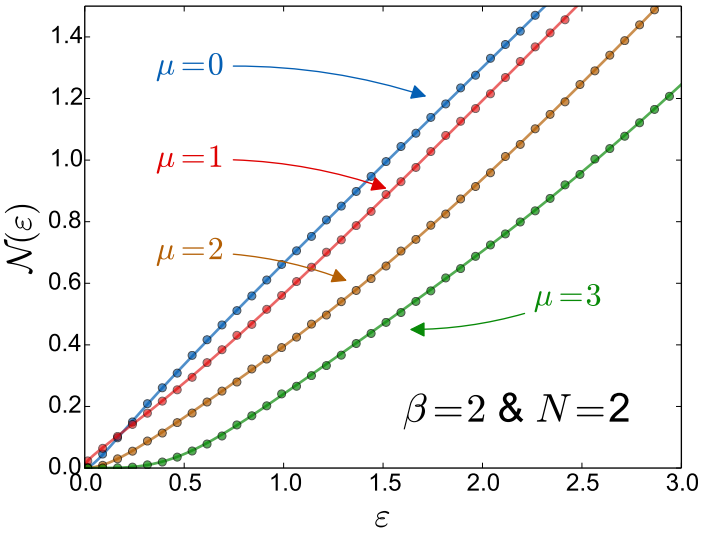

Figure 7.12: Integrated density of states $\mathcal{N}(\varepsilon)$ for $N = 2$ channels and $\beta = 2$, in the non-isotropic case $G = \mathrm{Diag}(\frac{1}{2}, \frac{3}{2})$. The points are obtained from numerical simulations, the lines are the analytic results (7.12,7.13,7.50).

Chapter 8

Topological phase transitions

In the 2000s, models of multichannel disordered wires have been reconsidered from the perspective of their topological properties. These models were indeed shown to support Majorana zero modes [192, 255]. A key feature of these modes is that their topological nature provides a protection under small perturbations (such as weak disorder). The aim of this chapter is to study the effect of strong disorder on these modes, as it was shown that the disorder can drive topological phase transitions [240, 264, 268].

In the previous chapters, we have introduced and studied a model of multichannel disordered wire, the Dirac equation with a random mass, belonging to the three chiral classes. We now investigate its topological properties. These properties are encoded in a quantum number of topological nature. The determination of this index relies on the bulk-edge correspondence: the topological quantum number, which characterises a bulk property, also counts the number of edge states (as in the integer quantum Hall effect). In the case of our chiral model, the edge states have zero energy. In order to count the number of zero modes, we will consider in this chapter the Witten index defined by [312]

$$\Delta(\tilde{\beta}) = \mathrm{tr}\left[\sigma_3\, \mathrm{e}^{-\tilde{\beta}\mathcal{H}^2}\right] , \tag{8.1}$$

where $\mathcal{H}$ is the Dirac Hamiltonian and $\tilde{\beta}$ is the inverse temperature (denoted with a tilde to distinguish it from the Dyson index). To show how this index can be used to characterise the topological properties of our model of disordered wires, we first consider a simple example.

8.1 A simple example

Let us first consider the strictly one-dimensional case $N = 1$, with a constant mass $m(x) = m_0$ for $x > 0$. The Dirac equation (6.2,6.3) reduces to

$$\begin{cases} (\partial_x + m_0)\xi(x) = \varepsilon\, \varphi(x) , \\ (-\partial_x + m_0)\varphi(x) = \varepsilon\, \xi(x) , \end{cases} \qquad \psi = \begin{pmatrix} \varphi \\ \xi \end{pmatrix} . \tag{8.2}$$

We choose the boundary condition $m(x) = -\infty$ for $x < 0$, corresponding to $\varphi(0) = 0$ (we could similarly consider the case $\xi(0) = 0$). If $m_0 \neq 0$, the spectrum of the Dirac

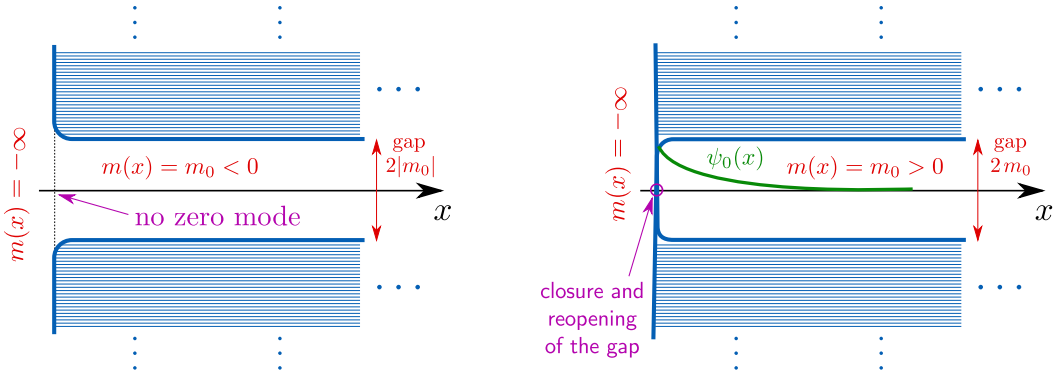

Figure 8.1: Spectrum of the 1D Dirac equation with a constant mass $m(x) = m_0$ for $x > 0$, while the mass is set to $-\infty$ for $x < 0$. Left: $m_0 < 0$, the mass does not change sign when crossing the origin thus the gap remains open. There is no zero mode in this case. Right: $m_0 > 0$, the gap closes and reopens when crossing the origin. This causes the appearance of a zero mode.

equation (8.2) is $]-\infty, -|m_0|] \cup [|m_0|, +\infty[$, with a gap $2|m_0|$. Inside the spectrum, the solutions take the form

$$\psi_\varepsilon(x) = A \begin{pmatrix} \varepsilon \sin \kappa x \\ -\kappa \cos \kappa x + m_0 \sin \kappa x \end{pmatrix}, \quad \kappa = \sqrt{\varepsilon^2 - m_0^2}, \tag{8.3}$$

where A is a normalisation constant. In the gap, we can formally write solutions of the Dirac equation (8.2) in the form

$$\psi_\varepsilon(x) = A \begin{pmatrix} \varepsilon \sinh \kappa x \\ -\kappa \cosh \kappa x + m_0 \sinh \kappa x \end{pmatrix}, \quad \kappa = \sqrt{m_0^2 - \varepsilon^2}, \tag{8.4}$$

which satisfy $\varphi(0) = 0$ but cannot be normalised. However, exactly at zero energy $\varepsilon = 0$, this solution becomes

$$\psi_0(x) = \begin{pmatrix} 0 \\ 1 \end{pmatrix} \sqrt{2m_0}\, \mathrm{e}^{-m_0 x}, \quad x > 0, \tag{8.5}$$

which can be normalised if $m_0 > 0$ (we imposed $m(x) = -\infty$ for $x < 0$). Therefore, this zero mode exists only if the mass is positive. This can be related to the change of sign of the mass when going from the region $x < 0$ to $x > 0$, associated to the closure and reopening of the gap (see Fig. 8.1). This is the signature of a topological phase transition. We will now see how to make use of the Witten index (8.1) to characterise this transition.

In the case of a discrete spectrum, the Witten index (8.1), which counts the number of zero modes, is independent of the temperature $\tilde{\beta}$ and is a quantum number of topological nature [253, 312]. Indeed, this index is expressed in terms of the squared Dirac Hamiltonian

$$\mathcal{H}^2 = (-\partial_x^2 + m^2)\mathbb{1}_2 + \partial_x m \sigma_3 = \begin{pmatrix} H_+ & 0 \\ 0 & H_- \end{pmatrix}, \quad H_\pm = -\partial_x^2 + m^2 \pm \partial_x m, \tag{8.6}$$

and therefore takes the form

$$\Delta(\tilde{\beta}) = \mathrm{tr}\left[\mathrm{e}^{-\tilde{\beta}H_+}\right] - \mathrm{tr}\left[\mathrm{e}^{-\tilde{\beta}H_-}\right] . \tag{8.7}$$

The index $\Delta(\tilde{\beta})$ thus measures the difference between the two spectra of the Hamiltonians H_+ and H_- [184]. These Hamiltonians have the same spectrum, except potentially at $\varepsilon = 0$ (is supersymmetry holds). Therefore, $\Delta(\tilde{\beta})$ should indicate the presence of the zero mode (8.5) for $m_0 > 0$ (H_+ corresponds to $m(x) = m_0$ and H_- to $m(x) = -m_0$).

However, in the situation considered here, the spectrum is continuous and $\Delta(\tilde{\beta})$ has a non-trivial $\tilde{\beta}$-dependence. However, in the zero temperature limit $\tilde{\beta} \to 0$, only the bottom of the spectrum contributes to $\Delta(\tilde{\beta})$ and

$$\Delta(\infty) = \lim_{\tilde{\beta}\to\infty} \Delta(\tilde{\beta}) \tag{8.8}$$

is a topological quantum number [253]. We will see on the example (8.2) that it is of the form

$$\Delta(\infty) = \frac{1}{2} \times \text{integer} \tag{8.9}$$

and indeed characterises the number of zero modes.

In order to compute the Witten index $\Delta(\infty)$ for the Dirac equation (8.2), we start from the definition (8.1). Let us denote $\rho_+(\varepsilon)$ the density of states in the case of a constant mass m_0, and $\rho_-(\varepsilon)$ for $-m_0$ (we make no assumption on the sign of m_0). We can rewrite (8.1) as

$$\Delta(\tilde{\beta}) = \int_0^\infty \mathrm{d}\varepsilon \, (\rho_+(\varepsilon) - \rho_-(\varepsilon)) \, \mathrm{e}^{-\tilde{\beta}\varepsilon^2} . \tag{8.10}$$

After integration by parts, we obtain

$$\Delta(\tilde{\beta}) = \int_0^\infty \mathrm{d}\varepsilon \, \frac{\delta_+(\varepsilon) - \delta_-(\varepsilon)}{2\pi} \, 2\tilde{\beta}\varepsilon \, \mathrm{e}^{-\tilde{\beta}\varepsilon^2} , \tag{8.11}$$

where $\delta_\pm = -\mathrm{i} \ln \det r_\pm(\varepsilon)$ are the scattering Friedel phases obtained from the reflection matrix $r_\pm(\varepsilon)$ introduced in Section 6.2. The topological index is obtained by taking the zero-temperature limit $\tilde{\beta} \to \infty$:

$$\Delta(\infty) = \frac{\delta_+(0) - \delta_-(0)}{2\pi} . \tag{8.12}$$

We have thus reduced the problem to computing the scattering Friedel phases $\delta_\pm$ at zero energy. To this end, we first come back to the scattering situation on the region $[0, L]$ introduced in Section 6.2 (see Fig. 6.1). For $x > L$, the solutions of the free Dirac equation are characterised by the reflection coefficient $r(\varepsilon)$:

$$\psi_\varepsilon(x) = \begin{pmatrix} 1 \\ \mathrm{i} \end{pmatrix} \mathrm{e}^{-\mathrm{i}\varepsilon(x-L)} + r(\varepsilon) \begin{pmatrix} -1 \\ \mathrm{i} \end{pmatrix} \mathrm{e}^{\mathrm{i}\varepsilon(x-L)} . \tag{8.13}$$

Matching with the solutions (8.3,8.4) of the Dirac equation (8.2) at $x = L$, we express the reflection coefficient as:

$$r(\varepsilon) = -\frac{\mathrm{i}\varphi_\varepsilon(L) - \xi_\varepsilon(L)}{\mathrm{i}\varphi_\varepsilon(L) + \xi_\varepsilon(L)} . \tag{8.14}$$

For example, if $\varepsilon < |m_0|$, we have:

$$r(\varepsilon) = -\frac{\mathrm{i}\varepsilon \sinh(\kappa L) + \kappa \cosh(\kappa L) - m_0 \sinh(\kappa L)}{\mathrm{i}\varepsilon \sinh(\kappa L) - \kappa \cosh(\kappa L) + m_0 \sinh(\kappa L)} , \quad \kappa = \sqrt{m_0^2 - \varepsilon^2} . \tag{8.15}$$

Therefore, in the limit $L \to \infty$, we obtain[1]

$$r(\varepsilon) = \frac{\sqrt{m_0^2 - \varepsilon^2} - m_0 + \mathrm{i}\varepsilon}{\sqrt{m_0^2 - \varepsilon^2} - m_0 - \mathrm{i}\varepsilon} . \tag{8.16}$$

Let us introduce the scattering Friedel phase $\delta(\varepsilon) = -\mathrm{i} \ln r(\varepsilon)$, which is related to the density of states by (6.27). In the limit $\varepsilon \to 0$, we have

$$r(\varepsilon) = \mathrm{e}^{\mathrm{i}\delta(\varepsilon)} \simeq \frac{|m_0| - m_0 + \mathrm{i}\varepsilon - \varepsilon^2/2\,|m_0|}{|m_0| - m_0 - \mathrm{i}\varepsilon - \varepsilon^2/2\,|m_0|} \simeq \begin{cases} -1 - \frac{\mathrm{i}\varepsilon}{m_0} & \text{if } m_0 > 0 , \\ 1 + \frac{\mathrm{i}\varepsilon}{|m_0|} & \text{if } m_0 < 0 , \end{cases} \tag{8.17}$$

from which we deduce

$$\delta(0) = \pi\, \Theta(m_0) , \tag{8.18}$$

where Θ is the Heaviside function. We can easily deduce the Witten index (8.12) by subtracting to this result the one where we substituted $m_0 \to -m_0$:

$$\Delta(\infty) = \frac{\delta_+(0) - \delta_-(0)}{2\pi} = \frac{1}{2}\left(\Theta(m_0) - \Theta(-m_0)\right) = \frac{1}{2}\ \mathrm{sign}(m_0) . \tag{8.19}$$

The sign of the Witten index $\Delta(\infty)$ indicates in which sector the zero mode is present ($m_0 < 0$ or $m_0 > 0$).

Having understood the behaviour of the Witten index in this simple one dimensional case, we can now go back to the multichannel case. The discussion above can be trivially extended to the situation where $M(x) = m_0 \mathbb{1}_N$, as all the channels are independent. A zero mode is present in each channel if $m_0 > 0$, thus:

$$\Delta(\infty) = \frac{N}{2}\ \mathrm{sign}(m_0) . \tag{8.20}$$

We have seen on this simple example with a continuous spectrum that $2\Delta(\infty)$ is an integer, which counts the number of zero modes. In the case of a constant mass, the spectrum is gapped, as illustrated in Fig. 8.1. However, this is not the case in the disordered case: as shown in Section 7.1, the introduction of the disorder closes the gap. We will show that even in the presence of disorder, $2\Delta(\infty)$ remains an integer, which indicates the presence of zero modes. It is remarkable that these zero modes still exist for a gapless spectrum, as it was pointed out in Refs. [267, 268].

[1] We first take the limit $L \to \infty$, before taking the limit $\varepsilon \to 0$. If we keep a finite size $L \gg 1/m_0$, the zero mode (8.5) is split into two low energy states, $\varepsilon_\pm = \pm 2m_0 \exp(-m_0 L)$ (for $\varphi(0) = \xi(L) = 0$).

8.2 Relation to the Riccati matrix

Our aim is now to extend the previous discussion to the disordered case. In Section 7.1, we have seen that we can extract the density of states from the distribution of Riccati matrix Z_ε. We will now see that we can compute the topological index $\Delta(\infty)$ from the stationary distribution (6.59).

Our starting point is again the scattering situation of Section 6.2. This scattering problem is characterised by the $N \times N$ reflection matrix $r(\varepsilon)$, which can be expressed in terms of the Riccati matrix Z_ε by Eq. (6.33). This allows us the express the Friedel phase, for $\langle M \rangle = +\mu G$ as

$$\delta_+(\varepsilon) = -\mathrm{i} \ln \det r(\varepsilon) = -\mathrm{i} \ln \det \left\{ [\varepsilon - \mathrm{i} Z_\varepsilon(L)][\varepsilon + \mathrm{i} Z_\varepsilon(L)]^{-1} \right\} . \tag{8.21}$$

Let us now introduce eigenvalues $\{z_n^+(L)\}$ of the Riccati matrix for $\langle M \rangle = +\mu G$. We have:

$$\delta_+(\varepsilon) = -\mathrm{i} \ln \det r(\varepsilon) = -\mathrm{i} \sum_{n=1}^N \ln \left(\frac{\varepsilon - \mathrm{i} z_n^+(L)}{\varepsilon + \mathrm{i} z_n^+(L)} \right) = -2 \sum_{n=1}^N \arctan \left(\frac{z_n^+(L)}{\varepsilon} \right) . \tag{8.22}$$

We have the same relation for the phase $\delta_-(\varepsilon)$ associated to the situation $\langle M \rangle = -\mu G$, in terms of the eigenvalues $\{z_n^-\}$ of the corresponding Riccati matrix. The difference of phases between the two situations thus reads:

$$\delta_+(\varepsilon) - \delta_-(\varepsilon) = -2 \sum_{n=1}^N \arctan \left(\frac{z_n^+(L)}{\varepsilon} \right) + 2 \sum_{n=1}^N \arctan \left(\frac{z_n^-(L)}{\varepsilon} \right) \tag{8.23}$$

Using the supersymmetry (6.35), which implies the relation

$$\{z_n^+\} \overset{(\mathrm{law})}{=} \left\{ -\varepsilon^2 / z_n^- \right\} , \tag{8.24}$$

we obtain:

$$\begin{aligned} \langle \delta_+(\varepsilon) - \delta_-(\varepsilon) \rangle &= \left\langle 2 \sum_{n=1}^N \arctan \left(\frac{\varepsilon}{z_n^-(L)} \right) + 2 \sum_{n=1}^N \arctan \left(\frac{z_n^-(L)}{\varepsilon} \right) \right\rangle \\ &= \pi \sum_{n=1}^N \left\langle \mathrm{sign}[z_n^-(L)] \right\rangle , \end{aligned} \tag{8.25}$$

where we used that $\arctan x + \arctan(1/x) = \pi \, \mathrm{sign}(x)/2$. For $L \to \infty$, the Riccati process is stationary, therefore the averaging can be performed with the stationary distribution of Z_ε. We thus obtain the Witten index (8.12) as

$$\boxed{\Delta(\infty) = \frac{\langle \delta_+(0) - \delta_-(0) \rangle}{2\pi} = \lim_{\varepsilon \to 0} \frac{1}{2} \sum_{n=1}^N \left\langle \mathrm{sign}(z_n^-) \right\rangle} \tag{8.26}$$

where the averaging is performed using the stationary distribution of Z_ε for $\langle M \rangle = -\mu G$. This relation links the topological properties of the disordered wire, encoded in the Witten index $\Delta(\infty)$, to the statistical properties of the Riccati matrix, encoded in the stationary distribution $f(Z)$, Eq. (6.59). However, we have obtained this distribution only

for purely imaginary energies. We thus reproduce the above derivation with the analytic continuation[2] $\varepsilon = ik$ to express the Witten index in terms of the distribution (6.59). For this purpose, it is convenient to rewrite the reflection matrix as

$$r(\varepsilon) = \left[\sqrt{-\varepsilon^2 - \mathrm{i}0^+} - Z_\varepsilon(L)\right]\left[\sqrt{-\varepsilon^2 - \mathrm{i}0^+} + Z_\varepsilon(L)\right]^{-1} , \tag{8.27}$$

from which we deduce

$$r(\mathrm{i}k) = \frac{k - Z_{\mathrm{i}k}(L) - \mathrm{i}0^+}{k + Z_{\mathrm{i}k}(L) - \mathrm{i}0^+} . \tag{8.28}$$

For $\langle M \rangle = \pm\mu G$, the associated Friedel phases are obtained from the eigenvalues $\{z_n^\pm\}$ of the Riccati matrix as

$$\delta_\pm(\mathrm{i}k) = -\mathrm{i}\ln\det r(\mathrm{i}k) = -\mathrm{i}\sum_{n=1}^N \ln\left(\frac{k - z_n^\pm(L) - \mathrm{i}0^+}{k + z_n^\pm(L) - \mathrm{i}0^+}\right) . \tag{8.29}$$

We can again compute the phase difference:

$$\begin{aligned}\langle \delta_+(\mathrm{i}k) - \delta_-(\mathrm{i}k)\rangle &= \left\langle -\mathrm{i}\sum_{n=1}^N \ln\left(\frac{k - z_n^+(L) - \mathrm{i}0^+}{k + z_n^+(L) - \mathrm{i}0^+}\right) + \mathrm{i}\sum_{n=1}^N \ln\left(\frac{k - z_n^-(L) - \mathrm{i}0^+}{k + z_n^-(L) - \mathrm{i}0^+}\right)\right\rangle \\ &= \left\langle -\mathrm{i}\sum_{n=1}^N \ln\left(\frac{z_n^-(L) - k - \mathrm{i}0^+}{k + z_n^-(L) - \mathrm{i}0^+}\right) + \mathrm{i}\sum_{n=1}^N \ln\left(\frac{k - z_n^-(L) - \mathrm{i}0^+}{k + z_n^-(L) - \mathrm{i}0^+}\right)\right\rangle ,\end{aligned} \tag{8.30}$$

where we used the supersymmetry (6.35). Using now that

$$\ln(x - \mathrm{i}0^+) = \ln(-x - \mathrm{i}0^+) + \mathrm{i}\pi\,\mathrm{sign}(x) , \quad x \in \mathbb{R} , \tag{8.31}$$

we obtain:

$$\langle \delta_+(\mathrm{i}k) - \delta_-(\mathrm{i}k)\rangle = \pi\sum_{n=1}^N \left\langle \mathrm{sign}(z_n^-(L) - k)\right\rangle . \tag{8.32}$$

In the limit $L \to \infty$, the averaging can be computed from the stationary distribution of the eigenvalues $\{z_n^-\}$. Therefore, we can write the Witten index (8.12) as

$$\boxed{\Delta(\infty) = \frac{\langle \delta_+(\mathrm{i}0^+) - \delta_-(\mathrm{i}0^+)\rangle}{2\pi} = \lim_{k\to 0}\frac{1}{2}\sum_{n=1}^N \langle \mathrm{sign}(z_n - k)\rangle} \tag{8.33}$$

where the averaging over the eigenvalues of the Riccati matrix must be performed with the stationary distribution (6.59) with μ replaced by $-\mu$ (since it must be computed in the case $\langle M \rangle = -\mu G$). We will now make use of this formula to compute the value of the topological index.

[2] One can check that the simple analysis performed in the $N = 1$ case in the absence of disorder (Section 8.1) can be extended to $\varepsilon = \mathrm{i}k$, $k \in \mathbb{R}$.

8.2.1 The one channel case

Let us start with the simplest case of $N = 1$ channel. For $\varepsilon = \mathrm{i}k$, the distribution of the Riccati variable (6.57) for $\langle M \rangle = -\mu g$ becomes

$$f_-(z) = \mathcal{C}_{1,\beta}^{-1}\, z^{\mu-1}\, \mathrm{e}^{-\frac{1}{2g}(z+k^2/z)}\,, \quad z > 0\,. \tag{8.34}$$

If $\mu > 0$, one can simply take the limit $k \to 0$ in this expression, and obtain the distribution of z at zero (imaginary) energy:

$$f_-(z) \to \mathcal{C}_{1,\beta}^{-1}\, z^{\mu-1}\, \mathrm{e}^{-z/2g}\,, \quad z > 0\,, \quad \text{for } k \to 0\,. \tag{8.35}$$

This limit can only be taken for $\mu > 0$ since the resulting distribution can be normalised only in this case. Therefore, z remains of order one as $k \to 0$ and is given by a Gamma distribution. We can thus easily compute

$$\lim_{k\to 0} \langle \mathrm{sign}(z-k) \rangle = 1\,, \tag{8.36}$$

from which we deduce the Witten index

$$\Delta(\infty) = \frac{1}{2}\,, \quad \text{for } \mu > 0\,. \tag{8.37}$$

Let us now investigate to case $\mu < 0$. We cannot simply take the limit $k \to 0$ in the distribution (8.34), as the resulting limit is not normalisable, due to the divergence at the origin. Let us instead consider the rescaled variable $y = z/k^2$. The distribution of y thus reads

$$P(y) \propto y^{\mu-1}\, \mathrm{e}^{-\frac{1}{2g}(k^2 y + 1/y)} \underset{k\to 0}{\longrightarrow} y^{\mu-1}\, \mathrm{e}^{-1/(2gy)}\,, \tag{8.38}$$

which can be normalised for $\mu < 0$. This shows that, in this case, the Riccati variable z condensates to zero as $\mathcal{O}(k^2)$ for $k \to 0$, and reaches an inverse Gamma distribution. Therefore, we can again evaluate the Witten index (8.33):

$$\Delta(\infty) = \frac{1}{2} \lim_{k\to 0} \Big\langle \mathrm{sign}(k^2 y - k) \Big\rangle = -\frac{1}{2}\,, \quad \text{for } \mu < 0\,. \tag{8.39}$$

Additionally, we can also investigate the case $\mu = 0$. The good scaling variable is now $u = z/k$, which has the distribution

$$P(u) \propto \frac{1}{u}\, \mathrm{e}^{-\frac{k}{2g}(u+1/u)}\,. \tag{8.40}$$

Using the symmetry $u \leftrightarrow 1/u$, which is simply the consequence of the supersymmetry (6.35). This yields

$$\Delta(\infty) = \frac{1}{2} \lim_{k\to 0} \langle \mathrm{sign}(ku - k) \rangle = 0\,, \quad \text{for } \mu = 0\,, \tag{8.41}$$

where the averaging is performed with respect to (8.40). To summarise, the Witten index is controlled by the mass over disorder ratio $\mu = \langle M \rangle / g$, as:

$$\Delta(\infty) = \begin{cases} \dfrac{1}{2} & \text{for } \mu > 0\,, \\ 0 & \text{for } \mu = 0\,, \\ -\dfrac{1}{2} & \text{for } \mu < 0\,. \end{cases} \tag{8.42}$$

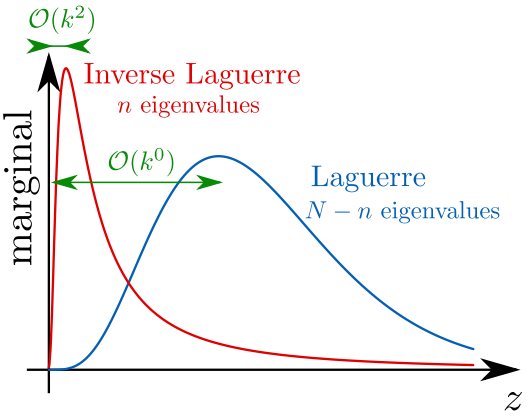

Figure 8.2: Condensation transition of the eigenvalues as $k \to 0$. If the mass over disorder ratio μ is in the interval (8.50), n eigenvalues "condensate" towards the origin as $\mathcal{O}(k^2)$, while the remaining $N-n$ remain of order 1.

This result is very similar to the one obtained in Section 8.1 in the case of a constant mass, Eq. (8.19). There is however an important difference between the two situations: for the constant mass the spectrum is gapped and the zero modes are midgap states. However here there is no gap in the spectrum due to the disorder. It is remarkable that these zero modes still exist in the case of gapless spectrum.

We have given an interpretation of the topological phase transition, driven by the mass over disorder ratio μ, in terms of the distribution of the Riccati variable z. We will now extend this picture to the multichannel case.

8.2.2 Condensation scenario in the isotropic case

We now go back to the multichannel situation $N > 1$ and consider first the isotropic case $G = g\mathbb{1}_N$ for simplicity. The joint distribution of eigenvalues (6.62) for $\langle M \rangle = -\mu g \mathbb{1}_N$ reads:

$$f_-(\{z_n\}) \propto \prod_{i<j} |z_i - z_j|^\beta \prod_{i=1}^N z_i^{\mu-1-\beta\frac{N-1}{2}} \, \mathrm{e}^{-\frac{1}{2g}(z_i + k^2/z_i)} \, . \tag{8.43}$$

For $\mu > \beta\frac{N-1}{2}$, one can directly take the limit $k \to 0$:

$$f_-(\{z_n\}) \underset{k\to 0}{\longrightarrow} \mathcal{L}_{N,\mu-\beta\frac{N-1}{2}}(z_1, \dots, z_N) \, , \tag{8.44}$$

where

$$\mathcal{L}_{N,\theta}(z_1, \dots, z_N) \propto \prod_{i<j} |z_i - z_j|^\beta \prod_{i=1}^N z_i^{\theta-1} \, \mathrm{e}^{-z_i/2g} \, , \quad z_i > 0 \, , \tag{8.45}$$

is the distribution of eigenvalues in the Laguerre ensemble of RMT. It is normalisable for $\theta > 0$. Therefore, all the eigenvalues of the Riccati matrix are of order $\mathcal{O}(1)$ as $k \to 0$, thus:

$$\Delta(\infty) = \frac{1}{2} \lim_{k\to 0} \sum_{n=1}^N \langle z_n - k \rangle = \frac{N}{2} \, , \quad \text{for } \mu > \beta\frac{N-1}{2} \, . \tag{8.46}$$

We now investigate the situation $\mu < \beta\frac{N-1}{2}$. In this case, the distribution obtained by taking the limit $k \to 0$ of (8.43) is not normalisable. Our aim is thus to find the distribution of the eigenvalues $\{z_n\}$ in this limit. Inspired from the discussion

of Section 8.2.1 in the one channel case, we rescale n eigenvalues as $z_i = k^2 y_i$, for $i \in \{1, \dots, n\}$. In the limit $k \to 0$, the Vandermonde determinant becomes:

$$\prod_{i<j} |z_i - z_j|^\beta = \prod_{1 \leqslant i < j \leqslant n} k^2 \, |y_i - y_j|^\beta \times \prod_{n < i < j \leqslant N} |z_i - z_j|^\beta \times \prod_{i=1}^{n} \prod_{j=n+1}^{N} \left| k^2 y_i - z_j \right|$$
$$\simeq k^{n(n-1)} \times \prod_{1 \leqslant i < j \leqslant n} |y_i - y_j|^\beta \times \prod_{n < i < j \leqslant N} |z_i - z_j|^\beta \times \prod_{j=n+1}^{N} z_j^{\beta n} \, . \tag{8.47}$$

Therefore, as $k \to 0$, the joint distribution of eigenvalues (8.43) factorises into two parts:

$$f_-(\{z_n\}) \underset{k \to 0}{\propto} \frac{1}{k^{2n}} \, \mathcal{I}_{n, -\mu + \beta \frac{N-2n+1}{2}} \left(\frac{z_1}{k^2}, \dots, \frac{z_n}{k^2} \right) \times \mathcal{L}_{N-n, \mu - \beta \frac{N-2n-1}{2}}(z_{n+1}, \dots, z_N) \, , \tag{8.48}$$

where $\mathcal{L}_{M,\theta}$ is the Laguerre distribution (8.45), and $\mathcal{I}_{M,\theta}$ is the "inverse Laguerre"

$$\mathcal{I}_{M,\theta}(\lambda_1, \dots, \lambda_M) \propto \prod_{i<j} |\lambda_i - \lambda_j|^\beta \prod_{i=1}^{M} \lambda_i^{-\theta - 1 - \beta(M-1)} \, \mathrm{e}^{-1/2\lambda_i} \, , \quad \lambda_i > 0 \, , \tag{8.49}$$

which is also normalisable for $\theta > 0$. This terminology means that $\{\lambda_i\}$ are the inverse of eigenvalues distributed according to the Laguerre distribution $\mathcal{L}_{M,\theta}$. Combining the conditions for the normalisability of both distributions $\mathcal{L}_{N,\theta}$ and $\mathcal{I}_{N,\theta}$ appearing in (8.48) yields the condition

$$\beta \frac{N-1}{2} - \beta n < \mu < \beta \frac{N-1}{2} - \beta(n-1) \, . \tag{8.50}$$

In this interval, n eigenvalues of the Riccati matrix condensate towards the origin as $\mathcal{O}(k^2)$, while the remaining $N - n$ stay of order $\mathcal{O}(1)$ as $k \to 0$. This mechanism is illustrated in Fig. 8.2. Henceforth, the Witten index (8.33) takes the value

$$\Delta(\infty) = \frac{1}{2} \lim_{k \to 0} \left(\sum_{p=1}^{n} \underbrace{\langle \mathrm{sign}(z_p - k) \rangle}_{\to -1} + \sum_{p=n+1}^{N} \underbrace{\langle \mathrm{sign}(z_p - k) \rangle}_{\to +1} \right) = \frac{N - 2n}{2} \, . \tag{8.51}$$

Note that for $\mu < -\beta \frac{N-1}{2}$, all the eigenvalues condensate into the inverse Laguerre distribution, thus

$$\Delta(\infty) = -\frac{N}{2} \, , \quad \text{for } \mu < -\beta \frac{N-1}{2} \, . \tag{8.52}$$

There only remains to study the transition points. Let us consider $\mu = \beta(N - 2n + 1)/2$, for a certain $n \in \{1, \dots, N\}$. From our discussion in the case $N = 1$, we already know that we should single out one eigenvalue, which will scale as $\mathcal{O}(k)$ for $k \to 0$. We can thus guess that the joint distribution of eigenvalues now factorises into three parts:

$$f_-(\{z_n\}) \underset{k \to 0}{\propto} \frac{1}{k^{2(n-1)}} \, \mathcal{I}_{n-1, \beta} \left(\frac{z_1}{k^2}, \dots, \frac{z_{n-1}}{k^2} \right) \times \frac{1}{z_n} \, \mathrm{e}^{-\frac{k}{2}(z_n/k + k/z_n)}$$
$$\times \, \mathcal{L}_{N-n, \beta}(z_{n+1}, \dots, z_N) \, . \tag{8.53}$$

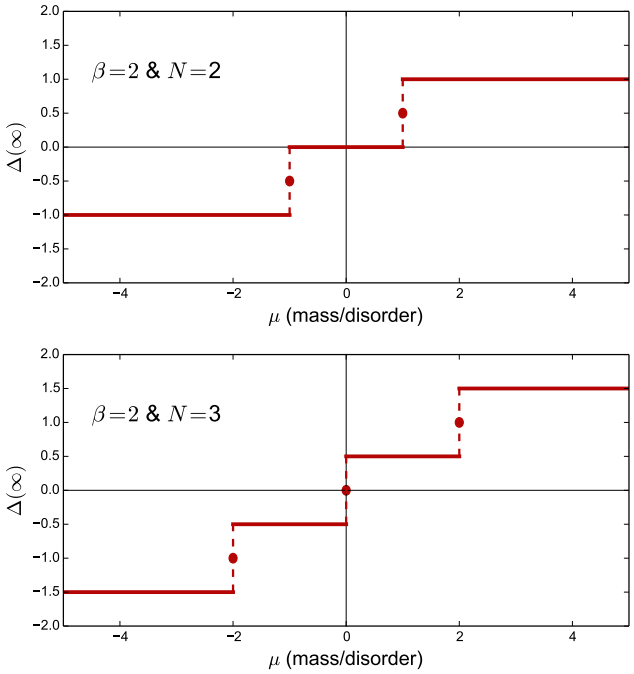

Figure 8.3: Witten index $\Delta(\infty)$ (half the number of zero modes), as a function of the mass over disorder ratio $\mu = \langle M \rangle G^{-1}$. This index goes from the value $N/2$ for $\mu > \beta\frac{N-1}{2}$ to $-N/2$ for $\mu < \beta\frac{N-1}{2}$ by steps of 1 through a series of N topological phase transitions. Exactly at each transition, it takes an intermediate value (represented by the dots).

The first $n-1$ eigenvalues give a contribution $-1/2$ to the Witten index (8.33), the $N-n$ last give a contribution $+1/2$, while the n^{th} averages to zero due to the supersymmetry (6.35). This gives that, at the transition,

$$\Delta(\infty) = \frac{N-2n+1}{2}\,, \quad \text{for } \mu = \beta\frac{N-2n+1}{2}\,, \quad n \in \{1,\dots,N\}\,. \tag{8.54}$$

The value of the topological index $\Delta(\infty)$ is shown as function of μ for different number of channels in Fig. 8.3.

8.2.3 Non-isotropic case

We have studied in details the isotropic case in the previous section. We now move to the non-isotropic case $G = \text{Diag}(g_1,\dots,g_N)$. The distribution of the Riccati matrix is given by (6.59). Let us introduce the eigenvalues and eigenvectors of Z as

$$Z = U^\dagger \mathcal{Z} U\,, \quad \mathcal{Z} = \text{Diag}(z_1,\dots,z_N)\,. \tag{8.55}$$

The Jacobian of this change of variable is given by (A.11). The joint distribution of eigenvalues and eigenvectors thus reads, for $\langle M \rangle = -\mu G$:

$$\mathcal{C}_{N,\beta}^{-1} \prod_{i<j} |z_i - z_j|^\beta \prod_{i=1}^N z_i^{\mu-1-\beta\frac{N-1}{2}} \exp\left\{-\frac{1}{2}[UGU^\dagger]_{ii}\left(z_i + \frac{k^2}{z_i}\right)\right\}\,. \tag{8.56}$$

The marginal distribution of the eigenvalues is then obtained by integration over the eigenvectors:

$$P_-(\{z_i\}) = \mathcal{C}_{N,\beta}^{-1} \int \mathrm{d}\mu(U) \prod_{i<j} |z_i - z_j|^\beta \prod_{i=1}^N z_i^{\mu-1-\beta\frac{N-1}{2}} \exp\left\{-\frac{1}{2}[UGU^\dagger]_{ii}\left(z_i + \frac{k^2}{z_i}\right)\right\}\,. \tag{8.57}$$

This form is more complicated that the one obtained in the isotropic case due to the additional integral over the eigenvectors, but it can be analysed similarly. For $\mu > \beta\frac{N-1}{2}$, we can straightforwardly take the limit $k \to 0$, as the resulting distribution can be normalised. If $\mu < \beta\frac{N-1}{2}$, we proceed as in Section 8.2.2 and rescale several eigenvalues by k^2. The additional integral over the compact group makes no difference in the discussion of the normalisability of the distribution. We can thus reproduce the exact same argument as before, and obtain the same value of the topological index. This shows that **the Witten index $\Delta(\infty)$ does not depend on the choice of the matrix G**, and thus that the topological phase transitions are robust against the addition of some anisotropy among the channels.

8.3 Summary and phase diagram

We have shown that the multichannel disordered wire undergoes a sequence of N distinct topological phase transitions, driven by the mass over disorder ratio $\mu = \langle M \rangle G^{-1}$. These transitions occur for

$$\mu = \beta\frac{N-2n+1}{2}\,, \quad n \in \{1,\dots,N\}\,. \tag{8.58}$$

At each transition point the topological index $\Delta(\infty)$ changes by one unit. This corresponds to the appearance or disappearance of a zero mode, located at the edge $x = 0$.

As we have seen in Chapter 7, the exponent α controlling the low energy behaviour of the density of states,

$$\mathcal{N}(\varepsilon) \sim \varepsilon^{\alpha}\,, \tag{8.59}$$

vanishes when μ is equal to one of the values given by Eq. (8.58). Additionally, one of the Lyapunov exponents (controlling the localisation properties) vanish at this point. We can summarise these phase transitions as

$$\text{Topological phase transition} \quad \Leftrightarrow \quad \begin{cases} \mu = \beta\dfrac{N-2n+1}{2}\,, \quad n \in \{1,\dots,N\}\,, \\ \alpha = 0 \quad \Rightarrow \quad \mathcal{N}(\varepsilon) \sim \dfrac{1}{\ln^2 \varepsilon}\,, \\ \exists p \quad \text{s.t.} \quad \gamma_p = 0\,. \end{cases} \tag{8.60}$$

These transitions are represented on the phase diagram in Fig. 8.4.

After submitting our paper (Article 5), Christopher Mudry pointed out his recent article, Ref. [239], in which a similar phase diagram is presented. In this article, the phase diagram is obtained from global considerations (such as in the DMPK approach), while here it is derived from a precise analysis of a microscopic model.

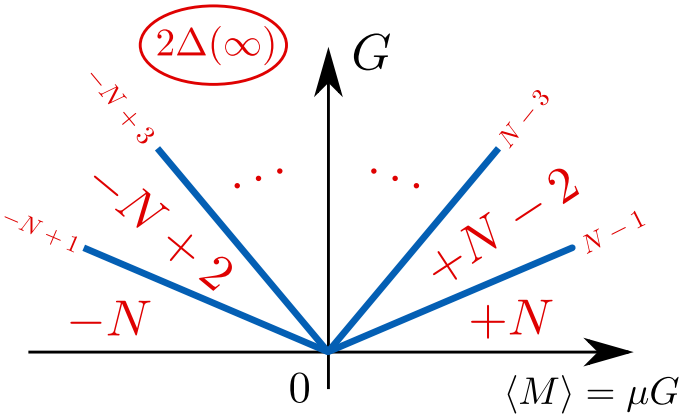

Figure 8.4: Phase diagram of the multichannel model, in the plane disorder strength (encoded in G) versus average mass $\langle M\rangle = \mu G$. The upper half plane is separated in $N+1$ sectors characterised by the value of the topological index $2\Delta(\infty)$. The transition lines are given by Eq. (8.58).

Article 5

Topological phase transitions and superuniversality in the 1D multichannel Dirac equation with random mass

A. Grabsch and C. Texier, Topological phase transitions in the 1D multichannel Dirac equation with random mass and a random matrix model, Europhys. Lett. **116**, 17004 (2016).

☞ http://dx.doi.org/10.1209/0295-5075/116/17004

Conclusion

Although random matrix theory has first been introduced almost a century ago, it is still a very active field of research as new applications and new types of questions keep arising. This thesis has provided several illustrations of this statement, as we have introduced and studied several new problems, in different physical contexts.

- In Chapter 3, we have reported the study of the joint distribution of two spectral linear statistics, motivated by the analysis of the impedance of a quantum RC-circuit.

  There has been a lot of works focusing on the stationary (DC) properties of quantum transport in coherent mesoscopic systems using a random matrix approach (see the review [30]). In this case, many physical quantities can be extracted from the transmission probabilities $\{T_n\}$, which can be shown to correspond to the eigenvalues of Jacobi random matrices (see Section 1.4). For example, the conductance is given by the Landauer formula $G = \frac{2e^2}{h} \sum_n T_n$, where e is the electronic charge. It takes the form of a linear statistics, which has been extensively studied, for example using the Coulomb gas method [301, 302].

  Here, we have studied the dynamical (AC) response of a quantum RC-circuit, built from a chaotic quantum dot, using a theory developed by Büttiker, Prêtre and Thomas [73–75]. In their formalism, the impedance of the circuit is expressed in terms of *two* linear statistics involving the eigenvalues of the celebrated Wigner-Smith matrix. For a chaotic cavity, the inverse of this matrix was shown to belong to the Laguerre ensemble of random matrices [57, 58].

  In this context, we have analysed the joint distribution of these two linear statistics and obtained a two dimensional phase diagram for the underlying Coulomb gas, which has a rich structure. This was the first study of a joint distribution of two linear statistics.

- In Chapter 4, we have introduced a new type of observable, which we have called *truncated linear statistics*. These are linear statistics in which only a fixed number K of the eigenvalues contribute. We have considered two situations: either only the largest (or equivalently, the smallest) eigenvalues contribute, or any subset of eigenvalues can contribute.

We have identified different universal mechanisms for the Coulomb gas in the two situations. The analysis of the first case has required that the function that appears in the linear statistics is monotonous.

- To the best of our knowledge, all previous studies of the statistical properties of linear statistics of the eigenvalues of random matrices in the limit $N \to \infty$ corresponded to the case where the first moments are finite. In Section 2.2.6 we have considered a case in which all the moments are infinite, motivated by the study of the Wigner time delay in disordered wires. This situation induces some technical difficulties and required us to go beyond the dominant energy term given by the Coulomb gas method and conjecture the form of the $1/N$ corrections.

- We have also reconsidered the well studied problem of Anderson localisation in disordered wires from a different point of view in Part II.

  Many works are based on the DMPK approach [106–109, 227] (for reviews see [30, 229]), which consists in studying the evolution of the eigenvalues of the transfer matrix upon increasing the length of the wire. Focusing on the eigenvalues, this approach relies on strong isotropy assumptions which restrict it to the quasi-1D situation (when the system is ergodic in the transverse direction).

  In this thesis, we have studied a matrix stochastic process instead of focusing on the eigenvalues. We have established a connection between a specific model of disordered wires (the multichannel Dirac equation with a random mass) and a random matrix model (Chapter 6). This connection has allowed to go beyond the usual isotropy assumption considered for such models and study the effect of the introduction of some anisotropy between the channels. At the level of the matrix model, the anisotropy breaks the rotational invariance of the distribution of the random matrix. Using this connection we have studied the density of states and the localisation properties of this model (Chapter 7). Finally, we have showed that this model exhibits a series of topological phase transitions, driven by the disorder, which are robust against the introduction of some anisotropy (Chapter 8).

As random matrix theory is still a very active field of research, both in mathematics and in theoretical physics, there remain many open questions. We can give a few examples in connection with the works presented in this thesis:

- The Coulomb gas method which has been extensively used in part I gives rise to transitions of different orders. Many of these transitions have been summarised in Table 2.1 (page 43).

  A particular attention has been put on the case of third order phase transitions (see the review [212]) in connection with the distribution of the largest eigenvalue of several random matrix ensembles. When the boundary of the spectrum is described by a soft edge, it is well-known that the typical fluctuations of the largest eigenvalue are characterised by a universal function (expressed in terms of a Painlevé transcendent): the Tracy-Widom distribution [294]. The atypical fluctuations are described by a nonuniversal large deviation function which smoothly matches with the tails of the Tracy-Widom distribution [101, 102, 300]. This matching by the smooth Tracy-Widom distribution corresponds in the limit $N \to \infty$

to the third order phase transition, which is generic for a soft edge/hard edge transition [212].

It is natural to question whether other universal scenarios, like the splitting of a charge for the second order transition (see Chapter 3 and also Refs. [250, 251, 286]), would be described by other universal functions similar to the Tracy-Widom distribution.

- In the context of the truncated linear statistics restricted to the K largest eigenvalues, we have obtained a universal scenario in the case where the function is monotonous. It is natural to question whether the universality remains for non monotonous functions.

  Additionally, we have only considered the situation in which a fixed fraction $\kappa = K/N \in]0, 1[$ of the eigenvalues contribute to the truncated linear statistics, while $N \to \infty$. We have stressed that both limits $\kappa \to 0$ and $\kappa \to 1$ are singular.

  At first sight, the fact that the limit $\kappa \to 1$ is singular might seem surprising as one would expect to recover the full linear statistics ($K = N$). However, we have shown that for $0 < \kappa < 1$, the Coulomb gas undergoes an infinite order phase transition, which is not generic for $\kappa = 1$ (see Table 2.1, page 43).

  In addition, taking the limit $\kappa \to 0$, we do not recover the result for $K = 1$ (largest eigenvalue), as in this latter case the Coulomb gas exhibits a third order phase transition [101, 102]. As discussed above, a more detailed analysis of the typical fluctuations of the largest eigenvalue shows that they are described by a universal function: the Tracy-Widom distribution, whose tails smoothly match with the large deviation function. Similarly, we expect that there exists a smooth function that interpolates between the case $K = \mathcal{O}(N)$ and $K = \mathcal{O}(1)$. The determination of this function is still an open problem.

- In the context of disordered wires discussed in Part II, the analytical study of the Lyapunov exponents, at any energy, remains a difficult question. It would be interesting to determine if the QR-formalism introduced in Section 7.2.2 could be successfully applied to this task.

  Finally, although we have introduced some anisotropy in the noise which couples the different channels, we have not considered the most general kind of disorder. The study of a more general anisotropic model, which would permit to reach the two dimensional limit, remains extremely challenging.

Appendices

Appendix A

Diverse tools from random matrix theory

In this Appendix, I regroup a few useful tools which are often needed in random matrix theory.

A.1 Measures and Jacobians

To define probability distributions and integrals over matrix spaces, we first need to introduce a measure on those spaces. For a matrix M of size $N \times N$, with no particular symmetry (all the entries are independent), the uniform measure is given by the Lebesgue measure

$$\mathrm{d}M = \prod_{i,j=1}^{N} \mathrm{d}M_{ij} \,. \tag{A.1}$$

In many cases, the matrices we consider have some particular symmetries. For example, for real symmetric matrices (Dyson index $\beta = 1$), the elements on the lower triangular part are equal to the one on the top triangular part and should contribute only once. Therefore, the Lebesgue measure is

$$\mathrm{d}M = \prod_{i \leqslant j} \mathrm{d}M_{ij} \,. \tag{A.2}$$

For complex Hermitian matrices ($\beta = 2$), one should split the matrix elements into their real and imaginary parts to consider only the independent *real* components. The diagonal elements of such matrices are real, and symmetric off-diagonal elements are complex-conjugate. The Lebesgue measure is thus

$$\mathrm{d}M = \prod_{i} \mathrm{d}M_{ii} \prod_{i<j} \mathrm{d}(\mathrm{Re}\, M_{ij})\, \mathrm{d}(\mathrm{Im}\, M_{ij}) \,. \tag{A.3}$$

In the quaternionic case $\beta = 4$, we decompose the off-diagonal matrix elements as $M_{ij} = M_{ij}^{(0)} + \mathrm{i}M_{ij}^{(1)} + \mathrm{j}M_{ij}^{(2)} + \mathrm{k}M_{ij}^{(3)}$, where i, j and k are the three imaginary units are the $M_{ij}^{(n)}$'s are real. The Lesbesgue measure is

$$\mathrm{d}M = \prod_{i} \mathrm{d}M_{ii} \prod_{i<j} \mathrm{d}M_{ij}^{(0)} \mathrm{d}M_{ij}^{(1)} \mathrm{d}M_{ij}^{(2)} \mathrm{d}M_{ij}^{(3)} \,. \tag{A.4}$$

For the corresponding compact groups it is convenient to introduce the Haar measure $\mathrm{d}\mu$, which is left and right-invariant:

$$\mathrm{d}\mu(VU) = \mathrm{d}\mu(UV) = \mathrm{d}\mu(U)\,, \quad \forall V \in \begin{cases} \mathrm{O}(N) & \text{for } \beta = 1\,, \\ \mathrm{U}(N) & \text{for } \beta = 2\,, \\ \mathrm{Sp}(N) & \text{for } \beta = 4\,. \end{cases} \tag{A.5}$$

Having defined the Lebesgue and Haar measures, we list a few Jacobians associated to some frequently encountered transforms. The proofs and a more exhaustive list can be found in [222]. Let X be a $N \times N$ real symmetric ($\beta = 1$), complex Hermitian ($\beta = 2$) or quaternionic self-dual ($\beta = 4$) matrix.

Product: For any $N \times N$ matrix A, we have:

$$Y = AXA^\dagger \quad \Rightarrow \quad \mathrm{d}Y = (\det A^2)^{1+\beta\frac{N-1}{2}}\mathrm{d}X\,. \tag{A.6}$$

The multiplication on the left by A and on the right by $A^\dagger$ ensures that the resulting matrix Y is still self-adjoint.

Inverse: The Jacobian for the inverse is

$$Y = X^{-1} \quad \Rightarrow \quad \mathrm{d}Y = (\det X^{-2})^{1+\beta\frac{N-1}{2}}\mathrm{d}X\,. \tag{A.7}$$

Eigendecomposition: The main features of the statistics of the eigenvalues of random matrices come from the Jacobian of the eigendecomposition

$$X = U^\dagger \Lambda U\,, \quad \Lambda = \mathrm{Diag}(\lambda_1, \dots, \lambda_N)\,, \quad U \in \begin{cases} \mathrm{O}(N) & \text{for } \beta = 1\,, \\ \mathrm{U}(N) & \text{for } \beta = 2\,, \\ \mathrm{Sp}(N) & \text{for } \beta = 4\,. \end{cases} \tag{A.8}$$

To ensure the uniqueness of this decomposition, we need to impose some conditions on U. For example, we can impose that its diagonal elements are real and positive. Then, the Jacobian is given by

$$\mathrm{d}X = \prod_{i<j} |\lambda_i - \lambda_j|^\beta \; \mathrm{d}\lambda_1 \dots \mathrm{d}\lambda_N \, \mathrm{d}\mu(U)\,, \tag{A.9}$$

where $\mathrm{d}\mu$ is the Haar measure on the corresponding group, which verifies[1]

$$\int \mathrm{d}\mu(U) \overset{\text{(def)}}{=} v_{N,\beta} = \frac{\pi^{\beta\frac{N(N-1)}{2}}\Gamma\left(\frac{\beta}{2}\right)^N}{\Gamma_{N,\beta}\left(\frac{\beta N}{2}\right)}\,, \tag{A.10}$$

which is expressed in terms of the multivariate Gamma function, see Appendix B.1. Note that the Jacobian (A.9) involves the Vandermonde determinant

$$\Delta(\lambda) = \det[\lambda_i^{j-1}]_{1\leqslant i,j\leqslant N} = \prod_{i<j}(\lambda_i - \lambda_j)\,. \tag{A.11}$$

[1] $v_{N,\beta}$ is not exactly the volume of the compact group, due to the conditions we imposed to ensure the uniqueness of the eigendecomposition. Relation (A.10) can be found for $\beta = 1$ and $\beta = 2$ in Ref. [222], and for general β in Ref. [135].

Cholesky: Sometimes, it is useful to perform a Cholesky decomposition[2]

$$X = LL^\dagger \,, \tag{A.12}$$

where L is a lower triangular matrix, with positive diagonal elements. The Jacobian is

$$\mathrm{d}X = 2^N \prod_{i=1}^{N} (L_{ii})^{\beta(n-j)+1} \,\mathrm{d}L \,. \tag{A.13}$$

We also have the Jacobian

$$X = L^\dagger L \quad \Rightarrow \quad \mathrm{d}X = 2^N \prod_{i=1}^{N} (L_{ii})^{\beta(j-1)+1} \,\mathrm{d}L \,. \tag{A.14}$$

QR-decomposition: Consider a $M \times N$ matrix X with independent elements, and introduce its QR-decomposition

$$X = QR \,, \tag{A.15}$$

where R is a $N \times N$ upper triangular with positive diagonal elements, and Q is $M \times N$ and pseudo-unitary[3]: $Q^\dagger Q = \mathbb{1}_N$. The Jacobian of this change of variables is

$$\mathrm{d}X = \left(\prod_{i=1}^{N} (R_{jj})^{\beta(M-j+1)-1} \right) \mathrm{d}R \,\mathrm{d}\mu(Q) \,, \tag{A.16}$$

where the measure $\mathrm{d}\mu$ verifies

$$\int \mathrm{d}\mu(Q) = \frac{2^N \pi^{\beta MN/2}}{\Gamma_{N,\beta}\left(\frac{\beta M}{2}\right)} \,, \tag{A.17}$$

expressed in terms of the multivariate Gamma function (B.5). If we introduce the matrix $Y = X^\dagger X = R^\dagger R$, we deduce from (A.16) and (A.13):

$$\mathrm{d}X = 2^{-N} (\det Y)^{\frac{\beta}{2}(M-N+1)-1} \,\mathrm{d}Y \,\mathrm{d}\mu(Q) \,. \tag{A.18}$$

This Jacobian proves the expression (1.35) for the expression of the Wishart distribution.

A.2 Derivatives

We are often led to consider functions of matrix argument $f(M)$. Such functions can then be differentiated with respect to any independent real parameter of the matrix M. If this matrix is real symmetric ($\beta = 1$), it can be parametrised by its upper triangular elements. It is thus convenient to define the differential operator [244]

$$\left(\frac{\partial f}{\partial M} \right)_{ij} = \frac{1 + \delta_{ij}}{2} \frac{\partial f}{\partial M_{ij}} \,, \qquad \beta = 1 \,. \tag{A.19}$$

[2] See for example Section B.1.

[3] Or pseudo-orthogonal or pseudo-symplectic.

The prefactor gives weight 1 to the diagonal elements, and 1/2 to the off-diagonal elements to compensate the fact that their appear twice. In the case $\beta = 2$, the complex-conjugate off-diagonal elements can be treated as independent, and we define this operator simply as

$$\left(\frac{\partial f}{\partial M}\right)_{ij} = \frac{\partial f}{\partial M_{ij}} \qquad \beta = 2\,. \tag{A.20}$$

With these two operators we can write compact expressions for the derivatives of simple functions. I give here a few examples which have been useful in this thesis. For a more exhaustive list see Ref. [262].

Traces:

$$\frac{\partial}{\partial X}\operatorname{tr}(AX) = \frac{1}{2}\left(A + A^{\mathrm{T}}\right)\,, \tag{A.21}$$

$$\frac{\partial}{\partial X}\operatorname{tr}(AX^{-1}) = -\frac{1}{2}X^{-1}\left(A + A^{\mathrm{T}}\right)X^{-1}\,. \tag{A.22}$$

Determinant:

$$\frac{\partial}{\partial X}\det(X) = X^{-1}\det(X)\,. \tag{A.23}$$

Inverse: For $\beta = 1$,

$$\frac{\partial (X^{-1})_{ab}}{\partial X_{ij}} = -\frac{1}{1+\delta_{ij}}\left((X^{-1})_{ai}(X^{-1})_{jb} + (X^{-1})_{aj}(X^{-1})_{ib}\right)\,, \tag{A.24}$$

and for $\beta = 2$:

$$\frac{\partial (X^{-1})_{ab}}{\partial X_{ij}} = -(X^{-1})_{ai}(X^{-1})_{jb}\,. \tag{A.25}$$

All these relations are needed to check that (6.59) is solution of the Fokker-Planck equation (6.37).

A.3 Integrals over the eigenvalues

In RMT, one is often led to consider integrals of the form

$$\int_{\mathcal{I}} \mathrm{d}\lambda_1 \ldots \int_{\mathcal{I}} \mathrm{d}\lambda_N \prod_{i<j} |\lambda_i - \lambda_j|^\beta \prod_{n=1}^{N} w(\lambda_n)\,, \tag{A.26}$$

where w is a given function and $\mathcal{I}$ an interval of $\mathbb{R}$. This integral can be expressed in terms of determinants or pfaffians, depending on the value of β [1, 135, 224].

A.3.1 Unitary case ($\beta = 2$)

As usual in RMT, the unitary case $\beta = 2$ is the simplest: the integral (A.26) can be expressed as a determinant thanks to Andréif's formula [19] (see also the historical review [136]):

$$\int_{\mathcal{I}} \mathrm{d}\lambda_1 \ldots \int_{\mathcal{I}} \mathrm{d}\lambda_N \prod_{i<j} |\lambda_i - \lambda_j|^2 \prod_{n=1}^{N} w(\lambda_n) = N!\,\det\left[\int_{\mathcal{I}} \mathrm{d}\lambda\, \lambda^{i+j-2}\, w(\lambda)\right]_{1\leqslant i,j\leqslant N}\,. \tag{A.27}$$

A.3.2 Orthogonal case ($\beta = 1$)

In the orthogonal case, De Bruijn [96] proved that Eq. (A.26) can be rewritten as the pfaffian of a skew-symmetric matrix A:

$$\int_{\mathcal{I}} \mathrm{d}\lambda_1 \dots \int_{\mathcal{I}} \mathrm{d}\lambda_N \prod_{i<j} |\lambda_i - \lambda_j|^2 \prod_{n=1}^{N} w(\lambda_n) = N!\ \mathrm{pf}\,[A]\ . \tag{A.28}$$

The expression of the matrix A depends on the parity of N.

• If N is even, the matrix A is of size $N \times N$, with elements are given by

$$A_{ij} = \int_{\mathcal{I}} \mathrm{d}x \int_{\mathcal{I}} \mathrm{d}y\ \mathrm{sign}(x-y)\, x^{i-1} y^{j-1}\, w(x) w(y)\ . \tag{A.29}$$

• If N is odd, the matrix A has size $(N+1) \times (N+1)$. For $1 \leqslant i, j \leqslant N$, the matrix elements A_{ij} are given by Eq. (A.29). The last row and columns read:

$$A_{i,N+1} = -A_{N+1,i} = \int_{\mathcal{I}} \mathrm{d}x\, x^{i-1}\, w(x)\ . \tag{A.30}$$

A.3.3 Symplectic case ($\beta = 4$)

In the symplectic case, the integral (A.26) can also be expressed as a pfaffian [1, Chapter 5]

$$\int_{\mathcal{I}} \mathrm{d}\lambda_1 \dots \int_{\mathcal{I}} \mathrm{d}\lambda_N \prod_{i<j} |\lambda_i - \lambda_j|^4 \prod_{n=1}^{N} w(\lambda_n) = N!\,\mathrm{pf}[A_{ij}]\ , \tag{A.31}$$

where the $2N \times 2N$ skew-symmetric matrix A is given by

$$A_{ij} = (j-i) \int_{\mathcal{I}} \mathrm{d}x\, x^{i+j-3}\, w(x)\ . \tag{A.32}$$

This formula comes from the relation [96]:

$$\int_{\mathcal{I}} \mathrm{d}x_1 \cdots \mathrm{d}x_N\ \det[(\phi_i(x_j), \psi_i(x_j))]_{\substack{1 \leqslant i \leqslant 2N \\ 1 \leqslant j \leqslant N}} = N!\,\mathrm{pf}\left[\int_{\mathcal{I}} (\phi_i(x)\psi_j(x) - \phi_j(x)\psi_i(x)) \mathrm{d}x\right]_{1 \leqslant i,j \leqslant 2N}\ , \tag{A.33}$$

where we denoted

$$\det[(\phi_i(x_j), \psi_i(x_j))]_{\substack{1 \leqslant i \leqslant 2N \\ 1 \leqslant j \leqslant N}} = \begin{vmatrix} \phi_1(x_1) & \psi_1(x_1) & \cdots & \phi_1(x_N) & \psi_1(x_N) \\ \vdots & \vdots & & \vdots & \vdots \\ \phi_{2N}(x_1) & \psi_{2N}(x_1) & \cdots & \phi_{2N}(x_N) & \psi_{2N}(x_N) \end{vmatrix}\ . \tag{A.34}$$

With the choice

$$\phi_i(x) = w(x)\, x^{i-1}\ , \qquad \psi_j(x) = (i-1) x^{i-2}\ , \tag{A.35}$$

relation (A.34) reduces to (A.33) by using [1]

$$\det[(x_j^{i-1}, (i-1)x_j^{i-2}))]_{\substack{1 \leqslant i \leqslant 2N \\ 1 \leqslant j \leqslant N}} = \prod_{i<j} (x_i - x_j)^4\ . \tag{A.36}$$

A.4 Integrals over the unitary group

Sometimes, we also need to evaluate some integrals over the compact groups. The simplest integral, with only the Haar measure, are given by Eq. (A.10). I list here more complicated integrals, only in the unitary case $\beta = 2$.

A.4.1 Products of matrix elements

Integrals involving product of matrix elements of unitary matrices over $\mathrm{U}(N)$ are given by [83]:

$$\int_{U(N)} U_{i_1 j_1} \cdots U_{i_n j_n}\, U^\star_{k_1 l_1} \cdots U^\star_{k_n l_n}\, \mathrm{d}\mu(U) = \sum_{\sigma \in S_n} \sum_{\tau \in S_n} W(N, \sigma\tau^{-1})\, \delta_{i_1,k_{\sigma(i)}} \cdots \delta_{i_n,k_{\sigma(n)}}\, \delta_{j_1,l_{\sigma(i)}} \cdots \delta_{j_n,l_{\sigma(n)}}\,, \quad \text{(A.37)}$$

where S_n is the group of permutations of n integers and $W(N,\sigma)$ is the Weingarten function. Often, the permutations are denoted by their cyclic shape: for example if $n = 2$, the two possible permutations 1^2 for the identity (two cycles of length 1) and 2^1 for the transposition (one cycle of length 2). In this case, Eq. (A.37) reduces to

$$\begin{aligned}\int_{U(N)} U_{i_1 j_1} U_{i_2 j_2} U^*_{k_1 l_1} U^*_{k_2 l_2} \mathrm{d}\mu(U) = {} & W(N, 1^2)\, (\delta_{i_1 k_1}\delta_{i_2 k_2}\delta_{j_1 l_1}\delta_{j_2 l_2} + \delta_{i_1 k_2}\delta_{i_2 k_1}\delta_{j_1 l_2}\delta_{j_2 l_1}) \\ & + W(N, 2)\, (\delta_{i_1 k_1}\delta_{i_2 k_2}\delta_{j_1 l_2}\delta_{j_2 l_1} + \delta_{i_1 k_2}\delta_{i_2 k_1}\delta_{j_1 l_1}\delta_{j_2 l_2})\,, \quad \text{(A.38)}\end{aligned}$$

where the Weingarten functions $W(N,\sigma)$ are given by:

$$W(N, 1^2) = \frac{1}{N^2 - 1}\,, \qquad W(N, 2) = -\frac{1}{N(N^2-1)}\,. \quad \text{(A.39)}$$

A.4.2 The Harish-Chandra–Itzykson–Zuber integral

Consider two Hermitian matrices A and B of size $N \times N$ with eigenvalues $\{a_n\}$ and $\{b_n\}$ respectively. The Harish-Chandra–Itzykson–Zuber integral is [174, 179]:

$$\int_{U(N)} \exp\left[t\ \mathrm{tr}(AUBU^\dagger)\right] \mathrm{d}\mu(U) = \left(\prod_{n=1}^{N-1} n!\right) t^{-n(n-1)/2}\, \frac{\det[\mathrm{e}^{t a_i b_j}]_{1 \leqslant i,j \leqslant N}}{\Delta(a)\Delta(b)}\,, \quad \text{(A.40)}$$

where $\Delta(a)$ and $\Delta(b)$ are the Vandermonde determinants of the eigenvalues of A and B, see Eq. (A.11).

A.5 Tricomi's theorem

In the Coulomb gas method described in Chapter 2, one often encounters integral equations of the from

$$⨍_a^b \frac{f(y)}{x - y} \mathrm{d}y = g(x)\,, \quad \forall x \in [a, b]\,, \quad \text{(A.41)}$$

where $⨍$ denotes the principal value integral. This relation can be inverted thanks to a formula due to Tricomi [296]:

$$f(x) = \frac{1}{\pi\sqrt{(x-a)(b-x)}} \left\{ A + ⨍_a^b \frac{\mathrm{d}t}{\pi} \frac{\sqrt{(t-a)(b-t)}}{t-x} \right\} , \tag{A.42}$$

where the constant A is a normalisation: $\int_a^b f = A$.

A.6 Saddle point estimate for integrals over matrix spaces

Consider the following integral

$$I_\beta(t) = \int f(X)\, \mathrm{e}^{t\phi(X)}\, \mathrm{d}X , \tag{A.43}$$

where f and ϕ are scalar function, and the integration runs over the space of real symmetric ($\beta = 1$), complex Hermitian ($\beta = 2$) or quaternionic self-dual matrices ($\beta = 4$). Our aim is to use a saddle point method to give an asymptotic behaviour for $t \to \infty$.

For integrals on $\mathbb{R}^n$ the result is well-known, and reads:

$$\int f(\vec{x})\, \mathrm{e}^{t\phi(\vec{x})}\, \mathrm{d}^n\vec{x} \underset{t\to\infty}{\simeq} \frac{(2\pi)^{n/2}}{\sqrt{t\,|\det \mathcal{H}|}} f(\vec{x}_0)\, \mathrm{e}^{t\phi(\vec{x}_0)}(1 + \mathcal{O}(t^{-1})) , \tag{A.44}$$

where $\vec{x}_0$ is the saddle point, given by $\frac{\partial\phi}{\partial\vec{x}} = 0$ and $\mathcal{H}$ is the Hessian matrix

$$\mathcal{H}_{ij} = \left.\frac{\partial^2\phi}{\partial x_i \partial x_j}\right|_{\vec{x}_0} . \tag{A.45}$$

The method to estimate integrals of the form (A.43) is the same as in the case of vectors. One simply has to map the independent real elements of the matrix onto a big vector. For example, with a mapping of the type

$$X_{ij} \longrightarrow y_n , \quad \text{with} \quad n = i + N(j-1) , \tag{A.46}$$

if X is a $N \times N$ matrix. Here, we considered all the matrix elements, but we can restrict their number depending on the symmetry class.

The saddle points X_0 (there might be several) are given by

$$\left.\frac{\partial\phi}{\partial X}\right|_{X_0} = 0 , \tag{A.47}$$

where the matrix derivatives are defined in Section A.2. The Hessian matrix is then

$$\mathcal{H}_{(i,j),(k,l)} = \left.\frac{\partial\phi}{\partial X_{ij}\partial X_{lk}}\right|_{X_0} . \tag{A.48}$$

Note that this is a formal expression: the derivatives must be taken with respect to independent real components (see example in Section B.2). Therefore, we have:

$$I_\beta(t) \underset{t\to\infty}{\simeq} \frac{(2\pi)^{\frac{N}{2}(1+\beta\frac{N-1}{2})}}{\sqrt{t\det\mathcal{H}}}\, f(X_0)\, \mathrm{e}^{t\phi(X_0)}(1+\mathcal{O}(t^{-1}))\,, \tag{A.49}$$

where the determinant of $\mathcal{H}$ runs over all *independent real elements* of X. We illustrate this method in Appendix B.2.

Appendix B

Special functions of matrix argument

In this Appendix, I introduce a few special functions defined by integrals over matrix spaces.

B.1 Multivariate Gamma and Beta functions

We first define generalisations of the Gamma and Beta functions, which are not functions of matrix argument, but which are useful. We define the multivariate Gamma function as [222, 244]

$$\boxed{\Gamma_{N,\beta}(a) = \int (\det X)^{a-1-\beta\frac{N-1}{2}} \, \mathrm{e}^{-\operatorname{tr} X} \, \mathrm{d}X} \tag{B.1}$$

where the integral is performed on $N \times N$ matrices $X = X^\dagger$, with positive eigenvalues. We can obtain an explicit form for this integral by using the Cholesky decomposition $X = LL^\dagger$, where L is lower triangular, with positive diagonal elements. Its off diagonal elements are either real ($\beta = 1$), complex ($\beta = 2$) or quaternionic ($\beta = 4$). We have

$$\det X = \prod_{i=1}^{N} (L_{ii})^2 \tag{B.2}$$

and

$$\operatorname{tr} X = \operatorname{tr}(LL^\dagger) = (L_{11}^2) + (|L_{12}|^2 + L_{22}^2) + \cdots + (|L_{n1}|^2 + \cdots + L_{nn}^2) \, . \tag{B.3}$$

Using the Jacobian (A.13), we can express the Gamma function as

$$\Gamma_{N,\beta}(a) = \left(\prod_{i=1}^{N} 2 \int_0^\infty (L_{ii})^{a-\beta\frac{j-1}{2}-\frac{1}{2}} \, \mathrm{e}^{-L_{ii}^2} \, \mathrm{d}L_{ii} \right) \left(\prod_{i>j} \int \mathrm{e}^{-|L_{ij}|^2} \, \mathrm{d}L_{ij} \right) \, . \tag{B.4}$$

The integrals over the off-diagonal terms are Gaussian, so they each yield a factor $\pi^{\beta/2}$. The diagonal terms give usual Gamma functions, thus:

$$\boxed{\Gamma_{N,\beta}(a) = \pi^{\beta N(N-1)/4} \prod_{j=1}^{N} \Gamma\left(a - \beta\frac{j-1}{2}\right)} \tag{B.5}$$

This function appears, for instance, in the normalisation constant of the Laguerre ensemble, Eq. (1.36).

The multivariate Beta function can be defined similarly, by the integral [222]

$$\boxed{\mathrm{B}_{N,\beta}(a,b) = \int_0^{\mathbb{1}_N} (\det X)^{a-1-\beta\frac{N-1}{2}} \det(\mathbb{1}_N - X)^{b-1-\beta\frac{N-1}{2}} \mathrm{d}X} \tag{B.6}$$

where the notation indicates that the integration is performed on self-adjoint matrices $X^\dagger = X$ with eigenvalues in $[0,1]$. Equivalently, it can be defined as

$$\mathrm{B}_{N,\beta}(a,b) = \int (\det X)^{a-1-\beta\frac{N-1}{2}} \det(\mathbb{1}_N + X)^{-a-b} \,\mathrm{d}X \,, \tag{B.7}$$

where $X^\dagger = X > 0$, to get rid of the upper bound. This function can be expressed in terms of the Gamma function (B.1) as [222]:

$$\boxed{\mathrm{B}_{N,\beta}(a,b) = \frac{\Gamma_{N,\beta}(a)\Gamma_{N,\beta}(b)}{\Gamma_{N,\beta}(a+b)}} \tag{B.8}$$

This expression reduces to the well-known relation for the Beta function in the case $N = 1$ [166]. Performing the eigendecomposition (A.8), the Beta function (B.6) reduces to the well-known Selberg integral [224, 273] (up to a constant arising from the integration over the eigenvectors, given by Eq. (A.10)).

B.2 Bessel function

We now introduce the generalisation of the modified Bessel function K_ν to the matrix argument case, which is useful in Chapter 7. This function was first introduced by Herz [176], in the case $\beta = 1$. Here, I use Bernadac's definition of the modified Bessel function of matrix argument [39], which I extend to $\beta \neq 1$. For two self-adjoint matrices A and B with positive eigenvalues, we define

$$\boxed{\mathbb{K}_{N,\beta}(\lambda|A,B) = \frac{(\det AB^{-1})^{\lambda/2}}{2^{N(1+\beta\frac{N-1}{2})}} \int (\det X)^{\lambda-1-\beta\frac{N-1}{2}} \,\mathrm{e}^{-\frac{1}{2}\operatorname{tr}(AX+BX^{-1})} \mathrm{d}X} \tag{B.9}$$

where the integral runs over self-adjoint matrices X with positive eigenvalues. With this definition, this function seems to depend on two matrices A and B. However, making the change of variables $X = A^{1/2}YA^{1/2}$, we obtain

$$\mathbb{K}_{N,\beta}(\lambda|A,B) = \mathbb{K}_{N,\beta}(\lambda|\mathbb{1}_N, A^{1/2}BA^{1/2}) \,. \tag{B.10}$$

Therefore, this Bessel function depends only on one matrix, which is $A^{1/2}BA^{1/2}$. More generally, for any self-adjoint matrix M with positive eigenvalues, one has the relation

$$\mathbb{K}_{N,\beta}(\lambda|A,B) = \mathbb{K}_{N,\beta}(\lambda|M^{1/2}AM^{1/2}, M^{-1/2}BM^{-1/2}) \,. \tag{B.11}$$

For $N = 1$, this function reduces to the usual modified Bessel function (7.29):

$$\mathbb{K}_{N=1,\beta}(\lambda|a,b) = K_\lambda(\sqrt{ab}) \,. \tag{B.12}$$

The integral (B.9) is in general very difficult to evaluate. However, its asymptotic form for large argument can be obtained by a saddle point estimate, as described in Section A.6. This procedure was carried out for $\beta = 1$ in Ref. [69]. We here present the derivation for all β of the asymptotic of $\mathbb{K}(\lambda|zA, zB)$, with $z \to \infty$. Introduce the matrix M such that $M^2 = A^{1/2}BA^{1/2}$. Let us make the change of variable $X = A^{-1/2}M^{1/2}YM^{1/2}A^{-1/2}$ in the integral. The Jacobian is given by (A.6), thus

$$\mathbb{K}_{N,\beta}(\lambda|zA, zB) = \frac{1}{2^{N(1+\beta\frac{N-1}{2})}} \int (\det Y)^{\mu-1-\beta\frac{N-1}{2}} \, \mathrm{e}^{-\frac{z}{2}\operatorname{tr}[M(Y+Y^{-1})]} \, \mathrm{d}Y \, . \tag{B.13}$$

We can assume without loss of generality that M is diagonal. Denote

$$\phi(X) = \operatorname{tr}[M(X + X^{-1})] \, , \qquad f(X) = (\det X)^{\lambda-1-\beta\frac{N-1}{2}} \, . \tag{B.14}$$

Equation (B.13) is thus of the form (A.43) and we can apply the procedure described in Section A.6. Using the properties of the matrix derivatives given in Section A.2, the saddle point is given by

$$\frac{\partial\phi}{\partial X} = 0 \quad \Rightarrow \quad M - X^{-1}MX^{-1} = 0 \, . \tag{B.15}$$

We can solve this equation by diagonalizing $X = U^\dagger DU$. This gives the equation

$$DUMU^\dagger = UMU^\dagger D^{-1} \, , \tag{B.16}$$

which we can rewrite in terms of components:

$$d_i(UMU^\dagger)_{ij} = (UMU^\dagger)_{ij}\frac{1}{d_j} \quad \forall i, j \, . \tag{B.17}$$

This equation imposes $d_i = 1$, $\forall i$, therefore the saddle point is

$$X_0 = \mathbb{1}_N \, . \tag{B.18}$$

Let us now compute the Hessian. For $\beta = 2$, we can consider each matrix element to be independent, thus:

$$\begin{aligned} \frac{\partial\phi}{\partial X_{ij}\partial X_{kl}} &= \frac{\partial}{\partial X_{ij}}(M - X^{-1}MX^{-1})_{lk} \\ &= (X^{-1})_{li}(X^{-1}MX^{-1})_{jk} + (X^{-1}MX^{-1})_{li}(X^{-1})_{jk} \, , \end{aligned} \tag{B.19}$$

where we used relation (A.25). Therefore, the Hessian is

$$\tilde{\mathcal{H}}_{(i,j),(k,l)} = \delta_{li}M_{jk} + M_{li}\delta_{jk} \, . \tag{B.20}$$

However, one has to be careful with the derivatives: the independent real elements are $\operatorname{Re} X_{ij}$ and $\operatorname{Im} X_{ij}$ for $i < j$, along with the diagonal elements X_{ii}. Therefore, we have for $i < j$:

$$\frac{\partial}{\partial \operatorname{Re} X_{ij}} = \frac{\partial}{\partial X_{ij}} + \frac{\partial}{\partial X_{ji}} \, , \tag{B.21}$$

$$\frac{\partial}{\partial \operatorname{Im} X_{ij}} = \frac{1}{\mathrm{i}} \left(\frac{\partial}{\partial X_{ji}} - \frac{\partial}{\partial X_{ij}} \right) , \tag{B.22}$$

and for the second derivatives:

$$\frac{\partial^2}{\partial (\operatorname{Re} X_{ij})^2} = \frac{\partial^2}{\partial X_{ij}^2} + \frac{\partial^2}{\partial X_{ji}^2} + 2 \frac{\partial^2}{\partial X_{ij} \partial X_{ji}} , \tag{B.23}$$

$$\frac{\partial^2}{\partial (\operatorname{Im} X_{ij})^2} = -\frac{\partial^2}{\partial X_{ij}^2} - \frac{\partial^2}{\partial X_{ji}^2} + 2 \frac{\partial^2}{\partial X_{ij} \partial X_{ji}} , \tag{B.24}$$

$$\frac{\partial^2}{\partial \operatorname{Re} X_{ij} \partial \operatorname{Im} X_{ij}} = \mathrm{i} \left(\frac{\partial^2}{\partial X_{ij}^2} - \frac{\partial^2}{\partial X_{ji}^2} \right) . \tag{B.25}$$

Using that M is diagonal, we obtain the true Hessian:

$$\mathcal{H}_{(i,j),(k,l)} = \frac{2}{1+\delta_{ij}} \left(\delta_{ki} M_{jl} + M_{ki} \delta_{jl} \right) . \tag{B.26}$$

It is non zero for $(i,j) = (k,l)$. So $\mathcal{H}$ is "diagonal", and its determinant is simply

$$\det \mathcal{H} = \prod_{i,j} \mathcal{H}_{(i,j),(i,j)} = 2^{N^2} \det M \left(\prod_{i<j} (M_{ii} + M_{jj}) \right)^2 . \tag{B.27}$$

For $\beta = 1$, one has to be more careful. The first derivative is:

$$\frac{\partial \phi}{\partial X_{ij}} = \frac{2}{1+\delta_{ij}} (M - X^{-1} M X^{-1})_{ij} , \tag{B.28}$$

and the derivative of an inverse is given by Eq. (A.24). Therefore:

$$\frac{\partial \phi}{\partial X_{ij} \partial X_{kl}} = \frac{2}{1+\delta_{kl}} \frac{1}{1+\delta_{ij}} \Big((X^{-1})_{ki} (X^{-1} M X^{-1})_{jl} + (X^{-1} M X^{-1})_{ki} (X^{-1})_{jl} + (i \leftrightarrow j) \Big) . \tag{B.29}$$

Finally, the Hessian is:

$$\mathcal{H}_{(i,j),(k,l)} = \frac{2}{1+\delta_{kl}} \frac{1}{1+\delta_{ij}} \left(\delta_{ki} M_{jl} + \delta_{jl} M_{ki} + \delta_{kj} M_{il} + \delta_{il} M_{kj} \right) . \tag{B.30}$$

$\mathcal{H}_{(i,j),(k,l)}$ is non zero iff $(i,j) = (k,l)$ or $(i,j) = (l,k)$. However, we will restrict ourselves to independent variables by imposing $i \leqslant j$ and $k \leqslant l$. So, we get:

$$\begin{aligned} \det \mathcal{H} &= \left(\prod_i \mathcal{H}_{(i,i),(i,i)} \right) \left(\prod_{i<j} \mathcal{H}_{(i,j),(i,j)} \right) = \left(\prod_i 2 M_{ii} \right) \left(\prod_{i<j} 2 (M_{ii} + M_{jj}) \right) \\ &= 2^{N(N+1)/2} \left(\prod_i M_{ii} \right) \left(\prod_{i<j} (M_{ii} + M_{jj}) \right) . \end{aligned} \tag{B.31}$$

We can summarise the two cases as:

$$\det \mathcal{H} = 2^{N(1+\beta \frac{N-1}{2})} \det M \left(\prod_{i<j} (M_{ii} + M_{jj}) \right)^\beta . \tag{B.32}$$

Using Eq. (A.49), we get the asymptotic form

$$\int (\det Y)^{\lambda-1-\beta\frac{N-1}{2}}\, \mathrm{e}^{-\frac{z}{2}\operatorname{tr}[M(Y+Y^{-1})]}\, \mathrm{d}Y \underset{z\to\infty}{\simeq} \left(\frac{2\pi}{z}\right)^{\frac{N}{2}(1+\beta\frac{N-1}{2})} \frac{1}{\sqrt{\det M}} \prod_{i<j}(M_{ii}+M_{jj})^{-\beta/2}\, \mathrm{e}^{-z\operatorname{tr} M}(1+\mathcal{O}(z^{-1}))\,. \quad \text{(B.33)}$$

Hence, finally

$$\boxed{\mathbb{K}_{N,\beta}(\lambda|zA,zB) \underset{z\to\infty}{\simeq} \left(\frac{\pi}{2z}\right)^{\frac{N}{2}(1+\beta\frac{N-1}{2})} \frac{\prod_{i<j}(m_i+m_j)^{-\beta/2}}{\prod_i \sqrt{m_i}}\, \mathrm{e}^{-z\operatorname{tr} M}(1+\mathcal{O}(z^{-1}))} \quad \text{(B.34)}$$

where $\{m_i\}$ are the eigenvalues of $M = \sqrt{A^{1/2}BA^{1/2}}$. We can check that this coincides for $\beta = 1$ with the result of Butler and Wood [69].

Appendix C

Table of integrals

C.1 Elliptic integrals

The complete elliptic integrals are given by:

$$E(m) = \int_0^1 \sqrt{\frac{1-mt^2}{1-t^2}}\,\mathrm{d}t, \tag{C.1}$$

$$K(m) = \int_0^1 \frac{\mathrm{d}t}{\sqrt{(1-t^2)(1-mt^2)}}, \tag{C.2}$$

$$\Pi(n,m) = \int_0^1 \frac{\mathrm{d}t}{(1-nt^2)\sqrt{(1-t^2)(1-mt^2)}}. \tag{C.3}$$

In the last integral, the Cauchy principal value should be taken if $n > 1$ (it corresponds to the real part of the value given by the function `EllipticPi` in `Mathematica`).

We assume that $a < b < c < d$. The following integrals are be useful in Chapter 4:

$$\int_c^d \frac{\mathrm{d}t}{\sqrt{(t-c)(d-t)(t-b)}} = \frac{2}{\sqrt{d-b}}\,K\left(\frac{d-c}{d-b}\right), \tag{C.4}$$

$$\int_c^d \sqrt{\frac{t-c}{(d-t)(t-b)}}\,\mathrm{d}t = 2\sqrt{d-b}\,E\left(\frac{d-c}{d-b}\right) - 2\frac{c-b}{\sqrt{d-b}}\,K\left(\frac{d-c}{d-b}\right), \tag{C.5}$$

$$\int_c^d \frac{\mathrm{d}t}{\sqrt{(t-c)(d-t)(t-b)}}\frac{1}{t-x} = \frac{2}{(d-x)\sqrt{d-b}}\,\Pi\left(\frac{d-c}{d-x}, \frac{d-c}{d-b}\right), \tag{C.6}$$

$$\int_a^b \frac{\mathrm{d}t}{(x-t)\sqrt{(t-a)(b-t)(c-t)(d-t)}} = \frac{2}{(x-b)(x-c)\sqrt{(d-b)(c-a)}} \times \left[(x-b)K\left(\frac{(d-c)(b-a)}{(d-b)(c-a)}\right) + (b-c)\Pi\left(\frac{(x-c)(b-a)}{(x-b)(c-a)}, \frac{(d-c)(b-a)}{(d-b)(c-a)}\right)\right], \tag{C.7}$$

$$\int_c^d \frac{\mathrm{d}t}{(x-t)\sqrt{(t-a)(b-t)(c-t)(d-t)}} = \frac{2}{(x-d)(x-a)\sqrt{(d-b)(c-a)}} \times \left[(x-d)K\left(\frac{(d-c)(b-a)}{(d-b)(c-a)}\right) + (d-a)\Pi\left(\frac{(x-a)(c-d)}{(x-d)(c-a)}, \frac{(d-c)(b-a)}{(d-b)(c-a)}\right)\right], \quad \text{(C.8)}$$

$$\int_a^b \frac{\mathrm{d}t}{\sqrt{(t-a)(b-t)(c-t)(d-t)}} = \int_c^d \frac{\mathrm{d}t}{\sqrt{(t-a)(b-t)(c-t)(d-t)}} = \frac{2}{\sqrt{(d-b)(c-a)}} K\left(\frac{(d-c)(b-a)}{(d-b)(c-a)}\right). \quad \text{(C.9)}$$

C.2 Principal value integrals

We always consider $x \in [a,b]$. The following integrals are useful when applying the Coulomb gas method (see Chapters 2 and 3):

$$⨍_a^b \frac{\mathrm{d}t}{\pi} \frac{\sqrt{(t-a)(b-t)}}{t-x} = \frac{a+b}{2} - x\,. \quad \text{(C.10)}$$

$$⨍_a^b \frac{\mathrm{d}t}{\pi} \frac{\sqrt{(t-a)(b-t)}}{t-x}\, t = \frac{(b-a)^2}{8} + \frac{a+b}{2}\, x - x^2\,. \quad \text{(C.11)}$$

$$⨍_a^b \frac{\mathrm{d}t}{\pi} \frac{\sqrt{(t-a)(b-t)}}{t-x}\, t^2 = \frac{(b-a)^2}{8}\frac{a+b}{2} + \frac{(b-a)^2}{8}x + \frac{a+b}{2}x^2 - x^3\,. \quad \text{(C.12)}$$

$$⨍_a^b \frac{\mathrm{d}t}{\pi} \frac{\sqrt{(t-a)(b-t)}}{t-x}\, t^3 = \frac{(b-a)^2}{128}(5a^2+6ab+5b^2) + \frac{(b-a)^2}{8}\frac{a+b}{2}x + \frac{(b-a)^2}{8}x^2 + \frac{a+b}{2}x^3 - x^4\,. \quad \text{(C.13)}$$

If $0 < a < x < b$:

$$⨍_a^b \frac{\mathrm{d}t}{\pi} \frac{\sqrt{(t-a)(b-t)}}{t-x}\, \frac{1}{t} = -1 + \frac{\sqrt{ab}}{x}\,. \quad \text{(C.14)}$$

$$⨍_a^b \frac{\mathrm{d}t}{\pi} \frac{\sqrt{(t-a)(b-t)}}{t-x}\, \frac{1}{t^2} = \frac{1}{\sqrt{ab}}\left(-\frac{a+b}{2x} + \frac{ab}{x^2}\right)\,. \quad \text{(C.15)}$$

$$⨍_a^b \frac{\mathrm{d}t}{\pi} \frac{\sqrt{(t-a)(b-t)}}{t-x}\, \frac{1}{t^3} = \frac{1}{(ab)^{3/2}}\left(\frac{(ab)^2}{x^3} - ab\frac{a+b}{2x^2} - \frac{(a-b)^2}{8x}\right)\,. \quad \text{(C.16)}$$

For $a < x < b$ and x_1 outside $[a,b]$:

$$⨍_a^b \frac{\mathrm{d}t}{\pi} \frac{\sqrt{(t-a)(b-t)}}{t-x}\, \frac{1}{t-x_1} = -1 + \frac{\sqrt{(a-x_1)(b-x_1)}}{|x_1-x|}\,. \quad \text{(C.17)}$$

Bibliography

[1] G. Akemann, J. Baik, and P. Di Francesco, *The Oxford handbook of random matrix theory*, Oxford University Press, 2011.

[2] G. Akemann, D. Villamaina, and P. Vivo, Singular-potential random-matrix model arising in mean-field glassy systems, Phys. Rev. E **89**, 062146 (2014).

[3] E. Akkermans and G. Montambaux, *Physique mésoscopique des électrons et des photons*, EDP Sciences, CNRS éditions, 2004.

[4] E. Akkermans and G. Montambaux, *Mesoscopic physics of electrons and photons*, Cambridge University Press, Cambridge, UK, 2007.

[5] I. L. Aleiner, P. W. Brouwer, and L. I. Glazman, Quantum effects in Coulomb blockade, Phys. Rep. **358**(5-6), 309–440 (2002).

[6] Y. Alhassid, The statistical theory of quantum dots, Rev. Mod. Phys. **72**, 895–968 (2000).

[7] J. Alicea, Y. Oreg, G. Refael, F. von Oppen, and M. P. A. Fisher, Non-Abelian statistics and topological quantum information processing in 1D wire networks, Nature Physics **7**, 412 (2011).

[8] R. Allez, J.-P. Bouchaud, and A. Guionnet, Invariant Beta Ensembles and the Gauss-Wigner Crossover, Phys. Rev. Lett. **109**, 094102 (2012).

[9] R. Allez, J.-P. Bouchaud, S. N. Majumdar, and P. Vivo, Invariant β-Wishart ensembles, crossover densities and asymptotic corrections to the Marčenko–Pastur law, J. Phys. A **46**(1), 015001 (2013).

[10] R. Allez, J. Touboul, and G. Wainrib, Index distribution of the Ginibre ensemble, J. Phys. A **47**(4), 042001 (2014).

[11] A. Altland, Spectral and transport properties of d-wave superconductors with strong impurities, Phys. Rev. B **65**, 104525 (2002).

[12] A. Altland, D. Bagrets, L. Fritz, A. Kamenev, and H. Schmiedt, Quantum Criticality of Quasi-One-Dimensional Topological Anderson Insulators, Phys. Rev. Lett. **112**, 206602 (2014).

[13] A. Altland, D. Bagrets, and A. Kamenev, Topology versus Anderson localization: Nonperturbative solutions in one dimension, Phys. Rev. B **91**, 085429 (2015).

[14] A. Altland and R. Merkt, Spectral and transport properties of quantum wires with bond disorder, Nucl. Phys. B **607**(3), 511 – 548 (2001).

[15] A. Altland and M. R. Zirnbauer, Random Matrix Theory of a Chaotic Andreev Quantum Dot, Phys. Rev. Lett. **76**, 3420–3423 (1996).

[16] A. Altland and M. R. Zirnbauer, Nonstandard symmetry classes in mesoscopic normal-superconducting hybrid structures, Phys. Rev. B **55**, 1142–1161 (1997).

[17] J. Ambjørn, L. Chekhov, C. Kristjansen, and Y. Makeenko, Matrix model calculations beyond the spherical limit, Nucl. Phys. B **404**(1), 127 – 172 (1993).

[18] P. W. Anderson, Absence of Diffusion in Certain Random Lattices, Phys. Rev. **109**, 1492–1505 (1958).

[19] C. Andréief, Note sur une relation entre les intégrales définies des produits des fonctions, Mém. de la Soc. Sci. (Bordeaux) **2**, 1–14 (1886).

[20] P. Appell, Sur les séries hypergéométriques de deux variables et sur des équations différentielles linéaires aux dérivés partielles., C. R. Acad. Sci., Paris **90**, 296–299, 731–735 (1880).

[21] C. Aslangul, N. Pottier, and D. Saint-James, Random walk in a one-dimensional random medium, Physica A **164**(1), 52 – 80 (1990).

[22] A. Auffinger, G. B. Arous, and J. Černý, Random Matrices and Complexity of Spin Glasses, Commun. Pure Appl. Math. **66**(2), 165–201 (2012).

[23] L. Balents and M. P. A. Fisher, Delocalization transition via supersymmetry in one dimension, Phys. Rev. B **56**, 12970–12991 (1997).

[24] H. U. Baranger and P. A. Mello, Mesoscopic transport through chaotic cavities: A random S-matrix theory approach, Phys. Rev. Lett. **73**, 142–145 (1994).

[25] J. Bardeen, L. N. Cooper, and J. R. Schrieffer, Microscopic Theory of Superconductivity, Phys. Rev. **106**, 162–164 (1957).

[26] E. L. Basor and C. A. Tracy, Variance calculations and the Bessel kernel, J. Stat. Phys. **73**(1), 415–421 (1993).

[27] H. Bateman, Higher transcendental functions, California Institute of Technology Bateman Manuscript Project, New York: McGraw-Hill, 1953-1955 (1955).

[28] C. W. J. Beenakker, Random-matrix theory of mesoscopic fluctuations in conductors and superconductors, Phys. Rev. B **47**, 15763–15775 (1993).

[29] C. W. J. Beenakker, Universality in the random-matrix theory of quantum transport, Phys. Rev. Lett. **70**, 1155–1158 (1993).

[30] C. W. J. Beenakker, Random-matrix theory of quantum transport, Rev. Mod. Phys. **69**, 731–808 (1997).

[31] C. W. J. Beenakker and B. Rajaei, Exact solution for the distribution of transmission eigenvalues in a disordered wire and comparison with random-matrix theory, Phys. Rev. B **49**, 7499–7510 (1994).

[32] C. W. J. Beenakker and B. Rejaei, Nonlogarithmic repulsion of transmission eigenvalues in a disordered wire, Phys. Rev. Lett. **71**, 3689–3692 (1993).

[33] C. Beenakker, Universality of Brézin and Zee's spectral correlator, Nucl. Phys. B **422**(3), 515 – 520 (1994).

[34] C. Beenakker and P. Brouwer, Distribution of the reflection eigenvalues of a weakly absorbing chaotic cavity, Physica E **9**(3), 463 – 466 (2001), Proceedings of an International Workshop and Seminar on the Dynamics of Complex Systems.

[35] I. Belyaev, L. Blinov, L. Yu, M. Labes, and B. Cano, Density of states in a one-dimensional random potential, Zh. Eksp. Teor. Fiz **73**, 650–661 (1977).

[36] G. Ben Arous and A. Guionnet, Large deviations for Wigner's law and Voiculescu's non-commutative entropy, Prob. Theo. Relat. Fields **108**(4), 517–542 (1997).

[37] G. Ben Arous and O. Zeitouni, Large deviations from the circular law, ESAIM: Prob. Stat. **2**, 123–134 (1998).

[38] T. Berggren and M. Duits, Mesoscopic Fluctuations for the Thinned Circular Unitary Ensemble, Math. Phys. Anal. Geom. **20**(3), 19 (2017).

[39] E. Bernadac, Random continued fractions and inverse Gaussian distribution on a symmetric cone, J. Theo. Prob. **8**(2), 221–259 (1995).

[40] T. Bienaimé and C. Texier, Localization for one-dimensional random potentials with large local fluctuations, J. Phys. A **41**(47), 475001 (2008).

[41] M. Bocquet and J. T. Chalker, Network models for localization problems belonging to the chiral symmetry classes, Phys. Rev. B **67**, 054204 (2003).

[42] E. Bocquillon, F. D. Parmentier, C. Grenier, J.-M. Berroir, P. Degiovanni, D. C. Glattli, B. Plaçais, A. Cavanna, Y. Jin, and G. Fève, Electron Quantum Optics: Partitioning Electrons One by One, Phys. Rev. Lett. **108**, 196803 (2012).

[43] E. Bocquillon, V. Freulon, F. D. Parmentier, J. Berroir, B. Plaçais, C. Wahl, J. Rech, T. Jonckheere, T. Martin, C. Grenier, D. Ferraro, P. Degiovanni, and G. Fève, Electron quantum optics in ballistic chiral conductors, Ann. Phys. **526**(1-2), 1–30 (2013).

[44] O. Bohigas, M. J. Giannoni, and C. Schmit, Characterization of Chaotic Quantum Spectra and Universality of Level Fluctuation Laws, Phys. Rev. Lett. **52**, 1–4 (1984).

[45] O. Bohigas, R. U. Haq, and A. Pandey, Fluctuation Properties of Nuclear Energy Levels and Widths : Comparison of Theory with Experiment, in *Nuclear Data for Science and Technology*, edited by K. H. Böckhoff, pages 809–813, Dordrecht, 1983, Springer Netherlands.

[46] O. Bohigas and M. P. Pato, Randomly incomplete spectra and intermediate statistics, Phys. Rev. E **74**, 036212 (2006).

[47] G. Borot, B. Eynard, S. N. Majumdar, and C. Nadal, Large deviations of the maximal eigenvalue of random matrices, J. Stat. Mech: Theory Exp. **2011**(11), P11024 (2011).

[48] G. Borot and A. Guionnet, Asymptotic Expansion of β Matrix Models in the One-cut Regime, Commun. Math. Phys. **317**(2), 447–483 (2013).

[49] J.-P. Bouchaud and M. Potters, *Theory of financial risk and derivative pricing: from statistical physics to risk management*, Cambridge University Press, 2003.

[50] J.-P. Bouchaud and M. Potters, Financial applications of random matrix theory: a short review, in *The Oxford handbook of random matrix theory*, edited by G. Akemann, J. Baik, and P. Di Francesco, pages 824–850, Oxford University Press, 2011.

[51] J. Bouchaud, A. Comtet, A. Georges, and P. Le Doussal, Classical diffusion of a particle in a one-dimensional random force field, Ann. Phys. **201**(2), 285–341 (1990).

[52] A. J. Bray and D. S. Dean, Statistics of Critical Points of Gaussian Fields on Large-Dimensional Spaces, Phys. Rev. Lett. **98**, 150201 (2007).

[53] E. Brézin, C. Itzykson, G. Parisi, and J. B. Zuber, Planar diagrams, Commun. Math. Phys. **59**(1), 35–51 (1978).

[54] P. W. Brouwer, Generalized circular ensemble of scattering matrices for a chaotic cavity with nonideal leads, Phys. Rev. B **51**, 16878–16884 (1995).

[55] P. W. Brouwer and C. W. J. Beenakker, Diagrammatic method of integration over the unitary group, with applications to quantum transport in mesoscopic systems, J. Math. Phys. **37**(10), 4904–4934 (1996).

[56] P. W. Brouwer and M. Büttiker, Charge-relaxation and dwell time in the fluctuating admittance of a chaotic cavity, Europhys. Lett. **37**(7), 441 (1997).

[57] P. W. Brouwer, K. M. Frahm, and C. W. J. Beenakker, Quantum Mechanical Time-Delay Matrix in Chaotic Scattering, Phys. Rev. Lett. **78**, 4737–4740 (1997).

[58] P. W. Brouwer, K. M. Frahm, and C. W. J. Beenakker, Distribution of the quantum mechanical time-delay matrix for a chaotic cavity, Waves in Random Media **9**, 91–104 (1999).

[59] P. W. Brouwer, A. Furusaki, I. A. Gruzberg, and C. Mudry, Localization and Delocalization in Dirty Superconducting Wires, Phys. Rev. Lett. **85**, 1064–1067 (2000).

[60] P. W. Brouwer, A. Furusaki, and C. Mudry, Universality of delocalization in unconventional dirty superconducting wires with broken spin-rotation symmetry, Phys. Rev. B **67**, 014530 (2003).

[61] P. W. Brouwer, C. Mudry, and A. Furusaki, Density of States in Coupled Chains with Off-Diagonal Disorder, Phys. Rev. Lett. **84**, 2913–2916 (2000).

[62] P. W. Brouwer, C. Mudry, B. D. Simons, and A. Altland, Delocalization in Coupled One-Dimensional Chains, Phys. Rev. Lett. **81**, 862–865 (1998).

[63] P. W. Brouwer, E. Racine, A. Furusaki, Y. Hatsugai, Y. Morita, and C. Mudry, Zero modes in the random hopping model, Phys. Rev. B **66**, 014204 (2002).

[64] P. Brouwer, *On the random matrix theory of quantum transport*, PhD thesis, Leiden University, 1997.

[65] P. Brouwer, C. Mudry, and A. Furusaki, Nonuniversality in quantum wires with off-diagonal disorder: a geometric point of view, Nucl. Phys. B **565**(3), 653 – 663 (2000).

[66] P. Brouwer, C. Mudry, and A. Furusaki, Transport properties and density of states of quantum wires with off-diagonal disorder, Physica E **9**(3), 333 – 339 (2001), Proceedings of an International Workshop and Seminar on the Dynamics of Complex Systems.

[67] J. Bun, *Application of Random Matrix Theory to High Dimensional Statistics*, PhD thesis, Université Paris-Saclay, 2016.

[68] J. Bun, J.-P. Bouchaud, and M. Potters, Cleaning large correlation matrices: Tools from Random Matrix Theory, Phys. Rep. **666**, 1 – 109 (2017), Cleaning large correlation matrices: tools from random matrix theory.

[69] R. W. Butler and A. T. Wood, Laplace approximation for Bessel functions of matrix argument, J. Comput. Appl. Math. **155**(2), 359 – 382 (2003).

[70] M. Büttiker, Absence of backscattering in the quantum Hall effect in multiprobe conductors, Phys. Rev. B **38**, 9375–9389 (1988).

[71] M. Büttiker, Scattering theory of current and intensity noise correlations in conductors and wave guides, Phys. Rev. B **46**, 12485–12507 (1992).

[72] M. Büttiker and T. Christen, Admittance and Nonlinear Transport in Quantum Wires, Point Contacts, and Resonant Tunneling Barriers, in *Mesoscopic Electron Transport*, edited by L. L. Sohn, L. P. Kouwenhoven, and G. Schön, pages 259–289, Dordrecht, 1997, Springer Netherlands.

[73] M. Büttiker, A. Prêtre, and H. Thomas, Dynamic conductance and the scattering matrix of small conductors, Phys. Rev. Lett. **70**, 4114–4117 (1993).

[74] M. Büttiker, H. Thomas, and A. Prêtre, Mesoscopic capacitors, Phys. Lett. A **180**(4), 364 – 369 (1993).

[75] M. Büttiker, H. Thomas, and A. Prêtre, Current partition in multiprobe conductors in the presence of slowly oscillating external potentials, Z. Phys. B **94**(1), 133–137 (1994).

[76] M. Büttiker, Chapter 4: The Quantum Hall Effect in Open Conductors, in *Semiconductors and Semimetals*, edited by M. Reed, volume 35, pages 191 – 277, Elsevier, 1992.

[77] P. Calabrese, P. Le Doussal, and S. N. Majumdar, Random matrices and entanglement entropy of trapped Fermi gases, Phys. Rev. A **91**, 012303 (2015).

[78] M. Caselle, Distribution of Transmission Eigenvalues in Disordered Wires, Phys. Rev. Lett. **74**, 2776–2779 (1995).

[79] M. Caselle, A new classification scheme for random matrix theories, arXiv cond-mat/9610017 (1996).

[80] C. Charlier and T. Claeys, Thinning and conditioning of the circular unitary ensemble, Random Matrices: Theory Appl. **06**(02), 1750007 (2017).

[81] L. Chekhov, Matrix models with hard walls: geometry and solutions, J. Phys. A **39**(28), 8857 (2006).

[82] L. Chekhov and B. Eynard, Hermitian matrix model free energy: Feynman graph technique for all genera, J. High Energy Phys. **2006**(03), 014 (2006).

[83] B. Collins, Moments and cumulants of polynomial random variables on unitary groups, the Itzykson-Zuber integral, and free probability, Int. Math. Res. Notices **2003**(17), 953–982 (2003).

[84] A. Comtet, J.-M. Luck, C. Texier, and Y. Tourigny, The Lyapunov Exponent of Products of Random 2×2 Matrices Close to the Identity, J. Stat. Phys. **150**(1), 13–65 (2013).

[85] A. Comtet, C. Texier, and Y. Tourigny, Products of random matrices and generalised quantum point scatterers, J. Stat. Phys. **140**, 426–466 (2010).

[86] A. Comtet, C. Texier, and Y. Tourigny, Supersymmetric quantum mechanics with Levy disorder in one dimension, J. Stat. Phys. **145**, 1291–1323 (2011).

[87] J. B. Conrey, L-Functions and Random Matrices, in *Mathematics Unlimited — 2001 and Beyond*, edited by B. Engquist and W. Schmid, pages 331–352, Berlin, Heidelberg, 2001, Springer.

[88] F. D. Cunden, P. Facchi, and P. Vivo, Joint statistics of quantum transport in chaotic cavities, Europhys. Lett. **110**(5), 50002 (2015).

[89] F. D. Cunden, P. Facchi, and P. Vivo, A shortcut through the Coulomb gas method for spectral linear statistics on random matrices, J. Phys. A **49**(13), 135202 (2016).

[90] F. D. Cunden, A. Maltsev, and F. Mezzadri, Fluctuations in the two-dimensional one-component plasma and associated fourth-order phase transition, Phys. Rev. E **91**, 060105 (2015).

[91] F. D. Cunden, F. Mezzadri, and N. O'Connell, Free fermions and the classical compact groups, arXiv preprint arXiv:1705.05932 (2017).

[92] F. D. Cunden, F. Mezzadri, N. Simm, and P. Vivo, Correlators for the Wigner-Smith time-delay matrix of chaotic cavities, J. Phys. A **49**(18), 18LT01 (2016).

[93] F. D. Cunden and P. Vivo, Universal Covariance Formula for Linear Statistics on Random Matrices, Phys. Rev. Lett. **113**, 070202 (2014).

[94] K. Damle, S. N. Majumdar, V. Tripathi, and P. Vivo, Phase transitions in the distribution of the Andreev conductance of superconductor-metal junctions with multiple transverse modes, Phys. Rev. Lett. **107**, 177206 (2011).

[95] R. Dashen, S.-k. Ma, and H. J. Bernstein, *S*-Matrix Formulation of Statistical Mechanics, Phys. Rev. **187**, 345–370 (1969).

[96] N. G. De Bruijn, On some multiple integrals involving determinants, J. Indian Math. Soc **19**, 133–151 (1955).

[97] C. de Carvalho and H. Nussenzveig, Time delay, Phys. Rep. **364**(2), 83 – 174 (2002).

[98] P. G. de Gennes, Soluble Model for Fibrous Structures with Steric Constraints, J. Chem. Phys. **48**, 2257 (1968).

[99] A. De Pasquale, P. Facchi, G. Parisi, S. Pascazio, and A. Scardicchio, Phase transitions and metastability in the distribution of the bipartite entanglement of a large quantum system, Phys. Rev. A **81**, 052324 (2010).

[100] D. S. Dean, P. L. Doussal, S. N. Majumdar, and G. Schehr, Universal ground-state properties of free fermions in a d -dimensional trap, Europhys. Lett. **112**(6), 60001 (2015).

[101] D. S. Dean and S. N. Majumdar, Large Deviations of Extreme Eigenvalues of Random Matrices, Phys. Rev. Lett. **97**, 160201 (2006).

[102] D. S. Dean and S. N. Majumdar, Extreme value statistics of eigenvalues of Gaussian random matrices, Phys. Rev. E **77**, 041108 (2008).

[103] L. Dieci, M. S. Jolly, and E. S. V. Vleck, Numerical Techniques for Approximating Lyapunov Exponents and Their Implementation, J. Comput. Nonlinear Dynam. **6**(1), 011003 (2010).

[104] L. Dieci and E. S. V. Vleck, Computation of a few Lyapunov exponents for continuous and discrete dynamical systems, Appl. Numer. Math. **17**(3), 275 – 291 (1995), Special Issue on Numerical Methods for Ordinary Differential Equations.

[105] B. Diu, C. Guthmann, D. Lederer, and B. Roulet, *Physique statistique*, Hermann, Paris, 1989.

[106] O. N. Dorokhov, Solvable model of multichannel localization, Phys. Rev. B **37**, 10526–10541 (1988).

[107] O. Dorokhov, Localization and transmission coefficient for two coupled metal chains with disorder, Solid State Comm. **44**(6), 915–919 (1982).

[108] O. Dorokhov, Transmission coefficient and the localization length of an electron in N bound disordered chains, JETP Lett. **36**(7), 318–321 (1982).

[109] O. Dorokhov, Electron localization in a multichannel conductor, Sov. Phys. JETP **58**, 606–615 (1983).

[110] A. Douglas, P. Markoš, and K. A. Muttalib, The generalized DMPK equation revisited: towards a systematic derivation, J. Phys. A **47**(12), 125103 (2014).

[111] A. Douglas and K. A. Muttalib, Distribution of conductance for Anderson insulators: A theory with a single parameter, Phys. Rev. B **80**, 161102 (2009).

[112] A. Douglas and K. A. Muttalib, Conductance distribution in three dimensions: Analytic solution of the generalized Dorokhov-Mello-Pereyra-Kumar equation in the strongly disordered regime, Phys. Rev. B **82**, 035121 (2010).

[113] I. Dumitriu and A. Edelman, Matrix models for beta ensembles, J. Math. Phys. **43**(11), 5830–5847 (2002).

[114] F. J. Dyson, A Brownian-Motion Model for the Eigenvalues of a Random Matrix, J. Math. Phys. **3**(6), 1191–1198 (1962).

[115] F. J. Dyson, Statistical Theory of the Energy Levels of Complex Systems. I, J. Math. Phys. **3**(1), 140–156 (1962),
F. J. Dyson, Statistical Theory of the Energy Levels of Complex Systems. II, J. Math. Phys. **3**(1), 157–165 (1962),
F. J. Dyson,Statistical Theory of the Energy Levels of Complex Systems. III, J. Math. Phys. **3**(1), 166–175 (1962).

[116] F. J. Dyson, The Threefold Way. Algebraic Structure of Symmetry Groups and Ensembles in Quantum Mechanics, J. Math. Phys. **3**, 1199–1215 (1962).

[117] F. J. Dyson and M. L. Mehta, Statistical Theory of the Energy Levels of Complex Systems. IV, J. Math. Phys. **4**(5), 701–712 (1963).

[118] K. B. Efetov, *Supersymmetry in chaos and disorder*, Cambridge University Press, 1997.

[119] K. B. Efetov and A. I. Larkin, Kinetics of a quantum particle in long metallic wires, Sov. Phys. JETP **85**, 764–778 (1983).

[120] R. S. Ellis, Large Deviations for a General Class of Random Vectors, Ann. Probab. **12**(1), 1–12 (1984).

[121] N. M. Ercolani and K. D. T.-R. McLaughlin, Asymptotics of the partition function for random matrices via Riemann-Hilbert techniques and applications to graphical enumeration, Int. Math. Res. Notices **2003**(14), 755–820 (2003).

[122] F. Evers and A. D. Mirlin, Anderson transitions, Rev. Mod. Phys. **80**, 1355–1417 (2008).

[123] B. Eynard, Topological expansion for the 1-hermitian matrix model correlation functions, J. High Energy Phys. **2004**(11), 031 (2004).

[124] B. Eynard and N. Orantin, Invariants of algebraic curves and topological expansion, Commun. Number Theory Phys. **1**(2), 347–452 (2007).

[125] P. Facchi, U. Marzolino, G. Parisi, S. Pascazio, and A. Scardicchio, Phase Transitions of Bipartite Entanglement, Phys. Rev. Lett. **101**, 050502 (2008).

[126] P. Facchi, G. Florio, G. Parisi, S. Pascazio, and K. Yuasa, Entropy-driven phase transitions of entanglement, Phys. Rev. A **87**, 052324 (2013).

[127] G. Fève, P. Degiovanni, and T. Jolicoeur, Quantum detection of electronic flying qubits in the integer quantum Hall regime, Phys. Rev. B **77**, 035308 (2008).

[128] G. Fève, *Quantization of the AC current : the quantum dot as a subnanosecond single electron source*, PhD thesis, Université Pierre et Marie Curie - Paris VI, 2006.

[129] D. S. Fisher, Random antiferromagnetic quantum spin chains, Phys. Rev. B **50**, 3799–3821 (1994).

[130] D. S. Fisher, Critical behavior of random transverse-field Ising spin chains, Phys. Rev. B **51**, 6411–6461 (1995).

[131] D. S. Fisher, P. Le Doussal, and C. Monthus, Random Walks, Reaction-Diffusion, and Nonequilibrium Dynamics of Spin Chains in One-Dimensional Random Environments, Phys. Rev. Lett. **80**, 3539–3542 (1998).

[132] D. S. Fisher and P. A. Lee, Relation between conductivity and transmission matrix, Phys. Rev. B **23**, 6851–6854 (1981).

[133] D. S. Fisher and A. P. Young, Distributions of gaps and end-to-end correlations in random transverse-field Ising spin chains, Phys. Rev. B **58**, 9131–9141 (1998).

[134] M. E. Fisher, Walks, Walls, Wetting, and Melting, J. Stat. Phys. **34**, 667 (1984).

[135] P. J. Forrester, *Log-gases and random matrices*, Princeton University Press, 2010.

[136] P. J. Forrester, Meet Andréief, Bordeaux 1886, and Andreev, Kharkov 1882-83, arXiv preprint arXiv:1806.10411 (2018).

[137] J. Friedel, XIV. The distribution of electrons round impurities in monovalent metals, Phil. Mag. **43**(337), 153–189 (1952).

[138] J. Friedel, Metallic alloys, Nuovo Cimento Suppl. **7**(2), 287–311 (1958).

[139] H. L. Frisch and S. P. Lloyd, Electron Levels in a One-Dimensional Random Lattice, Phys. Rev. **120**, 1175–1189 (1960).

[140] Y. V. Fyodorov and D. V. Savin, Resonance scattering of waves in chaotic systems, in *The Oxford handbook of random matrix theory*, edited by G. Akemann, J. Baik, and P. Di Francesco, pages 703–722, Oxford University Press, 2011.

[141] Y. V. Fyodorov, D. V. Savin, and H.-J. Sommers, Scattering, reflection and impedance of waves in chaotic and disordered systems with absorption, J. Phys. A **38**(49), 10731 (2005).

[142] Y. V. Fyodorov, H.-J. Sommers, and I. Williams, Density of stationary points in a high dimensional random energy landscape and the onset of glassy behavior, JETP Lett. **85**(5), 261–266 (2007).

[143] Y. V. Fyodorov and A. D. Mirlin, Statistical properties of eigenfunctions of random quasi 1D one-particle Hamiltonians, Int. J. Mod. Phys. B **08**(27), 3795–3842 (1994).

[144] Y. V. Fyodorov and C. Nadal, Critical Behavior of the Number of Minima of a Random Landscape at the Glass Transition Point and the Tracy-Widom Distribution, Phys. Rev. Lett. **109**, 167203 (2012).

[145] Y. V. Fyodorov and A. Ossipov, Distribution of the Local Density of States, Reflection Coefficient, and Wigner Delay Time in Absorbing Ergodic Systems at the Point of Chiral Symmetry, Phys. Rev. Lett. **92**, 084103 (2004).

[146] Y. V. Fyodorov, D. V. Savin, and H.-J. Sommers, Parametric correlations of phase shifts and statistics of time delays in quantum chaotic scattering: Crossover between unitary and orthogonal symmetries, Phys. Rev. E **55**, R4857–R4860 (1997).

[147] Y. V. Fyodorov and H.-J. Sommers, Parametric Correlations of Scattering Phase Shifts and Fluctuations of Delay Times in Few-Channel Chaotic Scattering, Phys. Rev. Lett. **76**, 4709–4712 (1996).

[148] Y. V. Fyodorov and H.-J. Sommers, Statistics of resonance poles, phase shifts and time delays in quantum chaotic scattering: Random matrix approach for systems with broken time-reversal invariance, J. Math. Phys. **38**(4), 1918–1981 (1997).

[149] Y. V. Fyodorov and I. Williams, Replica Symmetry Breaking Condition Exposed by Random Matrix Calculation of Landscape Complexity, J. Stat. Phys. **129**(5), 1081–1116 (2007).

[150] J. Gabelli, G. Fève, J.-M. Berroir, B. Plaçais, A. Cavanna, B. Etienne, Y. Jin, and D. C. Glattli, Violation of Kirchhoff's Laws for a Coherent RC Circuit, Science **313**(5786), 499–502 (2006).

[151] J. Gabelli, *Evidence of quantum coherence in dynamical electronic transport*, PhD thesis, Université Pierre et Marie Curie - Paris VI, 2006.

[152] R. Gade, Anderson localization for sublattice models, Nuclear Physics B **398**(3), 499 – 515 (1993).

[153] R. Gade and F. Wegner, The n = 0 replica limit of U(n) and U(n)SO(n) models, Nucl. Phys. B **360**(2), 213 – 218 (1991).

[154] A. García-Martín and J. J. Sáenz, Universal Conductance Distributions in the Crossover between Diffusive and Localization Regimes, Phys. Rev. Lett. **87**, 116603 (2001).

[155] C. Gardiner, *Stochastic Methods*, Springer-Verlag Berlin Heidelberg, 4th edition, 2009.

[156] A. Gogolin, Electron localization and hopping conductivity in one-dimensional disordered systems, Phys. Rep. **86**(1), 1 – 53 (1982).

[157] A. Gogolin and V. Mel'Nikov, Conductivity of disordered one-dimensional metal with half-filled band, Zh. Eksp. Teor. Fiz **73**, 706–720 (1977).

[158] A. O. Golosov, Localization of random walks in one-dimensional random environments, Commun. Math. Phys. **92**(4), 491–506 (1984).

[159] V. A. Gopar, P. A. Mello, and M. Büttiker, Mesoscopic Capacitors: A Statistical Analysis, Phys. Rev. Lett. **77**, 3005–3008 (1996).

[160] A. Grabsch, S. N. Majumdar, and C. Texier, Truncated Linear Statistics Associated with the Eigenvalues of Random Matrices II. Partial Sums over Proper Time Delays for Chaotic Quantum Dots, J. Stat. Phys. **167**(6), 1452–1488 (2017).

[161] A. Grabsch, S. N. Majumdar, and C. Texier, Truncated Linear Statistics Associated with the Top Eigenvalues of Random Matrices, J. Stat. Phys. **167**(2), 234–259 (2017), updated version arXiv:1609.08296.

[162] A. Grabsch, D. V. Savin, and C. Texier, Wigner-Smith time-delay matrix in chaotic cavities with non-ideal contacts, preprint arXiv:1804.09580 (2018).

[163] A. Grabsch and C. Texier, Capacitance and charge relaxation resistance of chaotic cavities —Joint distribution of two linear statistics in the Laguerre ensemble of random matrices, Europhys. Lett. **109**(5), 50004 (2015).

[164] A. Grabsch and C. Texier, Distribution of spectral linear statistics on random matrices beyond the large deviation function – Wigner time delay in multichannel disordered wires, J. Phys. A **49**, 465002 (2016).

[165] A. Grabsch, C. Texier, and Y. Tourigny, One-dimensional disordered quantum mechanics and Sinai diffusion with random absorbers, J. Stat. Phys. **155**, 237–276 (2014).

[166] I. S. Gradshteyn and I. M. Ryzhik, *Table of integrals, series and products*, 5th Edition (Academic Press), 1994.

[167] D. J. Gross and E. Witten, Possible third-order phase transition in the large-N lattice gauge theory, Phys. Rev. D **21**, 446–453 (1980).

[168] I. A. Gruzberg, N. Read, and S. Vishveshwara, Localization in disordered superconducting wires with broken spin-rotation symmetry, Phys. Rev. B **71**, 245124 (2005).

[169] T. Guhr, A. Müller-Groeling, and H. A. Weidenmüller, Random-matrix theories in quantum physics: common concepts, Phys. Rep. **299**(4/6), 189–425 (1998).

[170] J. Gärtner, On Large Deviations from the Invariant Measure, Theory Proba. Appl. **22**(1), 24–39 (1977).

[171] B. Hall, *Lie groups, Lie algebras, and representations: an elementary introduction*, volume 222, Springer, 2015, see also arXiv:math-ph/0005032.

[172] B. I. Halperin, Quantized Hall conductance, current-carrying edge states, and the existence of extended states in a two-dimensional disordered potential, Phys. Rev. B **25**, 2185–2190 (1982).

[173] B. I. Halperin, Green's Functions for a Particle in a One-Dimensional Random Potential, Phys. Rev. **139**, 104–117 (1965).

[174] Harish-Chandra, Differential Operators on a Semisimple Lie Algebra, Am. J. Math. **79**(1), 87–120 (1957).

[175] D. C. Herbert and R. Jones, Localized states in disordered systems, J. Phys. C **4**(10), 1145 (1971).

[176] C. S. Herz, Bessel functions of matrix argument, Ann. of Math. (2) **61**(3), 474–523 (1955).

[177] P. P. Hofer, D. Dasenbrook, and C. Flindt, Electron waiting times for the mesoscopic capacitor, Physica E **82**, 3 – 11 (2016), Frontiers in quantum electronic transport - In memory of Markus Büttiker.

[178] G. Hooft, A planar diagram theory for strong interactions, Nucl. Phys. B **72**(3), 461 – 473 (1974).

[179] C. Itzykson and J.-B. Zuber, The planar approximation. II, J. Math. Phys. **21**(3), 411–421 (1980).

[180] R. A. Jalabert, J.-L. Pichard, and C. W. J. Beenakker, Universal Quantum Signatures of Chaos in Ballistic Transport, Europhys. Lett. **27**(4), 255 (1994).

[181] B. Jancovici and P. J. Forrester, Derivation of an asymptotic expression in Beenakker's general fluctuation formula for random-matrix correlations near an edge, Phys. Rev. B **50**, 14599–14600 (1994).

[182] M. Janßen, O. Viehweger, U. Fastenrath, and J. Hajdu, *Introduction to the Theory of the Integer Quantum Hall Effect: Edited by J. Hajdu*, Wiley-VCH, 1994.

[183] K. Johansson, From Gumbel to Tracy-Widom, Probab. Theory Rel. **138**(1), 75–112 (2007).

[184] G. Junker, *Supersymmetric methods in quantum and statistical physics*, Springer-Verlag Berlin Heidelberg, 1996.

[185] V. A. Kaimanovich, Lyapunov exponents, symmetric spaces, and a multiplicative ergodic theorem for semisimple Lie groups, J. Sov. Math. **47**(2), 2387–2398 (1989).

[186] A. Karadimitrakis, A. L. Moustakas, and P. Vivo, Outage Capacity for the Optical MIMO Channel, IEEE Trans. Info. Theo. **60**(7), 4370–4382 (2014).

[187] P. Kazakopoulos, P. Mertikopoulos, A. L. Moustakas, and G. Caire, Living at the Edge: A Large Deviations Approach to the Outage MIMO Capacity, IEEE Trans. Info. Theo. **57**(4), 1984–2007 (2011).

[188] J. P. Keating, Random matrices and number theory, in *Applications of Random Matrices in Physics*, edited by É. Brézin, V. Kazakov, D. Serban, P. Wiegmann, and A. Zabrodin, pages 1–32, Dordrecht, 2006, Springer Netherlands.

[189] J. P. Keating and N. C. Snaith, Random matrices and L-functions, J. Phys. A **36**(12), 2859 (2003).

[190] H. Kesten, The limit distribution of Sinai's random walk in random environment, Physica A **138**(1), 299 – 309 (1986).

[191] B. A. Khoruzhenko, D. V. Savin, and H.-J. Sommers, Systematic approach to statistics of conductance and shot-noise in chaotic cavities, Phys. Rev. B **80**, 125301 (2009).

[192] A. Y. Kitaev, Unpaired Majorana fermions in quantum wires, Phys. Usp. **44**(10S), 131 (2001).

[193] A. Kitaev, Periodic table for topological insulators and superconductors, AIP Conference Proceedings **1134**(1), 22–30 (2009).

[194] T. Kottos, Statistics of resonances and delay times in random media: beyond random matrix theory, J. Phys. A **38**(49), 10761 (2005).

[195] B. Kramer and A. MacKinnon, Localization: theory and experiment, Rep. Prog. Phys. **56**(12), 1469 (1993).

[196] M. G. Krein, On the trace formula in perturbation theory, Matem. Sbornik **33**, 597–626 (1953).

[197] J. Lacroix, Computations of the sum of positive Lyapunov exponents for the Lloyd model in a strip, in *Lyapunov Exponents*, edited by L. Arnold and V. Wihstutz, pages 258–264, Berlin, Heidelberg, 1986, Springer Berlin Heidelberg.

[198] B. Lacroix-A-Chez-Toine, P. L. Doussal, S. N. Majumdar, and G. Schehr, Statistics of fermions in a d-dimensional box near a hard wall, Europhys. Lett. **120**(1), 10006 (2017).

[199] G. Lambert, Incomplete determinantal processes: from random matrix to Poisson statistics, preprint arXiv:1612.00806 (2016).

[200] R. Landauer, Spatial Variation of Currents and Fields Due to Localized Scatterers in Metallic Conduction, IBM J. Res. Dev. **1**(3), 223–231 (1957).

[201] P. Le Doussal, C. Monthus, and D. S. Fisher, Random walkers in one-dimensional random environments: Exact renormalization group analysis, Phys. Rev. E **59**, 4795–4840 (1999).

[202] Y. Le Jan, On isotropic Brownian motions, Z. Wahrsch. Verw. Geb. **70**(4), 609–620 (1985).

[203] N. Lehmann, D. V. Savin, V. V. Sokolov, and H.-J. Sommers, Time delay correlations in chaotic scattering: random matrix approach, Physica D **86**, 572–585 (1995).

[204] I. M. l. Lifshits, S. A. Gredeskul, and L. A. Pastur, *Introduction to the theory of disordered systems*, Wiley-Interscience, 1988.

[205] H. I. Liou, H. S. Camarda, S. Wynchank, M. Slagowitz, G. Hacken, F. Rahn, and J. Rainwater, Neutron-Resonance Spectroscopy. VIII. The Separated Isotopes of Erbium: Evidence for Dyson's Theory Concerning Level Spacings, Phys. Rev. C **5**, 974–1001 (1972).

[206] J.-M. Luck, *Systèmes désordonnés unidimentionnels*, Collection Aléa-Saclay, Commissariat à l'énergie atomique, 1992.

[207] A. W. W. Ludwig, M. P. A. Fisher, R. Shankar, and G. Grinstein, Integer quantum Hall transition: An alternative approach and exact results, Phys. Rev. B **50**, 7526–7552 (1994).

[208] A. W. W. Ludwig, H. Schulz-Baldes, and M. Stolz, Lyapunov Spectra for All Ten Symmetry Classes of Quasi-one-dimensional Disordered Systems of Non-interacting Fermions, J. Stat. Phys. **152**(2), 275–304 (2013).

[209] C. Mahaux and H. A. Weidenmüller, *Shell-Model Approach to Nuclear Reactions.*, North-Holland, Amsterdam, 1969.

[210] S. N. Majumdar, C. Nadal, A. Scardicchio, and P. Vivo, Index distribution of Gaussian random matrices, Phys. Rev. Lett. **103**, 220603 (2009).

[211] S. N. Majumdar, C. Nadal, A. Scardicchio, and P. Vivo, How many eigenvalues of a Gaussian random matrix are positive?, Phys. Rev. E **83**, 041105 (2011).

[212] S. N. Majumdar and G. Schehr, Top eigenvalue of a random matrix: large deviations and third order phase transition, J. Stat. Mech. **2014**(1), P01012 (2014).

[213] S. N. Majumdar and M. Vergassola, Large deviations of the maximum eigenvalue for Wishart and Gaussian random matrices, Phys. Rev. Lett. **102**, 060601 (2009).

[214] S. N. Majumdar and P. Vivo, Number of Relevant Directions in Principal Component Analysis and Wishart Random Matrices, Phys. Rev. Lett. **108**, 200601 (2012).

[215] M. Marciani, P. W. Brouwer, and C. W. J. Beenakker, Time-delay matrix, midgap spectral peak, and thermopower of an Andreev billiard, Phys. Rev. B **90**, 045403 (2014).

[216] R. Marino, *Number statistics in random matrices and applications to quantum systems*, PhD thesis, Université Paris Saclay, 2015.

[217] R. Marino, S. N. Majumdar, G. Schehr, and P. Vivo, Index distribution of Cauchy random matrices, J. Phys. A **47**(5), 055001 (2014).

[218] R. Marino, S. N. Majumdar, G. Schehr, and P. Vivo, Phase Transitions and Edge Scaling of Number Variance in Gaussian Random Matrices, Phys. Rev. Lett. **112**, 254101 (2014).

[219] R. Marino, S. N. Majumdar, G. Schehr, and P. Vivo, Number statistics for β-ensembles of random matrices: applications to trapped fermions at zero temperature, Phys. Rev. E **94**, 032115 (2016).

[220] T. Martin and R. Landauer, Wave-packet approach to noise in multichannel mesoscopic systems, Phys. Rev. B **45**, 1742–1755 (1992).

[221] V. A. Marčenko and L. A. Pastur, Distribution of eigenvalues for some sets of random matrices, Math. USSR-Sb **1**(4), 457 (1967).

[222] A. M. Mathai, *Jacobians of Matrix Transformations and Functions of Matrix Arguments*, World Scientific, 1997.

[223] R. H. McKenzie, Exact Results for Quantum Phase Transitions in Random XY Spin Chains, Phys. Rev. Lett. **77**, 4804–4807 (1996).

[224] M. L. Mehta, *Random matrices*, Elsevier, Academic, New York, third edition, 2004.

[225] M. L. Mehta and A. Pandey, On some Gaussian ensembles of Hermitian matrices, J. Phys. A **16**(12), 2655 (1983).

[226] P. A. Mello and H. U. Baranger, Interference phenomena in electronic transport through chaotic cavities: An information-theoretic approach, Waves Random Media **9**, 105–162 (1999).

[227] P. Mello, P. Pereyra, and N. Kumar, Macroscopic approach to multichannel disordered conductors, Ann. Phys. **181**(2), 290 – 317 (1988).

[228] P. A. Mello, Macroscopic approach to universal conductance fluctuations in disordered metals, Phys. Rev. Lett. **60**, 1089–1092 (1988).

[229] P. A. Mello and N. Kumar, *Quantum transport in mesoscopic systems – Complexity and statistical fluctuations*, Oxford University Press, 2004.

[230] P. A. Mello, P. Pereyra, and T. H. Seligman, Information theory and statistical nuclear reactions. I. General theory and applications to few-channel problems, Ann. Phys. **161**(2), 254 – 275 (1985).

[231] P. A. Mello and S. Tomsovic, Scattering approach to quantum transport: Toward a consistent physical picture, Phys. Rev. Lett. **67**, 342–345 (1991).

[232] F. Mezzadri and N. J. Simm, Tau-Function Theory of Quantum Chaotic Transport with beta=1,2,4, Commun. Math. Phys. **324**, 465–513 (2013).

[233] A. Migdal, Loop equations and 1/N expansion, Phys. Rep. **102**(4), 199 – 290 (1983).

[234] A. Mirlin, A. Mullergroeling, and M. Zirnbauer, Conductance Fluctuations of Disordered Wires: Fourier Analysis on Supersymmetric Spaces, Ann. Phys. **236**(2), 325 – 373 (1994).

[235] A. D. Mirlin, Statistics of energy levels and eigenfunctions in disordered systems, Phys. Rep. **326**(5), 259 – 382 (2000).

[236] L. G. Molinari, Identities and exponential bounds for transfer matrices, J. Phys. A **46**(25), 254004 (2013).

[237] H. L. Montgomery, The pair correlation of zeros of the zeta function, in *Proc. Symp. Pure Math*, volume 24, pages 181–193, 1973.

[238] C. Monthus and P. Le Doussal, Localization of thermal packets and metastable states in the Sinai model, Phys. Rev. E **65**, 066129 (2002).

[239] T. Morimoto, A. Furusaki, and C. Mudry, Anderson localization and the topology of classifying spaces, Phys. Rev. B **91**, 235111 (2015).

[240] O. Motrunich, K. Damle, and D. A. Huse, Griffiths effects and quantum critical points in dirty superconductors without spin-rotation invariance: One-dimensional examples, Phys. Rev. B **63**, 224204 (2001).

[241] A. L. Moustakas, S. H. Simon, and A. M. Sengupta, MIMO capacity through correlated channels in the presence of correlated interferers and noise: a (not so) large N analysis, IEEE Trans. Info. Theo. **49**(10), 2545–2561 (2003).

[242] C. Mudry, P. W. Brouwer, and A. Furusaki, Random magnetic flux problem in a quantum wire, Phys. Rev. B **59**, 13221–13234 (1999).

[243] C. Mudry, P. W. Brouwer, and A. Furusaki, Crossover from the chiral to the standard universality classes in the conductance of a quantum wire with random hopping only, Phys. Rev. B **62**, 8249–8268 (2000).

[244] R. J. Muirhead, *Aspects of Multivariate Statistical Theory*, Wiley, New York, 1982.

[245] K. A. Muttalib and V. A. Gopar, Generalization of the DMPK equation beyond quasi one dimension, Phys. Rev. B **66**, 115318 (2002).

[246] K. A. Muttalib and J. R. Klauder, Generalized Fokker-Planck Equation for Multichannel Disordered Quantum Conductors, Phys. Rev. Lett. **82**, 4272–4275 (1999).

[247] K. A. Muttalib, P. Markoš, and P. Wölfle, Conductance distribution in strongly disordered mesoscopic systems in three dimensions, Phys. Rev. B **72**, 125317 (2005).

[248] C. Nadal, *Matrices aléatoires et leurs applications à la physique statistique et physique quantique*, PhD thesis, Université Paris-Sud, 2011.

[249] C. Nadal and S. N. Majumdar, Nonintersecting Brownian interfaces and Wishart random matrices, Phys. Rev. E **79**, 061117 (2009).

[250] C. Nadal, S. N. Majumdar, and M. Vergassola, Phase Transitions in the Distribution of Bipartite Entanglement of a Random Pure State, Phys. Rev. Lett. **104**, 110501 (2010).

[251] C. Nadal, S. N. Majumdar, and M. Vergassola, Statistical Distribution of Quantum Entanglement for a Random Bipartite State, J. Stat. Phys. **142**(2), 403–438 (2011).

[252] C. M. Newman, The distribution of Lyapunov exponents: Exact results for random matrices, Commun. Math. Phys. **103**(1), 121–126 (1986).

[253] A. Niemi and G. Semenoff, Fermion number fractionization in quantum field theory, Phys. Rep. **135**(3), 99 – 193 (1986).

[254] B. Oksendal, *Stochastic Differential Equations: An Introduction with Applications*, Hochschultext / Universitext, Springer, 2003.

[255] Y. Oreg, G. Refael, and F. von Oppen, Helical Liquids and Majorana Bound States in Quantum Wires, Phys. Rev. Lett. **105**, 177002 (2010).

[256] V. I. Oseledec, A multiplicative ergodic theorem. Characteristic Ljapunov, exponents of dynamical systems, Tr. Mosk. Mat. Obs. **19**, 179–210 (1968).

[257] A. Ossipov and Y. V. Fyodorov, Statistics of delay times in mesoscopic systems as a manifestation of eigenfunction fluctuations, Phys. Rev. B **71**, 125133 (2005).

[258] D. N. Page, Average entropy of a subsystem, Phys. Rev. Lett. **71**, 1291–1294 (1993).

[259] A. Pandey and M. L. Mehta, Gaussian ensembles of random hermitian matrices intermediate between orthogonal and unitary ones, Commun. Math. Phys. **87**(4), 449–468 (1983).

[260] R. K. Pathria and P. D. Beale, *Statistical mechanics*, Academic Press, Elsevier, 2011, 3rd edition.

[261] N. Pavloff and N. Sator, *Physique statistique*, Vuibert, 2016.

[262] K. B. Petersen and M. S. Pedersen, *The Matrix Cookbook*, 2012.

[263] C. E. Porter and N. Rosenzweig, Statistical properties of atomic and nuclear spectra, Ann. Acad. Sci. Fennicae, Serie A, VI Physica **44**, 1–66 (1960).

[264] A. C. Potter and P. A. Lee, Multichannel Generalization of Kitaev's Majorana End States and a Practical Route to Realize Them in Thin Films, Phys. Rev. Lett. **105**, 227003 (2010).

[265] A. Prêtre, H. Thomas, and M. Büttiker, Dynamic admittance of mesoscopic conductors: Discrete-potential model, Phys. Rev. B **54**, 8130–8143 (1996).

[266] K. Ramola and C. Texier, Fluctuations of Random Matrix Products and 1D Dirac Equation with Random Mass, J. Stat. Phys. **157**(3), 497–514 (2014).

[267] M.-T. Rieder and P. W. Brouwer, Density of states at disorder-induced phase transitions in a multichannel Majorana wire, Phys. Rev. B **90**, 205404 (2014).

[268] M.-T. Rieder, P. W. Brouwer, and I. Adagideli, Reentrant topological phase transitions in a disordered spinless superconducting wire, Phys. Rev. B **88**, 060509 (2013).

[269] S. Ryu, A. P. Schnyder, A. Furusaki, and A. W. W. Ludwig, Topological insulators and superconductors: tenfold way and dimensional hierarchy, New J. Phys. **12**(6), 065010 (2010).

[270] D. V. Savin, Y. V. Fyodorov, and H.-J. Sommers, Reducing nonideal to ideal coupling in random matrix description of chaotic scattering: Application to the time-delay problem, Phys. Rev. E **63**, 035202 (2001).

[271] D. V. Savin and H.-J. Sommers, Delay times and reflection in chaotic cavities with absorption, Phys. Rev. E **68**, 036211 (2003).

[272] H. Schomerus, M. Marciani, and C. W. J. Beenakker, Effect of Chiral Symmetry on Chaotic Scattering from Majorana Zero Modes, Phys. Rev. Lett. **114**, 166803 (2015).

[273] A. Selberg, Berkninger om et multilet integral, Norsk, Mat. Tidsskr. **26**, 71–78 (1944).

[274] D. G. Shelton and A. M. Tsvelik, Effective theory for midgap states in doped spin-ladder and spin-Peierls systems: Liouville quantum mechanics, Phys. Rev. B **57**, 14242–14246 (1998).

[275] E. Shuryak and J. Verbaarschot, Random matrix theory and spectral sum rules for the Dirac operator in QCD, Nucl. Phys. A **560**(1), 306 – 320 (1993).

[276] Y. G. Sinai, Limiting behavior of a one-dimensional random walk in a random medium, Theor. Prob. Appl. **27**, 256–268 (1982).

[277] L. I. Smith, A tutorial on principal components analysis, 2002.

[278] H.-J. Sommers, W. Wieczorek, and D. V. Savin, Statistics of conductance and shot noise power for chaotic cavities, Acta Phys. Pol. A **112**, 691 (2007).

[279] H.-J. Sommers, D. V. Savin, and V. V. Sokolov, Distribution of Proper Delay Times in Quantum Chaotic Scattering: A Crossover from Ideal to Weak Coupling, Phys. Rev. Lett. **87**, 094101 (2001).

[280] M. Steiner, M. Fabrizio, and A. O. Gogolin, Random-mass Dirac fermions in doped spin-Peierls and spin-ladder systems: One-particle properties and boundary effects, Phys. Rev. B **57**, 8290–8306 (1998).

[281] H. Takayama, Y. R. Lin-Liu, and K. Maki, Continuum model for solitons in polyacetylene, Phys. Rev. B **21**, 2388–2393 (1980).

[282] C. Texier, *Quelques aspects du transport quantique dans les systèmes désordonnés de basse dimension*, PhD thesis, Université Paris-Sud, 1999.

[283] C. Texier, *Disorder, localisation and interaction. Quantum transport in metallic networks*, Habilitation à diriger des recherches, Université Paris-Sud, 2010.

[284] C. Texier, Wigner time delay and related concepts – Application to transport in coherent conductors, Physica E **82**, 16–33 (2016), Frontiers in quantum electronic transport - In memory of Markus Büttiker. See arXiv:1507.00075 for an updated version.

[285] C. Texier and C. Hagendorf, The effect of boundaries on the spectrum of a one-dimensional random mass Dirac Hamiltonian, J. Phys. A **43**(2), 025002 (2010).

[286] C. Texier and S. N. Majumdar, Wigner Time-Delay Distribution in Chaotic Cavities and Freezing Transition, Phys. Rev. Lett. **110**, 250602 (2013),
Erratum: Phys. Rev. Lett. **112**, 139902 (2014).

[287] C. Texier and G. Montambaux, Weak Localization in Multiterminal Networks of Diffusive Wires, Phys. Rev. Lett. **92**, 186801 (2004).

[288] C. Texier and G. Roux, *Physique statistique: des processus élémentaires aux phénomènes collectifs*, Dunod, Paris, 2017.

[289] D. J. Thouless, A relation between the density of states and range of localization for one dimensional random systems, J. Phys. C **5**(1), 77 (1972).

[290] D. J. Thouless, M. Kohmoto, M. P. Nightingale, and M. den Nijs, Quantized Hall Conductance in a Two-Dimensional Periodic Potential, Phys. Rev. Lett. **49**, 405–408 (1982).

[291] E. C. Titchmarsh, *Introduction to the theory of Fourier integrals*, Oxford University: Clarendon Press, 2nd edition, 1948.

[292] M. Titov, P. W. Brouwer, A. Furusaki, and C. Mudry, Fokker-Planck equations and density of states in disordered quantum wires, Phys. Rev. B **63**, 235318 (2001).

[293] H. Touchette, The large deviation approach to statistical mechanics, Phys. Rep. **478**(1), 1 – 69 (2009).

[294] C. A. Tracy and H. Widom, Level-spacing distributions and the Airy kernel, Commun. Math. Phys. **159**(1), 151–174 (1994).

[295] C. A. Tracy and H. Widom, On orthogonal and symplectic matrix ensembles, Commun. Math. Phys. **177**(3), 727–754 (1996).

[296] F. G. Tricomi, *Integral equations*, Interscience, London, 1957.

[297] J. J. M. Verbaarschot and I. Zahed, Spectral density of the QCD Dirac operator near zero virtuality, Phys. Rev. Lett. **70**, 3852–3855 (1993).

[298] J. Verbaarschot, H. Weidenmüller, and M. Zirnbauer, Grassmann integration in stochastic quantum physics: The case of compound-nucleus scattering, Phys. Rep. **129**(6), 367 – 438 (1985).

[299] J. Verbaarschot and T. Wettig, Random matrix theory and chiral symmetry in QCD, Annu. Rev. Nucl. Part. Sci. **50**(1), 343–410 (2000).

[300] P. Vivo, S. N. Majumdar, and O. Bohigas, Large deviations of the maximum eigenvalue in Wishart random matrices, J. Phys. A **40**(16), 4317 (2007).

[301] P. Vivo, S. N. Majumdar, and O. Bohigas, Distributions of Conductance and Shot Noise and Associated Phase Transitions, Phys. Rev. Lett. **101**, 216809 (2008).

[302] P. Vivo, S. N. Majumdar, and O. Bohigas, Probability distributions of linear statistics in chaotic cavities and associated phase transitions, Phys. Rev. B **81**, 104202 (2010).

[303] P. Vivo and E. Vivo, Transmission eigenvalue densities and moments in chaotic cavities from random matrix theory, J. Phys. A **41**(12), 122004 (2008).

[304] S. R. Wadia, $N = \infty$ phase transition in a class of exactly soluble model lattice gauge theories, Phys. Lett. B **93**(4), 403 – 410 (1980).

[305] J. Weidmann, *Spectral theory of ordinary differential operators*, Springer, 1987.

[306] E. P. Wigner, Characteristic Vectors of Bordered Matrices with Infinite Dimensions, Ann. Math. **62**, 548–564 (1955).

[307] E. Wigner, Gatlinburg conference on neutron physics by time-of-flight, Oak Ridge National Laboratory Report 2309, p. 59, 1957.

[308] E. Wigner, *Group theory and its application to the quantum mechanics of atomic spectra*, Academic, New-York, 1959.

[309] E. P. Wigner, On the statistical distribution of the widths and spacings of nuclear resonance levels, Math. Proc. Cambridge Philos. Soc. **47**(4), 790–798 (1951).

[310] E. P. Wigner, On the Distribution of the Roots of Certain Symmetric Matrices, Ann. Math. **67**(2), 325–327 (1958).

[311] J. Wishart, The Generalised Product Moment Distribution in Samples from a Normal Multivariate Population, Biometrika **20A**(1-2), 32–52 (1928).

[312] E. Witten, Dynamical breaking of supersymmetry, Nucl. Phys. B **188**(3), 513 – 554 (1981).

[313] M. R. Zirnbauer, Super Fourier analysis and localization in disordered wires, Phys. Rev. Lett. **69**, 1584–1587 (1992).

[314] M. R. Zirnbauer, Riemannian symmetric superspaces and their origin in random-matrix theory, J. Math. Phys. **37**(10), 4986–5018 (1996).

université PARIS-SACLAY
ÉCOLE DOCTORALE
Physique en île-de-France (EDPIF)

Titre : Théorie des matrices aléatoires en physique statistique : théorie quantique de la diffusion et systèmes désordonnés

Mots clés : matrices aléatoires, statistiques linéaires, grandes déviations, systèmes désordonnés, transport cohérent

Résumé : La théorie des matrices aléatoires a des applications dans des domaines variés : mathématiques, physique, finance, ... En physique, le concept de matrices aléatoires a été utilisé pour l'étude du transport électronique dans des structures mésoscopiques, de systèmes désordonnés, de l'intrication quantique, de modèles d'interfaces 1D fluctuantes en physique statistique, des atomes froids, ...
Dans cette thèse, on s'intéresse au transport AC cohérent dans un point quantique, à des propriétés d'interfaces fluctuantes 1D sur un substrat et aux propriétés topologiques de fils quantiques multicanaux.
La première partie commence par une introduction générale a la théorie des matrices aléatoires ainsi qu'a la principale méthode utilisée dans cette thèse : le gaz de Coulomb. Cette technique permet entre autres d'étudier la distribution d'observables qui prennent la forme de statistiques linéaires des valeurs propres, qui représentent beaucoup de quantités physiques pertinentes. Cette méthode est ensuite appliquée à des exemples concrets pour étudier le transport cohérent et les problèmes d'interfaces fluctuantes en physique statistique.
La seconde partie se concentre sur un modèle de fil désordonné : l'équation de Dirac multicanale avec masse aléatoire. Nous étendons le puissant formalisme utilisé pour l'étude de systèmes unidimensionnels au cas quasi-1D, et établissons une connexion avec un modèle de matrices aléatoires. Nous utilisons ce résultat pour obtenir la densité d'états et les propriétés de localisation. Nous montrons également que ce système présente une série de transitions de phases topologiques (changement d'un nombre quantique de nature topologique, sans changement de symétrie), contrôlées par le désordre.

Title: Random matrix theory in statistical physics: quantum scattering and disordered systems

Keywords: random matrices, linear statistics, large deviations, disordered systems, coherent transport

Abstract: Random matrix theory has applications in various fields: mathematics, physics, finance, ... In physics, the concept of random matrices has been used to study the electonic transport in mesoscopic structures, disordered systems, quantum entanglement, interface models in statistical physics, cold atoms, ... In this thesis, we study coherent AC transport in a quantum dot, properties of fluctuating 1D interfaces on a substrate and topological properties of multichannel quantum wires.
The first part gives a general introduction to random matrices and to the main method used in this thesis: the Coulomb gas. This technique allows to study the distribution of observables which take the form of linear statistics of the eigenvalues. These linear statistics represent many relevant physical observables, in different contexts. This method is then applied to study concrete examples in coherent transport and fluctuating interfaces in statistical physics.
The second part focuses on a model of disordered wires: the multichannel Dirac equation with a random mass. We present an extension of the powerful methods used for one dimensional systems to this quasi-1D situation, and establish a link with a random matrix model. From this result, we extract the density of states and the localisation properties of the system. Finally, we show that this system exhibits a series of topological phase transitions (change of a quantum number of topological nature, without changing the symmetries), driven by the disorder.

Université Paris-Saclay
Espace Technologique / Immeuble Discovery
Route de l'Orme aux Merisiers RD 128 / 91190 Saint-Aubin, France